

CR-133970

**CONTRACT NAS 9-12909**

**SD 73-SA-0036-3**

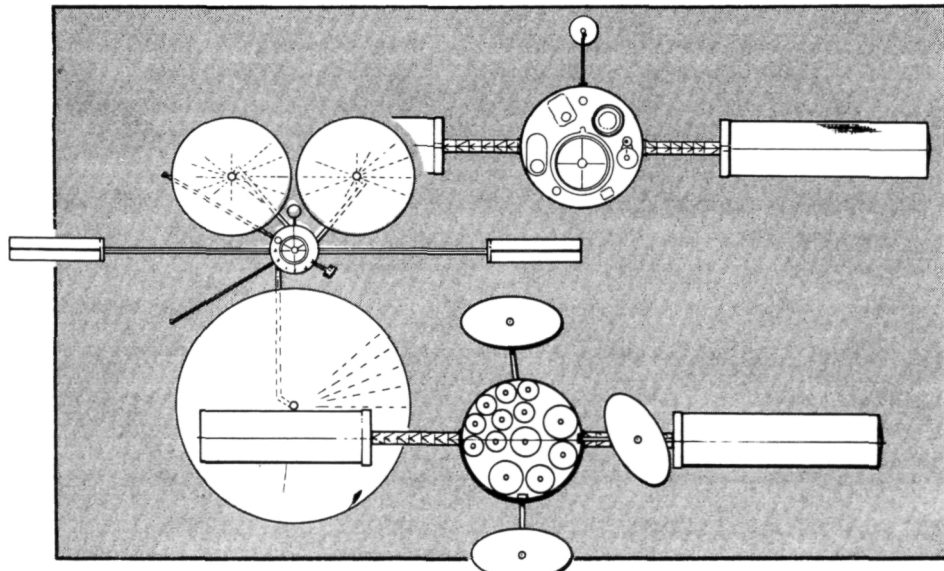
N73-28862

**GEOSYNCHRONOUS  
PLATFORM DEFINITION  
STUDY**

**CASE FILE**

**Volume III**      **COPY**

**GEOSYNCHRONOUS MISSION  
CHARACTERISTICS**



JUNE 1973



**Space Division**  
Rockwell International

1 2 2 1 4   Lakewood Boulevard  
Downey, California 90241

CONTRACT NAS 9-12909

SD 73-SA-0036-3

# GEOSYNCHRONOUS PLATFORM DEFINITION STUDY

## Volume III GEOSYNCHRONOUS MISSION CHARACTERISTICS

H. L. Myers

*H. L. Myers*  
*GPDS STUDY MANAGER*

JUNE 1973



1 2 2 1 4 Lakewood Boulevard,  
Downey, California 90241



## FOREWORD

The Geosynchronous Platform Definition Study was a pre-Phase A analysis conducted by the Space Division of Rockwell International Corporation (Rockwell) under Contract NAS9-12909 for the Lyndon B. Johnson Space Center of the National Aeronautics and Space Administration. The study explores the scope of geosynchronous traffic, the needs and benefits of multifunction space platforms, transportation system interfaces, and the definition of representative platform conceptual designs. The work was administered under the technical direction of Mr. David Brown (Telephone 713-483-6321) of the Program Planning Office/Future Programs Division of the Lyndon B. Johnson Space Center.

This report consists of the following seven volumes:

Volume I - Executive Summary	SD 73-SA-0036-1
Volume II - Overall Study Summary	SD 73-SA-0036-2
Volume III - Geosynchronous Mission Characteristics	SD 73-SA-0036-3
Volume IV, Part 1 - Traffic Analysis and System Requirements for the Baseline Traffic Model	SD 73-SA-0036-4 Part 1
Volume IV, Part 2 - Traffic Analysis and System Requirements for the New Traffic Model	SD 73-SA-0036-4 Part 2
Volume V - Geosynchronous Platform Synthesis	SD 73-SA-0036-5
Volume VI - Geosynchronous Program Evaluation and Recommendations	SD 73-SA-0036-6
Volume VII - Geosynchronous Transportation Requirements	SD 73-SA-0036-7

Acknowledgement is given to the following individuals for their participation in and contributions to the conduct of the study:

R. D. Meston	Mission and Program Analysis
L. R. Hogan	Systems Engineering and Spacecraft Design
E. Mehrbach	Communications and Avionics
Dr. K. A. Ehricke	Advanced Mission Analysis
M. R. Schall	Operations and Traffic Analysis
J. W. Patrick	Crew Systems and Servicing Analysis
E. L. Triman	Communications
E. G. Clegg	Spacecraft Design
K. B. Roberts	Operations Analysis
A. Gianformaggio	Cost Analysis
D. W. Earle	System Integration
R. E. Ogelvie	Guidance and Control
R. P. Arras	Thermal Control
W. C. Schmill	Electrical Power
J. B. Weddell	Astro-Physics Programs
E. F. Kraly	Sensor Systems Analysis

**Page intentionally left blank**



## CONTENTS

Section		Page
1.0	INTRODUCTION . . . . .	1-1
2.0	SUMMARY . . . . .	2-1
3.0	GEOSYNCHRONOUS ORBIT CHARACTERISTICS . . . . .	3-1
	3.1 GEOSYNCHRONOUS ORBIT GEOMETRIC CHARACTERISTICS . . . . .	3-3
	GROUND TRACE CHARACTERISTICS . . . . .	3-4
	EARTH COVERAGE CHARACTERISTICS . . . . .	3-13
	PREFERRED SATELLITE LOCATIONS . . . . .	3-32
	SOLAR TRANSIT OUTAGE . . . . .	3-56
	EARTH SHADOWING CHARACTERISTICS . . . . .	3-65
	3.2 ORBIT PERTURBATIONS . . . . .	3-71
	LUNI-SOLAR PERTURBATIONS . . . . .	3-77
	SOLAR PRESSURE PERTURBATIONS . . . . .	3-81
	PERTURBATION RESULTS . . . . .	3-85
	3.3 MISSION PROFILE CHARACTERISTICS . . . . .	3-93
	TRAJECTORY PROFILES . . . . .	3-94
	Ascent Profile (Single Delivery System) . . . . .	3-94
	Ascent Profile (Dual Reusable Tug) . . . . .	3-104
	Descent Profile . . . . .	3-112
	On-Orbit Operations . . . . .	3-112
	DELTA-V BUDGETS . . . . .	3-118
4.0	RELATED ORBIT CHARACTERISTICS . . . . .	4-1
	4.1 RELATED ORBIT GEOMETRIC CHARACTERISTICS . . . . .	4-3
	4.2 MISSION PROFILE CHARACTERISTICS . . . . .	4-13
5.0	ELECTROMAGNETIC SPECTRUM UTILIZATION . . . . .	5-1
	5.1 USABLE FREQUENCY SPECTRUM . . . . .	5-3
	5.2 ATMOSPHERIC WINDOWS . . . . .	5-13
	5.3 FREQUENCY ALLOCATIONS . . . . .	5-15
	5.4 ENVIRONMENTAL EFFECTS . . . . .	5-19
	ATMOSPHERIC ATTENUATION . . . . .	5-19
	Radio Frequencies . . . . .	5-19
	Infrared and Visible Frequencies . . . . .	5-24
	RAINFALL ATTENUATION . . . . .	5-24
	SKY NOISE . . . . .	5-31

Section	Page
5.5 FREQUENCY REUSE TECHNIQUES . . . . .	5-39
GROUND ANTENNA DISCRIMINATION . . . . .	5-39
Interference Relationships . . . . .	5-45
ORTHOGONAL POLARIZATION . . . . .	5-48
MULTIBEAM SPACECRAFT ANTENNA . . . . .	5-54
TIME DIVISION MULTIPLE ACCESS . . . . .	5-64
TDMA System Functional Description . . . . .	5-65
5.6 TECHNOLOGY STATUS . . . . .	5-69
FREQUENCY BAND AVAILABILITY . . . . .	5-69
COMPONENT AVAILABILITY . . . . .	5-69
RF Power Amplifier Components . . . . .	5-69
Receiver Front Ends . . . . .	5-71
Antennas . . . . .	5-72
Summary . . . . .	5-72
6.0 REFERENCES . . . . .	6-1

## ILLUSTRATIONS

Figure		Page
3.1-1	Geosynchronous Orbit Characteristics Definition . . . . .	3-4
3.1-2	Geographic Latitude Time-History . . . . .	3-8
3.1-3	Geographic Longitude Time-History ( $\lambda_0 = 0$ ) . . . . .	3-8
3.1-4	Geosynchronous Orbit Ground Trace ( $\lambda_0 = 0$ ) . . . . .	3-9
3.1-5	Relative Longitude Extrema . . . . .	3-12
3.1-6	Latitude at Longitude Extrema . . . . .	3-12
3.1-7	Time at Longitude Extrema . . . . .	3-12
3.1-8	Earth-Spacecraft Viewing Geometry . . . . .	3-13
3.1-9	Earth-Spacecraft Viewing Characteristics . . . . .	3-16
3.1-10	Earth Coverage Characteristics ( $\ell = 0$ ) . . . . .	3-18
3.1-11	Latitude Limits for Overlapping Coverage ( $\ell = 0$ ) . . . . .	3-19
3.1-12	World Coverage by Multiple Geostationary Satellite Systems . . . . .	3-21
3.1-13	General Earth Coverage Characteristics ( $\ell \neq 0$ ) . . . . .	3-24
3.1-14	Earth Coverage Geometry ( $\ell \neq 0$ ) . . . . .	3-24
3.1-15	Earth Coverage Characteristics ( $\ell = 60$ degrees) . . . . .	3-29
3.1-16	Generalized Time Varying Earth Coverage Characteristics ( $\ell \neq 0$ ) . . . . .	3-31
3.1-17	Definition of Geostationary Satellite Limits . . . . .	3-33
3.1-18	Geosynchronous Satellite Relative Longitude Limits . . . . .	3-35
3.1-19	Satellite Location Limits for Various Geographic Locations . . . . .	3-37
3.1-20	Utilization of Satellite Location Limits . . . . .	3-43
3.1-21	Satellite Locations Limits; At Least One U.S. Site . . . . .	3-45
3.1-22	Satellite Locations Limits; Single U.S. Site . . . . .	3-46
3.1-23	Satellite Location Limits; Any Contiguous U.S. Site . . . . .	3-47
3.1-24	Satellite Location Limits; Any U.S. Site Including Alaska and Hawaii . . . . .	3-48
3.1-25	Satellite Location Limits; European Coverage . . . . .	3-49
3.1-26	Satellite Location Limits; Atlantic Ocean Coverage (Including U.S. and Eastern Europe) . . . . .	3-50
3.1-27	Satellite Location Limits; Pacific Ocean Coverage . . . . .	3-51
3.1-28	Satellite Locations Limits; Indian Ocean Coverage . . . . .	3-52
3.1-29	Satellite Locations Limits; Meteorology (United States) . . . . .	3-53
3.1-30	Geostationary Satellite Location Summary . . . . .	3-55
3.1-31	Geosynchronous Satellite Shadow Trace on Earth . . . . .	3-59
3.1-32	Solar Declination Versus Time of Year . . . . .	3-60
3.1-33	Solar Outage Chart . . . . .	3-63
3.1-34	Ground Station/Geosynchronous Satellite Solar Outage Local Mean Time (Whenever Outage Occurs for that Station) . . . . .	3-64
3.1-35	Earth Shadow Geometry . . . . .	3-66
3.1-36	Earth Shadow Characteristics - Geosynchronous Orbit . . . . .	3-67
3.1-37	Annual Shadowing Characteristics . . . . .	3-68
3.1-38	Shadow Passage Time (Geostationary Orbit) . . . . .	3-69

Figure		Page
3.2-1	Perturbation Sources and Effects . . . . .	3-72
3.2-2	Perturbed Geosynchronous Satellite Mean Path . . . . .	3-74
3.2-3	Geosynchronous Satellite Gravitational Force . . . . .	3-74
3.2-4	Luni-Solar Perturbation Model . . . . .	3-78
3.2-5	Initial Orbital Geometry . . . . .	3-80
3.2-6	Eccentricity Buildup Due to Solar Pressure . . . . .	3-82
3.2-7	Eccentricity Circle Geometry . . . . .	3-83
3.2-8	Longitudinal Libration Period Due to Triaxial Earth, Equatorial Geosynchronous Orbit . . . . .	3-86
3.2-9	Longitudinal Drift Rate Due to Triaxial Earth, Equatorial Geosynchronous Orbit . . . . .	3-86
3.2-10	Geosynchronous Equatorial Satellite Longitudinal Drift Due to Triaxial Earth . . . . .	3-87
3.2-11	Geosynchronous Equatorial Satellite Altitude Deviation Due to Triaxial Earth . . . . .	3-87
3.2-12	Synchronous Equatorial Satellite Drift Velocity Due to Triaxial Earth . . . . .	3-88
3.2-13	Longitudinal Libration Amplitude Dispersion ( $\Delta\lambda_r$ ) Due to Triaxial Earth - degrees . . . . .	3-89
3.2-14	Mean Geosynchronous Luni-Solar Perturbation Effects . . .	3-90
3.2-15	Solar Pressure Perturbations on Geosynchronous Orbit . . .	3-90
3.2-16	Long Period Solar Pressure Maximum Perturbations (Period = One Year) . . . . .	3-91
3.2-17	Daily Longitudinal Libration Due to Solar Pressure . . . .	3-91
3.3-1	Geosynchronous Mission Ascent Profile . . . . .	3-95
3.3-2	Geosynchronous Mission Ascent Ground Trace . . . . .	3-96
3.3-3	Geosynchronous Transfer Orbit Position Time Histories . .	3-97
3.3-4	Geosynchronous Transfer Orbit Time Histories . . . . .	3-98
3.3-5	Geosynchronous Transfer Maneuvers . . . . .	3-100
3.3-6	Distributed Plane Change Delta-V Requirements . . . . .	3-103
3.3-7	Geosynchronous Transfer Incremental Velocity Requirements	3-105
3.3-8	Ascent Phasing Time Requirements . . . . .	3-106
3.3-9	Dual Reusable Tug Ascent Profile . . . . .	3-107
3.3-10	Dual Tug Incremental Velocities . . . . .	3-108
3.3-11	On-Orbit Phasing Requirements . . . . .	3-114
3.3-12	Plane Change Delta-V Requirements . . . . .	3-117
4.1-1	Eccentric "24-Hour" Orbit Ground Trace ( $\omega_p = 0$ ) . . . .	4-6
4.1-2	Eccentric "24-Hour" Orbit Ground Trace ( $\omega_p = 270^\circ$ ) . .	4-7
4.1-3	Earth Coverage Characteristics ( $\theta = 60$ degrees; $e = 0.2$ )	4-9
4.2-1	Elliptic Orbit Radii for "24-Hour" Orbits . . . . .	4-14
4.2-2	Impulsive Incremental Velocity Requirements (Eccentric "24-Hour" Orbits) . . . . .	4-15
5.1-1	Frequency Spectrum, 100 KHz to 1 GHz . . . . .	5-4
5.1-2	Frequency Spectrum, 1 GHz to 3 GHz . . . . .	5-5
5.1-3	Frequency Spectrum, 3 GHz to 10 GHz . . . . .	5-6
5.1-4	Frequency Spectrum, 10 GHz to 30 GHz . . . . .	5-7
5.1-5	Frequency Spectrum, 30 GHz to 100 GHz . . . . .	5-8
5.1-6	Frequency Spectrum, 100 GHz to 1000 GHz . . . . .	5-9
5.1-7	Frequency Spectrum, 1000 GHz ( $10^{12}$ Hz) to $10^{16}$ Hz . . . .	5-10



Figure		Page
5.1-8	Frequency Spectrum, $10^{16}$ Hz to $10^{20}$ Hz	5-11
5.2-1	Atmospheric Windows (Above 10 GHz)	5-13
5.4-1	Transmission Windows	5-20
5.4-2	Effects of Water Vapor and Oxygen	5-21
5.4-3	Atmospheric Attenuation (Between 150 and 350 GHz) (Theoretical Curves and Experimental Measurements)	5-22
5.4-4	Atmospheric Absorption Nomograph - Frequency vs. Elevation Angle	5-23
5.4-5	Atmospheric Absorption as a Function of Frequency and Elevation Angle (Sea Level Using an Atmosphere Typical of Washington, D.C. in August)	5-25
5.4-6	Atmospheric Transmission in Visible and Infrared Spectrum (Measurements Made Over Horizontal Paths)	5-26
5.4-7	RF Attenuation Due to Rainfall (3 - 20 GHz)	5-27
5.4-8	RF Attenuation Due to Rainfall (Above 10 GHz)	5-28
5.4-9	RF Attenuation Due to Rainfall	5-29
5.4-10	Point Rainfall Rates Measured in Several Places by Instruments with Rapid Response (Based on a One-Year sample made available through the courtesy of the Illinois State Water Survey)	5-30
5.4-11	Typical One-Way System Degradation Due to Rain	5-32
5.4-12	Precipitation Attenuation (dB) Equaled or Exceeded for Indicated Hours/Year	5-33
5.4-13	Atmospheric Attenuation at 16 and 30 GHz as Measured (Using the Sun as a Source)	5-34
5.4-14	Frequency of Occurrence of Rain Cells as a Function of Cell Diameter for Various Altitudes. (Based on half- year sample made available through the courtesy of McGill University, Montreal)	5-35
5.4-15	Ground Diversity Technique to Improve Communication Link Reliability	5-36
5.4-16	Diversity Advantage at 16 GHz as Measured for Two Earth Stations Located in New Jersey with Seven-Mile Separation	5-37
5.4-17	Sky-Noise Temperature Due to Oxygen and Water Vapor Absorption, the Angle of Elevation Above the Horizon is Attached to Each Curve	5-38
5.5-1	Interference Modes/Shared Frequency Operation	5-42
5.5-2	Interference Noise Versus Satellite Spacing	5-43
5.5-3	Downlink Interference	5-46
5.5-4	Uplink Interference	5-47
5.5-5	Polarization Isolation for Coincident Linear Beams	5-50
5.5-6	Horizontal Polarization (Antenna Without Grating - Angle Aligned) 5.925 to 6.425 GHz Uplink	5-51
5.5-7	Typical Frequency Plan Using Orthogonal Polarization	5-52
5.5-8	Cross Polarization Discrimination vs. Rain Rate Effects for a Horizontal Earth Link	5-53
5.5-9	Multi-Beam Satellite Antenna Use (Beam Separation vs. Beamwidth)	5-55
5.5-10	Two-Degree Spot Beam Template	5-56



Figure		Page
5.5-11	One-Degree Spot Beam Template . . . . .	5-57
5.5-12	Antenna Beamwidth vs. Size . . . . .	5-58
5.5-13	World Map for Use with Spot Beam Templates . . . . .	5-61
5.5-15	Satellite TDMA System . . . . .	5-66
5.5-16	Formats of a TDMA System . . . . .	5-67
5.6-1	Antenna Beamwidth vs. Antenna Gain . . . . .	5-70

## TABLES

Table		Page
3.1-1	Earth-Spacecraft Viewing Angles . . . . .	3-15
3.3-1	Single Tug Ascent Delta-V Budget (Inclination = 28.5 degrees) . . . . .	3-119
3.3-2	Single Tug Ascent Delta-V Budget (Geosynchronous Equatorial Orbit) . . . . .	3-119
3.3-3	Dual Tug Ascent/Return Delta-V Budget for Performance Calculations ( $i = 28.5$ degrees) . . . . .	3-120
3.3-4	Dual Tug Ascent/Return Delta-V Budget (Geosynchronous Equatorial Orbit) for Performance Calculations . . . . .	3-121
3.3-5	Reusable Tug Descent Delta-V Budget ( $i = 28.5$ deg) . . . . .	3-122
3.3-6	Reusable Tug Descent Delta-V Budget (Geosynchronous Equatorial Orbit) . . . . .	3-122
3.3-7	On-Orbit Maneuver Delta-V Budget . . . . .	3-123
5.3-1	World-Wide Spectrum Allocations for Space Services (Based on WARC-ST, 1971, Geneva) . . . . .	5-16
5.5-1	Allocated Frequency Spectrum and Projected Data Rate Capabilities . . . . .	5-40
5.5-2	Data Rate Forecast - Year 1990 (Derived from New Traffic Model) (Figures 3.4-3, 3.4-5 of Vol. IV, Part 2) . . . . .	5-41
5.5-3	Antenna Diameter to Wavelength Ratio . . . . .	5-44
5.5-4	Typical Interference Calculation . . . . .	5-49
5.5-5	Minimum Beamwidth Separation for Dual Beam Antennas . . . . .	5-59
5.6-1	Projection of Geosynchronous Orbit Data Rate Capability . . . . .	5-72

**Page intentionally left blank**



## ABBREVIATIONS

ASCS	Attitude stabilization and control system
ATS	Applications Technology Satellite
CCD	Charge coupled device
CCIR	Consultative Committee for International Radio
CM	Crew module
C/N	Carrier-to-noise ratio
COMM	Communications
Comsat	Communications Satellite
CSM	Common support module
DMS	Data management subsystem
Domsat	Domestic Communications Satellite
ECS	Environmental control subsystem
EIRP	Effective isotropic radiated power
EPS	Electrical power subsystem
FDMA	Frequency division multiplexing
FM	Frequency modulation
GEOPAUSE	Geodetic satellite in polar geosynchronous orbit
Geoseps	Geosynchronous solar electric propulsion stage
Intelsat	International Communication Satellite
IPACS	Integrated power and attitude control system
Mersat	Metrology and Earth Observations Satellite
Navsat	Navigation and Traffic Control Satellite

OTS	Orbital transportation system
PCM	Pulse code modulation
PSK	Phase shift keying
RCS	Reaction control subsystem
RSU	Remote service unit
SATA	Small Application Technology Satellite
SEP	Solar electric propulsion
SGLS	Space-ground link subsystem (part of U.S. Air Force Satellite Control Facility)
SNR	Signal-to-noise ratio
SSM	Spares storage module
STDN	Spaceflight tracking and data network
STS	Space transportation system
TDMA	Time division multiple access
TDRS	Tracking and Data Relay Satellite
TPS	Thermal protection subsystem
TT&C	Tracking, telemetry and command
UHF	Ultra high frequency
VHF	Very high frequency
WARC	World Administrative Radio Conference
XMTR	Transmitter

## 1.0. INTRODUCTION

The objectives of the Geosynchronous Platform Definitions Study were to examine the nature of currently planned and new evolutionary geosynchronous programs, to analyze alternative ways of conducting missions, to establish concepts for new systems to support geosynchronous programs in an effective and economical manner, and to define the logistic support to carry out these programs. In order to meet these objectives, it was necessary to define and examine general geosynchronous mission characteristics and the potentially applicable electromagnetic spectrum characteristics.

This volume contains an organized compilation of these data with emphasis on the development and use of the data. Fundamental geosynchronous orbit time histories, mission profile characteristics, and delivery system characteristics are presented. In addition, electromagnetic spectrum utilization is discussed in terms of the usable frequency spectrum, the spectrum potentially available considering established frequency allocations, and the technology status as it affects the ability to operate within specific frequency bands.

The data contained in this volume were used primarily to support the principal study tasks. Therefore, the material contained in the volume is general in nature and is not related to a given geosynchronous mission. As noted above, the fundamental data and relationships necessary to examine the characteristics of geosynchronous missions are presented. In this manner, additional data may be conveniently generated for cases not specifically covered by this report.

## 2.0 SUMMARY

Significant geosynchronous mission characteristics were derived and compiled in support of the Geosynchronous Platform Definition Study and for use during future mission planning activities. In general, there are natural phenomena which introduce specific constraints, limits, or parametric trends into the geosynchronous mission planning problem. The material presented here deals with these phenomena, showing which represent rigid constraints and which can be controlled or shaped to meet desired mission features. Delta-V maneuvers can be applied to modify orbital characteristics and frequency bands, and RF power levels can be selected to achieve desired communications capabilities.

Specifically included in this volume are the ground trace and earth coverage characteristics of geostationary, inclined, and other related geosynchronous orbits. Line-of-sight geometries are presented along with preferred satellite locations for various representative surface aim points and coverage zones. Earth-sun spacecraft geometry patterns are shown which affect solar noise levels in communication links and which define the period of solar occultation where solar array power output is reduced or terminated. Orbit perturbations are defined and their effects on orbital motions are summarized. Delta-V requirements to counter these perturbations are also presented. Typical mission profile characteristics are shown depicting all the major events required to place payloads at any specified location in geosynchronous orbit. Both placement and retrieval are considered along with their respective delta-V budgets.

The principal electromagnetic spectrum factors confronting the geosynchronous mission planner are the frequencies available, the environmental effects associated with these frequencies, the bandwidth needs for the services to be provided, and the earth coverage requirements related to the desired communications paths. To meet these needs, data are presented which define the usable spectrum in terms of natural phenomena effects (atmosphere and weather), frequency allocations through international agreements, and available technology. Important coverage enhancement and improved spectrum utilization factors are developed through frequency reuse techniques.

### 3.0 GEOSYNCHRONOUS ORBIT CHARACTERISTICS

This section presents a compilation of fundamental geosynchronous mission data. Basic relationships are derived, fundamental characteristics are discussed, and specific data are presented for select cases. These data constitute the fundamental geosynchronous mission characteristics which were used throughout the study for (1) defining preferred satellite locations for a variety of spacecraft types and/or mission functions, (2) defining the number of spacecraft required to satisfy earth-spacecraft line-of-sight requirements, (3) developing the time-phased geographic distributions of the satellites defined in the study traffic models, and (4) conducting geosynchronous orbit saturation analyses.

The data presented in this section are restricted to circular orbits which have a period equal to the mean rate of rotation of the earth. Included are circular geosynchronous orbits with zero as well as non-zero inclinations. Non-circular "24-hour" orbits and orbits with periods other than the geosynchronous orbit period are discussed in Section 4.0, Related Orbit Characteristics.

The initial sections present the fundamental orbital time history and earth coverage characteristics based on the restricted two-body equations of motion. The effects of orbit perturbations are then discussed. Geosynchronous mission profile characteristics are then developed with primary emphasis on the definition of delta-V budgets.

**Page intentionally left blank**

**Page intentionally left blank**

### 3.1 GEOSYNCHRONOUS ORBIT GEOMETRIC CHARACTERISTICS

The fundamental motion of a spacecraft in earth orbit is defined by the restricted two-body equations of motion. This motion defines the fundamental geometric characteristics which must be understood during the development and definition of geosynchronous missions. The restricted two-body equations of motion define the short-term spacecraft ground trace and the resultant line-of-sight characteristics between the spacecraft and given locations of earth. These characteristics also define the periods when solar transit outage will occur and when occultation of the sun by the earth will occur. These fundamental geosynchronous orbit geometric characteristics are presented in this section. The effects of orbit perturbations on these motions are discussed in Section 3.2, Orbit Perturbations.

The ground trace characteristics of geosynchronous orbits are presented first, considering both zero and non-zero inclination orbits. The resultant earth coverage characteristics are then presented. Based on these characteristics, preferred geographic locations are defined as a function of typical coverage requirements for representative mission functions.

Solar transit outage and solar occultation will affect either the number of spacecraft required or the spacecraft design requirements. Solar outage will dictate the number and spacing of satellites required to provide uninterrupted communications between specified ground stations. Without multiple satellites, there will be uniquely defined periods during the year when solar noise will negate the ability of a specified ground site to receive from a given geosynchronous data relay satellite.

There are two periods during the year when a geosynchronous satellite will pass through the earth shadow. During these periods, a non-solar electrical power system must provide the required power level and total energy. If communications are required during these periods, either multiple satellites must be utilized or a secondary electrical power system must provide the required power.

In general, the basic relationships are presented and fundamental data shown. Also, examples of specific data are presented. This approach permits the user to develop additional data for specific cases which are not presented in this report.



## GROUND TRACE CHARACTERISTICS

The ground trace characteristics of geosynchronous satellites are described by the definition of the geographic latitude and longitude of the subsatellite point as a function of time. The fundamental relationships defining the time-phased geographic latitude and longitude of the subsatellite point are shown in Figure 3.1-1

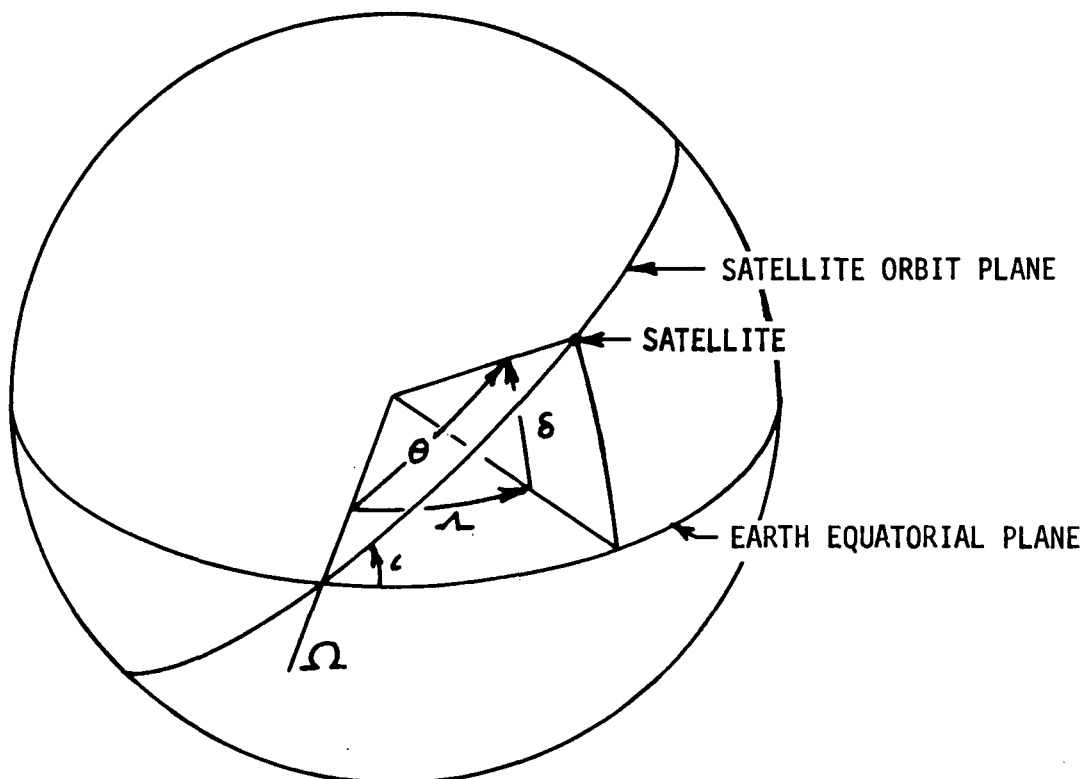


Figure 3.1-1. Geosynchronous Orbit Characteristics Definition

As can be seen from the figure, the latitude is given by:

$$\delta = \sin^{-1} (\sin \iota \sin \theta); \quad (-90^\circ \leq \delta \leq 90^\circ) \quad (3.1-1)$$

where

$\delta$  = the geographic latitude of the subsatellite point; measured from the earth equatorial plane (degrees)

$\iota$  = the inclination of the satellite orbit plane to the earth equatorial plane (degrees)

$\theta$  = the position of the satellite; measured in the satellite orbit plane from the orbit ascending node (degrees)

For circular orbits:

$$\theta = \eta t \quad (3.1-2)$$

where

$\eta$  = the mean orbital motion (degrees/hour)

$t$  = the time since ascending node passage (mean solar hours)

For geosynchronous orbits:

$$\eta = \omega_{\oplus}$$

= the earth mean rate of rotation

= 15.041 067 degrees per mean solar hour (Reference 3-1)

Therefore, the geographic latitude time-history of the subsatellite point of a satellite in circular geosynchronous orbit is given by:

$$\delta = \sin^{-1} [\sin \iota \sin (15.041067 t)] \quad (3.1-3)$$



From Equation (3.1-3) it can be seen that the subsatellite latitude extrema are defined by:

$$\delta_{MAX} = \epsilon$$

and

$$\delta_{MIN} = -\epsilon$$

and occur when

$$t = 5.98 \text{ hours } (\theta = 90 \text{ degrees})$$

and

$$t = 17.95 \text{ hours } (\theta = 270 \text{ degrees}),$$

respectively.

From Figure 3.1-1, the relative latitude of the subsatellite point is given by:

$$\begin{aligned} \lambda &= \cos^{-1} \left( \frac{\cos \theta}{\cos \delta} \right) \\ \text{or} \\ \lambda &= \cos^{-1} \left[ \frac{\cos (15.041067t)}{\cos \delta} \right] \end{aligned} \quad \left. \right\} 0 \leq \lambda \leq 360^\circ \quad (3.1-4)$$

The geographic longitude is then given by:

$$\lambda = \lambda_0 + \lambda - \omega_\oplus t ; \quad 0 \leq \lambda \leq 360^\circ \quad (3.1-5)$$

where

$\lambda$  = the relative longitude of the satellite; measured in the earth equatorial plane from the orbit ascending node (degrees)

$\lambda$  = the geographic longitude of the subsatellite point (degrees)

- $\lambda_0$  = the initial geographic longitude of the orbit  
ascending node (degrees)
- = the geographic longitude of the subsatellite point  
at  $t = 0$
- $\omega_\oplus$  = the earth mean rate of rotation
- = 15.041 067 degrees per mean solar hour

From Equations (3.1-3), (3.1-4), and (3.1-5), it can be seen that

$$\delta = 0$$

and

$$\lambda = \lambda_0$$

when

$$\theta = (n)(180 \text{ degrees})$$

or, equally,

$$t = (n) \left( \frac{180}{15.041067} \right) \quad n = \text{positive integer}$$

$$= (n)(11.967236).$$

Therefore, the geographic locations of the ascending and descending nodes are coincident.

The resultant geographic latitude and longitude time-histories defined by Equations (3.1-3), (3.1-4), and (3.1-5) are shown in Figures 3.1-2 and 3.1-3 for a range of inclinations assuming  $\lambda_0 = 0$ . The corresponding ground traces are shown in Figure 3.1-4.

As can be seen from Figure 3.1-4, the ground trace in general, defines a "figure-eight"; the only exception being the geostationary orbit ( $\iota = 0^\circ$ ). As noted previously, the latitude extrema are equal to the orbit inclination. The longitudinal extrema can be obtained by examining

$$\frac{d\lambda}{dt} = 0$$

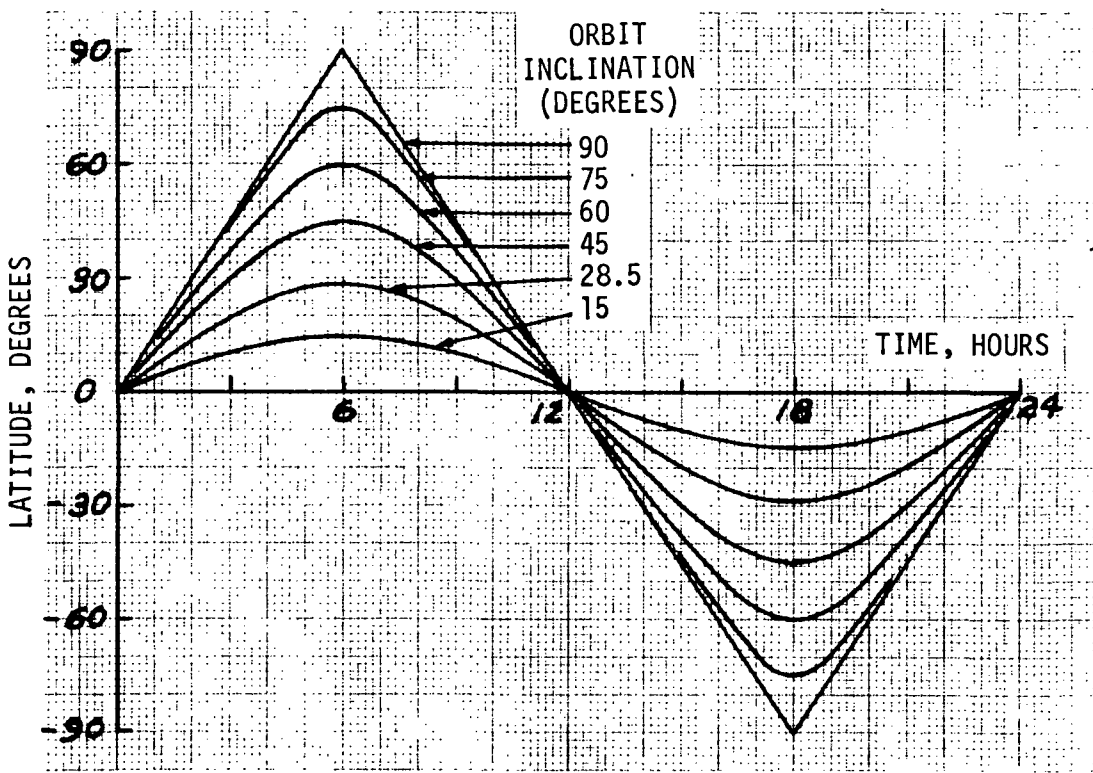


Figure 3.1-2. Geographic Latitude Time-History

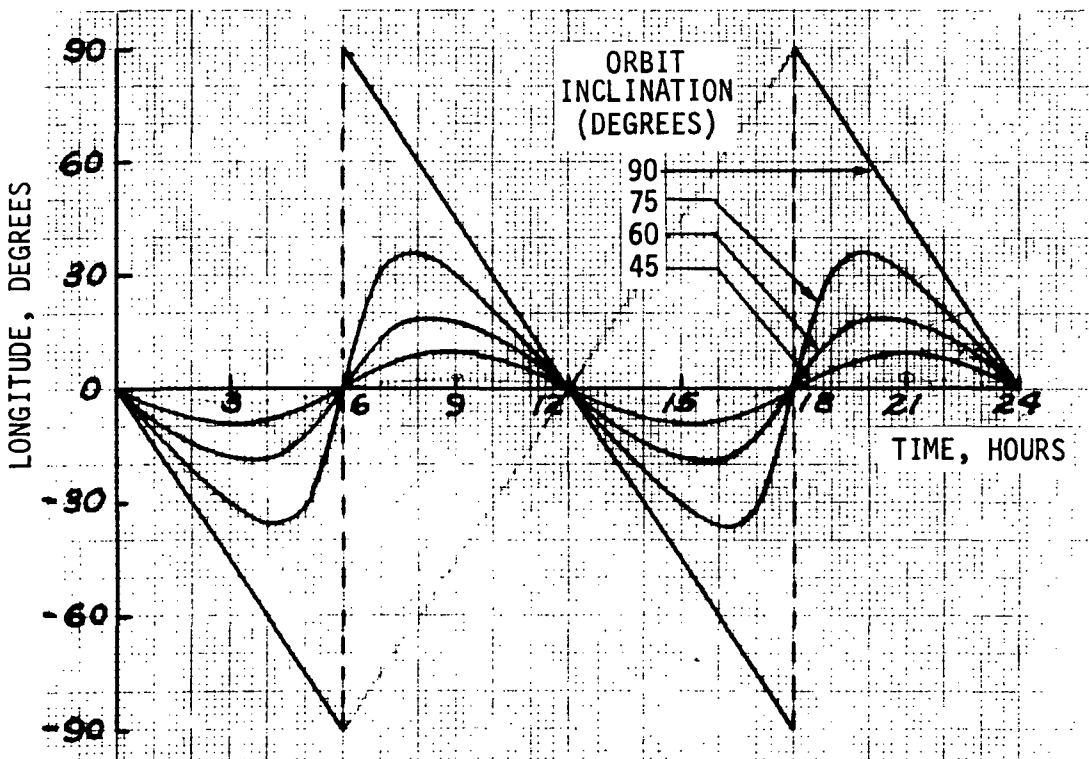


Figure 3.1-3. Geographic Longitude Time-History ( $\lambda_0 = 0$ )

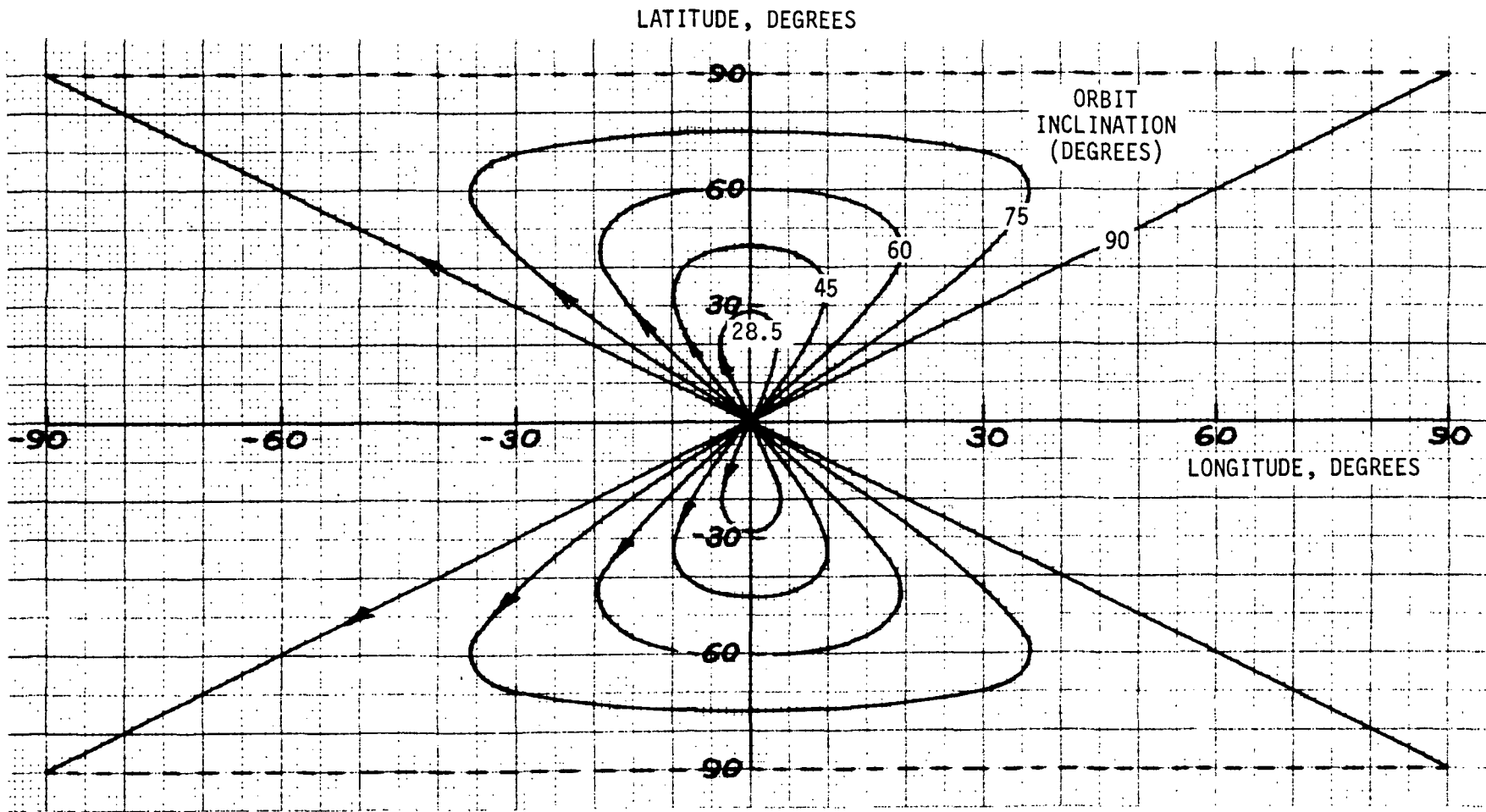


Figure 3.1-4. Geosynchronous Orbit Ground Trace ( $\lambda_0 = 0$ )

From Equation (3.1-5):

$$\frac{d\lambda}{dt} = \frac{d\lambda}{dt} - \omega_\oplus \quad (3.1-6)$$

From Equation (3.1-4):

$$\frac{d\lambda}{dt} = \frac{1}{\sin\lambda \cos\delta} \left[ \omega_\oplus \sin\theta - \frac{\sin\delta \cos\theta}{\cos\delta} \frac{d\delta}{dt} \right] \quad (3.1-7)$$

and from Equation (3.1-1):

$$\frac{d\delta}{dt} = \frac{\omega_\oplus \sin\lambda \cos\theta}{\cos\delta} \quad (3.1-8)$$

Combining Equations (3.1-7) and (3.1-8) and simplifying:

$$\frac{d\lambda}{dt} = \frac{\omega_\oplus}{\sin\lambda \cos\delta} \left[ \sin\theta - \frac{\sin\lambda \sin\delta \cos^2\theta}{\cos^2\delta} \right] \quad (3.1-9)$$

from which:

$$\frac{d\lambda}{dt} = \frac{\omega_\oplus}{\sin\lambda \cos\delta} \left[ \sin\theta - \frac{\sin\lambda \sin\delta \cos^2\theta}{\cos^2\delta} \right] - \omega_\oplus \quad (3.1-10)$$

Solving Equation (3.1-10) for

$$\frac{d\lambda}{dt} = 0,$$

the following relationships can be obtained:

$$\delta]_{\dot{\lambda}=0} = \pm \cos^{-1}(\sqrt{\cos\zeta}), \quad (3.1-11)$$

$$\theta]_{\dot{\lambda}=0} = (180)(n) \pm \cos^{-1} \left( \frac{\sqrt{\cos \iota} + \sqrt{1 - \cos \iota}}{\sin \iota} \right), \quad (3.1-12)$$

$n = 0$  and  $1$ ,

$$\lambda]_{\dot{\lambda}=0} = \pm \cos^{-1} \left( \frac{\sqrt{1 - \cos \iota}}{\sin \iota} \right), \quad (3.1-13)$$

and

$$\lambda]_{\dot{\lambda}=0} = \lambda_0 + \lambda]_{\dot{\lambda}=0} - \theta]_{\dot{\lambda}=0} \quad (3.1-14)$$

The resultant geographic longitude extrema, the corresponding latitude extrema, and the times at which the extrema occur are shown in Figures 3.1-5, 3.1-6, and 3.1-7, respectively. As can be seen from Figure 3.1-4, the maximum longitudinal excursion for posigrade ( $\iota \leq 90$  degrees) geosynchronous orbits is  $\pm 90$  degrees and occurs when  $\iota = 90$  degrees (polar orbit).

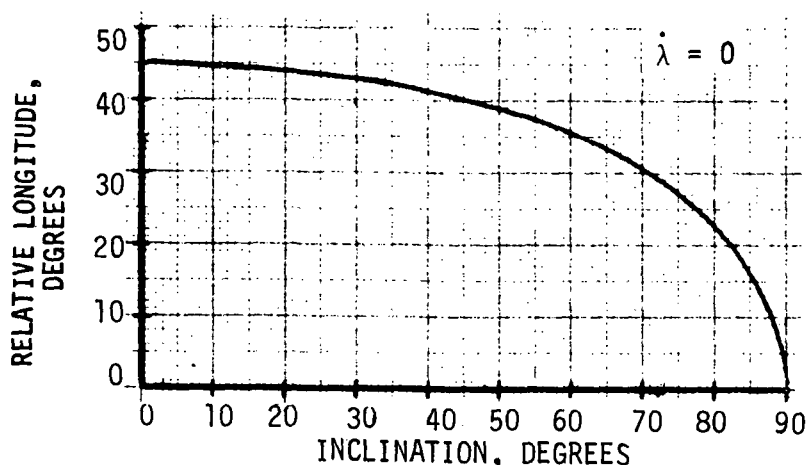


Figure 3.1-5. Relative Longitude Extrema

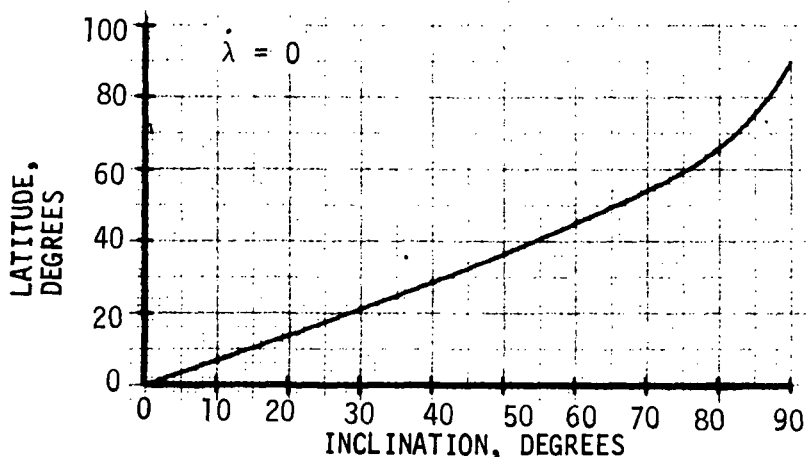


Figure 3.1-6. Latitude at Longitude Extrema

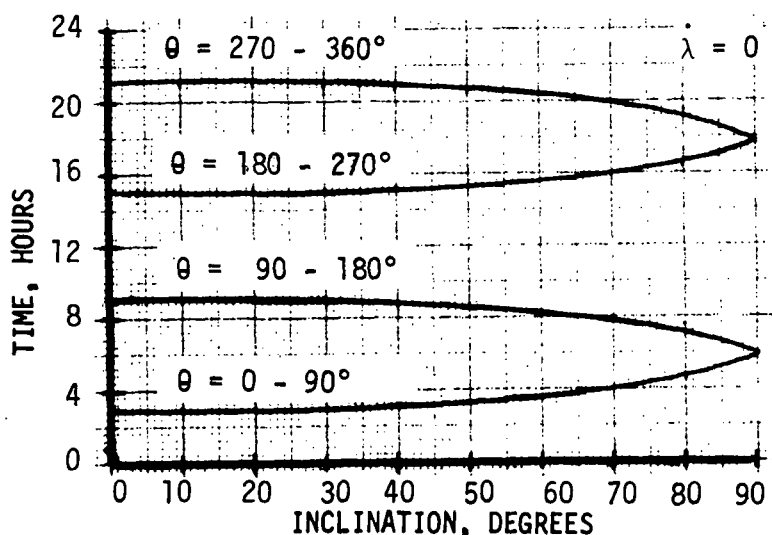


Figure 3.1-7. Time at Longitude Extrema

## EARTH COVERAGE CHARACTERISTICS

The general earth coverage characteristics are defined by the spacecraft radius and the minimum allowable earth surface view angle. The geometric relationships between these variables are illustrated in Figure 3.1-8.

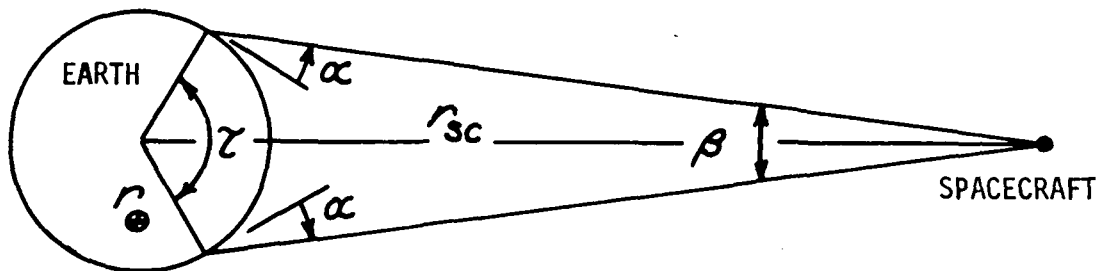


Figure 3.1-8. Earth-Spacecraft Viewing Geometry

As can be seen from the figure,

$$\beta = 2 \sin^{-1} \left[ \left( \frac{r_E}{r_{sc}} \right) \cos \alpha \right] \quad (3.1-15)$$

where

$\beta$  = the spacecraft view angle

$\alpha$  = the minimum allowable earth surface viewing incidence angle or

= the minimum allowable communications mask angle (angle of the spacecraft above the local horizon)

$r_E$  = the earth radius

=  $2.092\ 573\ 832 \times 10^7$  feet

and

$r_{sc}$  = the spacecraft radius

Also,

$$z = 180 - (2\alpha + \beta) \quad (3.1-16)$$

where

$$\gamma = \text{the total coverage earth central angle (degrees)}$$

The spacecraft radius is, for circular orbits, determined from

$$r = \sqrt{\frac{\mu}{\gamma^3}} \quad (\text{circular orbits})$$

from which

$$r_{sc} = \left( \frac{\mu}{\gamma^2} \right)^{1/3} \quad (3.1-17)$$

where

$$\begin{aligned} \mu &= \text{the earth gravitational constant} \\ &= 1.407\ 653\ 92 \times 10^{16} \text{ ft}^3/\text{sec}^2 \end{aligned}$$

and  $\gamma = \text{the mean orbital motion}$

As noted in the previous section, the mean orbital motion for circular geosynchronous orbits is equal to the earth mean rate of rotation ( $\omega_\oplus$ ). That is,

$$\begin{aligned} \gamma &= \omega_\oplus \\ &= 15.041\ 067 \text{ degrees per mean solar hour} \\ &= 6.300\ 387 \text{ radians per mean solar day} \end{aligned}$$

Therefore, the radius of a circular geosynchronous orbit is, from Equation (3.1-17), given by

$$[r_{sc}]_{\substack{\text{CIR.} \\ \text{GEO.}}} = r_{syn} = 1.383\ 342\ 191 \times 10^8 \text{ feet.}$$

The geosynchronous altitude, given by

$$h_{syn} = r_{syn} - r_\oplus$$

is then

$$h_{syn} = 1.174\ 084\ 808 \times 10^8 \text{ feet.}$$

Expressed in terms of alternate units,

$$r_{\oplus} = 3\ 443.933\ 6 \text{ nautical miles}$$

$$= 1.0 \text{ E.R. (Earth Radii)}$$

$$r_{SYN} = 22\ 766.884\ 38 \text{ nautical miles}$$

$$= 6.611 \text{ E.R.}$$

and

$$h_{SYN} = 19\ 322.950\ 78 \text{ nautical miles}$$

$$= 5.611 \text{ E.R.}$$

The resultant earth-spacecraft viewing characteristics defined by Equations (3.1-15) and (3.1-16) and the above constants are shown in Figure 3.1-9. The values of  $\beta$  and  $\tau$  evaluated at  $\alpha = 0$  correspond to the angle subtended by the earth from geosynchronous orbit and the corresponding earth central angle. From Equations (3.1-15) and (3.1-16),

$$\beta_{\alpha=0} = 17.40 \text{ degrees}$$

and

$$\tau_{\alpha=0} = 162.60 \text{ degrees}$$

For convenience, the view angles and the earth central angles for commonly used communications mask angles are tabulated in Table 3.1-1.

Table 3.1-1. Earth-Spacecraft Viewing Angles

Mask Angle ( $\alpha$ ) (degrees)	View Angle ( $\beta$ ) (degrees)	View Half-Angle ( $\beta/2$ ) (degrees)	Central Angle ( $\tau$ ) (degrees)	Central Half-Angle ( $\tau/2$ ) (degrees)
0	17.40	8.70	162.60	81.30
5	17.33	8.67	152.67	76.33
10	17.13	8.57	142.87	71.43
15	16.80	8.40	133.20	66.60
20	16.34	8.17	123.66	61.83



Space Division  
North American Rockwell

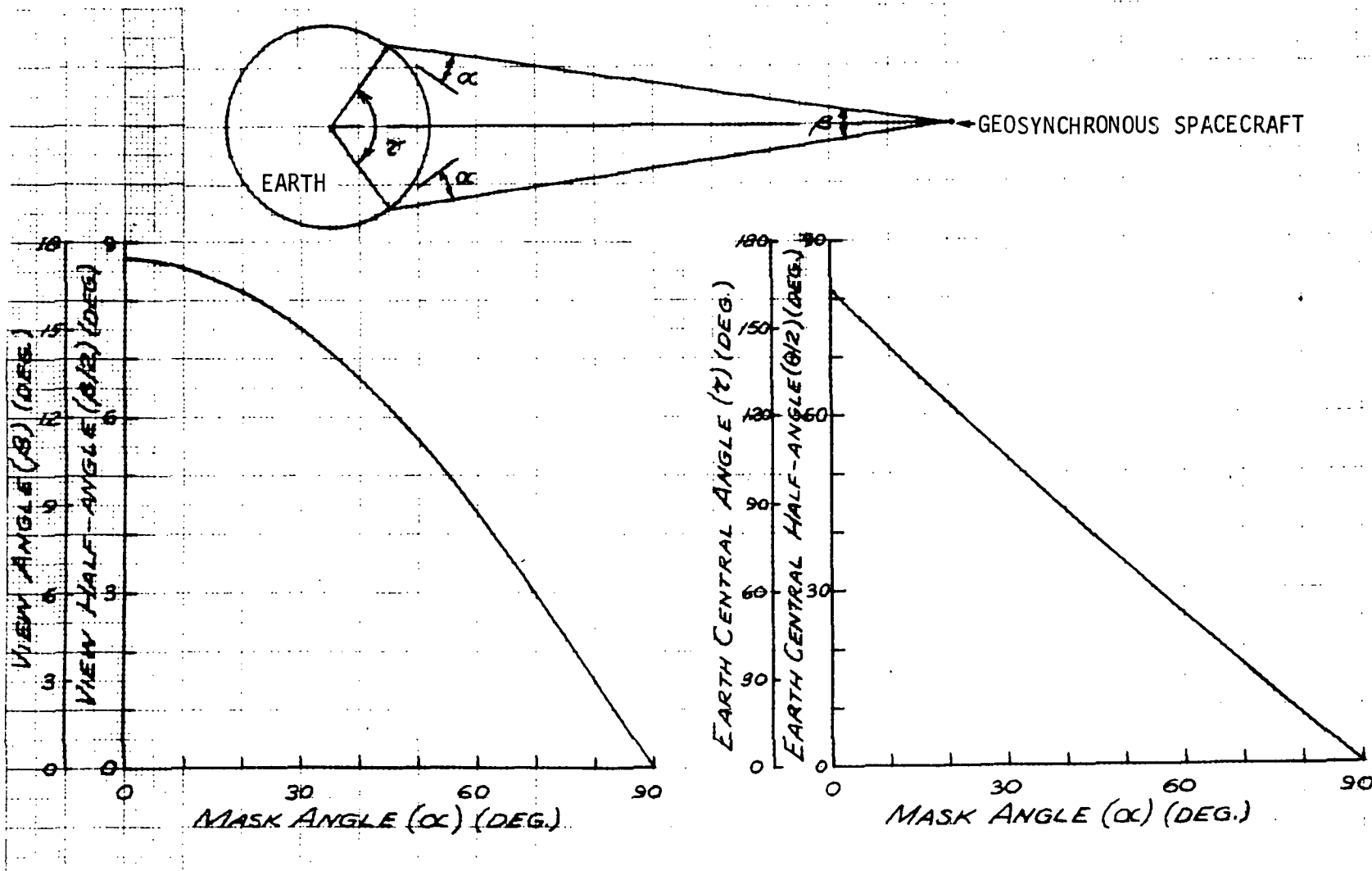


Figure 3.1-9. Earth-Spacecraft Viewing Characteristics

Representative earth coverage characteristics are shown in Figure 3.1-10 for a geosynchronous equatorial ( $\epsilon = 0$ ) orbit. For this figure, the spacecraft geostationary location was arbitrarily assumed to be at a geographic longitude of  $100^\circ W$ . The coverage provided by other geostationary satellites can be obtained by translating the coverage traces along the equator.

Multiple geostationary satellites provide overlapping coverage with the magnitude of the overlap dependent upon the longitudinal separation of the spacecraft. The coverage overlap is best expressed in terms of the maximum latitude of overlapping coverage as illustrated in Figure 3.1-11.

From the insert in Figure 3.1-11, it can be seen that

$$\delta_{LIMIT} = \pm \cos^{-1} \left[ \frac{\cos(\gamma/2)}{\cos(\Delta\lambda/2)} \right] \quad (3.1-18)$$

where

$\delta_{LIMIT}$  = the maximum latitude for overlapping coverage from adjacent geostationary satellites

$\Delta\lambda$  = the longitudinal separation of the spacecraft

From Equation (3.1-16)

$$\gamma/2 = 90 - (\alpha + \beta/2) \quad (3.1-19)$$

and, from Equation (3.1-15)

$$\beta/2 = \sin^{-1} \left[ \left( \frac{r_\theta}{r_{sc}} \right) \cos \alpha \right] \quad (3.1-20)$$

Combining Equations (3.1-18), (3.1-19), and (3.1-20), the latitude limit is given as a function of longitudinal separation ( $\Delta\lambda$ ) and mask angle ( $\alpha$ ) as:

$$\delta_{LIMIT} = \pm \cos^{-1} \left[ \frac{\sqrt{1 - \left( \frac{r_\theta}{r_{sc}} \right)^2 \cos^2 \alpha} \sin \alpha + \left( \frac{r_\theta}{r_{sc}} \right) \cos^2 \alpha}{\cos(\Delta\lambda/2)} \right] \quad (3.1-21)$$

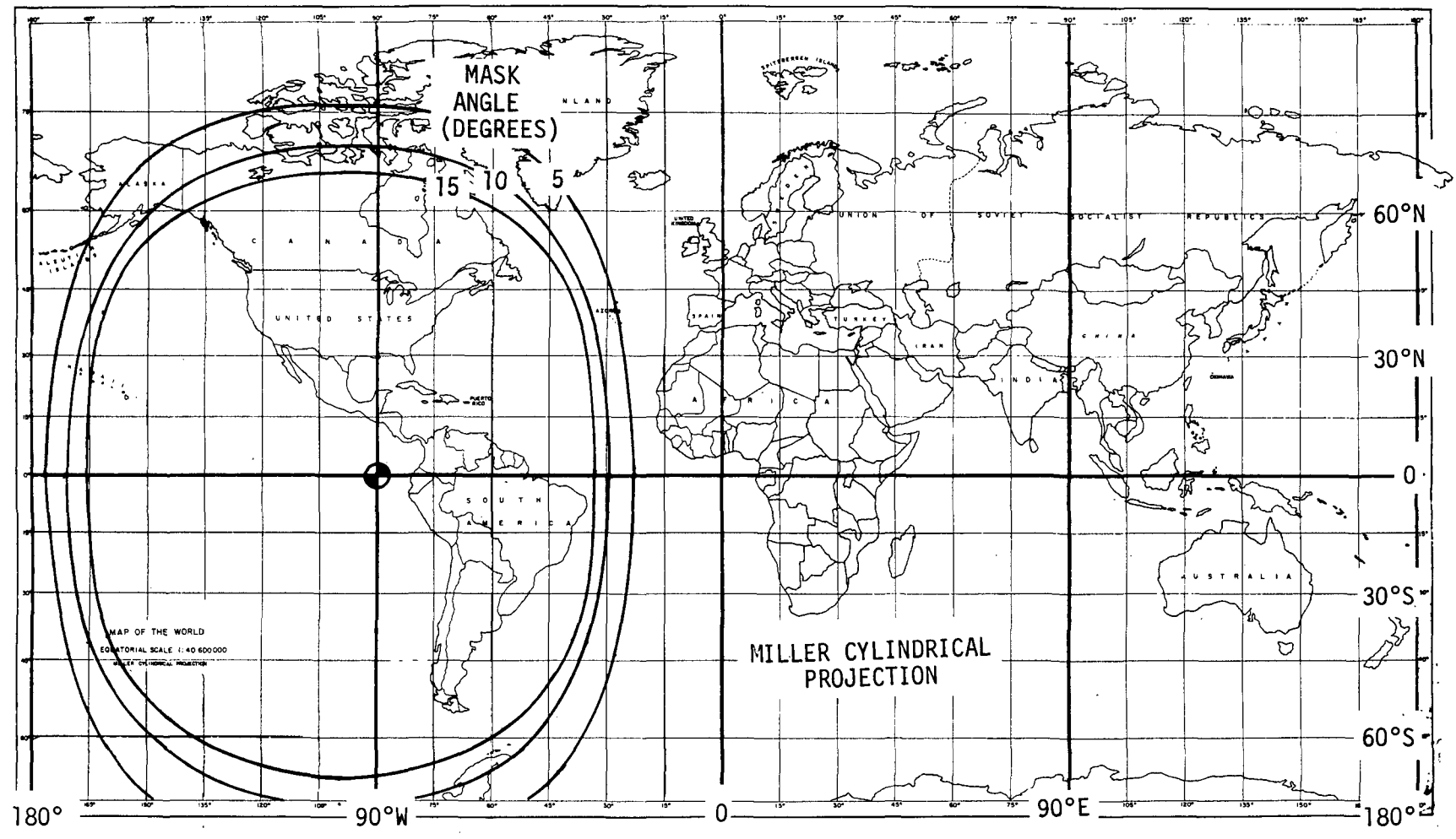


Figure 3.1-10. Earth Coverage Characteristics ( $\iota = 0$ )

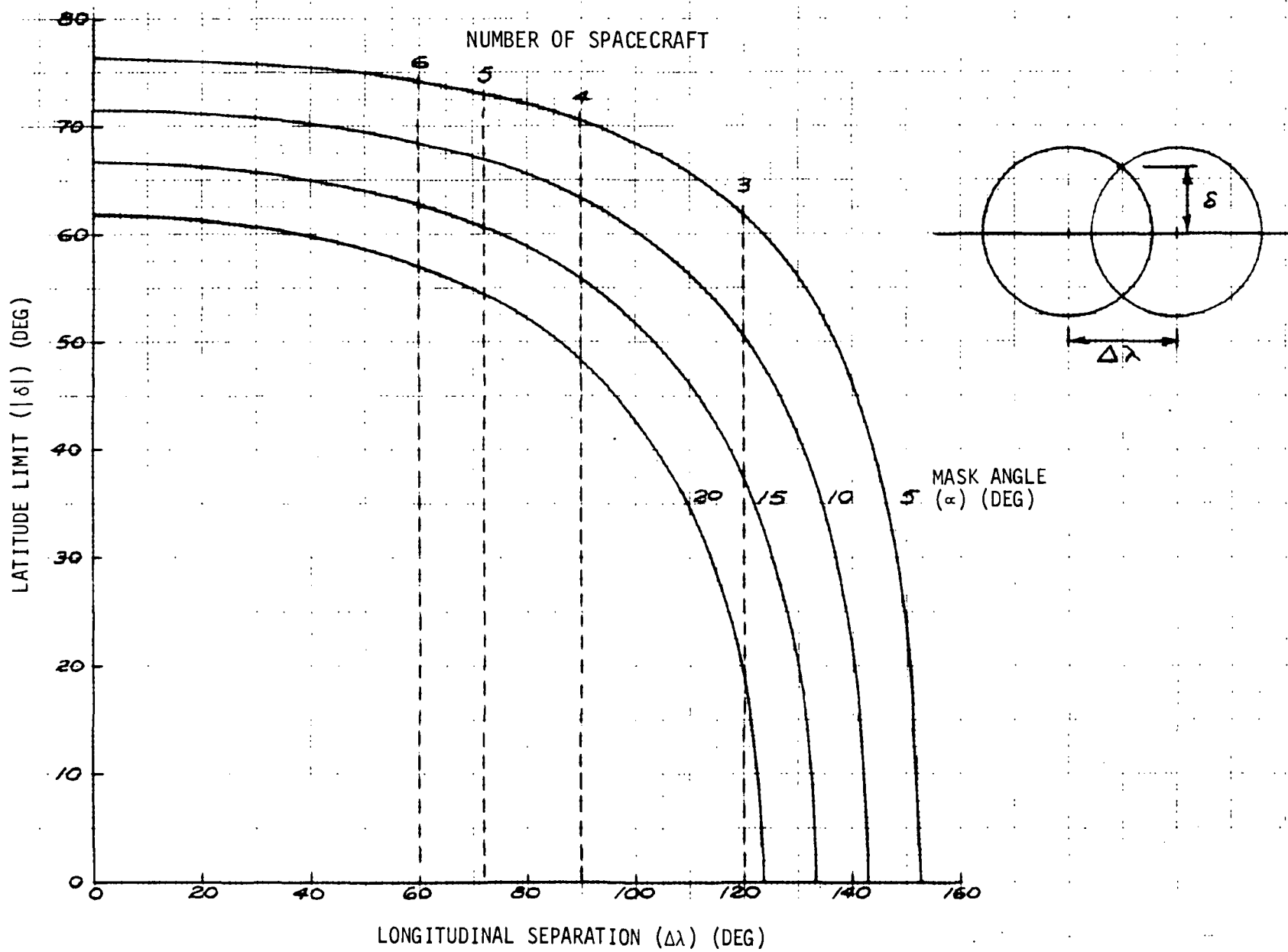


Figure 3.1-11. Latitude Limits for Overlapping Coverage ( $\iota = 0$ )



The resultant latitude limits are shown in Figure 3.1-11 for a range of mask angles ( $\alpha$ ). Also shown are the limits of continuous latitude coverage provided by multiple satellite networks ( $n > 2$ ) assuming a uniform longitudinal distribution, i.e.,

$$\Delta\lambda = \left(\frac{360}{n}\right)$$

$n$  = positive non-zero integer

As can be seen from the figure, a three-satellite, uniformly distributed satellite network will provide continuous coverage between 61.8 degrees north latitude and 61.8 degrees south latitude for a mask angle ( $\alpha$ ) of 5 degrees. By going to a uniformly distributed four-satellite network, the latitude band of continuous coverage is increased to +70.5 degrees.

The resultant world coverage characteristics for multiple geostationary satellite systems are shown in Figure 3.1-12 for representative mask angles. As can be seen from the figure, a four-satellite system with an allowable mask angle of 5 degrees will provide coverage of the world major land masses. The figure also illustrates the limited additional coverage provided by an increased uniformly distributed satellite population. Finally, the figures dramatically illustrate the impact of mask angle on the world-wide coverage capability of uniformly distributed multiple satellite systems.

As can be seen from Figures 3.1-10 and 3.1-12, coverage of the polar regions cannot be provided by geostationary satellites. It is necessary to utilize non-geostationary orbits ( $i \neq 0$ ) if coverage of the polar regions is required. As shown in the discussion of the ground trace characteristics of geosynchronous orbits, the ground trace of a non-geostationary orbit appears to describe a figure eight. Therefore, the coverage characteristics are a function of time and the time-phased coverage characteristics vary with inclination.

By combining the previously discussed ground trace and generalized earth coverage characteristics, the time-phased earth coverage characteristics of inclined geosynchronous orbits can be developed. The fundamental geometric relationships which must be considered are illustrated in Figure 3.1-13. The earth coverage at time  $t$  is dependent upon the spacecraft geographic latitude ( $\delta$ ) and longitude ( $\lambda$ ) at time  $t$  and the minimum allowable mask angle ( $\alpha$ ). The coverage at time  $t$  is then defined by a minor circle on the surface of the earth (spherical earth assumption) which is defined by the earth central angle  $\tau/2$ .

Let  $(\hat{i}, \hat{j}, \hat{k})$  represent an orthogonal unit vector set as shown in Figure 3.1-14. Also, let  $r$  = a unit vector in the direction of the spacecraft. Finally, let  $(\hat{r}, \hat{s}, \hat{t})$  represent the orthogonal unit vector set defined by a rotation about  $j$  through  $\delta$ . Then,

3-21

SD 73-SA-0036-3

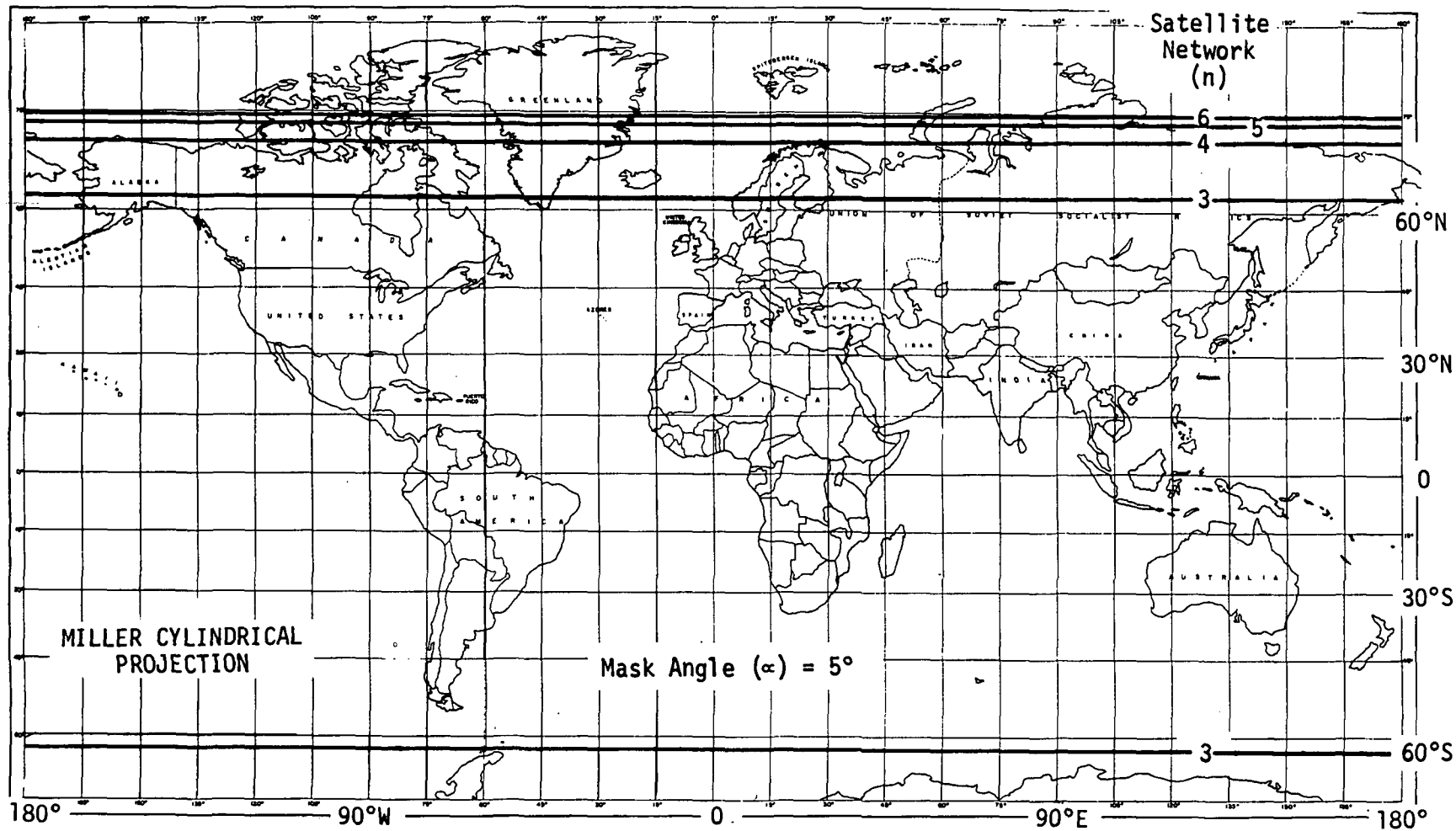


Figure 3.1-12. World Coverage by Multiple Geostationary Satellite Systems

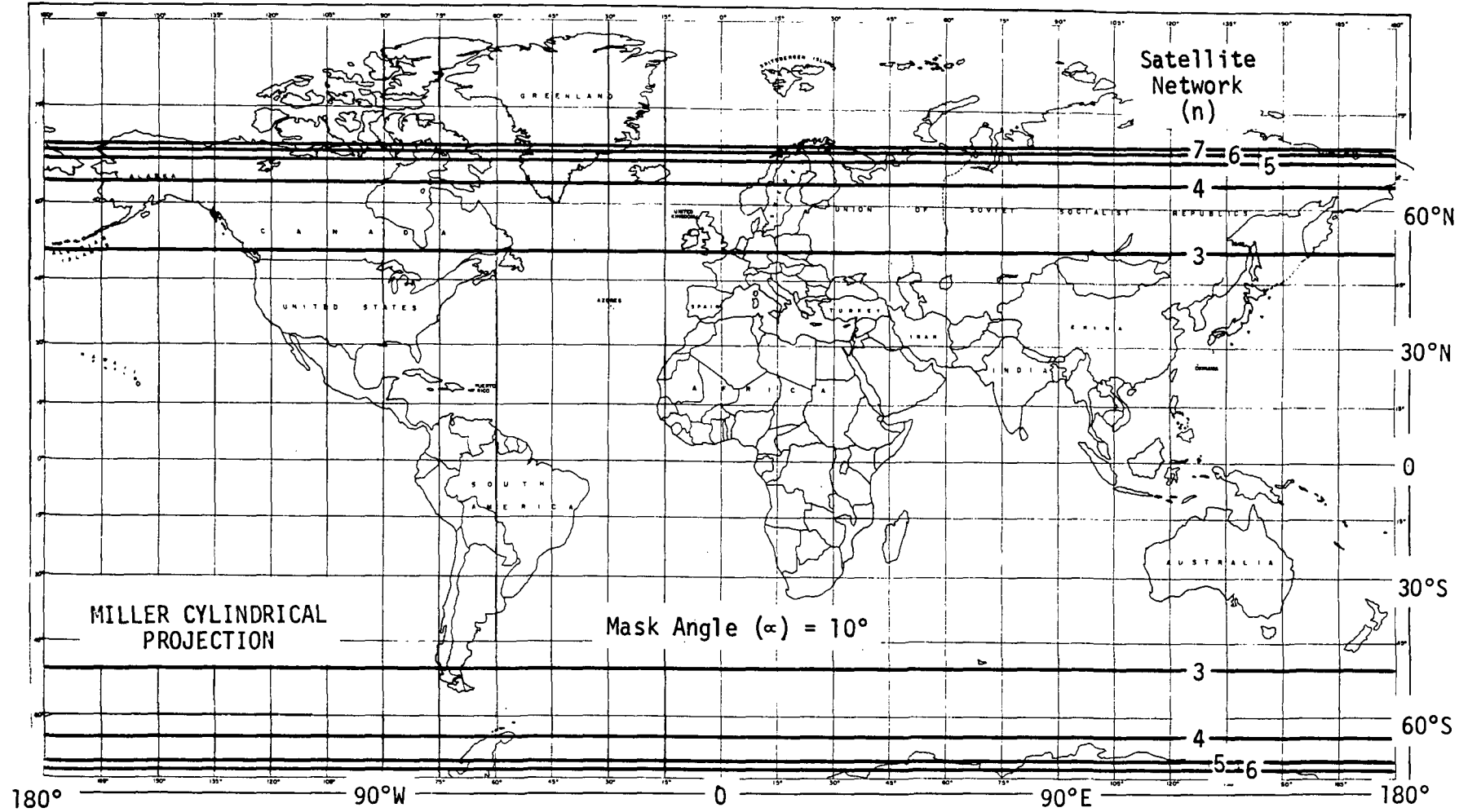


Figure 3.1-12. World Coverage by Multiple Geostationary Satellite Systems (continued)



Space Division  
North American Rockwell

3-23

SD 73-SA-0036-3

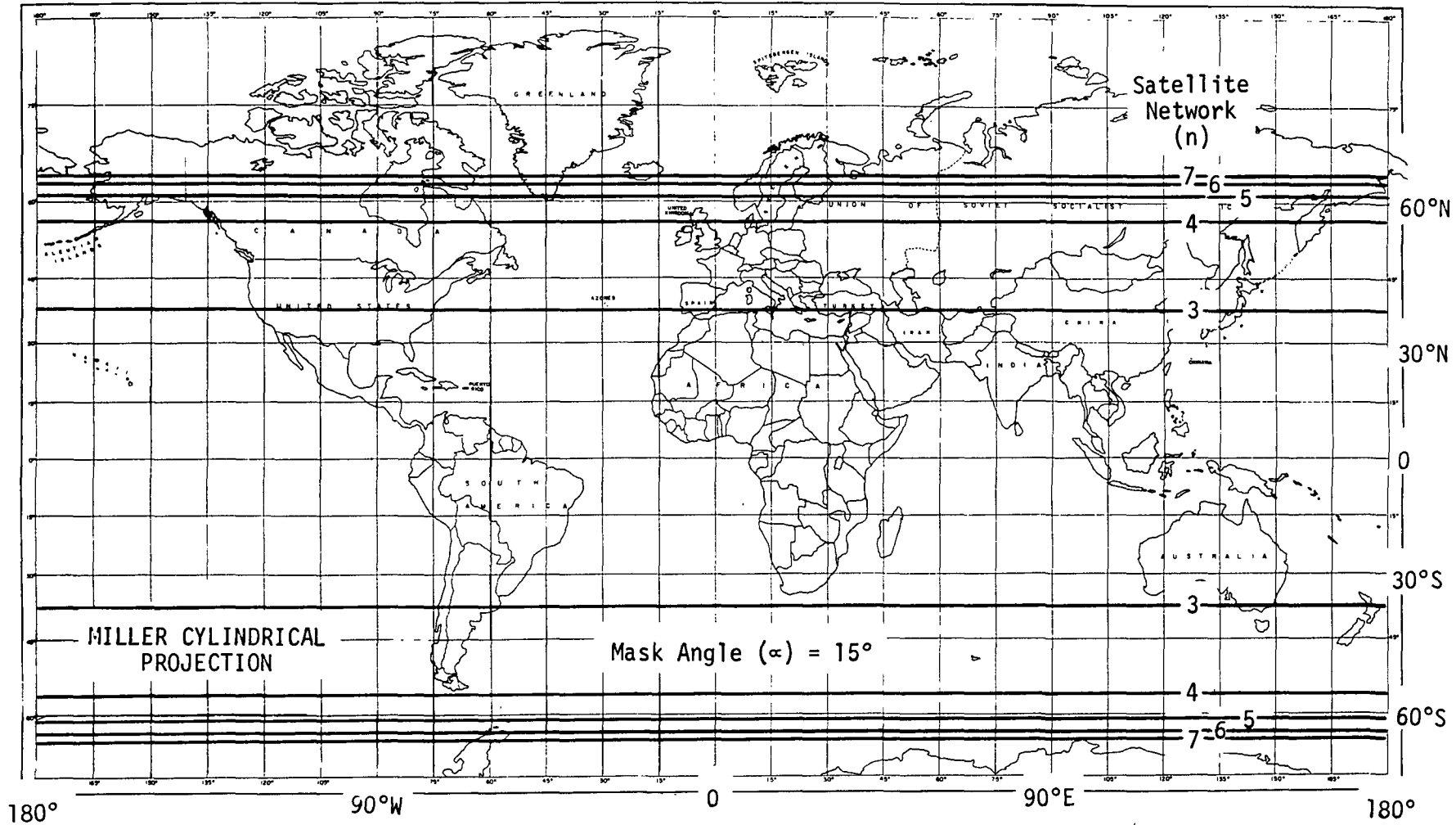


Figure 3.1-12. World Coverage by Multiple Geostationary Satellite Systems (continued)

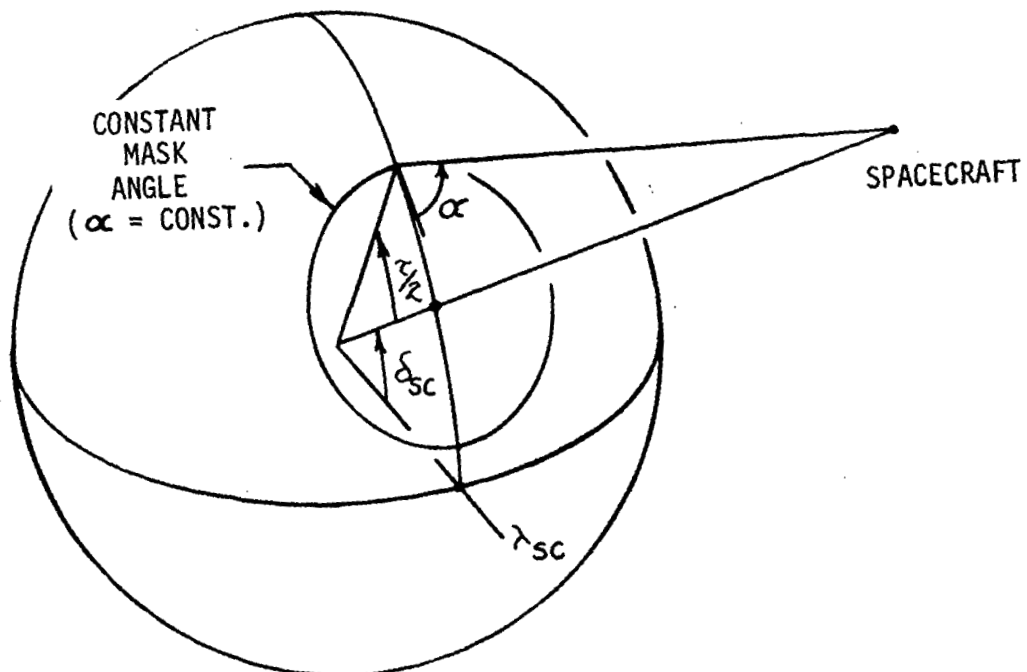


Figure 3.1-13. General Earth Coverage Characteristics ( $c \neq 0$ )

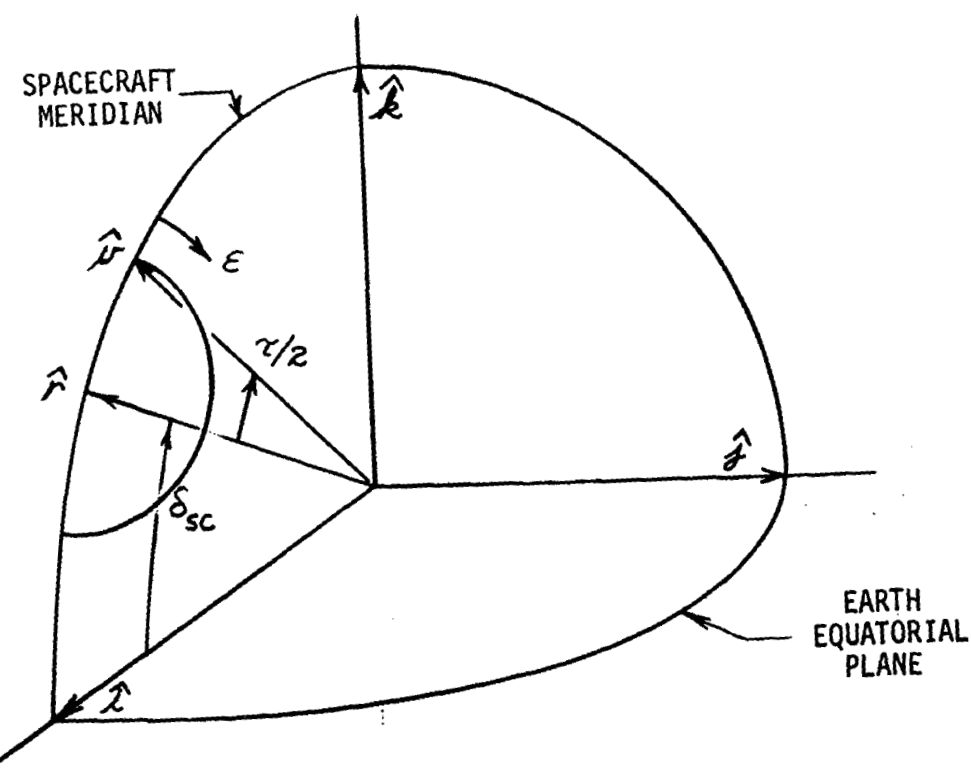


Figure 3.1-14. Earth Coverage Geometry ( $c \neq 0$ )



$$\begin{bmatrix} \hat{r} \\ \hat{s} \\ \hat{t} \end{bmatrix} = \begin{bmatrix} \cos \delta & 0 & \sin \delta \\ 0 & 1 & 0 \\ -\sin \delta & 0 & \cos \delta \end{bmatrix} \begin{bmatrix} \hat{i} \\ \hat{j} \\ \hat{k} \end{bmatrix}$$

(3.1-22)

$$\left. \begin{aligned} \hat{r} &= \cos \delta \hat{i} + \sin \delta \hat{k} \\ \hat{s} &= \hat{j} \\ \hat{t} &= -\sin \delta \hat{i} + \cos \delta \hat{k} \end{aligned} \right\}$$

Let

$\hat{\nu}$  = a unit vector defining the limit of earth viewing  
for a given mask angle

The earth coverage capability is then defined by the minor circle trace which results from a rotation of  $\hat{v}$  about  $\hat{r}$ .

The required unit vector  $\hat{v}$  is defined by

$$\hat{v} = \cos(\tau/2) \hat{r} + \sin \epsilon \sin(\tau/2) \hat{s} + \cos \epsilon \sin(\tau/2) \hat{t} \quad (3.1-23)$$

where

$\tau$  = the previously defined coverage earth central angle

$\epsilon$  = the angle of rotation about  $\hat{r}$ ; measured from the spacecraft meridian; clockwise as viewed from  $+\hat{r}$

Then, from Equation (3.1-22),

$$\begin{aligned} \hat{v} = & [\cos \delta \cos(\tau/2) - \cos \epsilon \sin \delta \sin(\tau/2)] \hat{x} \\ & + [\sin \epsilon \sin(\tau/2)] \hat{j} \\ & + [\sin \delta \cos(\tau/2) + \cos \epsilon \cos \delta \sin(\tau/2)] \hat{k}. \quad (3.1-24) \end{aligned}$$

The unit vector  $\hat{v}$  is defined in terms of geographic coordinates by

$$\begin{aligned}\hat{v} = & \cos \delta_{v_i} \cos \Delta \lambda_{v_i} \hat{i} \\ & + \cos \delta_{v_i} \sin \Delta \lambda_{v_i} \hat{j} \\ & + \sin \delta_{v_i} \hat{k}\end{aligned}\quad (3.1-25)$$

where

$\delta_{v_i}$  = the geographic latitude of the earth viewing limit evaluated at  $\epsilon_i$  ; and

$\Delta \lambda_{v_i}$  = the relative geographic longitude of the earth viewing limit evaluated at  $\epsilon_i$  ; measured in the earth equatorial plane from the spacecraft meridian.

By equating Equations (3.1-24) and (3.1-25) and solving,  $\delta_{v_i}$  and  $\Delta \lambda_{v_i}$  are expressed as the following functions of  $\delta$ ,  $\tau/2$  and  $\epsilon$  :

$$\delta_{v_i} = \sin^{-1} [\sin \delta \cos(\tau/2) + \cos \epsilon \cos \delta \sin(\tau/2)]$$

$$\Delta \lambda_{v_i} = \sin^{-1} \left[ \frac{\sin \epsilon \sin(\tau/2)}{\cos \delta_{v_i}} \right]$$

and

$$\Delta \lambda_{v_i} = \cos^{-1} \left[ \frac{\cos \delta \cos(\tau/2) - \cos \epsilon \sin \delta \sin(\tau/2)}{\cos \delta_{v_i}} \right]$$

Then

$$\lambda_{v_i} = \lambda + \Delta \lambda_{v_i}; \quad (0 \leq \lambda_{v_i} \leq 360^\circ). \quad (3.1-27)$$

Since

$$-90^\circ \leq \delta_{v_i} \leq 90^\circ$$

and

$$0 \leq \Delta \lambda_{v_i} \leq 360^\circ,$$



Equation (3.1-26) defines the total coverage capability without ambiguity by letting  $\epsilon$  vary from 0 to 360 degrees.

Representative earth coverage traces are shown in Figure 3.1-15 for a geosynchronous orbit within an inclination of 60 degrees assuming a mask angle of 5 degrees. For convenience, the coverage for the first twelve hours since ascending nodal passage is shown. The coverage for the remainder of the orbit is obtained by symmetry with respect to the equator of the earth. As can be seen from Figure 3.1-13, the spacecraft will be capable of "over-the-pole" viewing when the spacecraft latitude is

$$|\delta| > 90 - \frac{\pi}{2} \text{ (degrees)}$$

From Figure 3.1-9 and Table 3.1-1,

$$\left. \frac{\pi}{2} \right]_{\alpha=5^\circ} = 76.33 \text{ degrees}$$

Therefore, the north pole of the earth will be within line of sight of the spacecraft when the spacecraft latitude is greater than 13.67 degrees north. By symmetry, the south pole of the earth will be within line of sight when the spacecraft latitude is less than 13.67 degrees south.

The times during which polar coverage will occur can be obtained from Figure 3.1-2. By referring to the figure, it can be seen that line of sight of the north pole will begin 1.05 hours after ascending nodal crossing and cease 9.86 hours later. Since the orbit is circular, the south pole will be within line of sight for the same duration but will begin 13.02 hours after and cease 22.82 hours after the ascending nodal crossing.

The resultant general characteristics of the earth coverage provided by inclined geosynchronous orbits are illustrated in Figure 3.1-16. As shown in the figure, four basic types of coverage generally exist. A region of continuous coverage (①) generally exists with the dimensional characteristics of the region dependent upon the orbit inclination and the ground station mask angle. The second region (②) is that area of the surface of the earth which is never within line of sight of a geosynchronous satellite. The remaining regions (③ and ④) are periodically within line of sight with the duration of the periods of visibility dependent upon the orbit inclination, the mask angle, and the relative location within the regions. Ground stations (or terrestrial traffic elements, ships, aircraft, etc.) in region ③ are within line of sight during a single continuous period of less than 24 hours each day. Ground stations within region ④ have two periods each day when a geosynchronous satellite will be within line of sight. The two daily periods are, in general, unequal; the exception being sites along the equator viewing a satellite in a circular, inclined 24-hour orbit. These sites will be within line of sight during two equal periods each day.

**Page intentionally left blank**

**Page intentionally left blank**

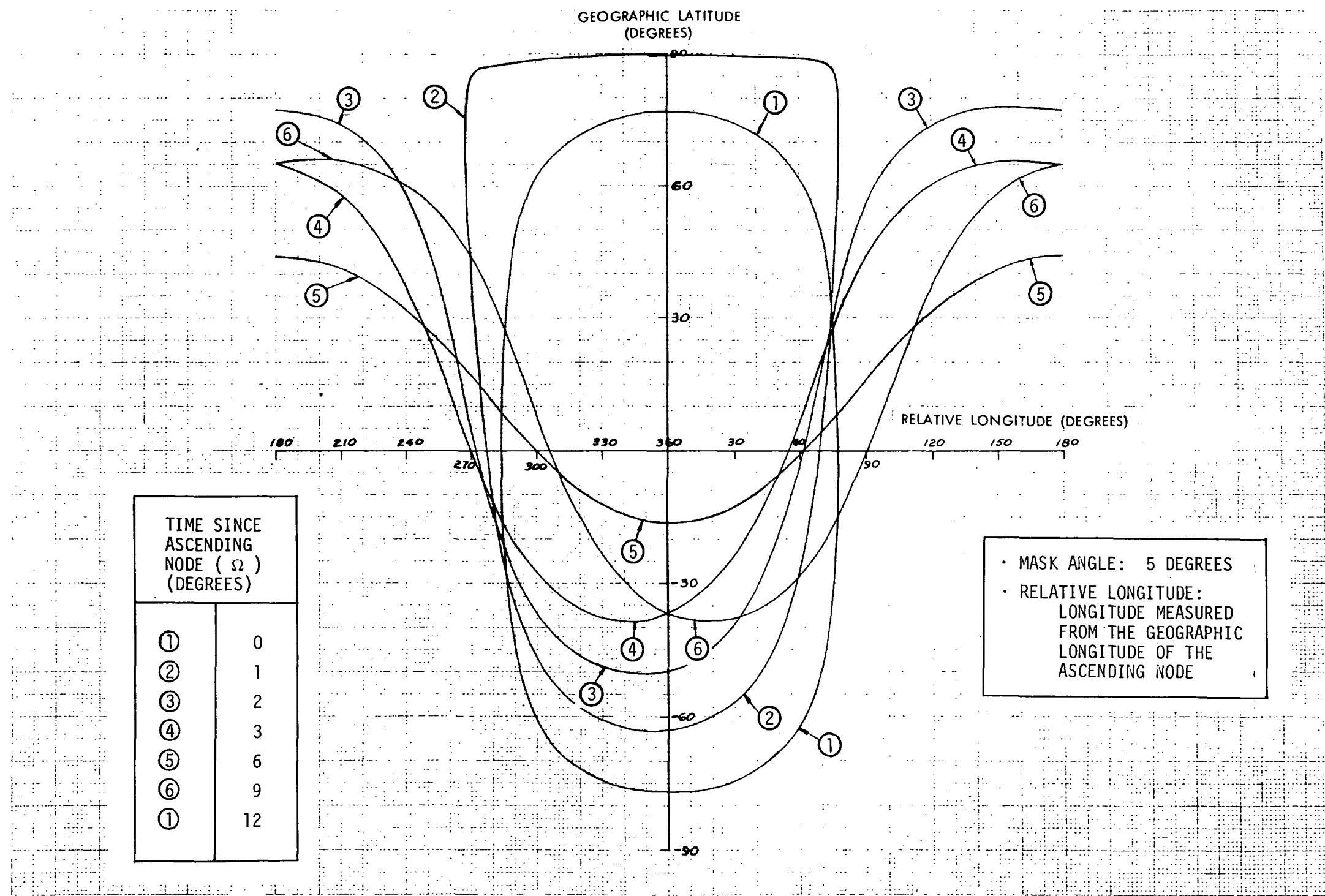


Figure 3.1-15. Earth Coverage Characteristics ( $i = 60$  degrees)

3-31

SD 73-SA-0036-3

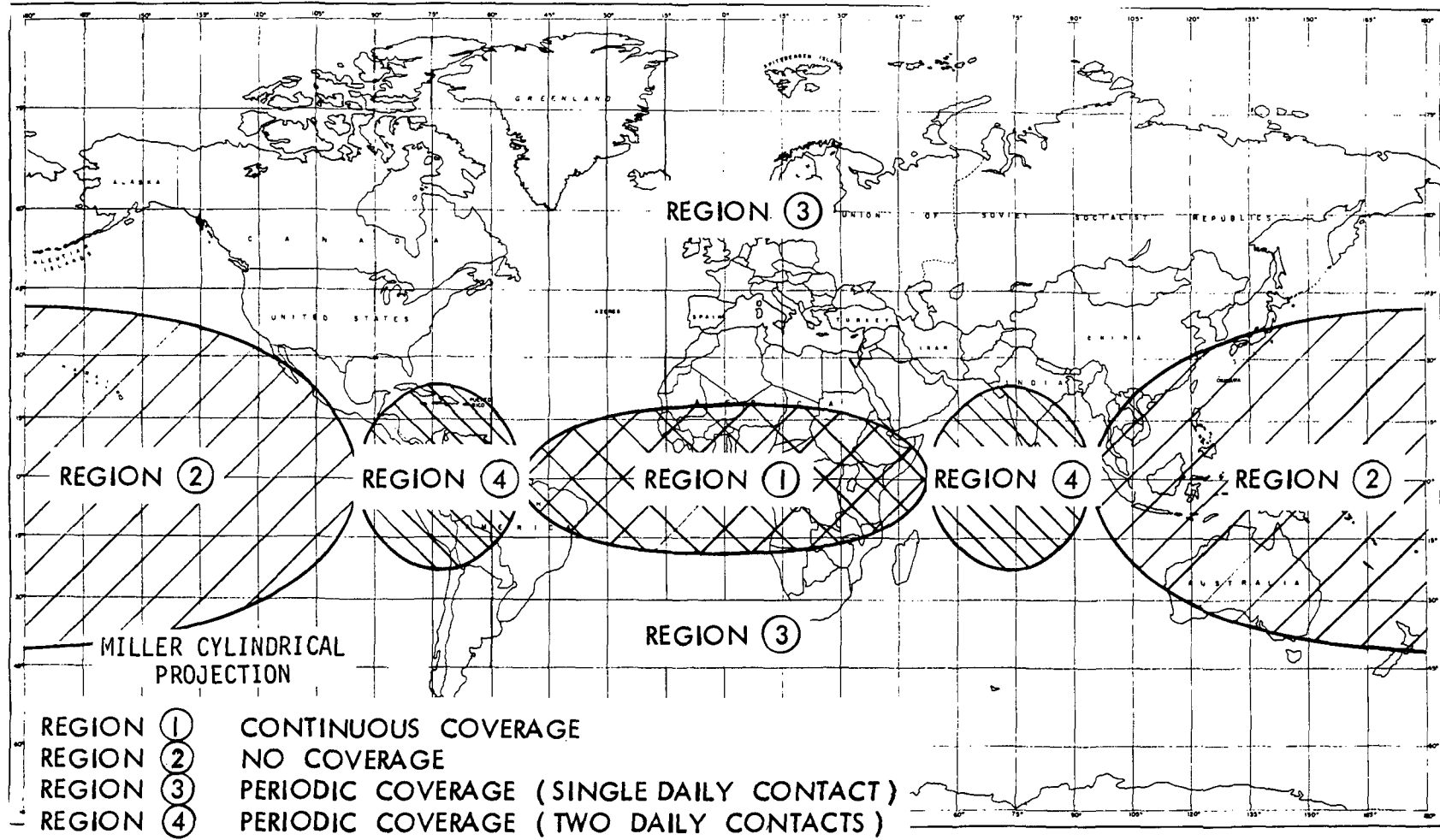


Figure 3.1-16. Generalized Time Varying Earth Coverage Characteristics ( $\ell \neq 0$ )



## PREFERRED SATELLITE LOCATIONS

The preferred locations of geosynchronous satellites with respect to the earth are dependent upon the satellite coverage and ground trace characteristics and the geographic area or areas which must be within line of sight of the satellite. For inclined geosynchronous orbits, the duration of line of sight must also be considered since, as discussed previously, the earth coverage characteristics of inclined orbits vary with time.

The fundamental geometric considerations which must be considered when establishing preferred geosynchronous satellite locations are illustrated in Figure 3.1-17. From the figure it can be seen that the limiting relative longitude of a geosynchronous satellite with respect to a given geographic location is given by:

$$\cos(\gamma/2) = \cos(90 - \delta_{sc}) \cos(90 - \delta_{site}) + \sin(90 - \delta_{sc}) \sin(90 - \delta_{site}) \cos \Delta \lambda$$

or

$$\cos(\gamma/2) = \sin \delta_{sc} \sin \delta_{site} + \cos \delta_{sc} \cos \delta_{site} \cos \Delta \lambda$$

from which

$$\Delta \lambda = \cos^{-1} \left[ \frac{\cos(\gamma/2) - \sin \delta_{sc} \sin \delta_{site}}{\cos \delta_{sc} \cos \delta_{site}} \right] \quad (3.1-28)$$

where

$\Delta \lambda$  = the relative longitude of the geosynchronous satellite; measured from the meridian of a specified ground site to the meridian of the geosynchronous satellite

$\delta_{site}$  = geographic latitude of the specified ground site

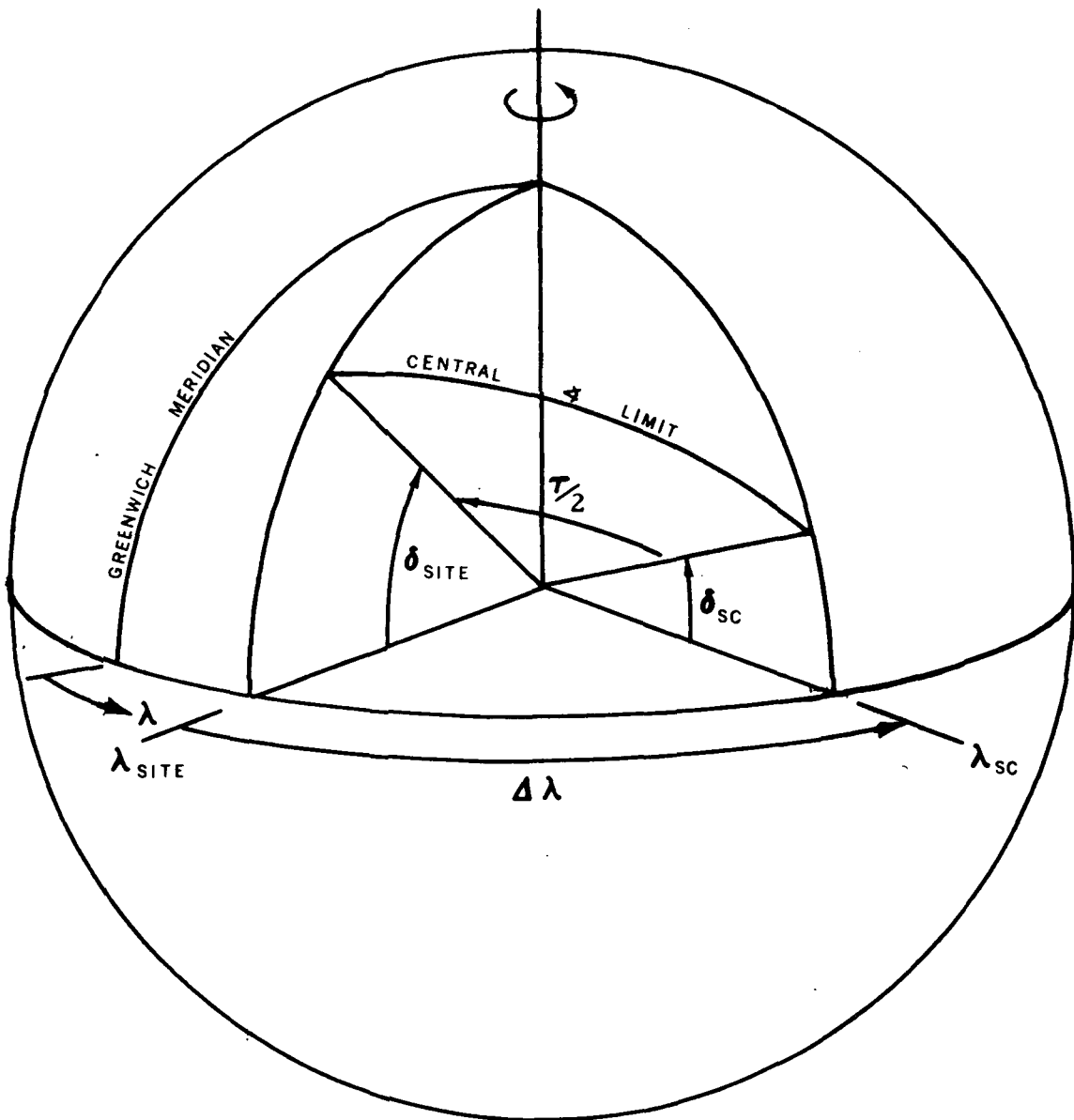


Figure 3.1-17. Definition of Geostationary Satellite Limits



$\delta_{sc}$  = geographic latitude of the subsatellite point

$\tau/2$  = limiting earth central angle for a given mask angle

The limiting range for the geographic longitude which permits line of sight between the geosynchronous satellite and a given geographic location is then given by:

$$\lambda_{sc} = \lambda_{site} \pm \Delta\lambda \quad (3.1-29)$$

For geostationary satellites,

$$\delta_{sc} = 0$$

and Equation (3.1-28) becomes:

$$\Delta\lambda]_{\delta_{sc}=0} = \cos^{-1} \left[ \frac{\cos(\tau/2)}{\cos \delta_{site}} \right] \quad (3.1-30)$$

The resultant allowable relative longitude is shown in Figure 3.1-18 as a function of the geographic latitude of the ground site for a range of values of surface mask angle. For a mask angle ( $\alpha$ ) of five degrees, the limiting earth central angle ( $\tau/2$ ) is 76.3329 degrees. Therefore, a geostationary satellite, or an inclined geosynchronous satellite when at either the ascending or descending node, will be within line of sight of points on the earth's equator between plus or minus 76.3329 degrees of the subsatellite point. Also, the maximum latitude that will be within line of sight is also 76.3329 degrees at a relative longitude of zero.

The allowable geographic longitude limits for geostationary satellites are shown in Figure 3.1-19 for a representative set of geographic locations within major world-wide geographic areas. For example, 14 locations are shown which grossly define the limiting geographic boundaries of Canada and the United States (including Alaska and Hawaii).

The utility of Figure 3.1-19 is illustrated in Figure 3.1-20. For this illustration, three specific sites have been chosen: Inuvik, Northwest Territories, Canada; St. John's, Island of Newfoundland; and London, England. In this example, a Canadian domestic satellite (Domsat) must be located between 122 degrees west longitude and 83 degrees west longitude if total coverage of

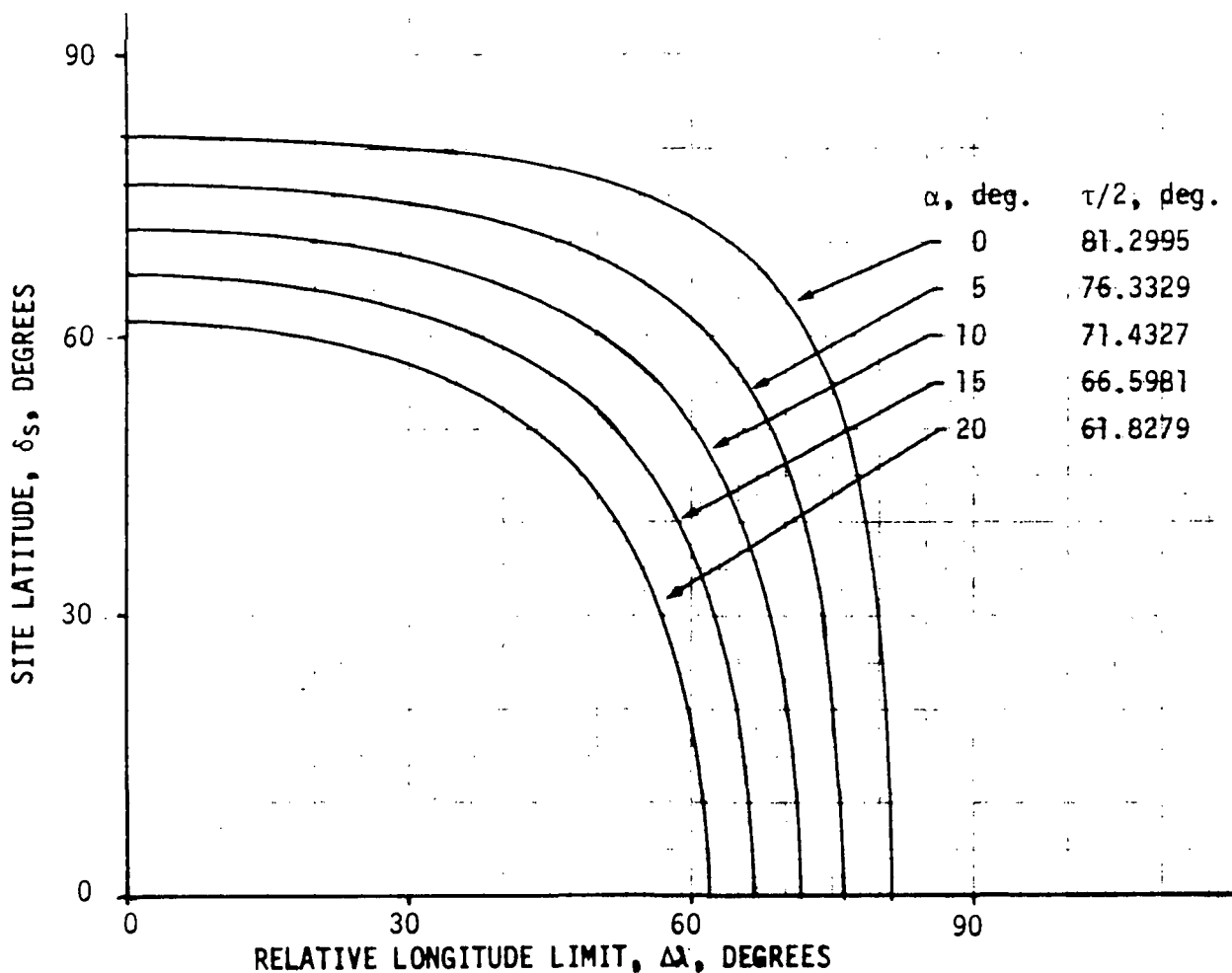


Figure 3.1-18. Geosynchronous Satellite Relative Longitude Limits

**Page intentionally left blank**

**Page intentionally left blank**

Geographic Area	Location	Latitude Degrees	Longitude Degrees	Satellite Location Limits <sup>(1)</sup>			
				180°W	90°W	0°	90°E
North America							
Canada	Inuvik	68.0 N	133.8 W				
	St. Johns	47.4 N	52.8 W				
United States	Pt. Hope, Alaska	68.5 N	166.5 W				
	Neah Bay, Wash.	48.36 N	124.64 W				
	Brewster, Wash.	48.10 N	119.8 W				
	Eureka, Calif.	40.8 N	124.16 W				
	Barstow, Calif.	34.9 N	117.03 W				
	San Diego, Calif.	32.72 N	117.15 W				
	Kauai, Hawaii	21.95 N	159.45 W				
	Eastport, Maine	44.9 N	67.0 W				
	Andover, Maine	44.63 N	70.75 W				
	Greenbelt, Maryland	39.0 N	76.87 W				
	Rossmann, N. Carolina	35.13 N	82.82 W				
	Savannah, Georgia	32.075 N	81.10 W				
Central America	Tijuana, Mexico	32.5 N	117.0 W				
	Panama, Panama	9.03 N	79.4 W				
South America	Guayaquil, Ecuador	2.12 S	80.0 W				
	Recife, Brazil	8.20 S	35.0 W				
	Punta Arenas, Chile	53.2 S	70.95 W				
North Atlantic	Sondre Stronfjord, Greenland	67.15 N	50.5 W				
	Reykjavik, Iceland	64.15 N	21.5 W				
	Bermuda	32.3 N	64.75 W				
	Sao Miguel, Azores	37.7 N	25.9 W				

(1) Geostationary

Figure 3.1-19. Satellite Location Limits  
for Various Geographic Locations

Geographic Area	Location	Latitude Degrees	Longitude Degrees	180°	Satellite Location Limits(1)				180°
					90°W	0°	90°E	180°	
Europe + USSR (W)	Erris Head, Ireland	54.3 N	10.0 W	180°					
	Murmansk, USSR	68.85 N	33.0 E						
	Lisboa, Portugal	38.75 N	9.15 W						
	Madrid, Spain	40.45 N	3.70 W						
	London, England	51.30 N	0.1 W						
	Paris, France	48.85 N	2.33 E						
	Bruxelles, Belgium	50.86 N	4.35 E						
	Amsterdam, Holland	52.36 N	4.9 E						
	Kobenhavn, Denmark	55.7 N	12.55 E						
	Oslo, Norway	60.0 N	10.75 E						
	Stockholm, Sweden	59.3 N	18.05 E						
	Helsinki, Finland	60.23 N	24.9 E						
	Wiesbaden, Germany	50.08 N	8.23 E						
	Berlin, Germany	52.55 N	13.4 E						
	Warszawa, Poland	52.3 N	21.0 E						
	Praha, Czech	50.1 N	14.4 E						
	Moscow, USSR	55.8 N	37.5 E						
	Ankara, Turkey	39.95 N	32.9 E						
Africa	Dakar, Senegal	14.6 N	17.5 W	180°					
	Ashkhabad, Turkmen SSR	37.9 N	58.35 E						
	Tehran, Iran	35.65 N	51.5 E						
	Baghdad, Iraq	33.4 N	44.4 E						
	Bahrain, Saudi Arabia	26.15 N	50.6 E						
	Tananarive, Malagasy	18.9 S	47.25 E						
	Johannesburg, S.Africa	25.75 S	28.1 E						
	Lubumbashi, Republic of Congo	11.6 S	27.5 E						
	Dar es Salaam, Tanzania	6.8 S	39.25 E						
	Brazzaville, Congo	4.15 S	15.2 E						
	Addis Ababa, Ethiopia	9.1 N	38.8 E						
	Khartoum, Sudan	15.2 N	32.5 E						
	El Qahira, UAR	30.0 N	31.5 E						
	Lagos, Nigeria	6.5 N	3.4 E						
	Tripoli, Libya	32.75 N	13.1 E						
	Tunis, Tunisia	36.75 N	10.15 E						
	Algiers, Algeria	36.7 N	3.1 E						
	Casablanca, Morocco	33.6 N	7.7 W						
	Monrovia, Liberia	6.4 N	10.7 W						
	Accra, Ghana	5.6 N	0.3 W						

Figure 3.1-19. Satellite Location Limits  
for Various Geographic Locations (Cont)

(1) Geostationary

Geographic Area	Location	Latitude Degrees	Longitude Degrees	Satellite Location Limits (1)			
				180°	90°W	0°	90°E
Asia							
USSR	Perm, USSR	58.1 N	55.6 E				
	Petropavlovsk, Kamchatskiy	53.2 N	159.0 E				
	Magadana, USSR	59.7 N	151.0 E				
	Yakutsk, USSR	62.1 N	129.3 E				
	Irkutsk, USSR	52.4 N	104.2 E				
	Bratsk, USSR	56.4 N	101.5 E				
	Kandahar, Afgan.	31.67 N	65.85 E				
	Karachi, Pakistan	24.95 N	67.1 E				
India	Ahmadabad, India	23.05 N	72.7 E				
	Calcutta, India	22.55 N	88.45 E				
	Kathmandu, Nepal	27.7 N	85.3 E				
China	Ining, China	44.0 N	81.35 E				
	Haerhpin, China	45.7 N	126.8 E				
	Olgiy, Mongolia	49.0 N	90.0 E				
	Tamsagbulag, Mongolia	47.1 N	117.1 E				
	Lhasa, Tibet	29.75 N	91.1 E				
	Rangoon, Burma	15.65 N	96.2 E				
	Bangkok, Thailand	13.75 N	100.6 E				
Indonesia	Medan, Sumatra	3.7 N	98.6 E				
	Djajapura, Irian	2.4 S	140.7 E				
	Quezon City, Phillip.	14.8 N	121.15 E				
	Saigon, S. Vietnam	10.7 N	106.75 E				
	Hanoi, N. Vietnam	21.0 N	105.75 E				
	Hong Kong, China	22.0 N	114.25 E				
	Taipei, Taiwan	25.0 N	121.4 E				
	Seoul, South Korea	37.6 N	126.9 E				
Japan	Kagoshima, Japan	31.67 N	130.45 E				
	Kushiro, Japan	43.03 N	144.35 E				
	Guam, U.S.	13.4 N	144.6 E				
Australia	Port Moresby, Aust.	9.35 S	147.2 E				
	Perth, Australia	31.8 S	115.7 E				
	Hobart, Tasmania	43.0 S	147.5 E				
	Brisbane, Australia	27.5 S	153.1 E				
	Wellington, N.Z.	42.5 S	174.8 E				
Oceana	Palau Islands	7.0 N	134.4 E				
	Tahiti	17.6 S	149.3 W				

Figure 3.1-19. Satellite Location Limits  
for Various Geographic Locations (Cont)

(1) Geostationary

Geographic Area	Location	Latitude Degrees	Longitude Degrees	Satellite Longitude Location Limits, Deg.
Canada	Inuvik	68.0 N	133.8 W	180 90W 0 90E 180
Canada	St. Johns	47.4 N	52.8 W	
England	London	51.3 N	0.1 W	

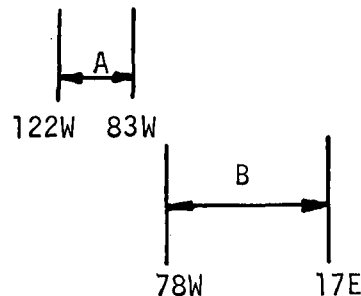


Figure 3.1-20. Utilization of Satellite Location Limits



Canada from Inuvik to St. John's is required. Canadian Domsats which are west of this longitude band will exclude coverage of Newfoundland and those which are to the east of the band will lose coverage of the western parts of Canada. The other example which is shown in Figure 3.1-20 illustrates the required geographic longitude of an international communications satellite (Intelsat) for communications between St. John's, Canada, and London, England. Communications between St. John's and London, England can be provided via an Intelsat satellite which is located anywhere between 78 degrees west longitude and 17 degrees east longitude assuming St. John's is an acceptable Canadian terminal. If a more westerly Canadian ground site is required, the allowable eastern limit of the satellite location must be decreased. Also, if more easterly sites within Europe must be considered, the western limit quoted above must be decreased.

A representative set of preferred satellite locations for geostationary satellites is illustrated in Figures 3.1-21 through 3.1-29. The first set of figures, Figures 3.1-21 through 3.1-24, show the effects of the desired United States coverage on the allowable location of geostationary satellites. Figure 3.1-21 shows that the allowable location of a geostationary satellite which has the capability to communicate with at least one site within the contiguous U.S. must be located between a longitude of approximately zero degrees westward to a longitude of approximately 165 degrees east longitude. Figure 3.1-22 is a representative illustration of the decrease associated with requiring the capability to communicate with a single ground site within the United States from two geosynchronous satellites. The effects of requiring the capability to communicate with any site in the United States is illustrated in Figure 3.1-23. For this case, a geostationary satellite must be located between 55 degrees west longitude and 135 degrees west longitude. A further decrease in the allowable location of a geostationary satellite is illustrated in Figure 3.1-24. For this case, communications capability is required for any site within the United States including Alaska and Hawaii. This case is the most restrictive case and illustrates the required location of a United States domestic communications satellite if communications between any points within the United States are required.

A representative geostationary satellite location constraint for European coverage is illustrated in Figure 3.1-25. In addition, Figures 3.1-26 through 3.1-28 illustrate typical satellite location requirements for coverage of the major world ocean areas.

An example of the preferred locations for applications-type U.S. meteorological satellites are shown in Figure 3.1-29. The locations shown in the figure permit coverage of the major U.S. weather sources as well as communications with a single U.S. ground site in the central U.S. The satellite located at 150 degrees west longitude provides coverage of the Aleutian low pressure center area, which is a major source of U.S. weather during the winter. The satellite located at 30 degrees west longitude provides overlapping coverage over the central United States as well as coverage of the Atlantic equatorial region, which is the spawning ground for tropical storms which become hurricanes in the Gulf of Mexico, Caribbean, and continental east coast areas. The satellite at 30 degrees west longitude also provides coverage of the major winter weather source for western Europe; the Icelandic low pressure center area.

3-45

SD 73-SA-0036-3

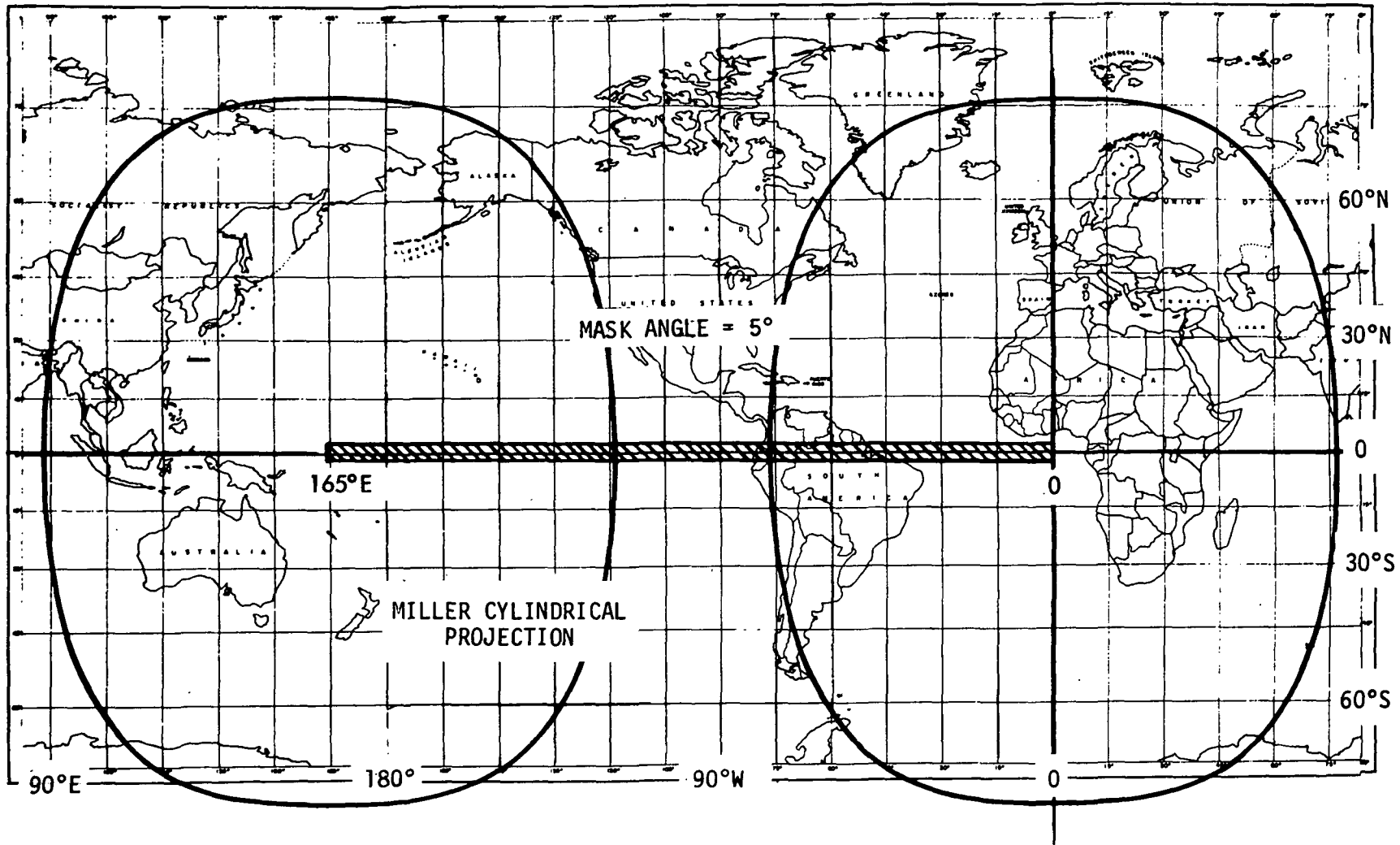


Figure 3.1-21. Satellite Locations Limits; At Least One U.S. Site

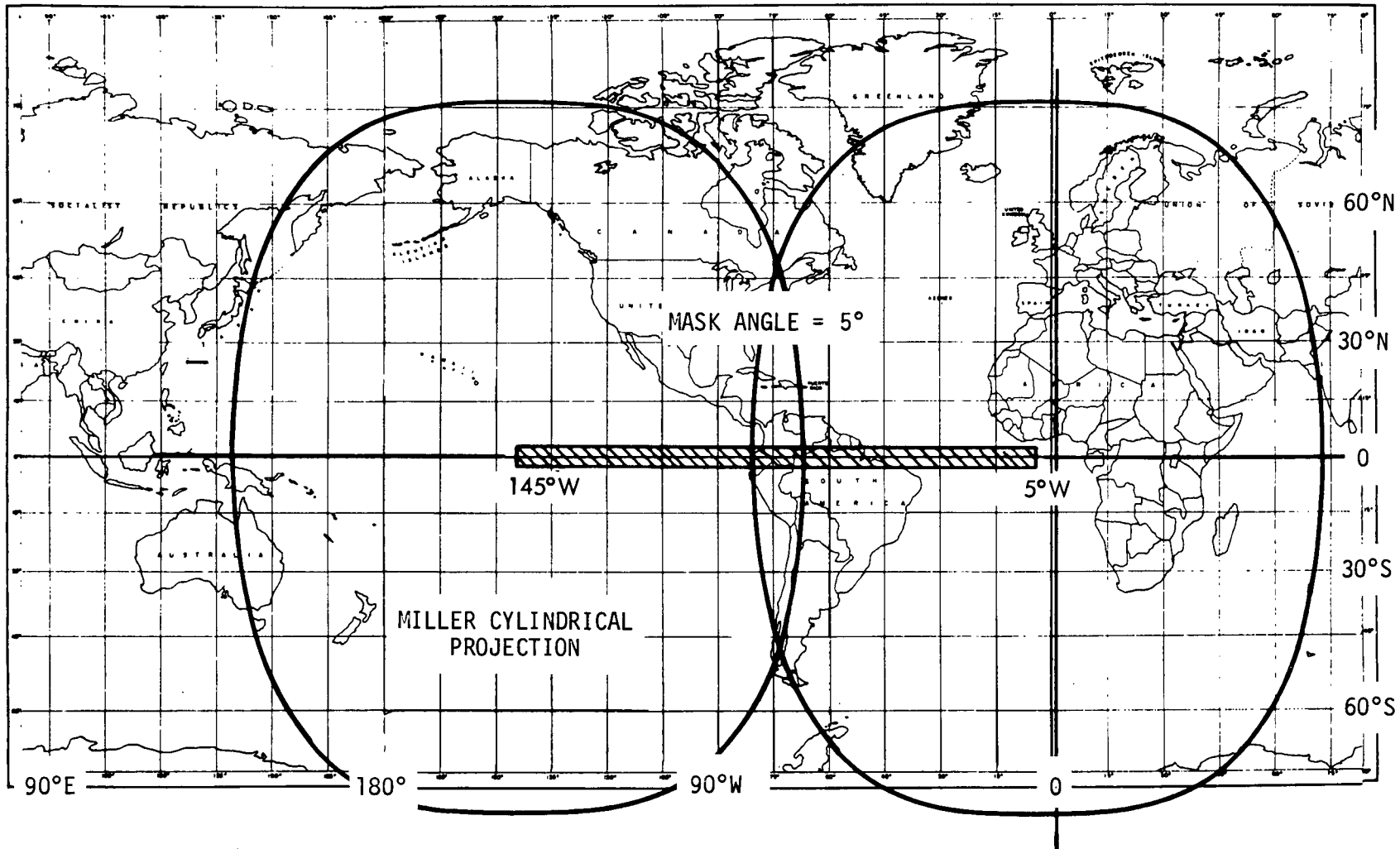


Figure 3.1-22. Satellite Locations Limits; Single U.S. Site

3-47

SD 73-SA-0036-3

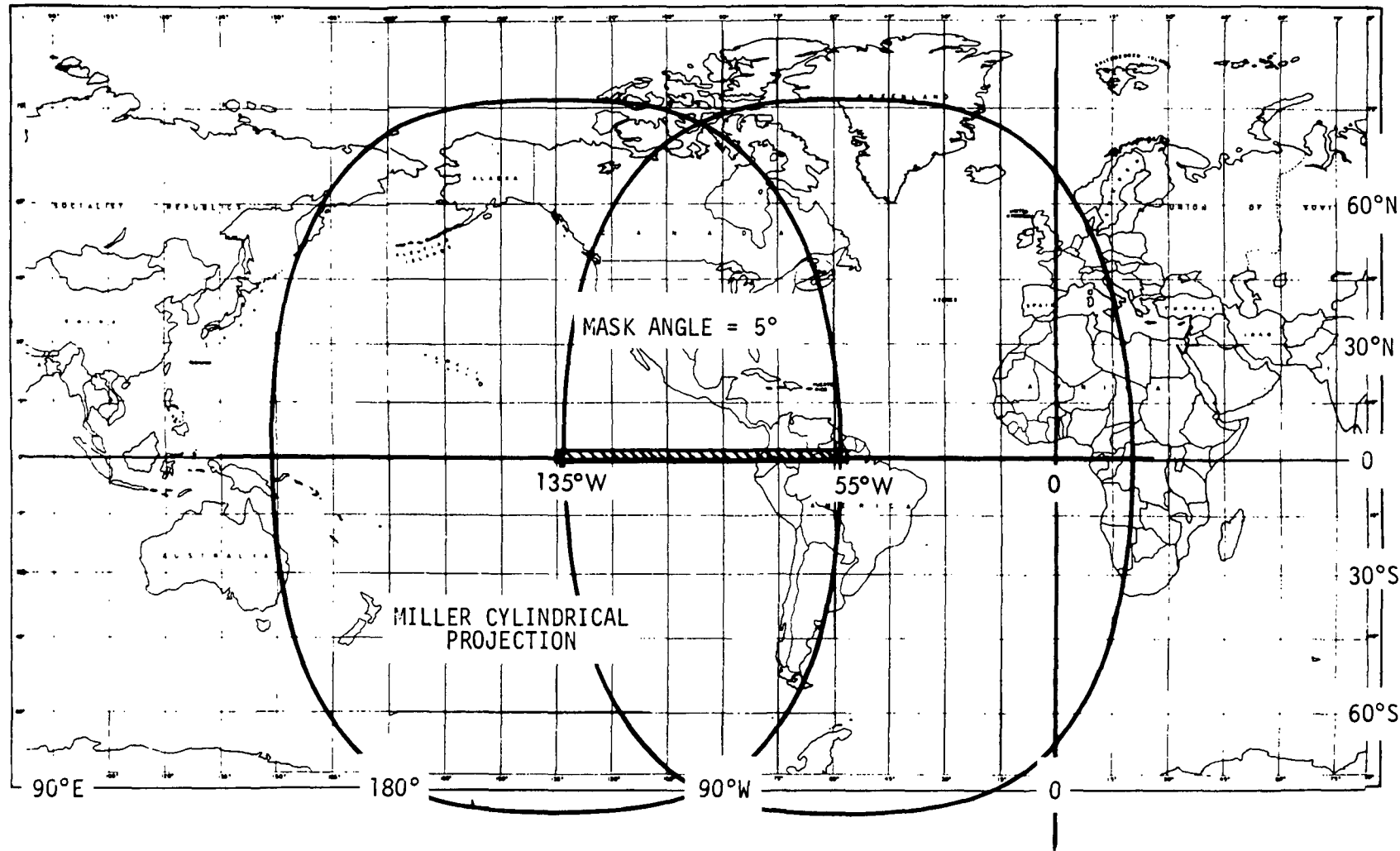


Figure 3.1-23. Satellite Location Limits; Any Contiguous U.S. Site



Space Division  
North American Rockwell

3-48

SD 73-SA-0036-3

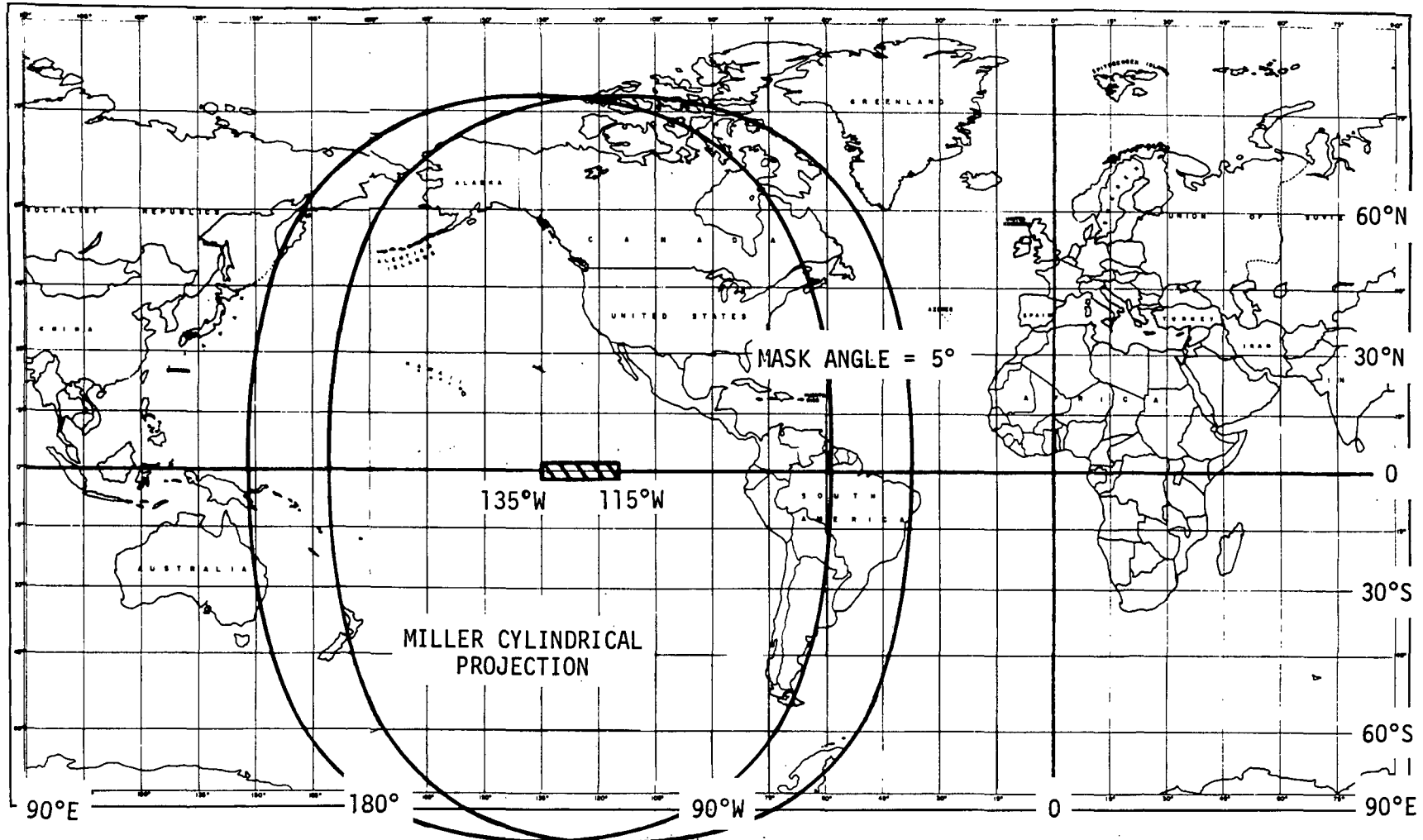


Figure 3.1-24. Satellite Location Limits; Any U.S. Site Including Alaska & Hawaii

3-49

SD 73-SA-0036-3

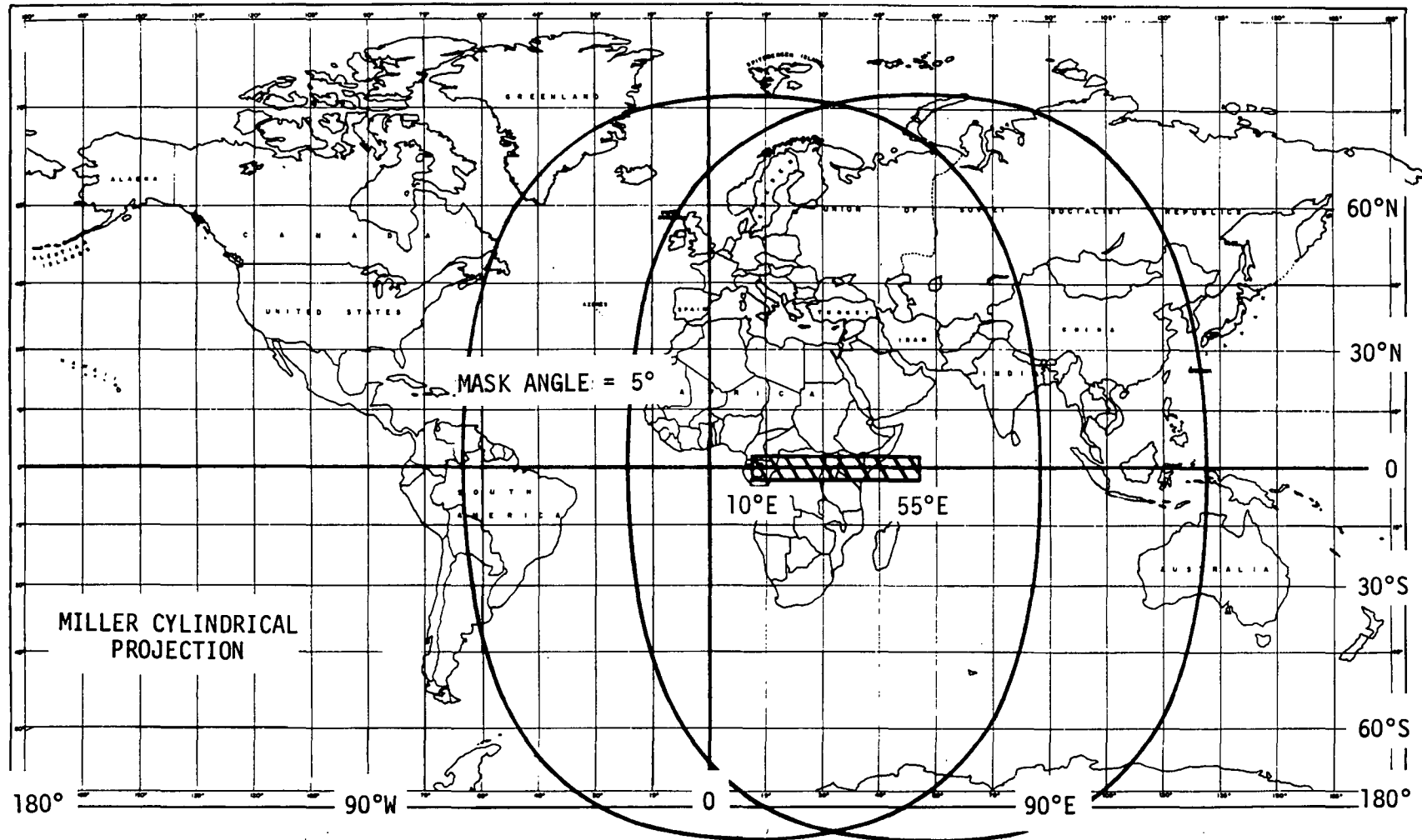


Figure 3.1-25. Satellite Location Limits; European Coverage



Space Division  
North American Rockwell

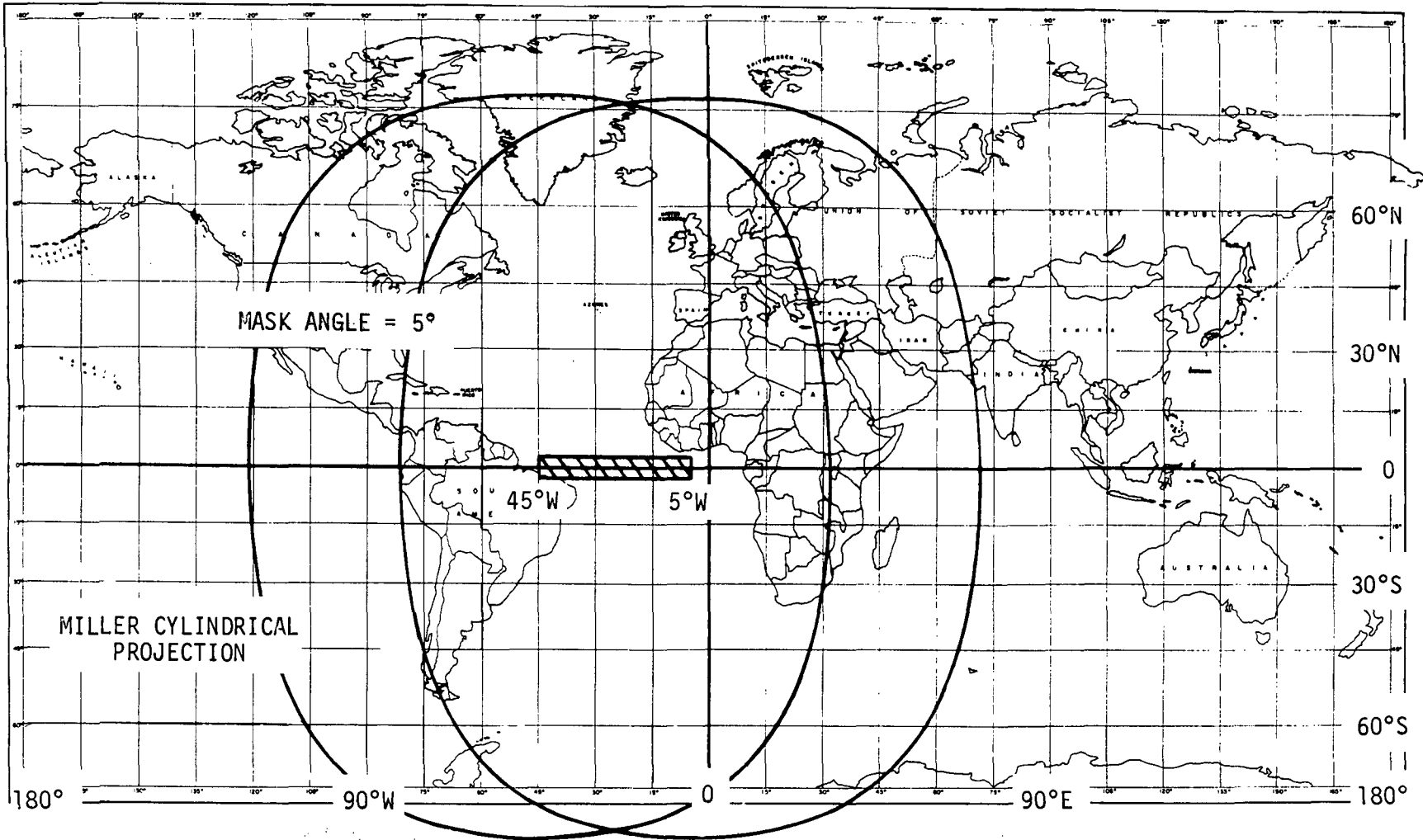


Figure 3.1-26. Satellite Location Limits; Atlantic Ocean Coverage  
(Including U.S. and Eastern Europe)

3-50

SD 73-SA-0036-3



Space Division  
North American Rockwell

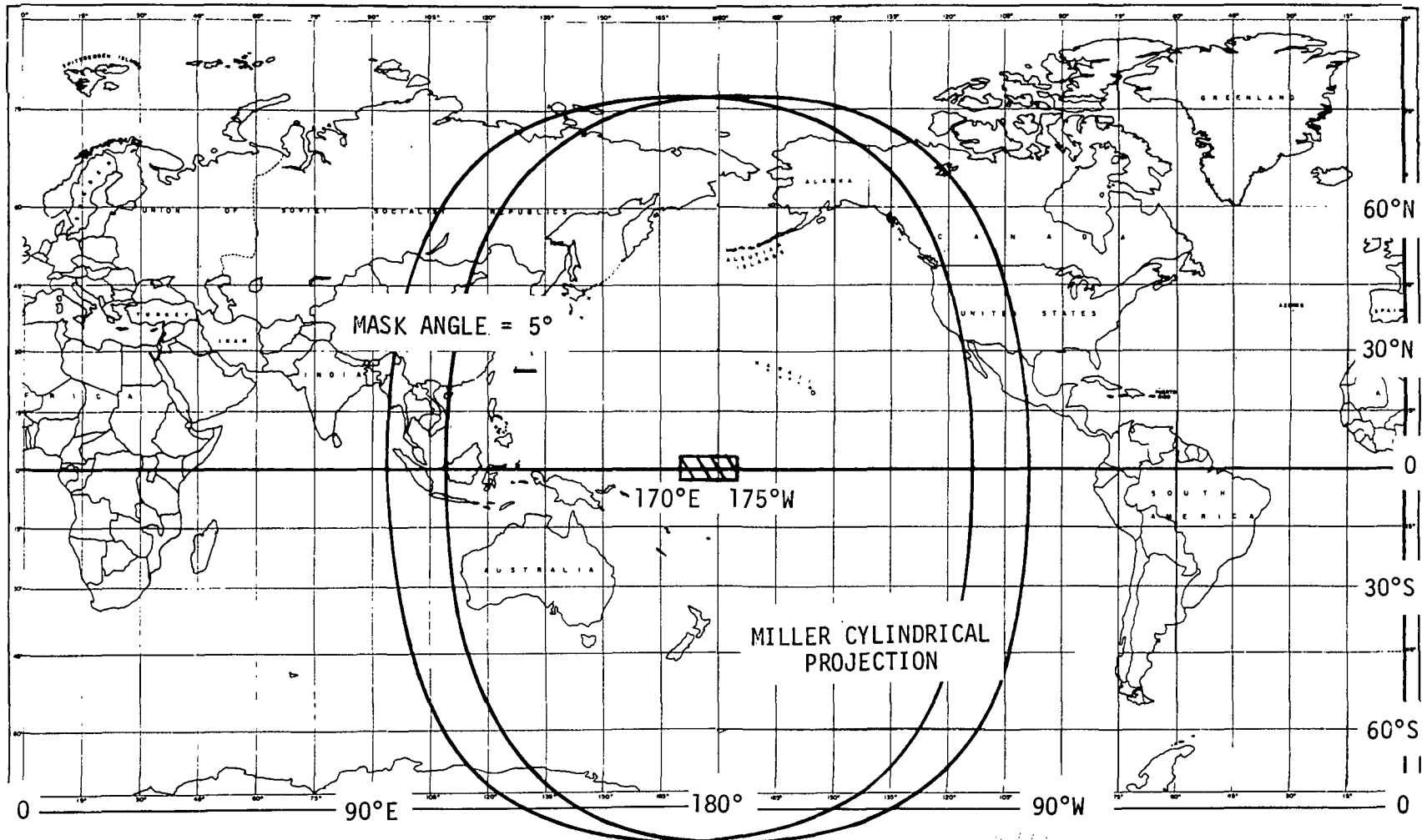


Figure 3.1-27. Satellite Location Limits; Pacific Ocean Coverage

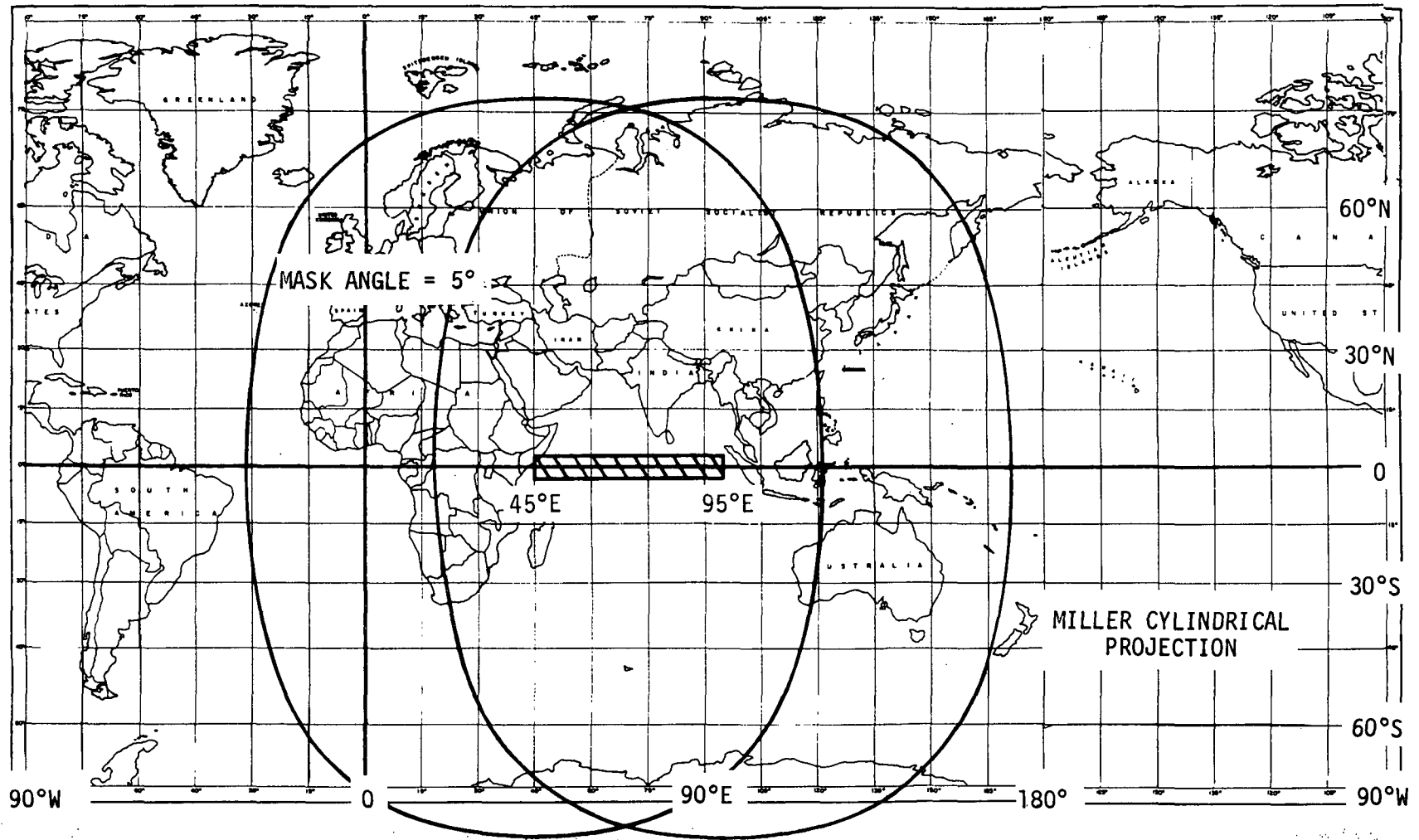


Figure 3.1-28. Satellite Locations Limits; Indian Ocean Coverage

3-53

SD 73-SA-0036-3

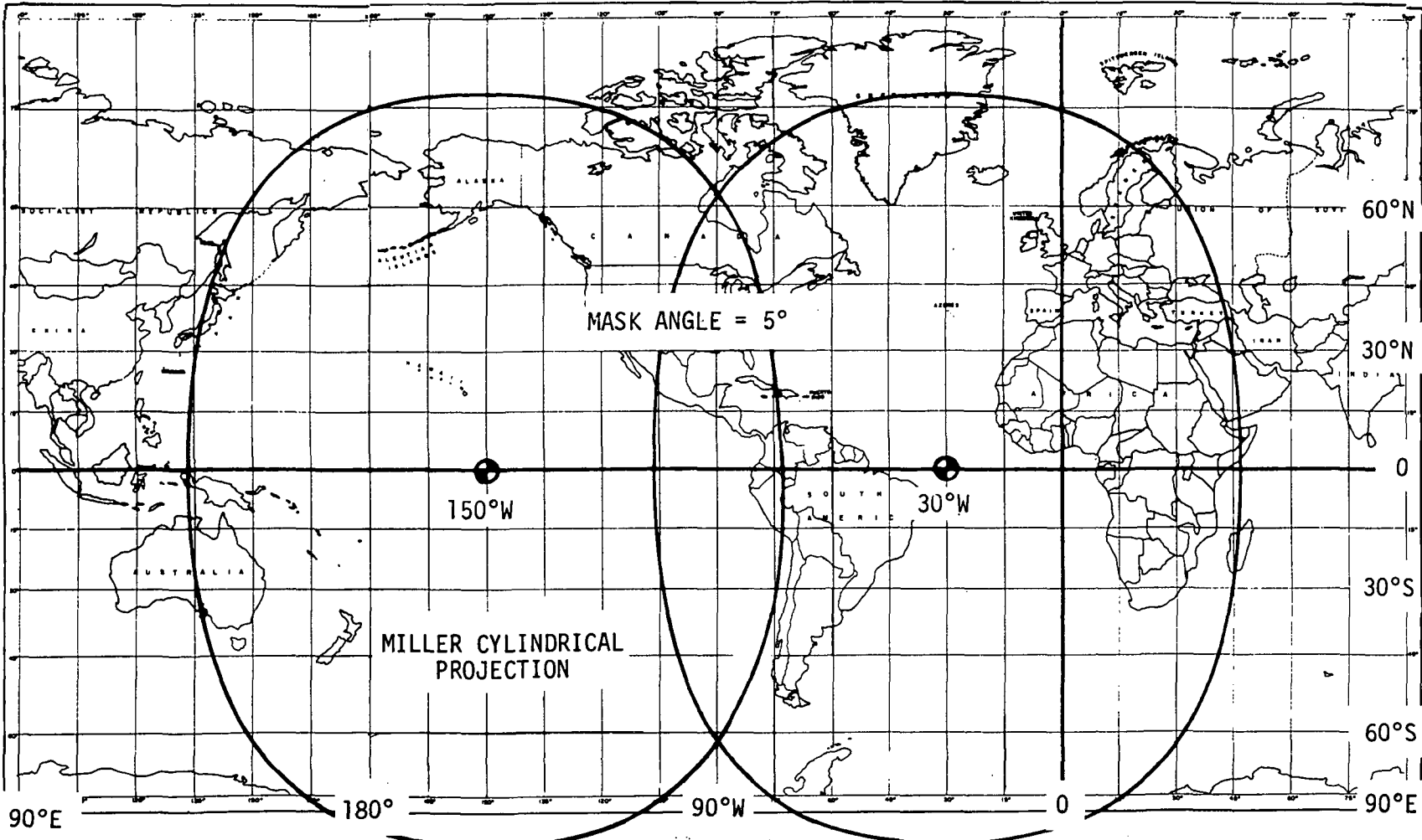


Figure 3.1-29. Satellite Locations Limits; Meteorology (United States)

A summary of the preferred satellite locations for world-wide coverage is shown in Figure 3.1-30. The satellite locations which are shown are representative only, since the particular earth coverage which is required will dictate the required geostationary satellite locations. As can be seen from the figure, geostationary satellites can be located essentially anywhere along the equator when world-wide earth coverage is considered.

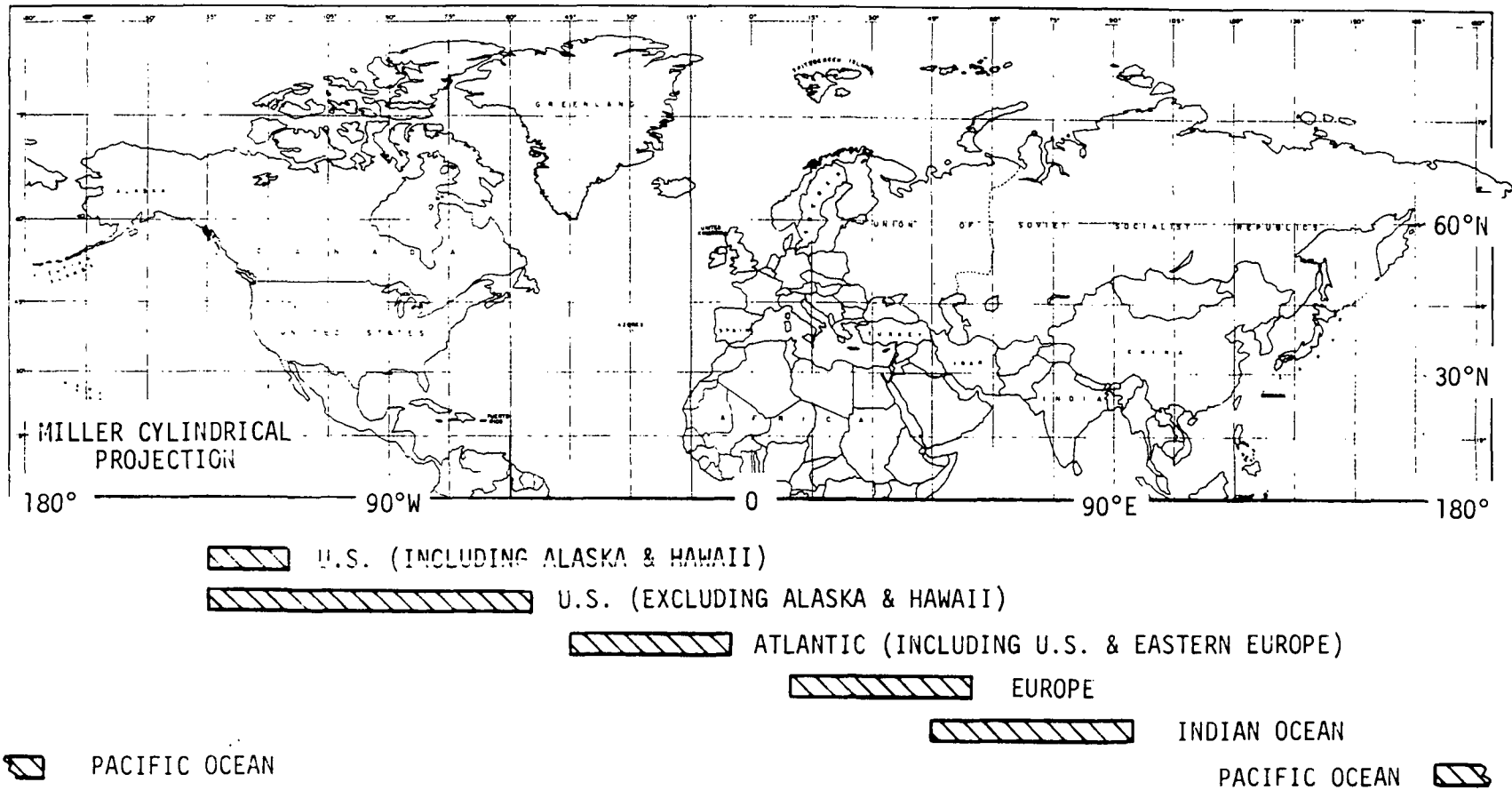


Figure 3.1-30. Geostationary Satellite Location Summary



## SOLAR TRANSIT OUTAGE

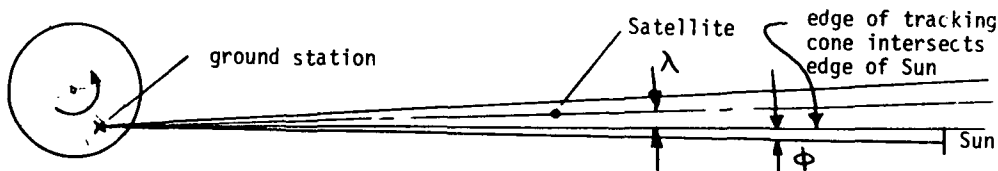
Solar transit outage occurs when a satellite passes in the vicinity of the solar disk and communications are interrupted due to solar interference. The duration of the outage and mean solar time at which it occurs is a function of the ground station antenna beamwidth, the geographic latitude and longitude of the ground station, and the geographic latitude and longitude of the satellite.

A summary of the analyses used to compute the solar outage characteristics for ground stations tracking equatorial geosynchronous satellites are presented below. The analyses were based primarily on an "outage cone" principle for defining points having solar outage at any particular time. Solar transit outage will occur at any ground station which is within the "outage cone" defined in the following sketch:



where  $\alpha$  = the outage cone half angle.

For the purpose of these analyses, two basic assumptions were made. First, solar outage occurs when the satellite tracking cone intersects any part of the sun as seen from the ground station as illustrated below:



In the previous sketch,

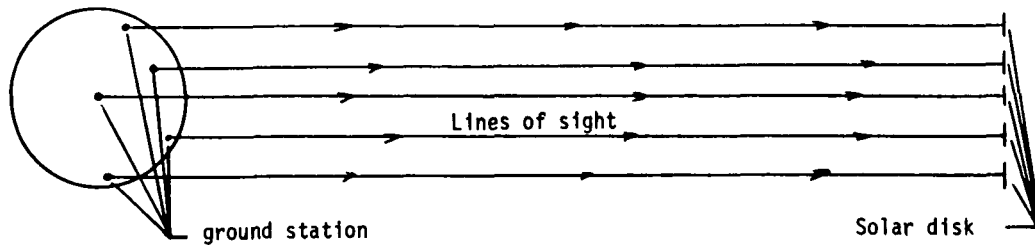
$\phi$  = the half angle of the solar disk as viewed from earth  
= 0.2666 degree

and  $\lambda$  = the half angle of the ground station tracking cone.

If  $\lambda$  = 0.5 degree

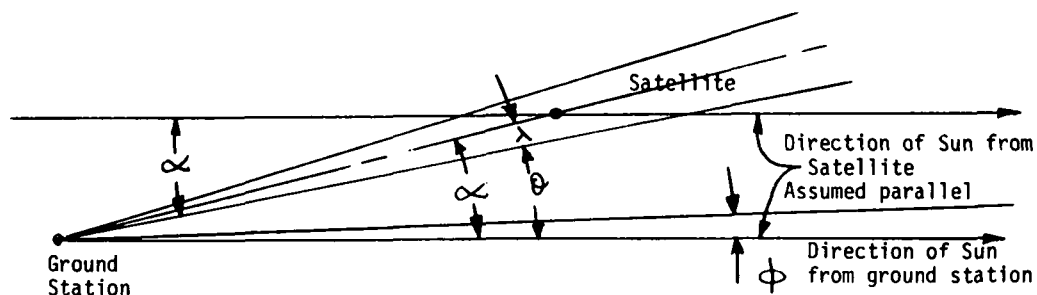
then  $\alpha$  = 0.7666 degree.

It was also assumed that the line of sight from all ground stations (or points within the vicinity of the earth) to the center of the sun are parallel as illustrated below:



The justification for this assumption is that the maximum angle between lines of sight is 0.00489 degree (two points, one earth diameter apart).

Using the previous assumptions, the following relationship can be derived from the sketch below:



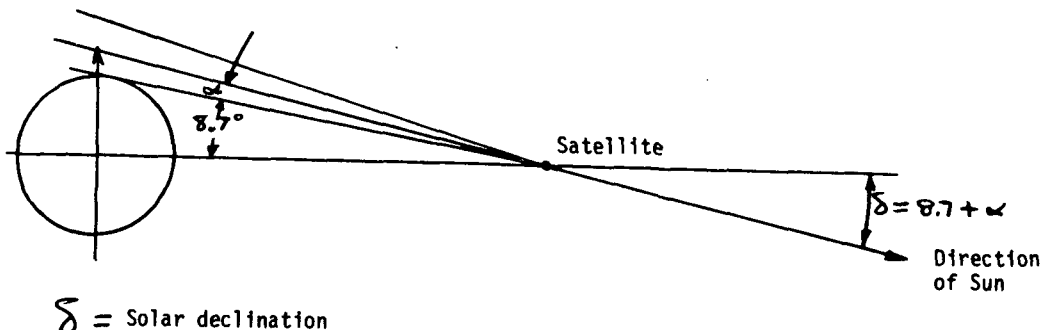
$$\alpha = \lambda + \theta$$

The tracking cone angle will intersect the sun's edge when  $\theta \leq \phi$   
Therefore, solar outage will occur when

$$\alpha = \phi + \lambda$$

The same outage relationships can be shown to hold for any ground station.  
Therefore, rotation of the angle  $\alpha$  about the line of sight to the sun will  
yield an "outage cone" within which all points will experience solar outage.

The projection of the outage cone on the earth's surface locates a region  
where ground station outage occurs. For equatorial geosynchronous satellites  
the outage cone axis will intersect the earth only when the solar declination  
is less than +8.7 degrees. There is no solar outage on the earth at solar  
declinations greater than  $8.7 + \alpha$  as illustrated below.



As a satellite moves between the sun and earth its outage cone traverses  
a path across the earth. This path is dependent upon the solar declination  
as well as the relative position of the satellite with respect to the earth.  
The solar declination required for the center of the outage cone to pass  
through a given ground station is shown in Figure 3.1-31. At a solar declina-  
tion of 8.7 degrees, the center of the outage cone no longer intersects the  
earth. At smaller declinations the center point traces out a path of varying  
latitude at each longitude relative to the satellite. When the solar declina-  
tion is zero the trace follows the earth's equator.

The solar declination varies with time of year as shown in Figure 3.1-32.  
Since solar outage is directly related to solar declination, outage will occur  
twice a year at any ground station. Yearly times of solar outage can be  
obtained (for any ground station relative to a given satellite) by combining  
the information in Figures 3.1-31 and 3.1-32. This time should be called a  
mean time since it corresponds to the time when the center of the outage cone  
crosses the ground station. Actual outage begins when the outage cone first  
reaches the ground station and ends when the outage cone passes the station.



Space Division  
North American Rockwell

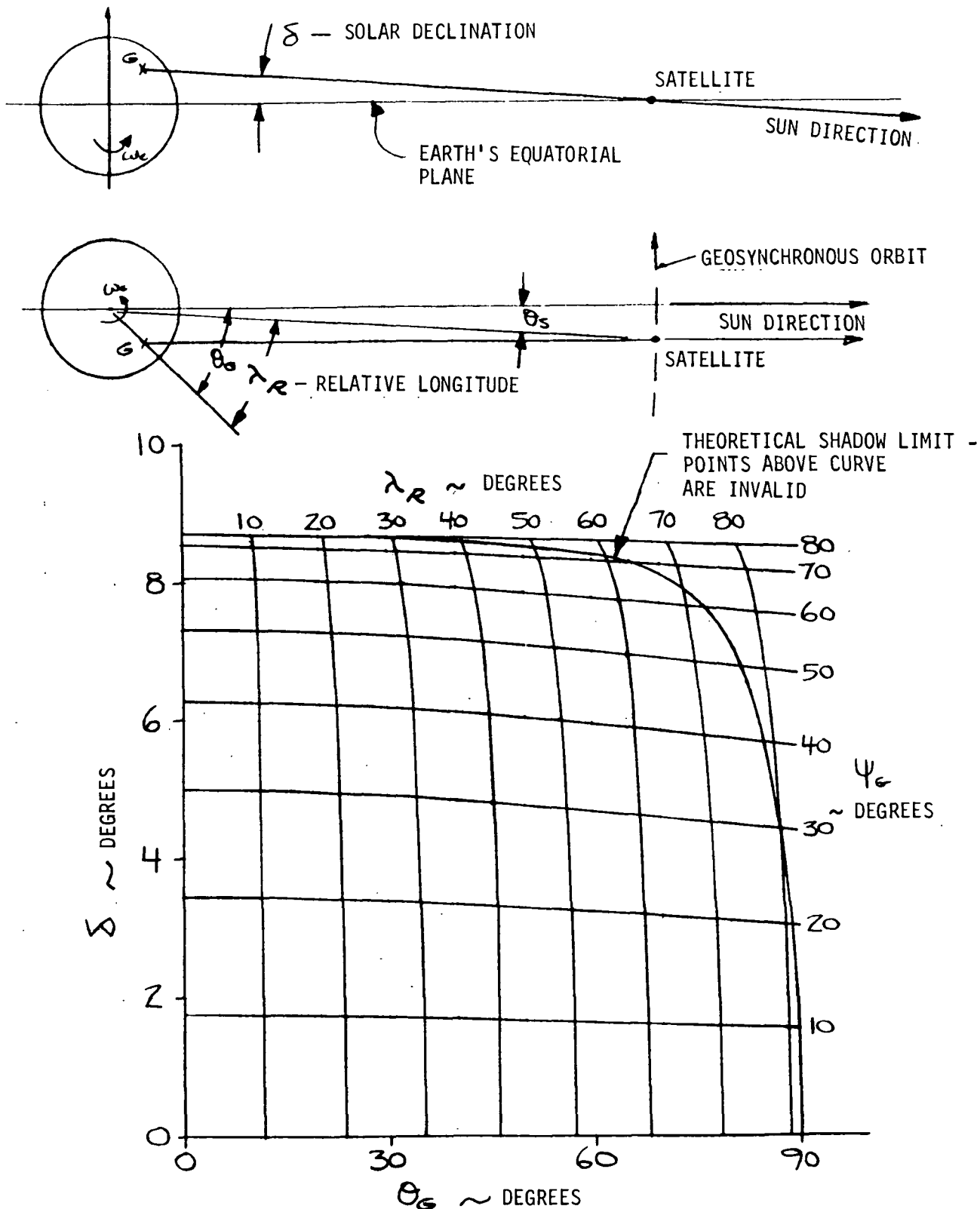


Figure 3.1-31. Geosynchronous Satellite Shadow Trace on Earth

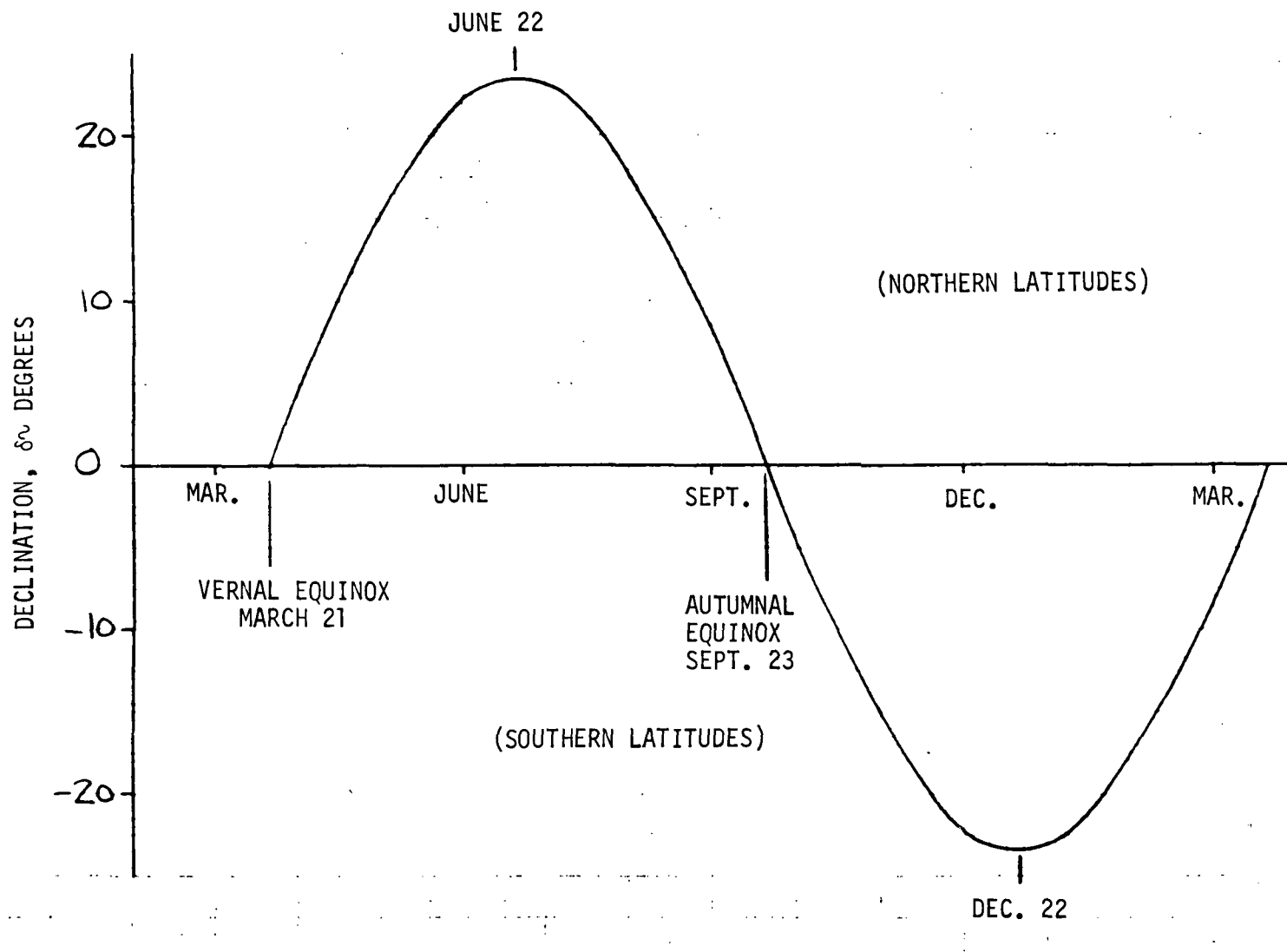


Figure 3.1-32. Solar Declination Versus Time of Year



For any ground station, the mean duration of yearly outage can be computed from the following expression:

$$\Delta T = \frac{2\alpha}{\dot{\sigma}}$$

where

$\Delta T$  = duration of solar outage, twice yearly; days

$\alpha$  = outage cone half angle; degrees

$\dot{\sigma}$  = solar declination rate of change; degrees/day

Assuming a mean sun motion, the declination rate varies with declination angle as shown below:

$$\dot{\sigma} = 0.985626 \frac{\sqrt{\sin^2 23.5 - \sin^2 \delta}}{\cos \delta} \text{ (deg /day)}$$

The range of declination rates where solar outage occurs is shown below:

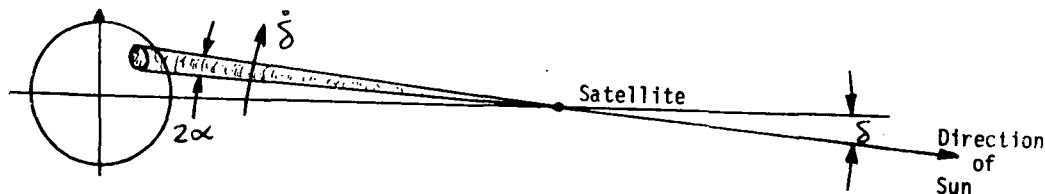
$$\delta = 0 \text{ degrees}$$

$$\dot{\sigma} = 0.393 \text{ deg/day}$$

$$\delta = 8.7 \text{ degrees}$$

$$\dot{\sigma} = 0.368 \text{ deg/day}$$

For a tracking half angle of 0.5 degree, the twice yearly outage amounts to four days for any ground station; i.e., 3.78 days at the equator to 4.05 days at high latitudes. The sketch below shows how yearly duration of solar outage was determined.



Outage cone passes through all points with rate  $\dot{\sigma}$ .



For any ground station, the mean duration of solar outage can be computed from the following expression:

$$\Delta t = \frac{2\alpha}{\omega_{\oplus}}$$

where

$\Delta t$  = duration of solar outage; minutes per day

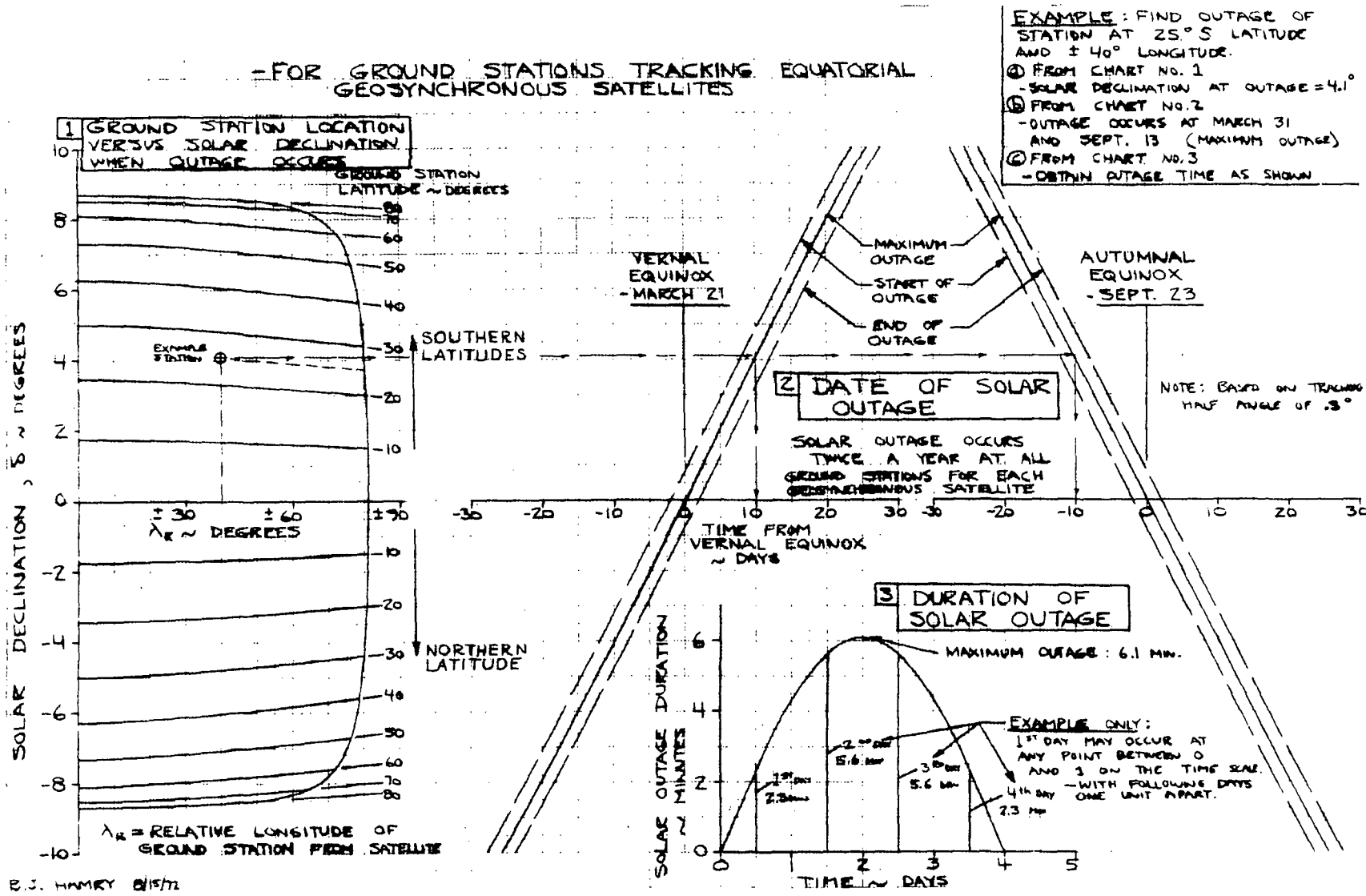
$\alpha$  = outage cone half angle; degrees

$\omega_{\oplus}$  = earth's rotation rate; 15.041 067 degrees per mean solar hour

For a tracking half angle of 0.5 degree, the mean outage time amounts to 6.10 minutes. This is the maximum time solar outage would last. At any period of outage during the year a ground station will experience varying lengths of daily outage. The outage time will rise to a maximum of 6.1 minutes or less and then fall off as the outage cone passes the ground station.

The solar outage characteristics for geosynchronous equatorial satellites are summarized in Figure 3.1-33 for a representative antenna beamwidth of 1.0 degree. As can be seen from the figure, outage occurs during two 4-day periods when the sun is in the vicinity of either the vernal equinox or the autumnal equinox. The maximum daily outage duration of 6.1 minutes occurs approximately two days after outage onset. It should be noted that the number of days during which outage will occur and the maximum outage duration is essentially independent of the relative location of ground station. The ground station relative location only affects the calendar dates during which outage will occur. For example, outage with respect to an equatorial ground station will occur as the sun appears to pass through the equinoctial points. Also, as illustrated in Figure 3.1-33, maximum outage for a ground station located at 25 degrees south latitude and a relative longitude of + 40 degrees will occur ten days after vernal equinox and ten days before autumnal equinox. Solar outage characteristics may play an influential role in the amount of grouping permissible or desirable for communications payloads.

The local mean time solar outage which will occur at any ground station is dependent upon the relative longitude and latitude between the ground station and satellite. The local mean solar time at outage which will occur is shown in Figure 3.1-34 as a function of relative longitude for a range of values of relative latitude. In general, stations west of the satellite will have outage before noon and those east will have outage after noon.



3-63

SD 73-SA-0036-3

Figure 3.1-33. Solar Outage Chart

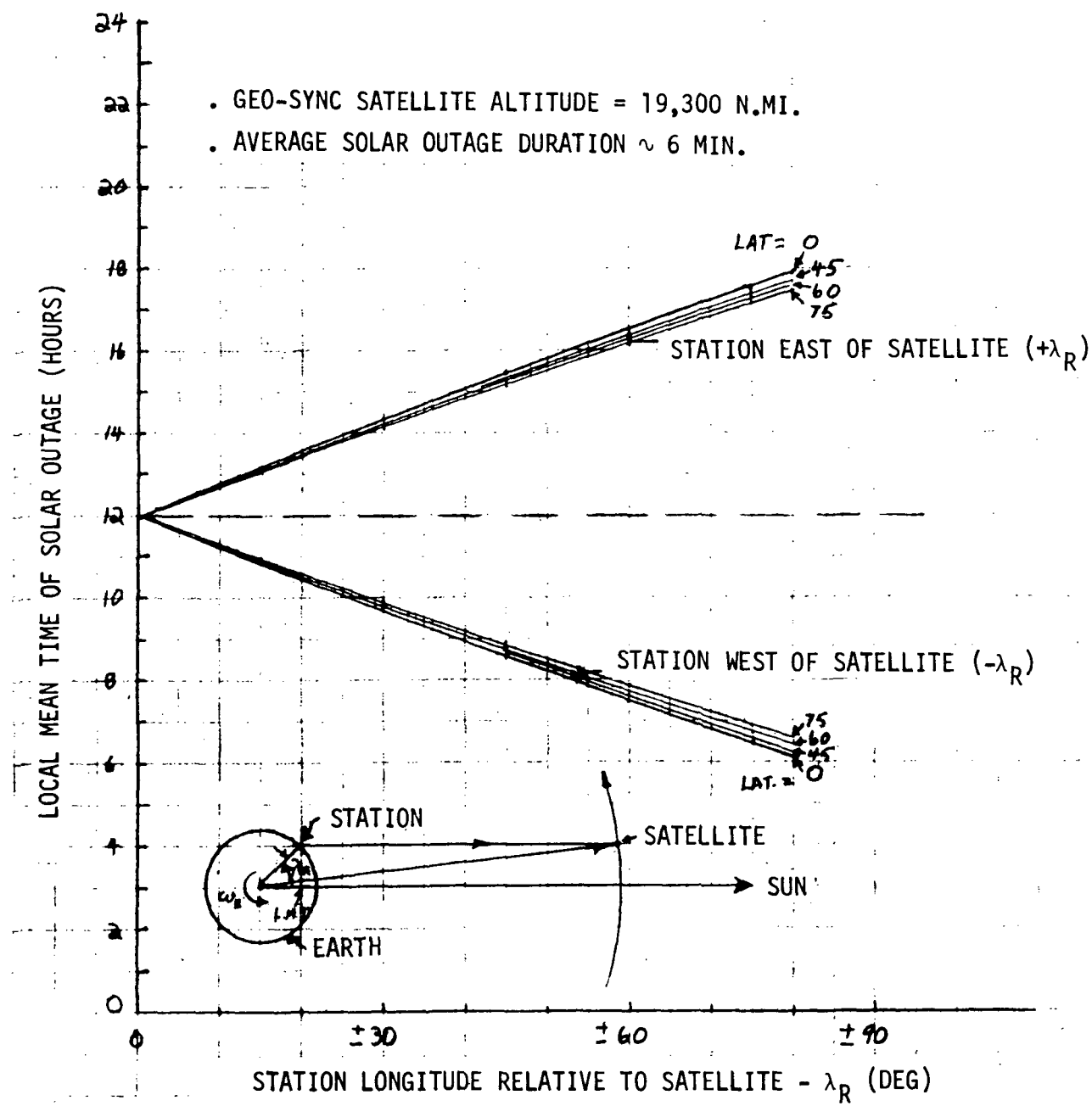


Figure 3.1-34. Ground Station/Geosynchronous Satellite Solar Outage  
Local Mean Time  
(Whenever Outage Occurs for that Station)

## EARTH SHADOWING CHARACTERISTICS

A satellite operating at geosynchronous altitude will periodically be eclipsed by the earth. The frequency and duration of the eclipse periods will have an impact on the design of spacecraft whose primary electrical power system is based on the use of solar arrays. The general characteristics, the frequency, and the mean duration of the eclipse periods are discussed below.

The geometric characteristics of the earth shadow are shown in Figure 3.1-35. Based on a mean distance of earth from sun of  $80.7 \times 10^6$  nautical miles ( $1.495 \times 10^8$  km; Reference 3.1-1), the umbra extends to a distance of approximately  $0.75 \times 10^6$  nautical miles ( $1.383 \times 10^6$  km). For comparison, the mean distance of moon from earth is approximately  $0.21 \times 10^6$  nautical miles ( $0.3844 \times 10^6$  km). Therefore, the umbra of earth extends to approximately 3.6 times the mean distance of moon from earth.

The resultant characteristics of the earth shadow in a geosynchronous orbit at a radius of 22,767 nautical miles are illustrated in Figure 3.1-36. From the geometry it can be determined that the earth central angle subtended by the umbra at geosynchronous altitude is 16.35 degrees based on a mean earth-sun distance. The earth central angle subtended by the penumbra is slightly greater, being 17.94 degrees.

The period of time during which a geosynchronous satellite will be within the earth shadow is dependent upon the orientation of the spacecraft orbital plane with respect to the earth-sun line of centers. The maximum time within the shadow is given by:

$$t_i = \frac{\alpha_i}{\pi} \quad (3.1-31)$$

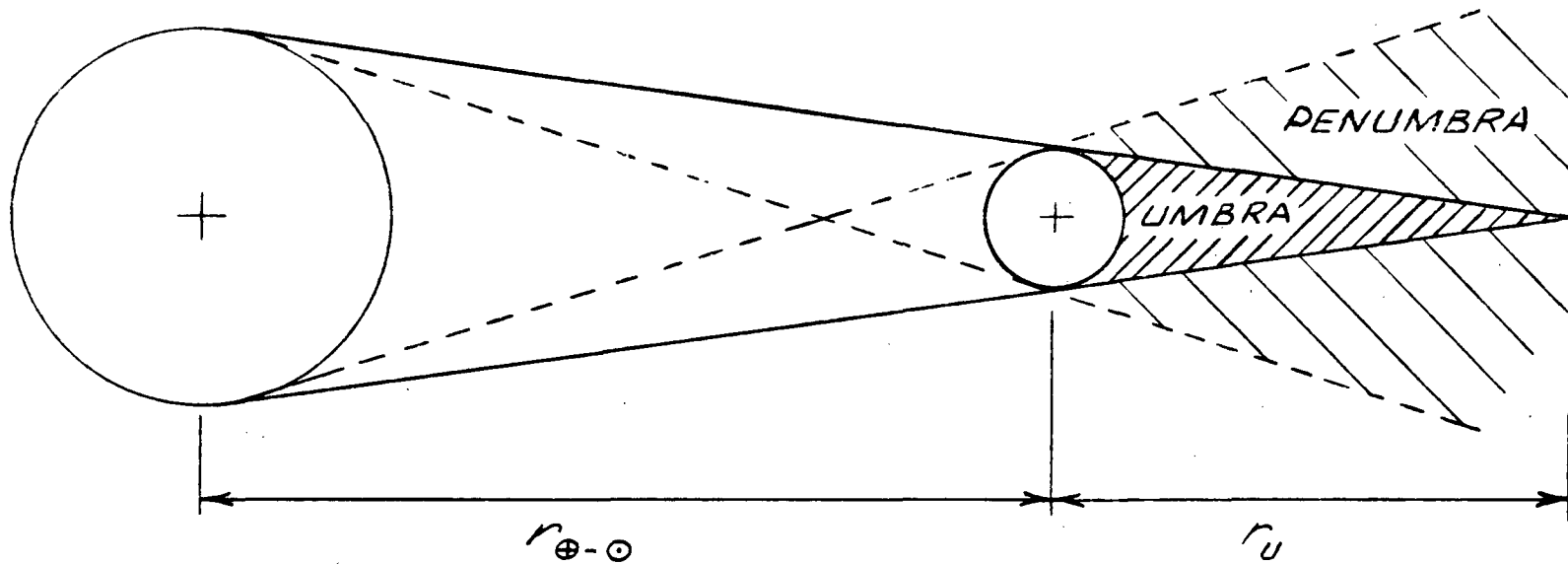
where

$t_i$  = the maximum time a spacecraft is within the umbra ( $\alpha_u$ ) or the penumbra plus umbra ( $\alpha_p$ )

$\alpha_i$  = the earth central angle defining the umbra ( $\alpha_u$ ) and the penumbra ( $\alpha_p$ )

$\pi$  = the mean orbital motion

For a geosynchronous orbit, the mean orbital motion is equal to the earth rotation rate of 15.041 067 degrees per mean solar hour. Therefore, the maximum time a geosynchronous satellite will be within the earth shadow (entry into the penumbra until exit from the penumbra) is 71.57 minutes. The maximum time within the umbra alone is 65.21 minutes.



3-66

$$r_{\oplus-\odot} = 80.4 \times 10^6 \text{ n.mi.}$$

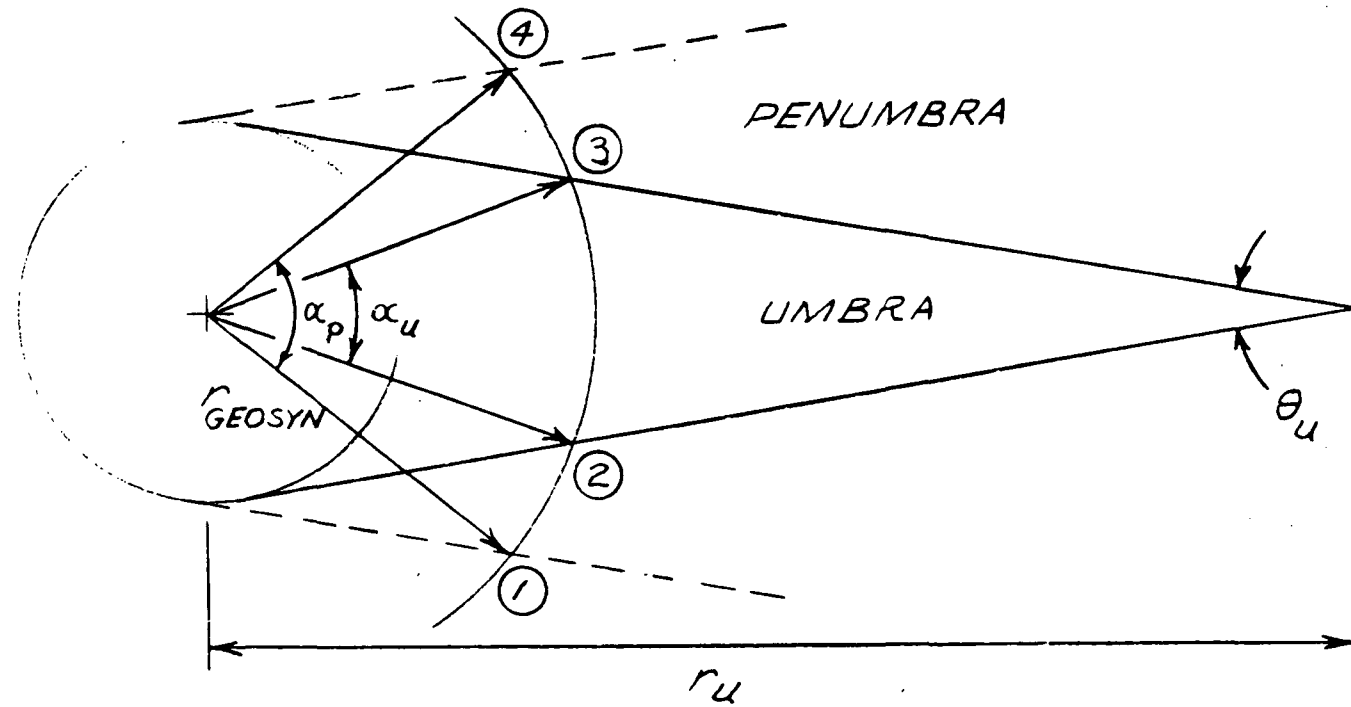
$$r_{\oplus-\odot} = 81.0 \times 10^6 \text{ n.mi.}$$

$$a_{\oplus} = 80.7 \times 10^6 \text{ n.mi.}$$

$$r_U = 0.75 \times 10^6 \text{ n.mi.}$$

$$(a_{\epsilon} = 0.21 \times 10^6 \text{ n.mi.})$$

Figure 3.1-35. Earth Shadow Geometry

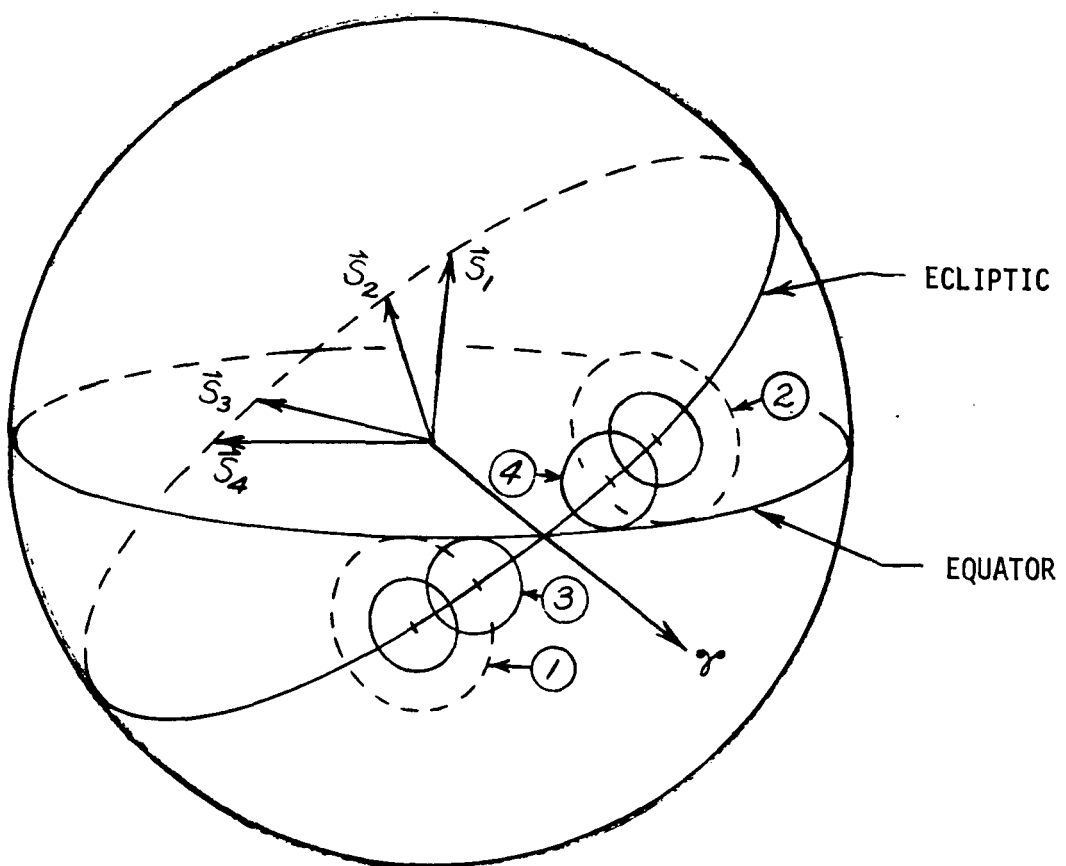


$r_u$ $r_{\oplus-\odot} = \alpha_{\oplus}$ $GEOSYN = 22,767 \text{ n.mi.}$	$\alpha_u = 16.35 \text{ deg.}$ $\alpha_p = 17.94 \text{ deg.}$ $\theta_u = 0.53 \text{ deg.}$	$t_{1-2 MAX} = t_{3-4 MAX} = 3.18 \text{ min.}$ $t_{2-3 MAX} = 65.21 \text{ min.}$ $t_{1-4 MAX} = 71.57 \text{ min.}$
----------------------------------------------------------------------------------	------------------------------------------------------------------------------------------------------	-----------------------------------------------------------------------------------------------------------------------------

Figure 3.1-36. Earth Shadow Characteristics - Geosynchronous Orbit



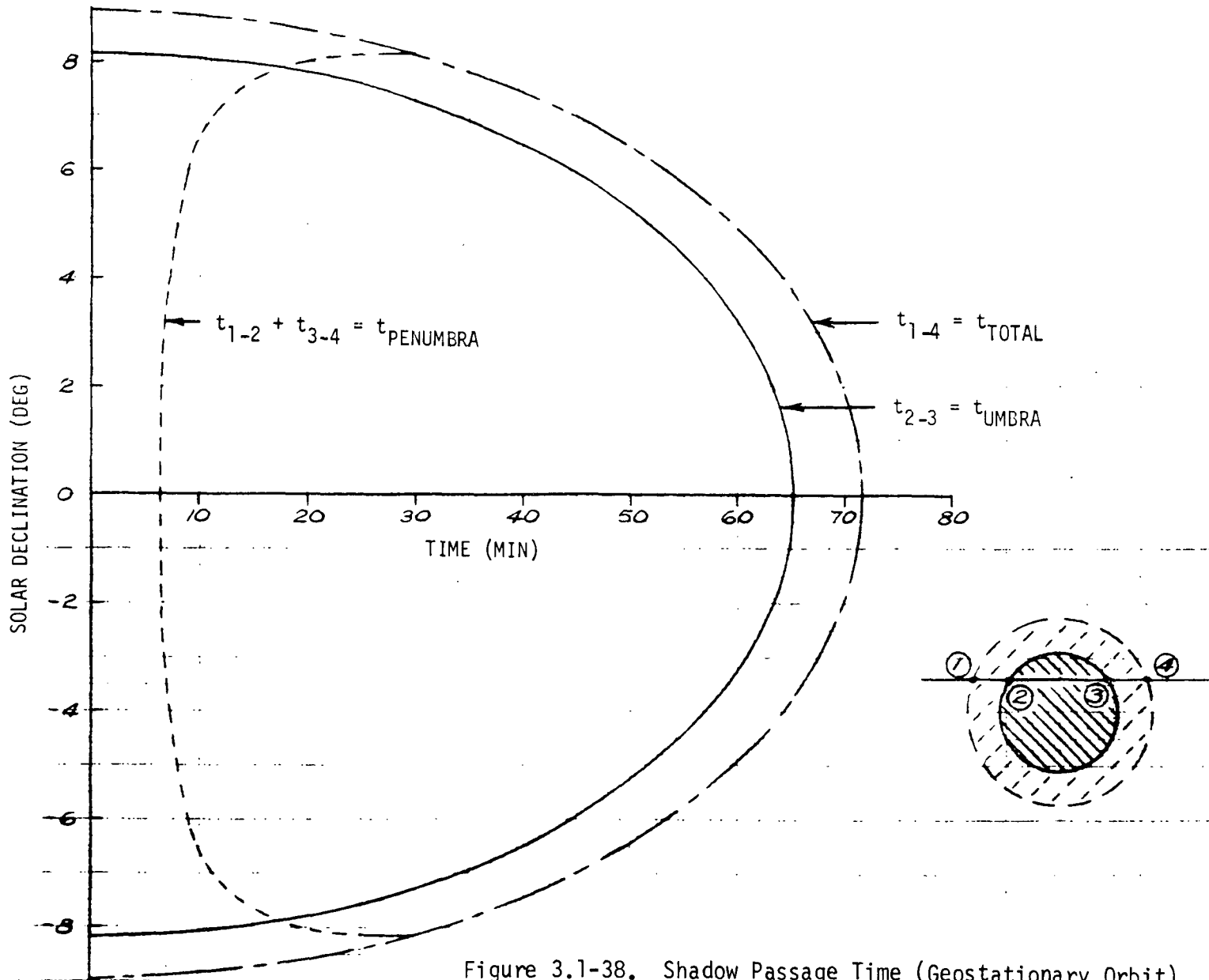
The effects of time of year for an equatorial geosynchronous satellite are shown in Figure 3.1-37. As can be seen from the figure, the earth shadow will be in the direction of vernal equinox when the sun is in the vicinity of autumnal equinox. Since the obliquity of the ecliptic is greater than the earth central angle subtended by the umbra or the penumbra, a geostationary satellite will not pass through the earth shadow on a daily basis at all times during the year. There are two periods during the year of approximately 47 days (sun in the vicinity of vernal equinox and sun in the vicinity of autumnal equinox) when a geostationary satellite will pass either through the penumbra or through the penumbra and the umbra. The characteristics of this shadow passage time are shown in Figure 3.1-38, which shows the time a geostationary satellite will be in the earth shadow as a function of solar declination.



$$t_{1-2} = 46.84 \text{ DAYS}$$

$$t_{3-4} = 42.50 \text{ DAYS}$$

Figure 3.1-37. Annual Shadowing Characteristics



3-69

SD 73-SA-0036-3

**Page intentionally left blank**

**Page intentionally left blank**

### 3.2 ORBIT PERTURBATIONS

A principal task of the Geosynchronous Platform Definition Study was the development and evaluation of a geosynchronous mission traffic model over approximately a twenty-year period. As part of the model evaluation, a physical contention analysis was conducted in order to determine possible physical interference between the many satellites and/or platforms which will be placed in orbit over the study time period.

Of particular interest are the potential problems that may occur when a geosynchronous satellite ceases stationkeeping because of a failure or because it reaches the end of its operational lifetime. When stationkeeping ceases, a geosynchronous satellite will begin an uncontrolled drift in accordance with perturbed geosynchronous orbit characteristics. Of principal concern is that an inactive satellite may, after months or years, drift into the vicinity of an active satellite and present a physical contention hazard.

Accordingly, the perturbations considered here are those long period perturbations which affect the mean satellite motion over a period of several months or years. The shorter period perturbations which are neglected cause small amplitude oscillations about the mean paths determined from the long period effects. Where appropriate, some of these shorter period effects are noted.

The dominant perturbations which must be considered for geosynchronous orbits are perturbations due to the tesseral harmonic term in the gravitational potential function of the earth (triaxial earth), luni-solar perturbations, and perturbations due to solar pressure. The effects of these perturbations are illustrated in Figure 3.2-1. The tesseral harmonics produce an apparent longitudinal "drift" about two stable points ( $75^{\circ}\text{E}$  and  $105^{\circ}\text{W}$  longitude) with the amplitude of the drift equal to the initial displacement from the stable points. The luni-solar perturbations produce a long term perturbation of the orbit inclination with the characteristics of the perturbations dependent upon the initial orientation of the orbital plane. Solar pressure perturbations produce a cyclic variation in the orbit eccentricity. The general characteristics of these perturbations are discussed in the following sections.

#### TRIAXIAL EARTH PERTURBATIONS

The major perturbation due to the triaxiality of the earth is a geographic longitudinal oscillation of the satellite about the semi-minor axis of the earth's equatorial ellipse and a radial oscillation about the mean geosynchronous radius. These perturbations are due primarily to the  $J_{2,2}$  tesseral harmonic term in the earth's potential and have periods of more than two years depending on the initial longitude of the satellite.

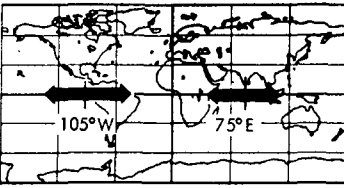
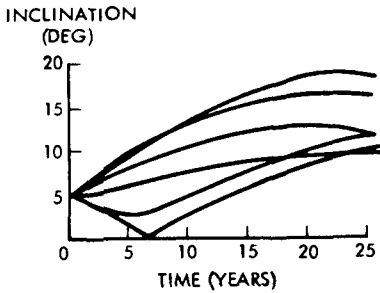
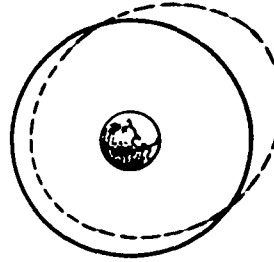
PERTURBATION SOURCE	TESSERAL HARMONIC	LUNI-SOLAR PERTURBATIONS	SOLAR PRESSURE
PERTURBATION EFFECT	 APPARENT LONGITUDINAL DRIFT	 INCLINATION PERTURBATION	 ORBIT ECCENTRICITY PERTURBATION

Figure 3.2-1. Perturbation Sources and Effects



Figure 3.2-2 illustrates the mean path of the perturbed equatorial geosynchronous satellite with respect to the earth and the nominal 24-hour orbit altitude. A satellite initially located at a longitude  $\lambda_{r_0}$  relative to the semi-minor axis (stable point) will oscillate about the stable point with an amplitude equal to the initial relative longitude ( $\lambda_{r_0}$ ). Also, while drifting in a westerly direction, the satellite radius will increase above the nominal orbit altitude reaching a maximum at the stable axis location. After reaching its maximum westerly longitude, the satellite radius drops below the nominal orbit radius and begins its easterly drift. The drifting satellite thus forms a closed mean path contour which is unique for each discrete initial location.

The motion of the drifting geosynchronous satellite may be examined as follows. Because of the elliptical shape of the earth's equatorial cross section, the gravitational acceleration vector ( $\bar{g}$ ) does not lie along the satellite radius. Figure 3.2-3 illustrates the gravitational forces acting on the satellite due to the ellipticity of the earth's equator. As can be seen from the figure, the gravitational force is directed slightly away from the center of the earth. The gravitational acceleration may be resolved into a component along the radius vector and a component ( $\bar{A}$ ) normal to the radius vector in the equatorial plane. The normal gravitational component is directed easterly toward the semi-major axis if the satellite is east of the stable axis and westerly if the satellite is west of the stable axis.

An approximate impulsive velocity analogy may be used to explain the satellite's mean path due to these gravitational forces. Consider a satellite located east of the stable axis in an orbit where mean angular motion is the same as the earth's rotational angular rate and is, therefore, stationary with respect to the earth. The satellite is traveling east and since the normal gravitational component is also in an easterly direction, the satellite will experience a velocity increase which will tend to raise its altitude and increase its orbital period. The earth will, therefore, be rotating faster than the satellite angular rate and the satellite will begin to drift above the nominal orbit in a westerly direction. As the satellite drifts to a point west of the stable axis, the normal gravitational component changes direction and the satellite experiences a decrease in velocity. The orbit altitude will begin to decrease and as it crosses the nominal orbit altitude, the earth will be rotating slower than the satellite's angular rate. The satellite will then begin a westerly drift at altitudes below the nominal. This motion continues causing an oscillatory motion about the stable axis and the nominal orbit radius.

The primary gravitational effects due to the equator's elliptical shape may be expressed in terms of the  $J_{2,2}$  tesseral harmonic term in the earth's potential function. Perkins (Reference 3-2) has shown that the longitudinal drift rate of a perturbed geosynchronous satellite may be expressed in terms of the  $J_{2,2}$  tesseral harmonic coefficient as:

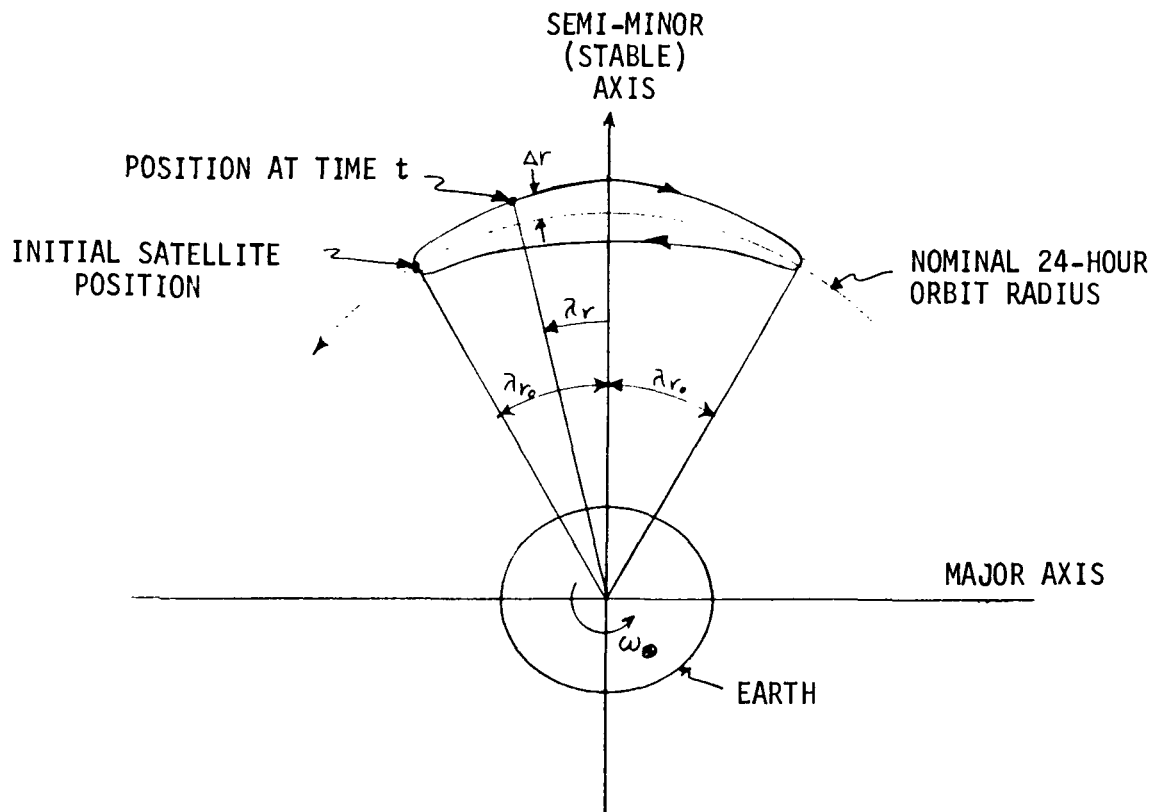


Figure 3.2-2. Perturbed Geosynchronous Satellite Mean Path

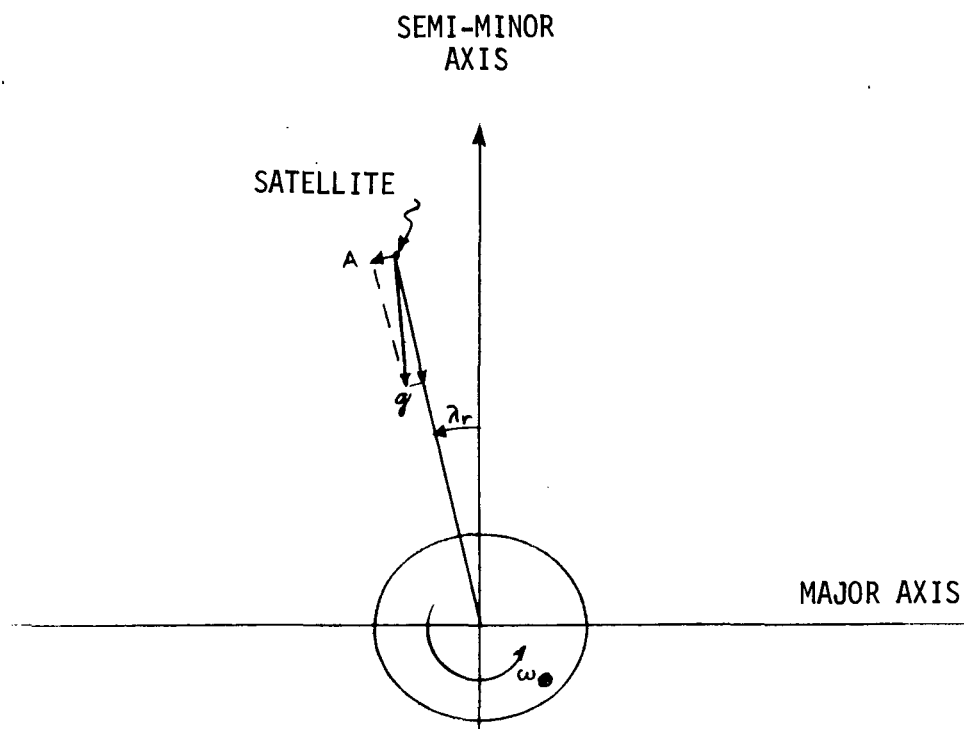


Figure 3.2-3. Geosynchronous Satellite Gravitational Force

$$\dot{\lambda}_r = \left[ \frac{-18\mu R_\oplus^2 J_{2,2}}{r_0^5} (\cos 2\lambda_r - \sin 2\lambda_{r_0}) \right]^{1/2} \quad (3.2-1)$$

where

- $\dot{\lambda}_r$  = longitudinal drift rate (rad/sec)
- $\mu$  = gravitational constant ( $\text{ft}^3/\text{sec}^2$ )
- $R_\oplus$  = earth's equatorial radius (ft)
- $r_0$  = nominal 24-hour synchronous radius (ft)
- $\lambda_r$  = longitude relative to stable axis ( $75^\circ\text{E}$  or  $105^\circ\text{W}$ )
- $\lambda_{r_0}$  = initial relative longitude, also equal to amplitude of longitudinal oscillation

and that the radial oscillation may be described by:

$$\Delta r = \frac{2}{\omega_\oplus} \left[ \frac{-2\mu R_\oplus^2 J_{2,2}}{r_0^3} (\cos 2\lambda_r - \cos 2\lambda_{r_0}) \right]^{1/2} \quad (3.2-2)$$

where

- $\Delta r$  = radial deviation from nominal (ft)
- $\omega_\oplus$  = earth's angular rotation rate (rad/sec)

By substituting Equation (3.2-1) into

$$dt = \frac{d\lambda}{\dot{\lambda}} \quad (3.2-3)$$

and changing variables, the oscillation period may be found from the resulting elliptical integral



$$\tau = \frac{2}{3} \sqrt{\frac{-r_0^5}{\mu R_\oplus^2 J_{2,2}}} \int_0^{\pi/2} \frac{d\phi}{(1 - \sin^2 \lambda_{r_0} \sin^2 \phi)^{1/2}} \quad (3.2-4)$$

where

$$\sin \theta = \frac{\sin \lambda_r}{\sin \lambda_{r_0}}$$

$\tau$  = oscillation period (sec)

The longitudinal position time history for a quarter period is sufficient to deduce the complete mean path since the motion is symmetrical. Therefore, by changing the limits of Equation (3.2-4) and adjusting the constant, the relationship between time and relative longitude for any given initial position  $\lambda_{r_0}$  is the elliptical integral:

$$t = \frac{1}{6} \sqrt{\frac{-r_0^5}{\mu R_\oplus^2 J_{2,2}}} \int_0^\phi \frac{d\phi}{(1 - \sin^2 \lambda_{r_0} \sin^2 \phi)^{1/2}} \quad (3.2-5)$$

where

$t$  = time from  $\lambda_r = 0$  to  $\lambda_r$

$$\phi = \sin^{-1} \left( \frac{\sin \lambda_r}{\sin \lambda_{r_0}} \right)$$

Another relationship of interest is the velocity of the satellite along its mean path relative to the nominal 24-hour satellite orbital velocity ( $V_r$ ) given by:

$$V_r = \left[ \frac{-2\mu R_\oplus^2 J_{2,2}}{r_0^3} (\cos 2\lambda_r - \cos 2\lambda_{r_0}) \right]^{1/2} \quad (3.2-6)$$



It was noted earlier that the amplitude of the oscillation is equal to the value of the initial relative longitudinal position ( $\lambda_{r_0}$ ). An oscillation amplitude of  $\lambda_{r_0}$  assumes perfect nominal conditions at the initiation of the perturbed orbital drift. In actual practice, and of special interest for physical contention analyses, the satellite will most probably have a small residual velocity at the cessation of stationkeeping. A residual velocity at initiation of uncontrolled drift will result in some amplitude dispersion between  $\lambda_{r_0}$  and  $\lambda_{r_{max}}$  corresponding to the maximum possible value of the residual velocity. The maximum amplitude dispersion value can easily be found from Equation (3.2-6) by rearrangement of the equation into:

$$\lambda_{r_{max}} = \frac{1}{2} \cos^{-1} \left[ \cos 2\lambda_{r_0} + \frac{r_0^3 \Delta V_r^2}{2\mu R_0^2 J_{2,2}} \right] \quad (3.2-7)$$

where

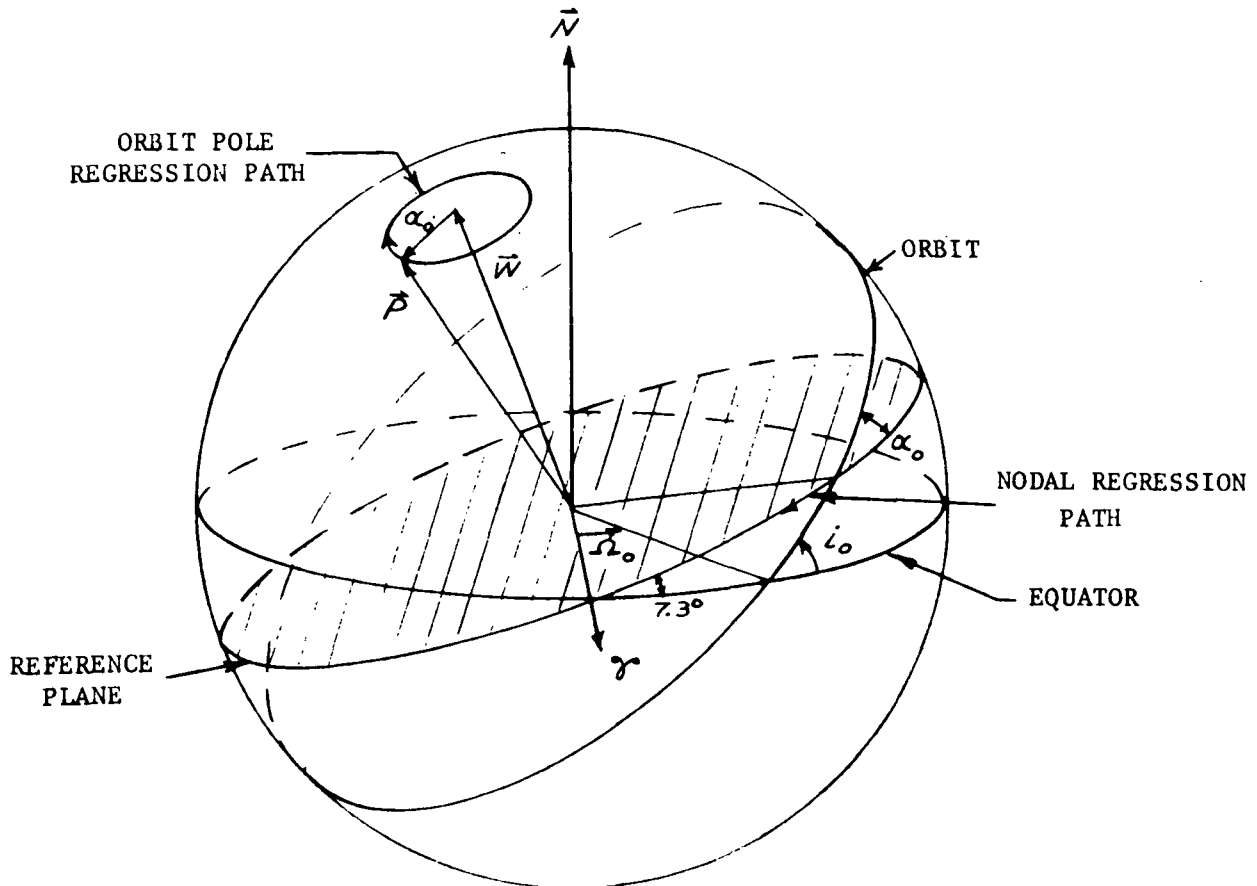
$\lambda_{r_{max}}$  = amplitude corresponding to maximum possible value of  $V_r$

$\Delta V_r$  = maximum possible residual velocity

#### LUNI-SOLAR PERTURBATIONS

Lunar and solar gravitational perturbations produce a very long period (over 50 years) oscillation of the geosynchronous orbit inclinations. Frick (Reference 3-3) has shown that the inclination perturbations are actually the result of an effective orbit plane nodal regression along a fictitious reference plane. The motion is similar to the lunar orbit plane inclination cycle caused by the lunar orbit plane node on the ecliptic regressing due to solar gravitational effects. The lunar orbit plane regresses around the ecliptic in a period of 18.6 years. The lunar orbit plane inclination to the ecliptic remains constant as the nodes regress which results in an oscillation of the lunar orbit plane inclination to the earth's equator. The lunar orbit plane inclination varies between 18.4 and 28.6 degrees during the 18.6-year cycle.

The orbit plane motion due to lunar solar gravitation is quite similar except that the geosynchronous orbit plane node regresses along a reference plane inclined 7.33 degrees to the earth's equator. The nodal regression period is about 53 years while the inclination varies between  $7.33 + \alpha_0$  degrees where  $\alpha_0$  is the inclination of the orbit plane to the reference plane. The value of  $\alpha_0$  is determined from the geometry of the orbit plane's initial inclination and right ascension of the ascending node with respect to the equator. The node of the reference plane is at the vernal equinox. Figure 3.2-4 defines the regression geometry.



$\vec{P}$  = Reference plane normal vector  
 $\vec{W}$  = Orbit plane normal vector  
 $\vec{N}$  = North  
 $\Omega_0$  = Orbit plane right ascension of ascending node  
 $\alpha_0$  = Orbit inclination to reference plane  
 $i_0$  = Initial orbit inclination

Figure 3.2-4. Luni-Solar Perturbation Model

The following analytical results are valid within approximately one-half degree for the near-circular geosynchronous orbits with initial inclinations less than about 75 degrees. The rotation of the earth around the sun, the rotation of the earth-moon system about its barycenter, and the regression of the lunar orbit plane about the normal to the ecliptic have been taken into account in the analysis by Frick (Reference 3-3).

From the definition of the reference plane, the inclination of an equatorial geosynchronous orbit  $\alpha_0(0)$  to the reference plane is seen to be 7.33 degrees. Frick also shows that the inertial nodal regression rate of an equatorial geosynchronous orbit  $\dot{\psi}(0)$  about the normal to the reference plane is a constant value equal to -6.816 degrees/year. The general case of the inclined 24-hour geosynchronous orbit can be discussed in terms of the above constants  $\alpha_0(0)$  and  $\dot{\psi}(0)$  for the equatorial geosynchronous orbit and the conventional orbit initial inclination and node.

The initial geometric conditions for an orbit plane of arbitrary inclination ( $\iota_0$ ) and right ascension of ascending node ( $\Omega_0$ ) are illustrated in Figure 3.2-5. From the figure, the inclination of the orbit plane to the reference plane is given by:

$$\alpha_0 = \cos^{-1}(\cos\epsilon \cos\iota_0 + \sin\epsilon \sin\iota_0 \cos\Omega_0) \quad (3.2-8)$$

where

$\alpha_0$  = orbit plane inclination to reference plane (= constant)

$\iota_0$  = initial orbit plane inclination to the equatorial plane

$\Omega_0$  = initial right ascension of the orbit plane ascending node

$\epsilon$  = inclination of reference plane to equator = 7.33 degrees

The regression rate of the orbit plane about the normal to the reference plane is

$$\dot{\psi} = \dot{\psi}(0) \cos \alpha_0 \quad (3.2-9)$$

where  $\dot{\psi}(0) = -6.816$  degrees/year

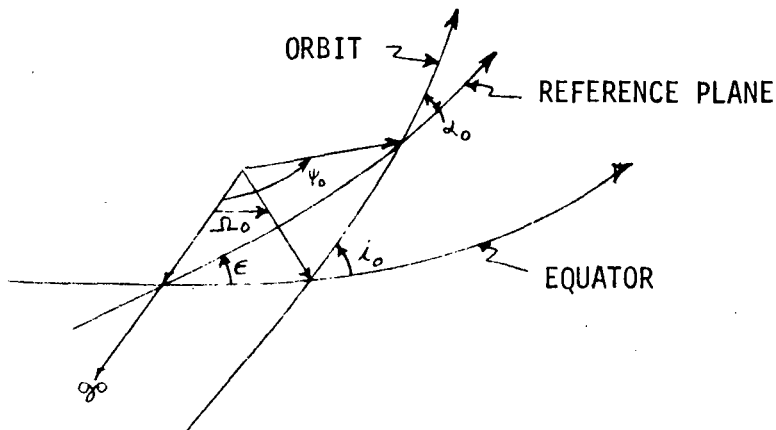


Figure 3.2-5. Initial Orbital Geometry

The nodal regression period ( $T_R$ ) is

$$T_R = \frac{360}{|\dot{\psi}|} \text{ (years)} \quad (3.2-10)$$

The initial argument of latitude ( $\psi_0$ ) measured in the reference plane to the orbit plane node on the reference plane is obtained from

$$\begin{aligned} \cos \psi_0 &= \frac{\cos \epsilon \cos \alpha_0 - \cos \Omega_0}{\sin \epsilon \sin \alpha_0} \\ \sin \psi_0 &= \frac{\sin \Omega_0 \sin \Omega_0}{\sin \alpha_0} \end{aligned} \quad (3.2-11)$$

After  $t$  years have elapsed, the argument of latitude of the orbit plane node on the reference plane ( $\psi$ ) is given by:

$$\psi = \psi_0 + \dot{\psi} t \quad (3.2-12)$$

The inclination of the orbit plane to the equator after  $t$  years is thus given by

$$\iota = \cos^{-1} [\csc \epsilon \cos \alpha_0 - \sin \epsilon \sin \alpha_0 \cos(\psi_0 + \dot{\psi} t)] \quad (3.2-13)$$

The preceding steady-state relationships adequately describe the lunisolar inclination perturbations to an accuracy of about one-half degree for values of  $\alpha_0$  below about 75 degrees. Above 75 degrees, higher order effects begin to significantly modify the steady-state relationships. For initial inclinations to the equator above 79 degrees, the normal to the orbit plane begins to trace an elliptical regression pattern around the reference plane normal.

#### SOLAR PRESSURE PERTURBATIONS

The major effects of solar radiation pressure on a geosynchronous orbit is a yearly oscillation in eccentricity and a rotation of the line of apsides. For an initially circular geosynchronous orbit, solar pressure will cause the eccentricity to increase to some maximum value after six months and return to circular after one year. The maximum value for the eccentricity is a function of the satellite effective area-to-weight ratio. Figure 3.2-6 illustrates the eccentric orbit producing forces of solar pressure. At point 1, the integrated solar pressure forces may be thought of as producing a small  $\Delta V$  in the same direction as the circular velocity vector thus raising the altitude at point 2. At point 2, the  $\Delta V$  is in the opposite direction of the circular velocity vector which then tends to reduce the altitude at point 1. Since the energy going into the orbit due to solar pressure for half of the orbit is essentially the same as the energy taken out of the orbit during the other half of a revolution, the semi-major axis remains unchanged while the eccentricity slowly builds up. Assuming that the satellite always remain in the sunlight (true within approximately one percent annually), that the effective cross-sectional area is constant, that earth's orbit about the sun is circular, and that the sun is always near or in the orbit plane, then the following procedure can be used to estimate the solar pressure perturbations within 10 percent. Actually, the approach is conservative so that at most the perturbations may be about 10 percent high.

Consider an eccentricity vector  $\bar{e}$  directed from the occupied focus toward apogee with magnitude  $(e)$  equal to the eccentricity. The rate of change of the eccentricity vector  $\bar{e}$  is a vector  $\dot{\bar{e}}$  which is normal to the earth-sun direction. Since the derivative of a vector is tangent to the path swept out by the tip of the vector and since  $\dot{\bar{e}}$  remains normal to the earth-sun line as the earth moves around the sun, the eccentricity vector traces out a circle during one complete revolution of the earth around the sun. The occupied focus of the synchronous orbit is on the circumference of the circle if the orbit is initially circular.

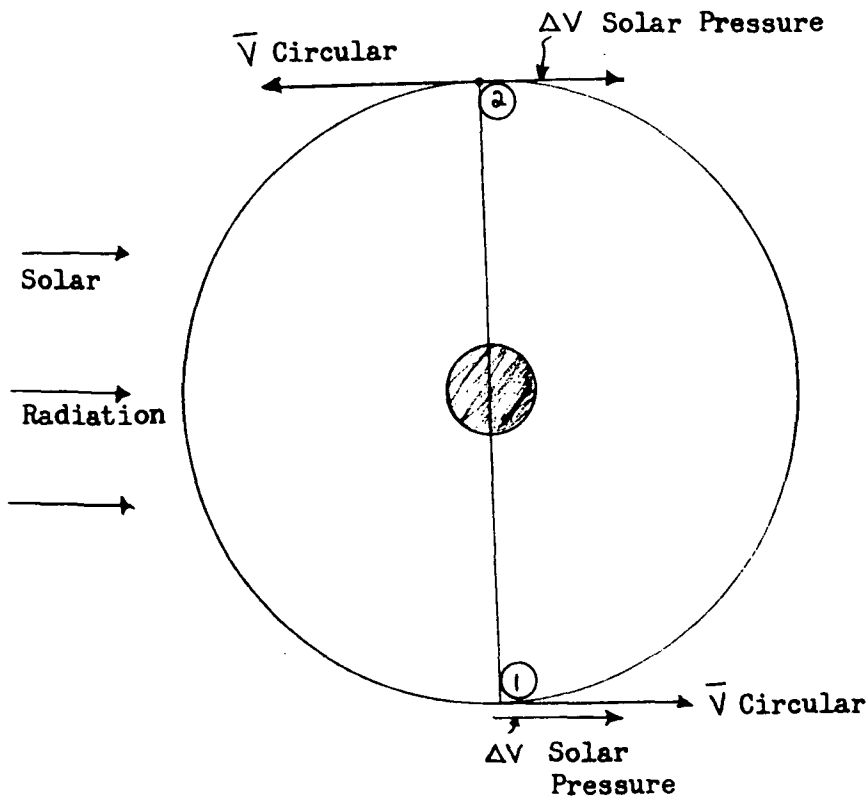


Figure 3.2-6. Eccentricity Buildup Due to Solar Pressure

The magnitude of the vector  $\dot{\vec{e}}$  is defined by Reference 3-4 as:

$$|\dot{\vec{e}}| = \frac{3gF}{2V_c} \left( \frac{A}{W_{EFF}} \right) (8.64 \times 10^{-4}) ; \text{ days}^{-1} \quad (3.2-14)$$

where

$V_c$  = circular velocity = 10,088 ft/sec for a geosynchronous orbit

$g$  = acceleration due to gravity

$F$  = solar pressure for a perfectly reflecting flat surface at 1 a.u. =  $1.945 \times 10^{-7}$  lb/ft<sup>2</sup>

$A$  = projected area of the satellite (ft<sup>2</sup>)

$W$  = satellite weight (pounds)

$\left(\frac{A}{W}\right)_{EFF}$  = effective area to weight ratio ( $\text{ft}^2/\text{lb}$ )

It can then be shown that the radius ( $\rho$ ) of the circle swept out by the eccentricity vector  $\bar{e}$  is

$$\rho = \left( \frac{365.25}{2\pi} \right) |\dot{\bar{e}}| \quad (3.2-15)$$

Figure 3.2-7 illustrates the eccentricity circle geometry and concepts. The angle  $n_\Theta t$  is the angle the earth has moved through after time  $t$  days at the earth's mean orbital motion ( $n_\Theta$ ).

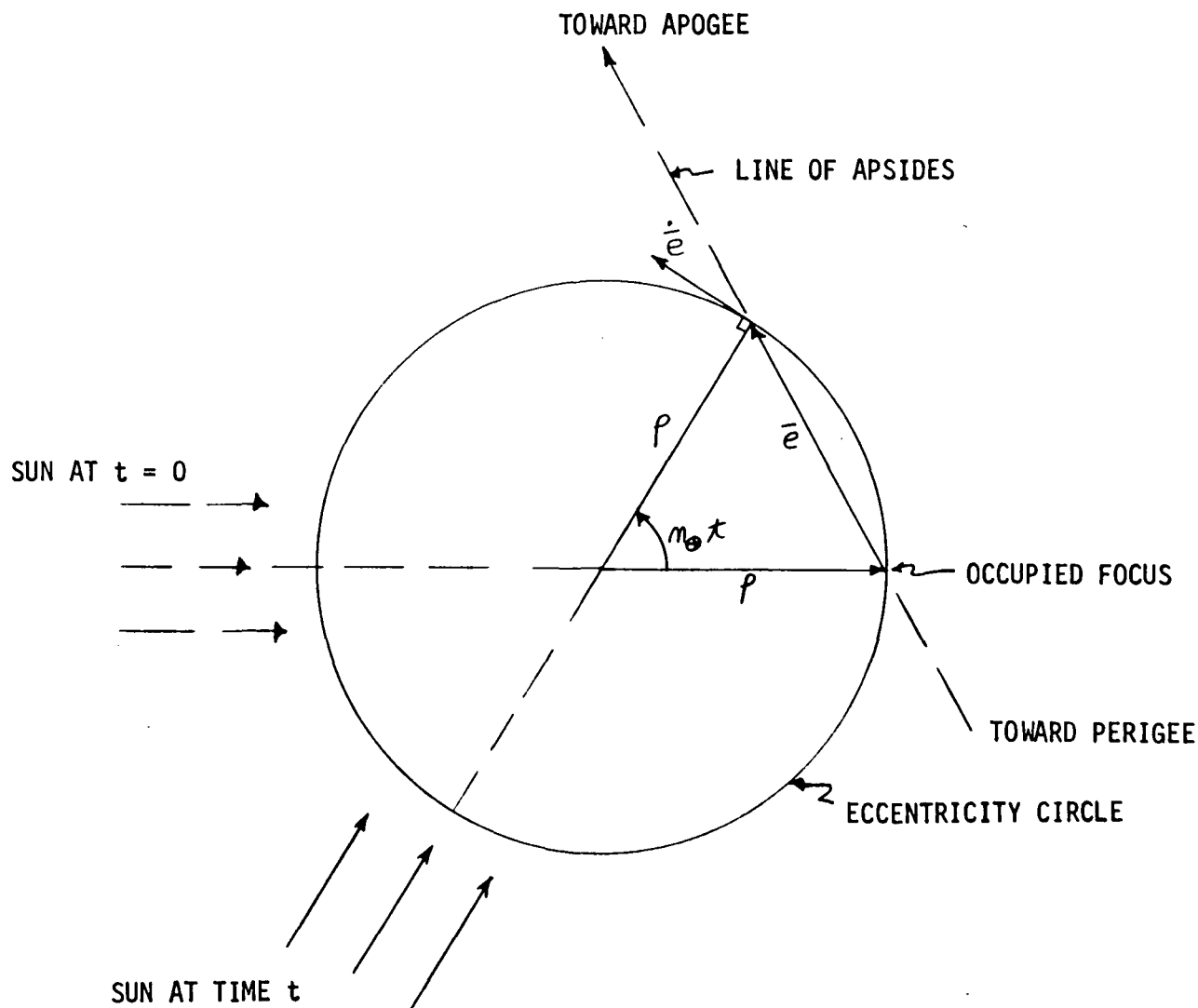


Figure 3.2-7. Eccentricity Circle Geometry

Since the length of  $\bar{e}$  is the eccentricity at time  $t$ , the eccentricity can be obtained from Figure 3.2-7 as:

$$e = 2\rho \sin\left(\frac{1}{2}\eta_{\oplus} t\right) \quad (3.2-16)$$

The period of the eccentricity cycle is one year with  $e$  reaching a maximum value of

$$e_{max} = 2\rho \quad (3.2-17)$$

at  $t =$  six months. Examination of Figure 3.2-7 will also reveal that the line of apsides rotates 180 degrees in one year. After one year, the orbit is again circular and the line of apsides begins the 180-degree rotation again. The line of apsides rotates at a rate ( $\dot{\omega}$ ) equal to one-half of the earth's mean orbital motion. That is:

$$\dot{\omega} = \frac{\pi}{2} \quad (3.2-18)$$

It can easily be shown that for a geosynchronous equatorial orbit, the satellite librates daily about the mean stationary longitude with a maximum deviation of:

$$\Delta\lambda = 2e \text{ (radians)} \quad (3.2-19)$$

Some comments on the effect of the assumptions made are relevant. The effect of the slight ellipticity of the earth's orbit is that although nearly the same eccentricity circle results, the speed at which it is traced out is variable. Out-of-plane effects of the sun produce a slight elliptical shape in the eccentricity circle. The ratio of the minor to major axis of the eccentricity ellipse is about 0.92 due to the 23.5 degree obliquity of the equator. The in-plane assumption of the sun's position is somewhat conservative. That is, the actual change in eccentricity is slightly less than that predicted by the above equations. Other second order effects cause minor deviations in the radius of the eccentricity circle, the rotational rate of the line of apsides, and the non-normal orientations of the earth-sun vector and  $\bar{e}$ . However, all of the above effects are second order and the computed solar pressure perturbations should be well within 10-percent accuracy and conservative.

## PERTURBATION RESULTS

Figures 3.2-8 through 3.2-13 present data which describe the mean path of a synchronous equatorial satellite under those perturbations due primarily to the  $J_{2,2}$  tesseral harmonic term in the earth potential. The mean path with respect to a rotating earth and a nominal 24-hour synchronous equatorial orbit is described. The curves in Figures 3.2-8 through 3.2-13 were generated from the equations discussed in the perturbations section. They correspond as follows:

<u>Figure</u>	<u>Equation</u>
3.2-8	3.2-4
3.2-9	3.2-1
3.2-10	3.2-5
3.2-11	3.2-2
3.2-12	3.2-6
3.2-13	3.2-7

In Figure 3.2-13, the increase in the satellite libration amplitude due to a small residual velocity at the initiation of uncontrolled drift is presented. Nominally the satellite would have zero velocity relative to the 24-hour geosynchronous equatorial orbital velocity at the beginning of uncontrolled drift and the amplitude of the oscillation would be equal to the initial relative longitude. The curves show the increase in amplitude with respect to the nominal amplitude if residual relative velocities are present at the beginning of the satellite drift along its mean geographical path.

Figure 3.2-14 presents the inclination perturbation data for a geosynchronous orbit due to luni-solar gravitational effects. Two cases are shown. The first case is for a geosynchronous orbit which is initially inclined at 5 degrees to the equator of the earth. Several values of the initial ascending node position are shown to illustrate the orientation effect. A single curve is given for the geosynchronous orbit which is initially equatorial since the node is undefined. Equations (3.2-8) through (3.2-13) were used to generate these data.

Figure 3.2-15 shows the eccentricity perturbation time history due to solar pressure on 24-hour circular geosynchronous orbits for several satellite area to weight ratios. The curves were generated using Equation (3.2-16) of the solar pressure perturbation discussion. Figure 3.2-16 shows the maximum eccentricity perturbation which will be experienced during the yearly eccentricity cycle as a function of the satellite area to weight ratio. The curve was generated with Equation (3.2-17) in the perturbation discussion.

The satellite daily longitude libration which occurs for the maximum eccentricity perturbation is shown in Figure 3.2-17 as a function of the satellite area-to-weight ratio. The curve was generated with Equation (3.2-19) in the perturbation discussion.

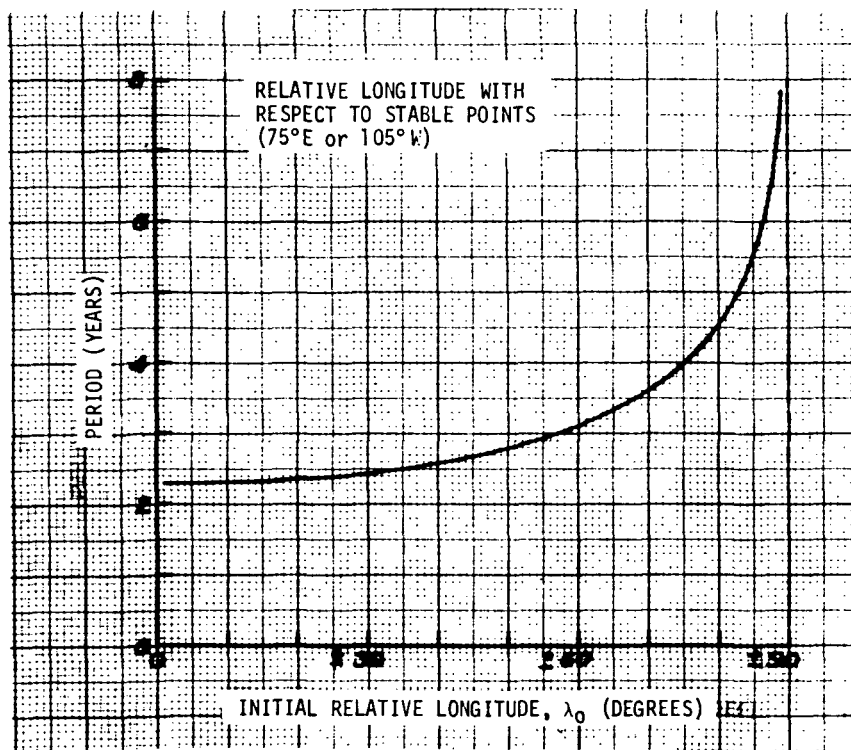


Figure 3.2-8. Longitudinal Libration Period Due to Triaxial Earth,  
Equatorial Geosynchronous Orbit

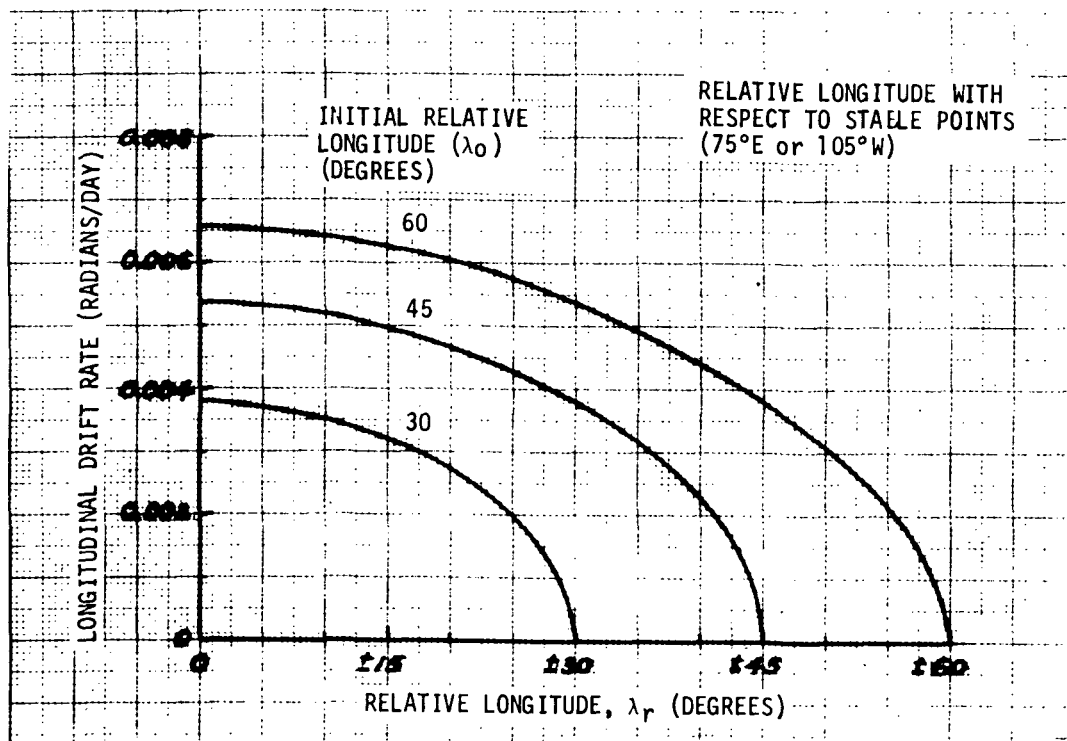


Figure 3.2-9. Longitudinal Drift Rate Due to Triaxial Earth,  
Equatorial Geosynchronous Orbit

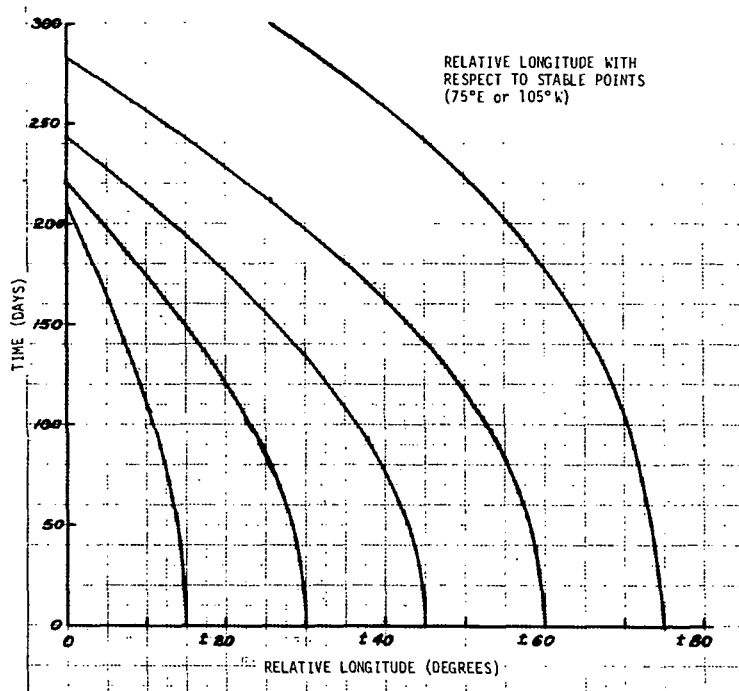


Figure 3.2-10. Geosynchronous Equatorial Satellite Longitudinal Drift Due to Triaxial Earth

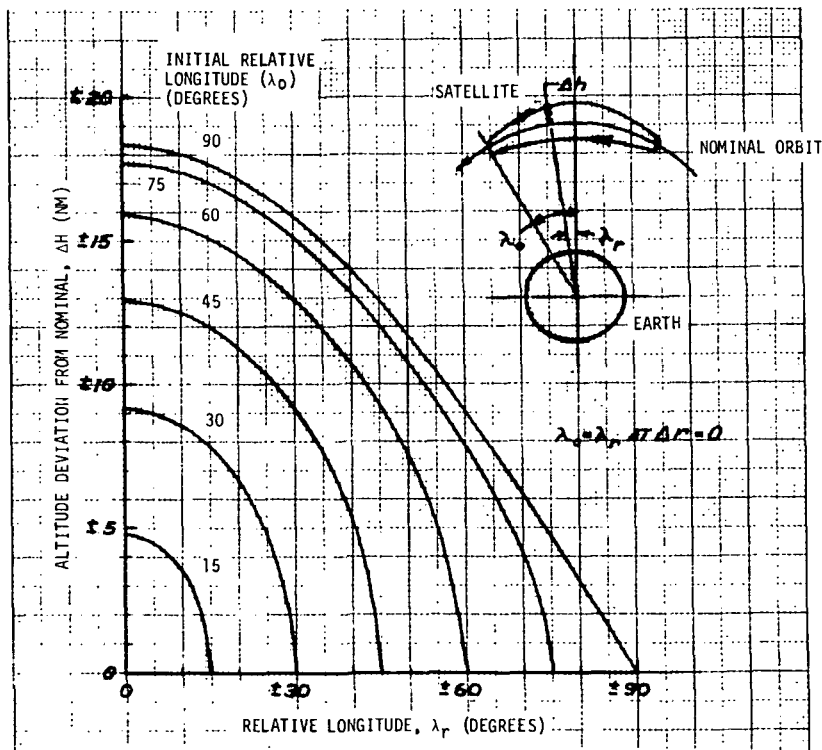


Figure 3.2-11. Geosynchronous Equatorial Satellite Altitude Deviation Due to Triaxial Earth

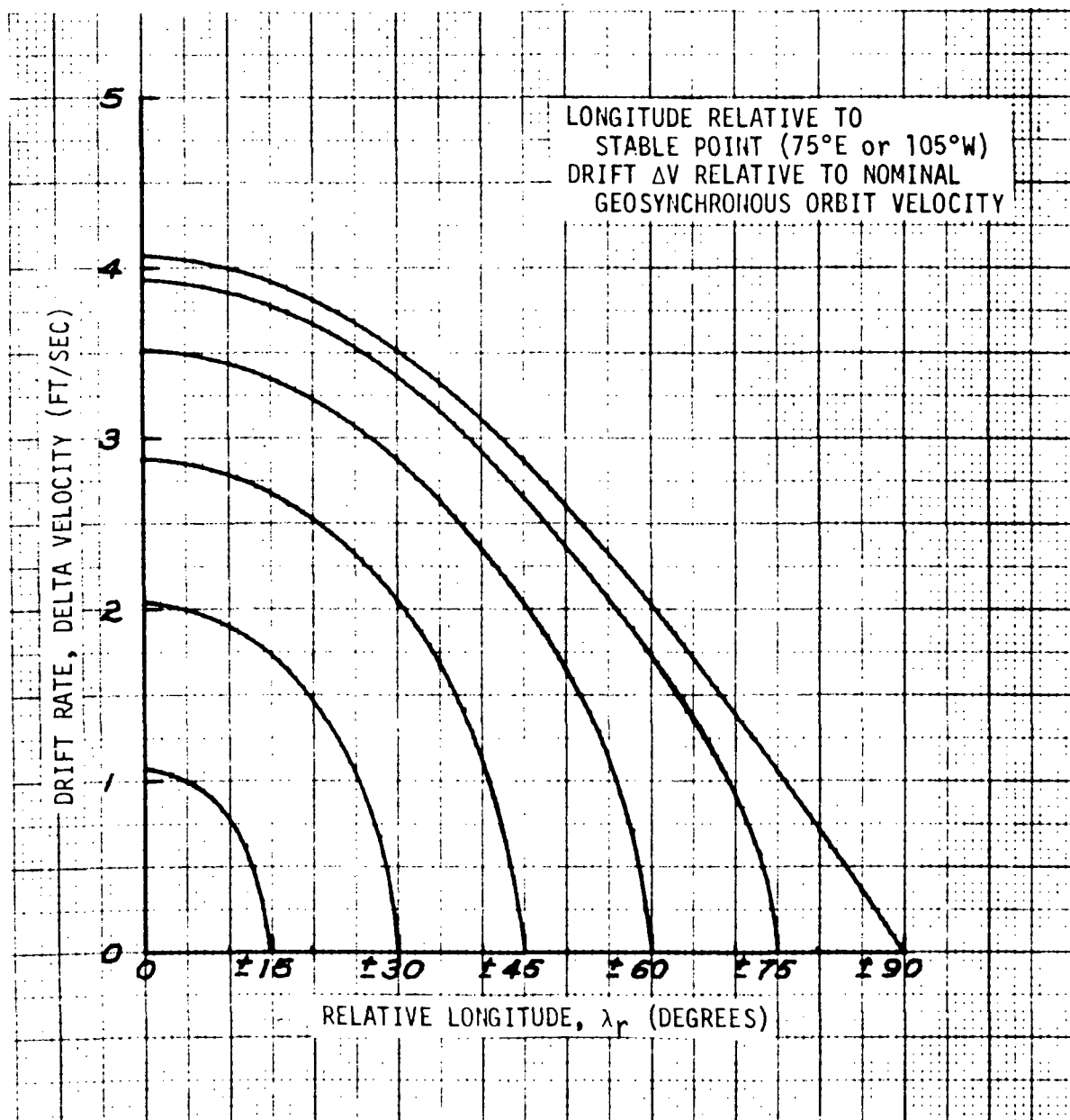


Figure 3.2-12. Synchronous Equatorial Satellite Drift Velocity  
Due to Triaxial Earth



Space Division  
North American Rockwell

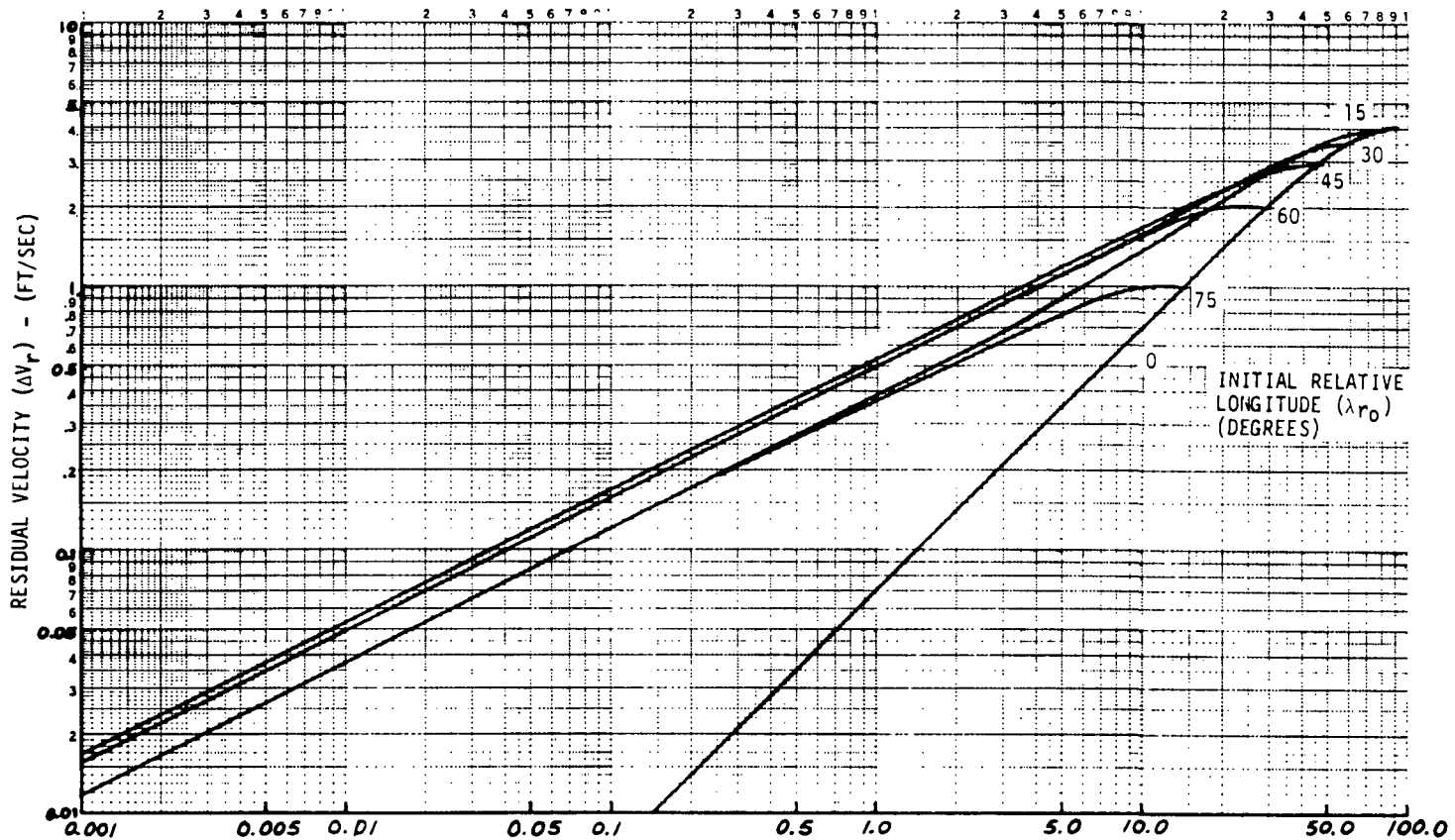


Figure 3.2-13. Longitudinal Libration Amplitude Dispersion ( $\Delta\lambda_r$ )  
Due to Triaxial Earth - degrees

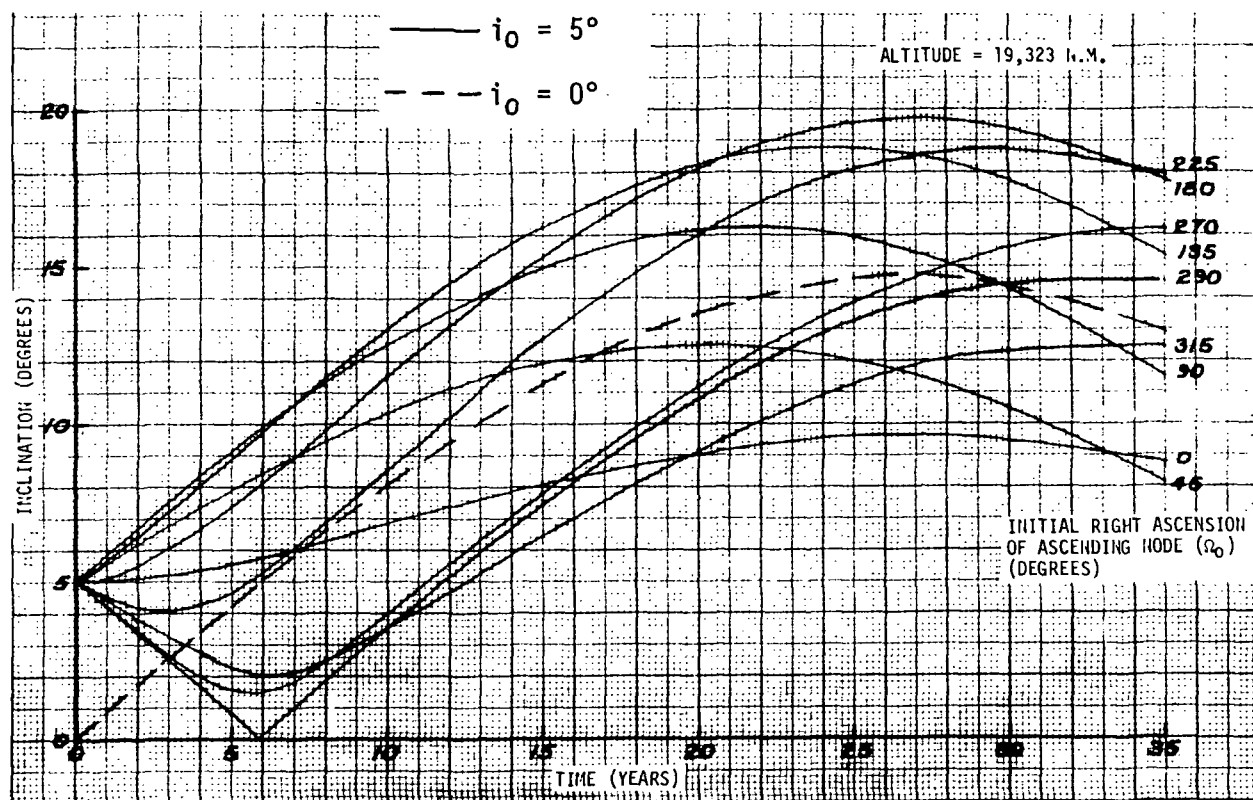


Figure 3.2-14. Mean Geosynchronous Luni-Solar Perturbation Effects

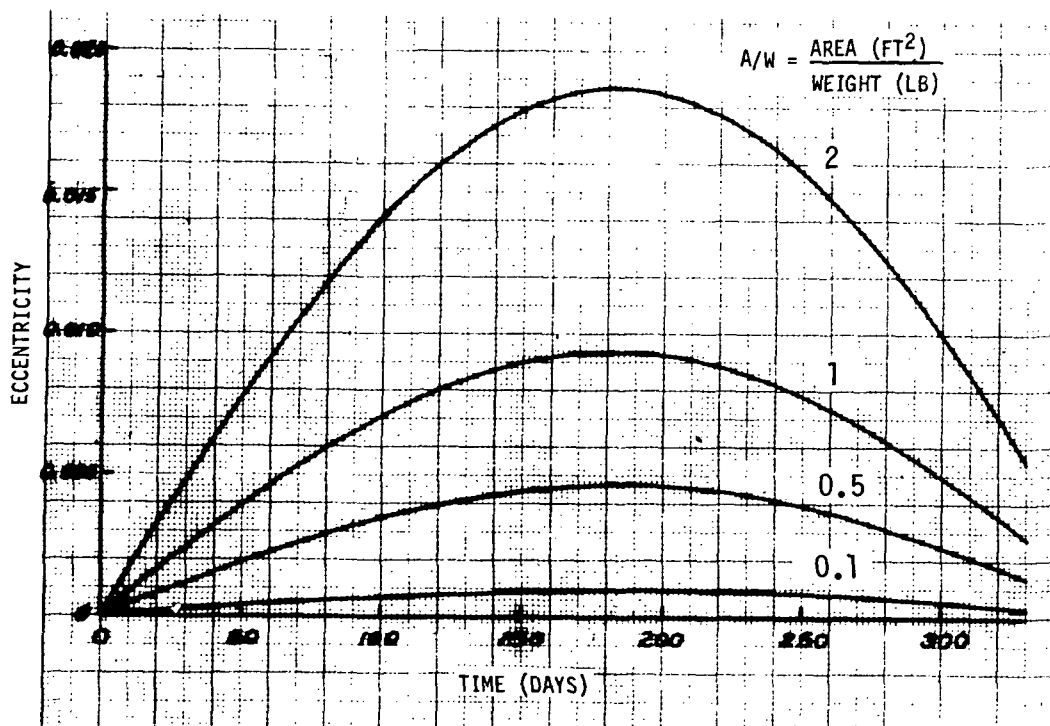


Figure 3.2-15. Solar Pressure Perturbations on Geosynchronous Orbit



Space Division  
North American Rockwell

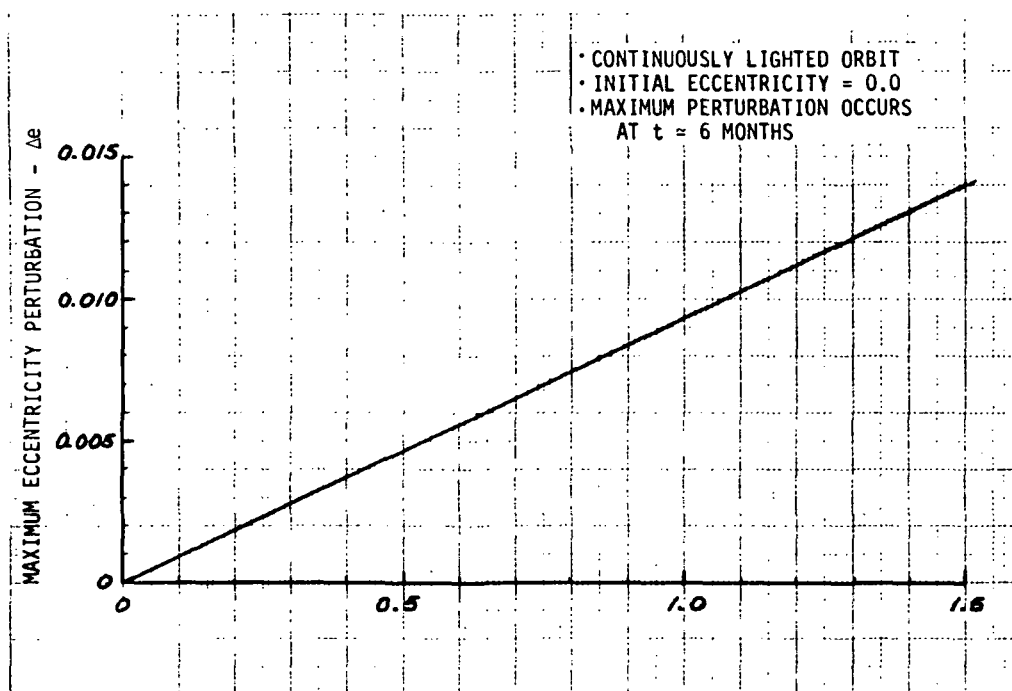


Figure 3.2-16. Long Period Solar Pressure Maximum Perturbations  
(Period = One Year)

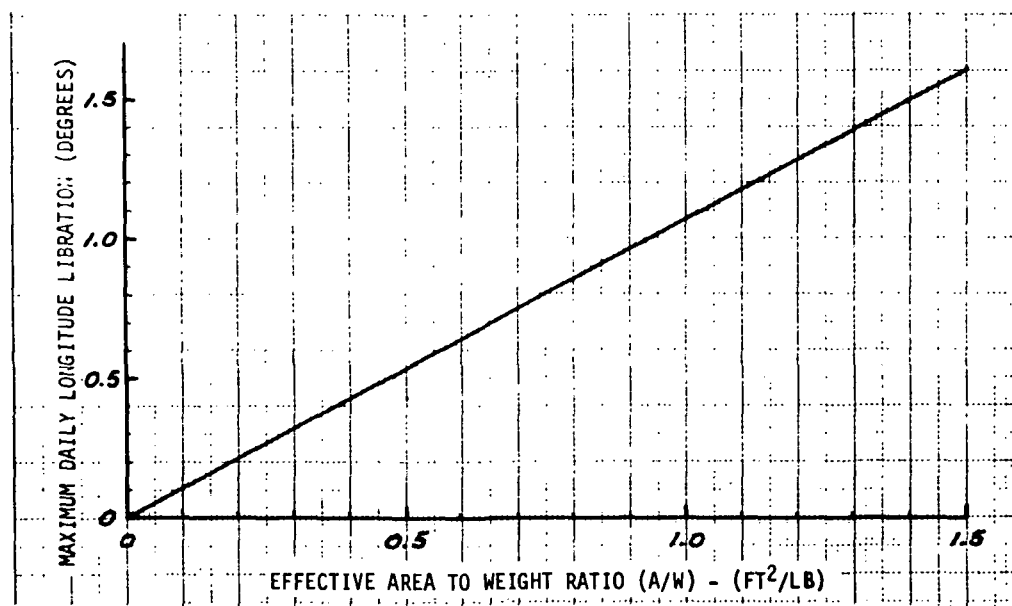


Figure 3.2-17. Daily Longitudinal Libration  
Due to Solar Pressure



The orbit perturbation data presented herein provide a quick-reference tool for mission planning activities. Trends in orbital motions including the effects of initial satellite placement and orbit orientation may be readily derived either directly from the graphical data or from the equations for intermediate parameter values. These data were also utilized in the orbit saturation analyses reported in Volume IV.

### 3.3 MISSION PROFILE CHARACTERISTICS

The overall performance requirements of the systems within a geosynchronous program are, in part, dependent upon the mission profile characteristics. In this context, mission profile characteristics include ascent to geosynchronous orbit, on-orbit operations, and return from geosynchronous orbit. The ascent profile defines, for example, the time from separation of the payload and payload delivery system from the shuttle orbiter until insertion of the payload into the final operational orbit. The ascent profile also defines the number, magnitude, and time-phasing of the major propulsive maneuvers which must be performed by the payload delivery system. The on-orbit operations define, for example, satellite propulsive maneuver requirements to correct orbit perturbations if such corrections are required to satisfy satellite mission objectives and constraints.

This section develops and presents the general characteristics of geosynchronous missions beginning with shuttle lift-off and ending with, for the case of a reusable payload delivery system, return of the system to the shuttle orbiter for subsequent return to earth. Fundamental characteristics are presented as well as the major propulsive maneuver requirements which are imposed on the payload delivery system. In general, the data are presented in parametric form with the final required geosynchronous orbit orientation treated as the principal variable. Based on these data, generalized delta-V budgets are developed for the payload delivery system.

The data contained within this section are presented in sufficiently generalized form to permit the synthesis of a broad family of geosynchronous missions. As a result, the data in this section plus the data contained in Section 3.1, Geosynchronous Orbit Time Histories, and Section 3.2, Orbit Perturbations, provide the fundamental data necessary to define the characteristics of geosynchronous orbits.



## TRAJECTORY PROFILES

The fundamental characteristics of geosynchronous trajectories are presented by major mission phase. Where appropriate, the fundamental relationships defining the trajectory characteristics are developed. In this manner, additional data can be conveniently generated to cover additional cases not specifically discussed in this report.

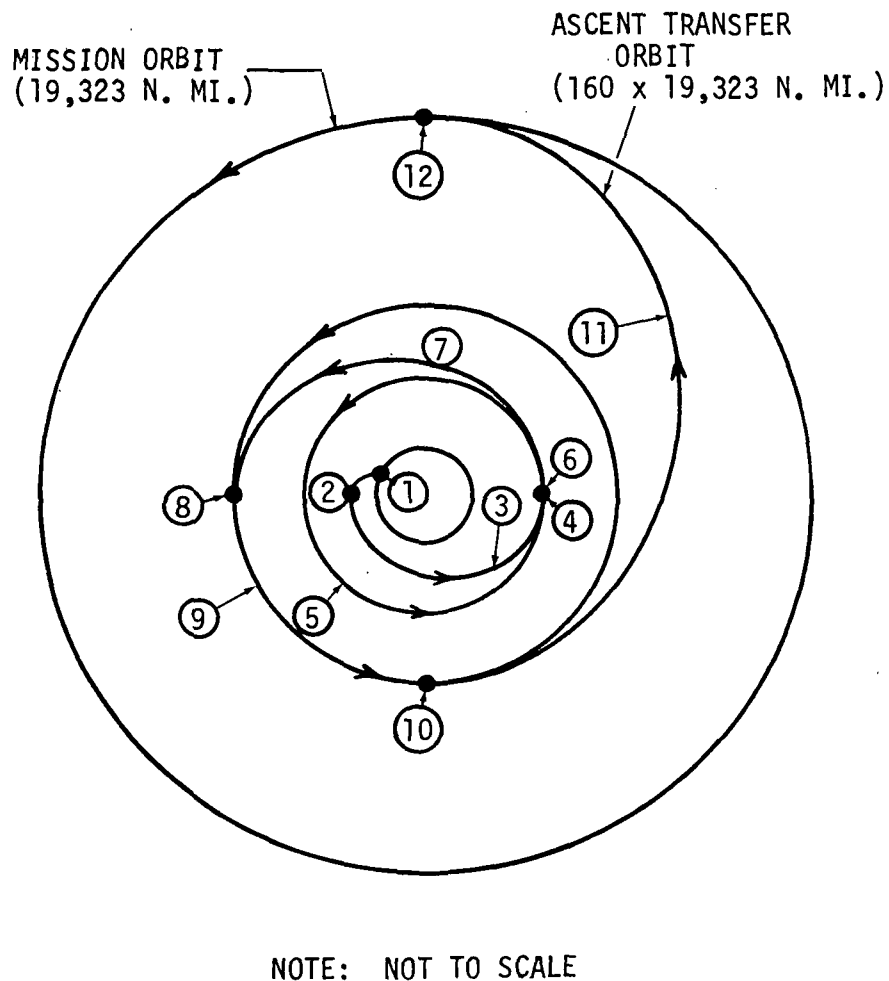
### Ascent Profile (Single Delivery System)

For illustrative purposes, the basic characteristics of a geosynchronous ascent profile utilizing the baseline shuttle and tug discussed in Volume VI are shown in Figure 3.3-1. Also shown in the figure are the major mission events, the time since shuttle lift-off that the events nominally occur, and the mission event duration. The ascent profile begins with shuttle lift-off and is completed following final insertion into the operational geosynchronous orbit. The profile includes, in general, an initial coast period in a low-altitude earth orbit, injection into a phasing orbit for the purpose of achieving the final operational characteristics, and the final insertion into the geosynchronous transfer orbit.

The ground trace of a representative ascent profile which does not include a phasing orbit is illustrated in Figure 3.3-2. For the case shown, it is assumed that the shuttle initially ascends to a 100-nautical mile circular orbit, coasts for approximately one revolution, and then transfers to a 160-nautical mile circular orbit. Separation of the payload and payload delivery system from the shuttle orbiter occurs in the 160-nautical mile circular parking orbit. The payload delivery system then performs a direct injection into the geosynchronous transfer orbit approximately one and one-fourth revolutions after initial insertion into the 160-nautical mile parking orbit.

As can be seen from Figure 3.3-2, the characteristics of the geosynchronous transfer orbit are such that the geographic longitude of the first apogee occurs approximately 101 degrees east of the geographic longitude of perigee. As a result, for this particular mission profile, the final geosynchronous orbit insertion will occur at a geographic longitude of approximately 35 degrees east longitude. If geosynchronous orbit insertion were not performed at first apogee, the vehicle would make one full revolution in a 160 by 19,323-nautical mile elliptic orbit with perigee occurring at approximately 136 degrees east longitude and second apogee occurring approximately 122 degrees west longitude. Additional revolutions would result in a geographic displacement of the possible geosynchronous orbit insertion location of approximately 203 degrees.

The latitude and relative longitude time histories of the geosynchronous transfer orbit are shown in Figure 3.3-3. The transfer orbit characteristics presented in the figure are based on a transfer orbit inclination of 28.5 degrees. The characteristics of the transfer orbit for other inclinations are essentially the same as those presented in the figure; however, the maximum latitude of the ground trace is equal to the inclination of the transfer orbit. There is also some slight change in the relative longitude time history; however, the relative longitude and time at which geosynchronous orbit insertion occurs is the same as that shown in Figure 3.3-3. The altitude, velocity, and flight path angle time histories of the transfer orbit are shown in Figure 3.3-4. These data are independent of the inclination of the transfer orbit.



Seq. No.	Event	Time (Hrs)	Duration (Hrs)
1	Liftoff	0	
2	Shuttle MECO	0.15	
3	Coast to 100 n.mi.		0.73
4	Circularize at 100 n.mi.	0.88	
5	Coast one revolution at 100 n.mi.		1.47
6	100 x 160 n.mi. transfer orbit injection	2.35	
7	Coast to 160 n.mi.		0.74
8	Circularize at 160 n.mi.	3.09	
9	Coast 1-1/4 revolution at 160 n.mi.		1.83
10	Geosynchronous transfer orbit injection	4.92	
11	Coast to apogee		5.27
12	Geosynchronous orbit insertion	10.19	

Figure 3.3-1. Geosynchronous Mission Ascent Profile

3-96

SD 73-SA-0036-3

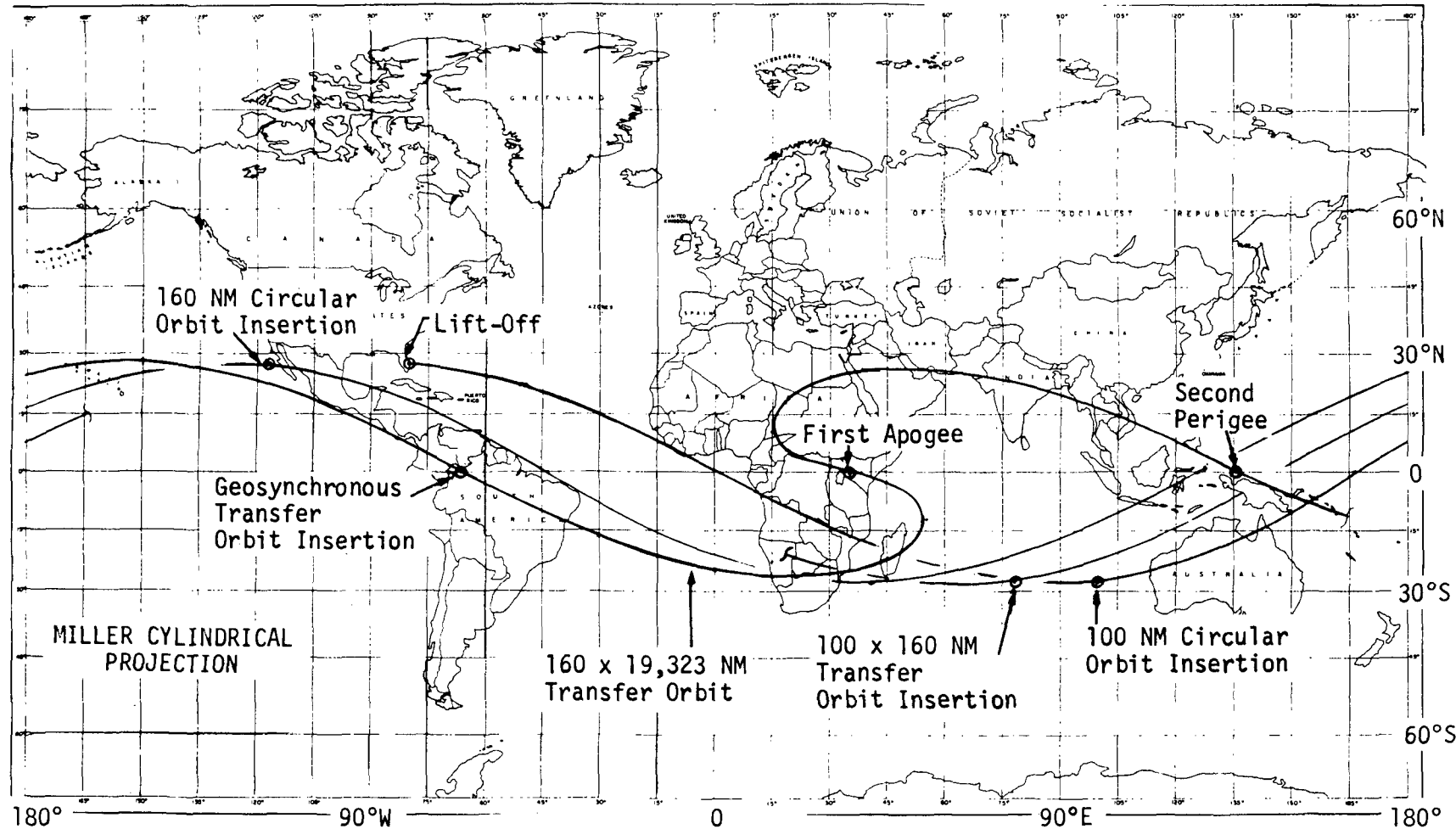


Figure 3.3-2. Geosynchronous Mission Ascent Ground Trace



Space Division  
North American Rockwell

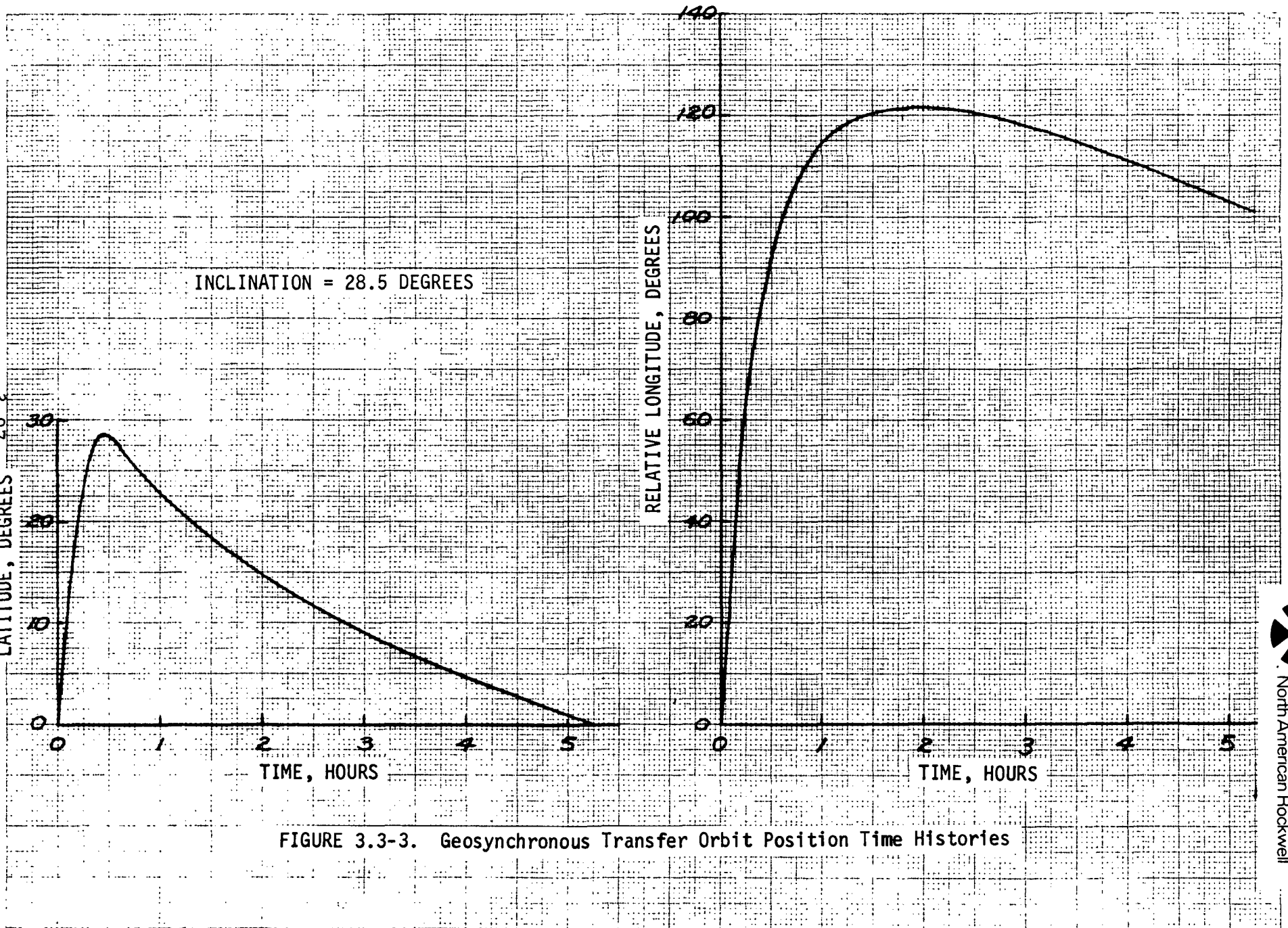


FIGURE 3.3-3. Geosynchronous Transfer Orbit Position Time Histories

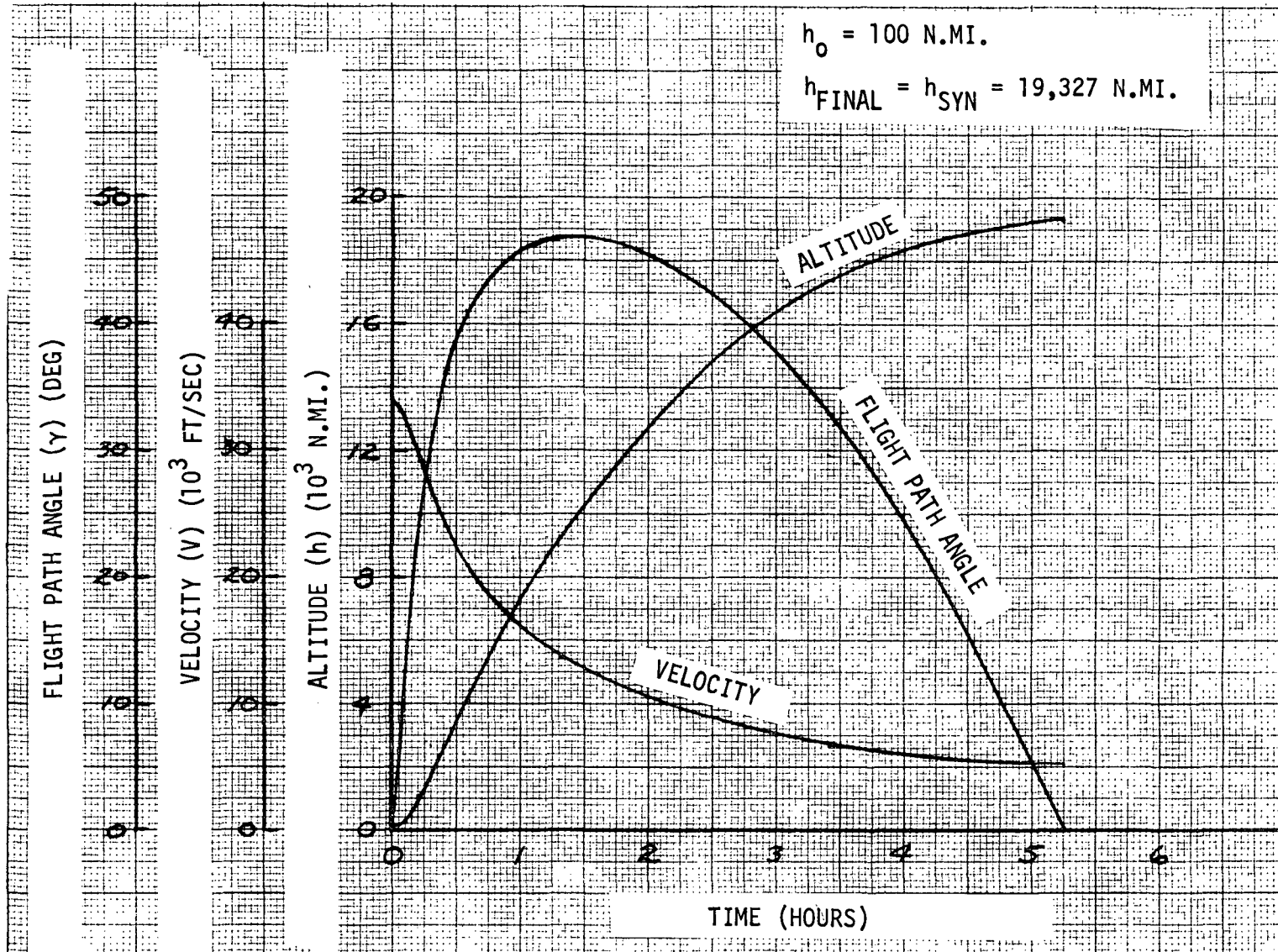


Figure 3.3-4. Geosynchronous Transfer Orbit Time Histories

The propulsive maneuvers which must be performed by the payload delivery system are illustrated in Figure 3.3-5. As stated previously, the shuttle orbiter ascends into an initial low-altitude circular orbit. The payload delivery system must then perform the necessary propulsive maneuvers to deliver the payload to the final operational geosynchronous orbit. As shown in the figure, the payload delivery system performs an initial insertion into a transfer orbit followed by the final insertion into the operational orbit. The total impulsive velocity increment which must be provided by the payload delivery system is given by:

$$\vec{\Delta V}_{tot} = \vec{\Delta V}_p + \vec{\Delta V}_a \quad (3.3-1)$$

where

$\vec{\Delta V}_p$  = the impulsive velocity increment at perigee

$\vec{\Delta V}_a$  = the impulsive velocity increment at apogee

The impulsive velocity increment at perigee is given by

$$\vec{\Delta V}_p = \vec{V}_p - \vec{V}_{c_p}$$

from which

$$\vec{\Delta V}_p = (V_{c_p}^2 + V_p^2 - 2V_{c_p} V_p \cos \epsilon_p)^{1/2} \quad (3.3-2)$$

where

$V_{c_p}$  = the circular orbit speed at the initial circular orbit altitude

$V_p$  = the speed at perigee of the transfer orbit

$\epsilon_p$  = the magnitude of the simultaneous plane change performed at perigee of the transfer orbit

Similarly, the impulsive velocity increment at apogee is given by:

$$\vec{\Delta V}_a = \vec{V}_{c_a} - \vec{V}_a$$

from which

$$\vec{\Delta V}_a = (V_{c_a}^2 + V_a^2 - 2V_{c_a} V_a \cos \epsilon_a)^{1/2} \quad (3.3-3)$$

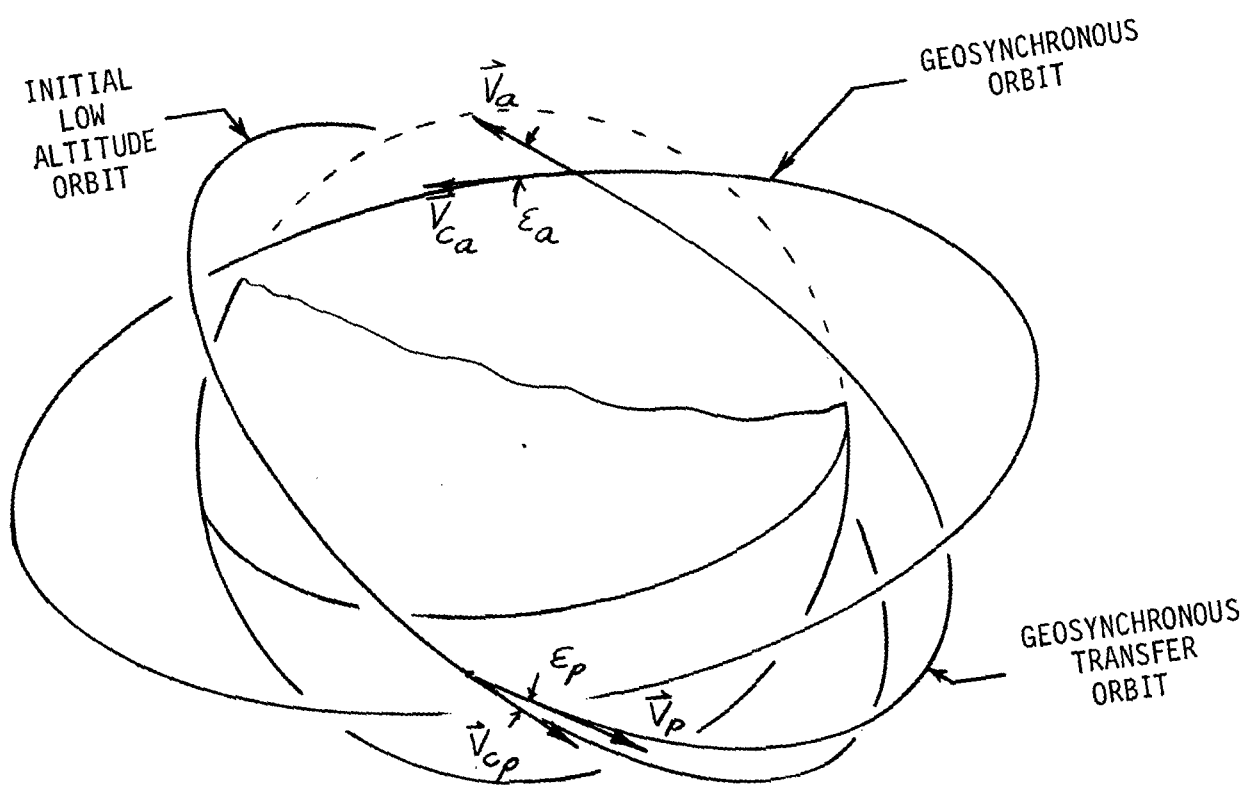


Figure 3.3-5. Geosynchronous Transfer Maneuvers

where

$v_{ca}$  = the circular orbit speed at the final, geosynchronous altitude

$v_a$  = the speed at apogee of the transfer orbit

$\epsilon_a$  = the magnitude of the simultaneous plane change performed at apogee of the transfer orbit

The circular orbit speeds at perigee and apogee are given by:

$$v_{cp} = \sqrt{\frac{\mu}{r_p}} \quad (3.3-4)$$

and

$$v_{ca} = \sqrt{\frac{\mu}{r_a}} \quad (3.3-5)$$

where

$\mu$  = the earth gravitational constant

=  $1.407\ 653\ 192 \times 10^{16}\ \text{ft}^3/\text{sec}^2$

$r_p$  = the transfer orbit perigee radius

= the radius of the initial low-altitude orbit

$r_a$  = the transfer orbit apogee radius

= the geosynchronous radius

=  $1.383\ 342\ 191 \times 10^8\ \text{ft}$

The perigee and apogee speeds of the transfer orbit are given by:

$$v_p = \sqrt{\frac{\mu}{r_p}} \sqrt{\frac{2}{1 + r_p/r_a}}$$

$$v_a = \sqrt{\frac{\mu}{r_a}} \sqrt{\frac{2}{1 + r_a/r_p}}$$

$$V_p = V_{cp} \sqrt{\frac{2}{1 + r_p/r_a}} \quad (3.3-6)$$

$$V_a = V_{ca} \sqrt{\frac{2}{1 + r_a/r_p}} \quad (3.3-7)$$

For an initial low-altitude orbit of 160 nautical miles,

$$r_p = 2.189\ 791\ 680 \times 10^7 \text{ feet}$$

Therefore,

$$V_{cp}]_{160} = 25\ 354 \text{ ft/sec}$$

$$V_p]_{160 \times 19323} = 33\ 316 \text{ ft/sec}$$

$$V_{ca}]_{19323} = 10\ 087 \text{ ft/sec}$$

$$V_a]_{160 \times 19323} = 5\ 274 \text{ ft/sec}$$

Substituting the above values into Equations (3.3-2) and (3.3-3),

$$\Delta V_p]_{160 \times 19323} = (17.423 - 16.894 \cos e_p)^{1/2} (10^4) \quad (3.3-8)$$

$$\Delta V_a]_{160 \times 19323} = (1.296 - 1.064 \cos e_a)^{1/2} (10^4) \quad (3.3-9)$$



As illustrated previously in Figure 3.3-5 and shown in Equations (3.3-2) and (3.3-3), one or more plane change maneuvers must be performed if the inclination of the final geosynchronous orbit is not equal to the inclination of the initial low-altitude shuttle orbit. For one limiting case, no plane change maneuver is performed at perigee ( $\epsilon_p = 0$ ) and the total plane change is performed at apogee ( $\epsilon_a = \epsilon_{TOT}$ ). By distributing the total plane change between perigee and apogee, however, the total impulsive incremental velocity requirement can be minimized. The effects of varying the plane change distribution on the total velocity increment are shown in Figure 3.3-6 for a range of total plane change values. As can be seen from the figure, there exists an initial plane change value ( $\epsilon_p$ ) which minimizes the total impulsive velocity requirement. For a total plane change requirement of 28.5 degrees, the total incremental velocity requirement is minimized by performing a simultaneous plane change/transfer orbit insertion maneuver which includes an initial plane change of approximately 2.2 degrees. The remaining required plane change of 26.3 degrees is performed concurrently with the final orbit insertion maneuver at apogee of the transfer orbit.

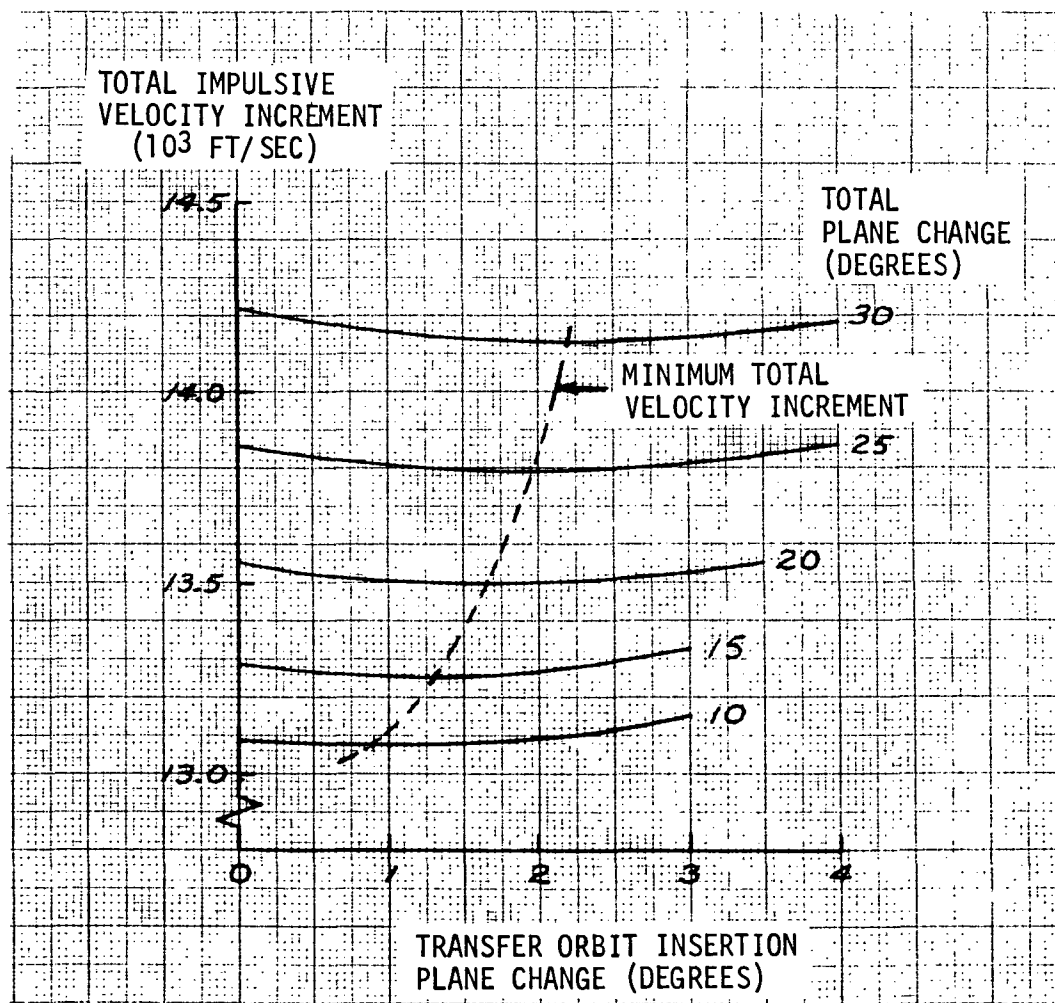


Figure 3.3-6. Distributed Plane Change  
Delta-V Requirements



The resultant incremental velocity requirements are shown in Figure 3.3-7 as a function of the total plane change requirement. Shown in the figure are the velocity requirements at perigee, at apogee, and the total impulsive velocity requirement. The data shown in Figure 3.3-7 defines, therefore, the total impulsive incremental velocity which must be provided by the payload delivery system in order to deliver payloads to circular geosynchronous orbits.

As illustrated previously in Figure 3.3-2, the geographic location at which final geosynchronous orbit insertion will occur is constrained by the characteristics of the ground trace of the initial low-altitude circular orbit and the ground trace characteristics of the geosynchronous transfer orbit. It is necessary, in general, to inject into an intermediate phasing orbit as previously illustrated in Figure 3.3-1. By injecting into the phasing orbit, any final orbit geosynchronous location can be achieved. The required period of the intermediate phasing orbit is shown in Figure 3.3-8 as a function of the incremental geographic longitude required to achieve a given final geosynchronous orbit insertion longitude. As can be seen from the figure, phasing orbit durations of up to 14.25 hours are required in order to achieve any geographic longitude for final geosynchronous orbit insertion and thus establish the stationkeeping position of a geosynchronous satellite. Following geosynchronous orbit insertion, the ground trace of the geosynchronous satellite will be as previously discussed in Section 3.1, Geosynchronous Orbit Time Histories.

#### Ascent Profile (Dual Reusable Tug)

An alternate typical ascent profile involves the use of two reusable space tugs operating in series. The fundamental characteristics of this dual reusable tug ascent profile are shown in Figure 3.3-9. The ascent profile is initiated by the launch of two shuttles; each carrying a tug and, in general, a mission-related payload. On-orbit assembly is then performed in a low-altitude earth orbit resulting in the payload and dual tug delivery system configuration illustrated in Figure 3.3-9. In the general case, the first tug (Tug A) performs the phasing orbit insertion maneuver plus part of the insertion into the geosynchronous transfer orbit. Prior to completing the geosynchronous transfer orbit insertion maneuver, the two tugs separate, Tug B completes the insertion maneuver, and Tug A performs a series of maneuvers resulting in the return of Tug A to Shuttle A for recovery and return to earth. The percentage of the total delta-V for the geosynchronous transfer orbit insertion maneuver performed by Tug A is, for a given tug design, dependent upon the total payload weight and the propellant loadings of each tug.

The major mission-related velocity increments which must be provided in the dual tug ascent mode are illustrated in Figure 3.3-10. Assuming impulsive velocity increments, the total incremental velocity which must be provided by Tug A and Tug B at perigee is given by

$$\vec{\Delta V}_{PA} + \vec{\Delta V}_{PB} = \vec{\Delta V}_P \quad (3.3-10)$$

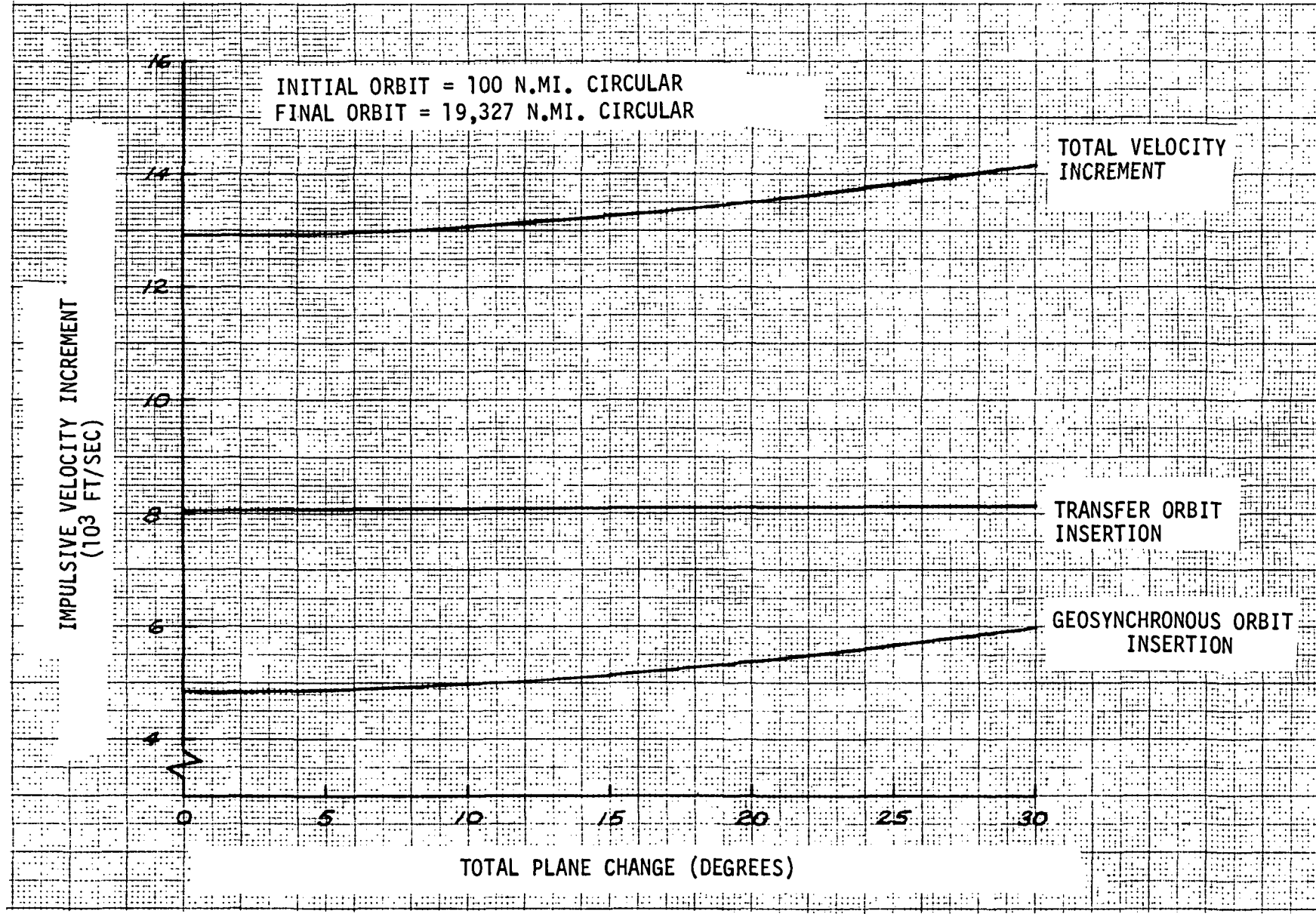


Figure 3.3-7. Geosynchronous Transfer Incremental Velocity Requirements

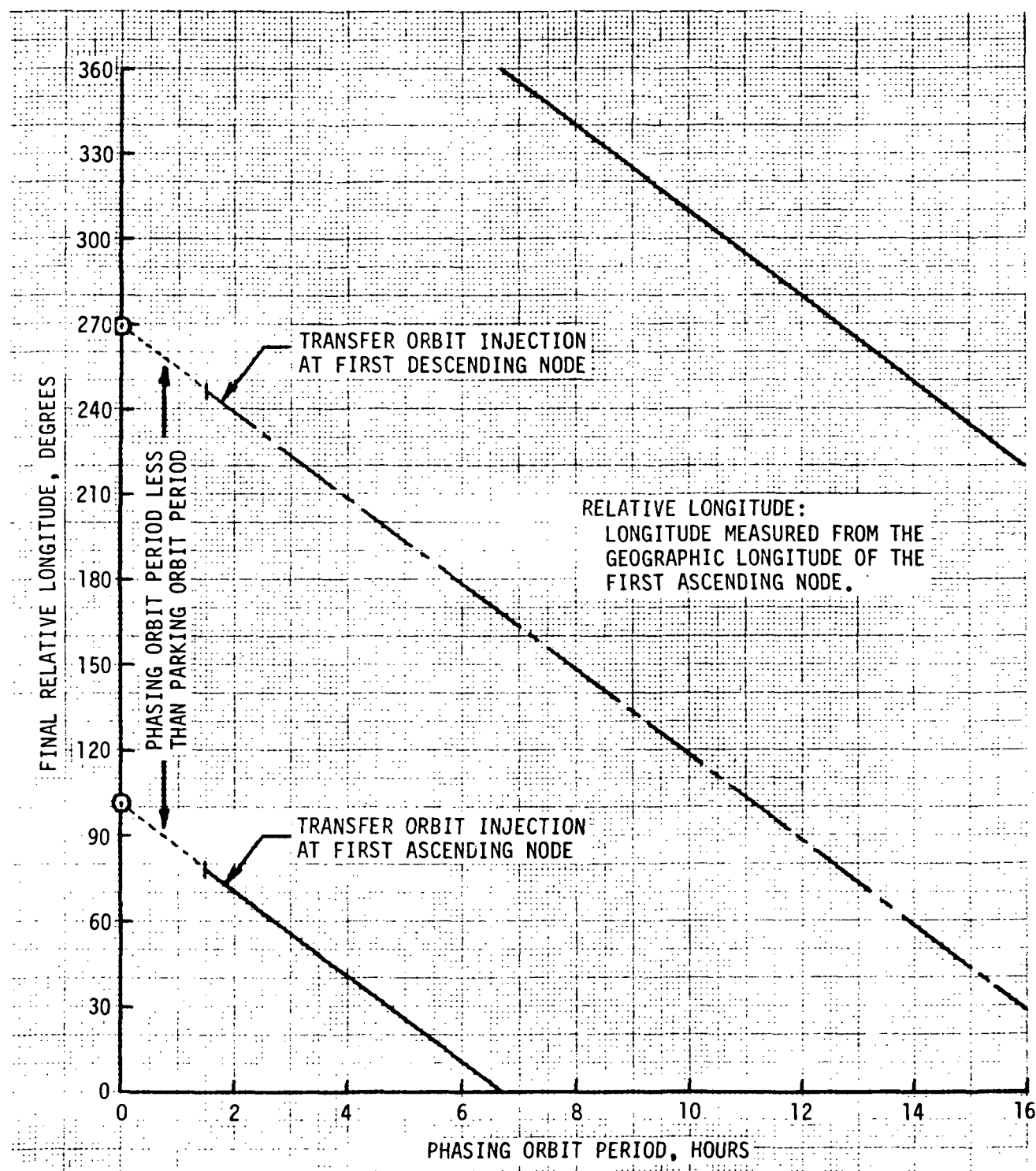


Figure 3.3-8. Ascent Phasing Time Requirements

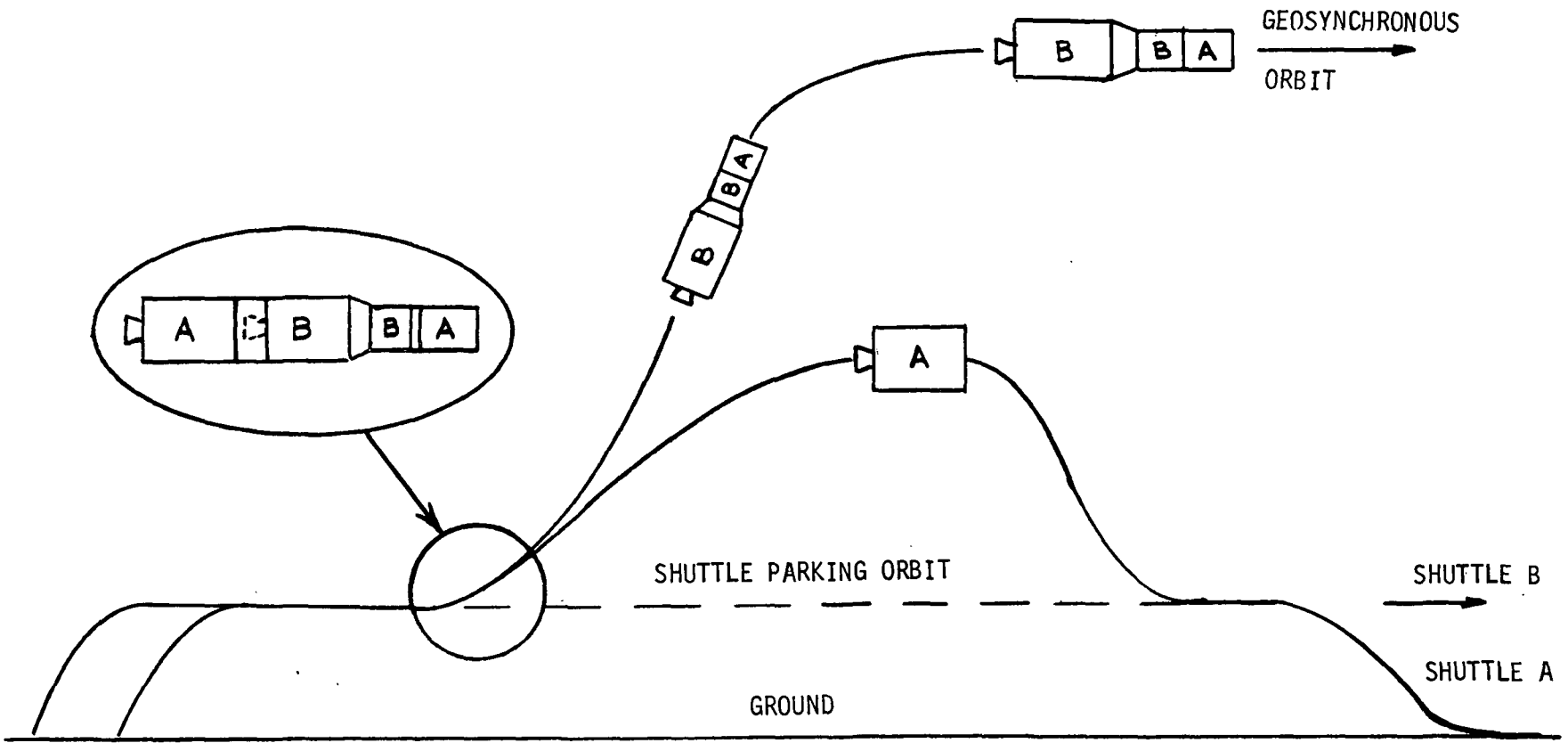


Figure 3.3-9. Dual Reusable Tug Ascent Profile

3-107

SD 73-SA-0036-3

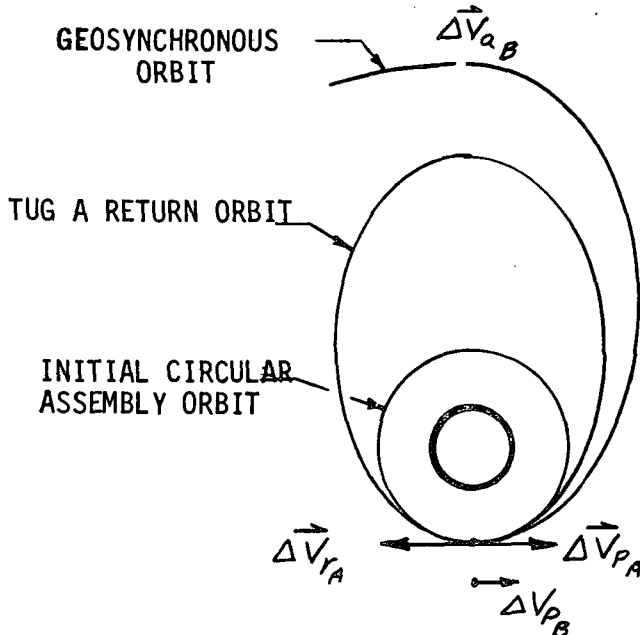


Figure 3.3-10. Dual Tug Incremental Velocities

where

$\vec{\Delta V}_{PA}$  = the initial transfer orbit insertion delta-V provided by Tug A

$\vec{\Delta V}_{PB}$  = the remaining transfer orbit insertion delta-V provided by Tug B

$\vec{\Delta V}_P$  = the total delta-V required to perform the transfer orbit insertion maneuver

= the impulsive velocity increment at perigee  
(Equation 3.3-1)

By assuming that the magnitude of the impulsive velocity increment required to return Tug A to Shuttle A is equal to the magnitude of the initial mission velocity increment provided by Tug A ( $|\vec{\Delta V}_{pA}|$ ) plus an additional velocity increment for orbit correction and plane change maneuvers, a closed form solution can be obtained for the initial velocity increment which can be provided by Tug A. That is, let the magnitude of the total velocity increment required to return Tug A ( $\Delta V_{rA}$ ) be given by

$$\Delta V_{TA} = \Delta V_{PA} + \Delta V_{RENO} \quad (3.3-11)$$

where

$\Delta V_{RENO}$  the sum of all velocity increments required by Tug A for orbit correction and plane change maneuvers

For impulsive  $\Delta V$ 's,

$$\Delta V_i = I_{sp} g \ln \mu_i \quad (3.3-12)$$

where

$\Delta V_i$  = the impulsive velocity increment (ft/sec)

$I_{sp}$  = the stage specific impulse (sec)

$g$  = the earth gravitational acceleration constant (ft/sec<sup>2</sup>)  
= 32.174 ft/sec<sup>2</sup>

$\mu_i$  = the ratio of the total weight prior to performing  $\Delta V_i$  to the end-boost weight

$$= \frac{W_{INITIAL}}{W_{END-BOOST}}$$

From Equations (3.3-11) and (3.3-12),

$$\mu_{TA} = EXP[(\Delta V_{PA} + \Delta V_{RENO}) / I_{sp} g]$$

$$= [EXP(\Delta V_{PA} / I_{sp} g)] [EXP(\Delta V_{RENO} / I_{sp} g)]$$

$$\mu_{TA} = (\mu_{PA})(\mu_{RENO}) \quad (3.3-13)$$

However, from the definition of

$$\mu_A = \frac{W_{STGA} + W_{PROPA}}{W_{STGA}} \quad (3.3-14)$$

where

$W_{PROPA}$  = the propellant required by Tug A to perform the maneuvers for return to Shuttle A

$W_{STGA}$  = the burnout weight of Tug A

Also,

$$\mu_A = \frac{W_0}{W_0 - W_{PROPA}} \quad (3.3-15)$$

where

$W_{PROPA}$  = the propellant available in Tug A for initiating the geosynchronous transfer orbit insertion maneuver

$W_0$  = the total weight prior to initiating the insertion into the geosynchronous transfer orbit

For a given geosynchronous mission

$$W_0 = W_{STGA} + W_{PROPA} + W_{STGB} + W_{PROPB} + W_{PL} \quad (3.3-16)$$

where, in addition to the previous definitions,

$W_{STGB}$  = the burnout weight of Tug B

$W_{PROPB}$  = the total usable propellant in Tug B

$W_{PL}$  = the total payload weight

By combining Equations (3.3-13) through (3.3-15)

$$\frac{W_{STGA} + W_{PROPrA}}{W_{STGA}} = \left( \frac{W_0}{W_0 - W_{PROPrA}} \right) (\mu_{RENO})$$

Since

$$W_{PROPrA} = W_{PA} + W_{rA}$$

then

$$\frac{W_{STGA} + W_{PROPrA}}{W_{STGA}} = \left( \frac{W_0}{W_0 + W_{PROPrA} - W_{PROPrA}} \right) (\mu_{RENO}) \quad (3.3-17)$$

For a given geosynchronous mission, all terms in Equation (3.3-17) are known except the propellant required by Tug A for return to Shuttle A ( $W_{PROPrA}$ ). Solving Equation (3.3-17),

$$\begin{aligned} W_{PROPrA} &= -\left(\frac{1}{2}\right)(W_0 + W_{STGA} - W_{PROPrA}) \\ &\quad + \left(\frac{1}{2}\right)\left\{(W_0 + W_{STGA} - W_{PROPrA})^2 \right. \\ &\quad \left. - 4[(1-\mu_{RENO})W_0 - W_{PROPrA}]W_{STGA}\right\}^{1/2} \end{aligned} \quad (3.3-18)$$

The magnitude of the initial mission incremental velocity provided by Tug A is then determined from Equations (3.3-11), (3.3-12) and (3.3-14) as



$$\Delta V_{PA} = I_{sp} g \ln \left[ \frac{W_{STGA} + W_{PROPA}}{W_{STGA}} \right] - \Delta V_{REND} \quad (3.3-19)$$

Then, from Equation (3.3-10), the magnitude of the remaining velocity increment which must be provided by Tug B at insertion into the geosynchronous transfer orbit is given by

$$\Delta V_{PB} = \Delta V_p - \Delta V_{PA} \quad (3.3-20)$$

### Descent Profile

The descent trajectory profile characteristics are essentially the inverse of the ascent profiles shown in the previous discussion of the ascent profiles for single delivery systems. The impulsive incremental velocity requirements for injection into a descent transfer orbit are equal to the delta-V requirements for initial insertion into the geosynchronous orbit. Also, the incremental velocity requirements for injection into a low-altitude orbit for recovery of a reusable payload delivery system are equal to the initial requirements for insertion into the geosynchronous transfer orbit. Therefore, the incremental velocity requirements which have been previously discussed for the ascent profiles are equally applicable to the descent profile of a reusable payload delivery system (e.g., a reusable tug).

The characteristics of the descent profile in terms of altitude, velocity, and flight path angle are also, by symmetry, equal to the inverse of the data previously presented in Figure 3.3-4. In addition, the latitude and relative longitude time histories shown in Figure 3.3-3 are also equivalent to the inverse of the latitude and relative longitude time histories of the descent profile. This effect can be seen by examining Figure 3.2-2 which shows the trace of a 160 by 19,323-nautical mile elliptic orbit which has first perigee at a longitude of approximately 65 degrees west, apogee at approximately 35 degrees east, and second perigee at approximately 136 degrees east longitude. The ground trace of a descent trajectory would be equivalent to the ground trace shown from first apogee to second perigee. Upon reaching perigee, the reusable payload delivery system injects into a circular orbit for subsequent recovery and return to earth using a shuttle orbiter.

### On-Orbit Operations

There are two basic types of on-orbit maneuvers which must be performed by the geosynchronous program systems. The first are those maneuvers which must be performed by the space transportation system (e.g., space tug) for the placement and/or servicing of multiple geosynchronous satellites which have a phase angle separation. The second maneuvers are those necessary to perform plane changes either by the geosynchronous satellite for correcting the effects of luni-solar perturbations or by the space transportation system

for performing plane change maneuvers when servicing multiple geosynchronous satellites which do not have the same orbit orientation.

The characteristics of the in-plane phasing requirements and the associated impulsive incremental velocity requirements are shown in Figure 3.3-11. The required phasing is achieved by modifying the time required to make one full revolution and is established as follows. Let  $\Delta\theta$  equal the desired phase change angle. Then, for interior phasing, the period of the phasing orbit is given by

$$\rho_{\phi I} = \frac{360 - \Delta\theta}{\pi} \quad (3.3-21)$$

where

- $\pi$  = the mean orbital motion
- = 15.041 067 degrees per mean solar hour

The period of the phasing orbit is also defined by

$$\rho_{\phi I} = 2\pi \sqrt{\frac{a_{\phi I}^3}{\mu}}$$

from which

$$a_{\phi I} = \left[ \mu \left( \frac{\rho_{\phi I}}{2\pi} \right)^2 \right]^{1/3} \quad (3.3-22)$$

where

- $a_{\phi I}$  = the semi-major axis of the interior phasing orbit
- $\mu$  = the earth gravitational constant
- = 1.407 653 92  $\times 10^{16}$  ft<sup>3</sup>/sec<sup>2</sup>

Combining Equations (3.3-21) and (3.3-22) in terms of consistent units:

$$a_{\phi I} = \left\{ \mu \left[ \left( \frac{1800}{\pi} \right) \left( \frac{360 - \Delta\theta}{\pi} \right) \right]^2 \right\}^{1/3} \quad (3.3-23)$$

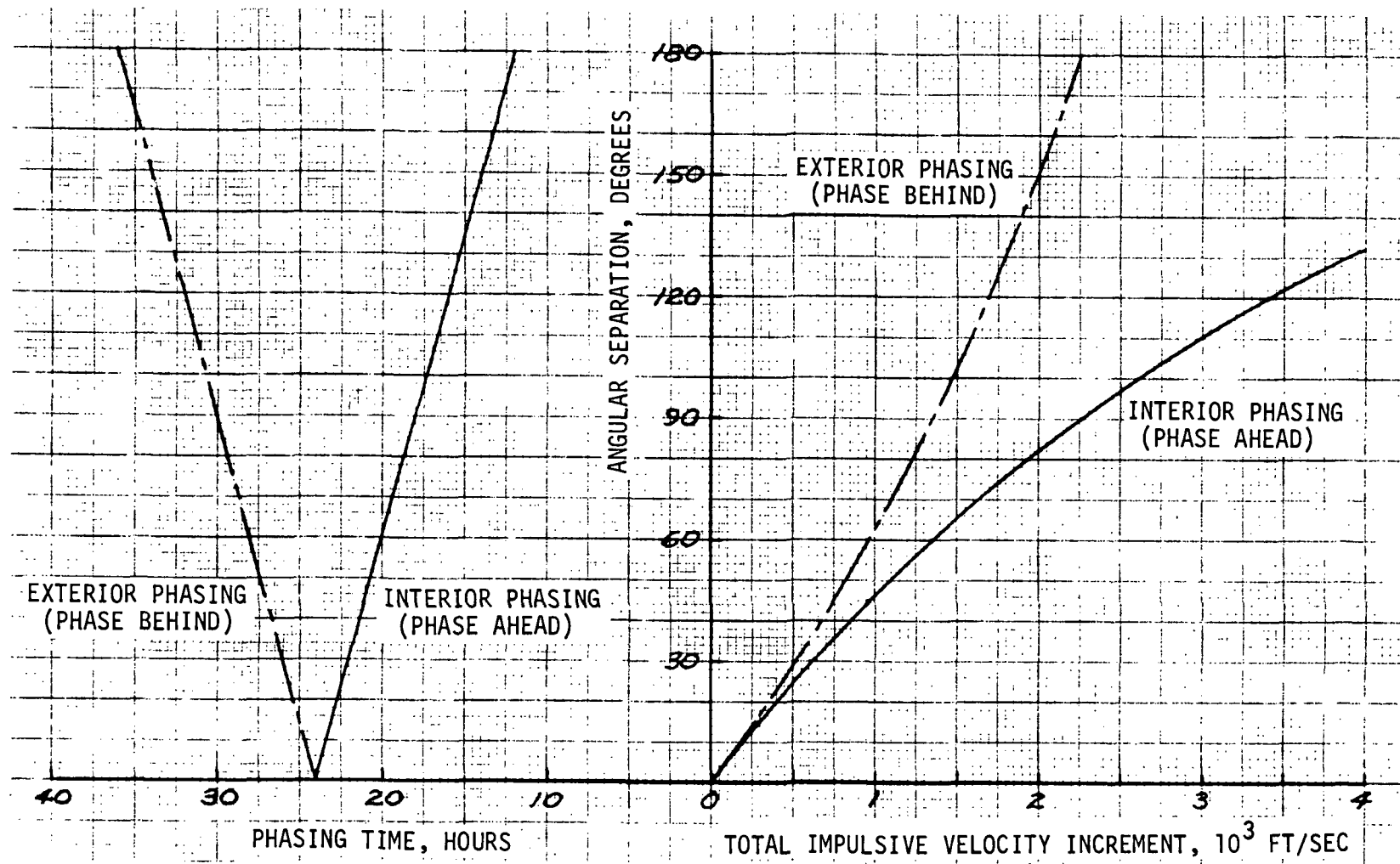


Figure 3.3-11. On-Orbit Phasing Requirements

The interior phasing orbit semi-major axis is defined as

$$a_{\phi I} = \frac{r_{a\phi} + r_{p\phi}}{2}$$

from which

$$r_{p\phi} = 2a_{\phi I} - r_{a\phi} \quad (3.3-24)$$

where

- $r_{a\phi}$  = the apogee radius of the phasing orbit
- = the geosynchronous orbit radius for interior phasing
- =  $r_{syn} = 1.383\ 342\ 191 \times 10^8$  feet
- $r_{p\phi}$  = the perigee radius of the phasing orbit

Having defined the period and the perigee radius of the interior phasing orbit, the required total impulsive velocity increment for insertion into the phasing orbit plus returning to a geosynchronous orbit is given by

$$\Delta V_{\phi I} = 2(V_{syn} - V_{a\phi}) \quad (3.3-25)$$

where

- $V_{syn}$  = the geosynchronous circular orbit speed
- $V_{a\phi}$  = the apogee speed of the elliptic phasing orbit

As previously defined, the geosynchronous circular orbit speed is given by:

$$V_{syn} = \sqrt{\frac{\mu}{r_{syn}}} \quad (3.3-26)$$

Also, the speed at apogee of the interior phasing orbit is given by:

$$V_{a\phi} = \sqrt{\frac{\mu}{r_{syn}}} \sqrt{\frac{2}{1 + r_{syn}/r_{p\phi}}} \quad (3.3-27)$$



Substituting into Equation (3.3-25), the total impulsive velocity requirement is then given by

$$\Delta V_{\phi I} = 2 \sqrt{\frac{\mu}{r_{SYN}}} \left( 1 - \sqrt{\frac{2}{1 + r_{SYN}/r_{P\phi}}} \right)$$

or, for  $V_{syn} = 10,087$  ft/sec,

$$\Delta V_{\phi I} = (20,174) \left( 1 - \sqrt{\frac{2}{1 + r_{SYN}/r_{P\phi}}} \right) \quad (3.3-28)$$

From the definition of interior phasing given in Equation (3.3-21), it can be seen that a space transportation system will, after one revolution in the phasing orbit, be "ahead" of a satellite which remains in the initial geosynchronous orbit by the phase change angle  $\Delta\theta$ . In a manner analogous to that presented above, the total impulsive velocity increment required for exterior phasing can be developed. Such phasing will cause the space transportation system to be, after one full revolution, "behind" a satellite which remained in the initial geosynchronous orbit. The required total impulsive velocity is defined by the following expressions:

$$\Delta V_{\phi E} = 2 \sqrt{\frac{\mu}{r_{SYN}}} \left( \sqrt{\frac{2}{1 + r_{SYN}/r_{a\phi}}} - 1 \right) \quad (3.3-29)$$

$$r_{a\phi} = 2a_{\phi E} - r_{SYN} \quad (3.3-30)$$

and

$$a_{\phi E} = \left\{ \mu \left[ \left( \frac{1800}{\pi} \right) \left( \frac{360 + \Delta\theta}{\pi} \right) \right]^2 \right\}^{1/3} \quad (3.3-31)$$



where, in addition to the previously defined terms,

$a_{\phi e}$  = the semi-major axis of the exterior phasing orbit

$r_{ap}$  = the apogee radius of the exterior phasing orbit

The impulsive incremental velocity requirements for pure plane change maneuvers ( $\Delta V_{pc}$ ) is given by:

$$\Delta V_{pc} = 2V_{syn} \sin\left(\frac{\epsilon}{2}\right) \quad (3.3-32)$$

where

$\epsilon$  = the magnitude of the plane change maneuver

The resultant impulsive velocity requirements are shown in Figure 3.3-12 as a function of the magnitude of the plane change. As can be seen from the figure, the magnitude of the velocity requirement is essentially linear for small plane change angles. From Equation (3.3-32)

$$\Delta V_{pc} \approx (V_{syn})(\epsilon) \quad (3.3-33)$$

for small values of  $\epsilon$ . Therefore,

$$\Delta V_{pc} \approx (10087)\left(\frac{\pi}{180}\right)(\epsilon)$$

from which

$$\Delta V_{pc} \approx 176 \text{ ft/sec/deg.} \quad (3.3-34)$$

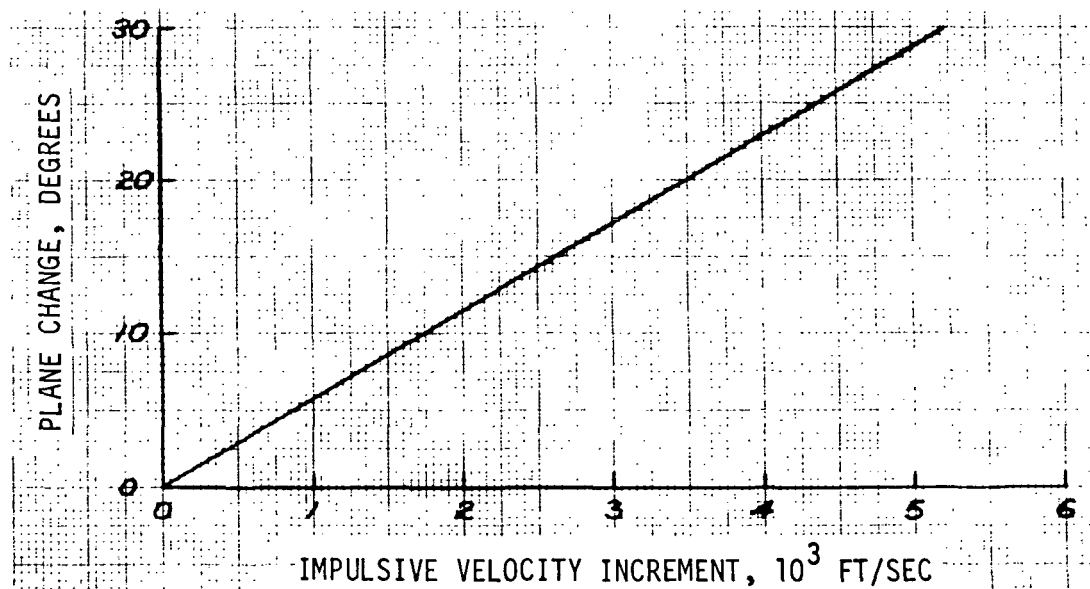


Figure 3.3-12. Plane Change Delta-V Requirements



## DELTA-V BUDGETS

A family of payload delivery system delta-V budgets was developed based primarily on the performance requirements shown in the previous section. The delta-V budgets include the impulsive incremental velocity requirements discussed previously plus estimates of the losses due to finite burning. In addition, the incremental velocity requirements for performing maneuvers such as midcourse corrections, payload/delivery system separation, and payload/delivery system rendezvous and docking are included. As a result, the budgets are considered to be defined in sufficient detail to permit the conduct of preliminary delivery system performance analyses. The delta-V budgets presented are, in general, based on the use of a reusable space tug since missions involving the tug impose the most demanding requirements in terms of the number and variety of maneuvers required. The budgets are applicable, however, to all payload delivery systems by selection of the appropriate incremental velocities for a given mission.

The first budget, presented in Table 3.3-1, defines the delta-V requirements for delivery of payloads to a 28.5-degree inclination geosynchronous orbit using a single payload delivery system. The corresponding delta-V budget for delivery of payloads to a geosynchronous equatorial orbit is presented in Table 3.3-2. The additional incremental velocity requirements which must be accounted for when considering the effects of finite burning and the required midcourse correction delta-V's are also shown in the budgets. For the purpose of conducting performance calculations, an equivalent main propulsion system (MPS) delta-V budget has been defined for the space tug. As noted in the tables, the major propulsive maneuvers are performed by the tug MPS and the relatively small midcourse correction and separation maneuvers are performed by the tug auxiliary propulsion system (APS). Based on a MPS specific impulse ( $I_{sp}$ ) of 470 seconds and an APS specific impulse of 380 seconds, the APS delta-V requirements were translated into an equivalent MPS delta-V. In this manner, the total available space tug propellant could be treated as mission propellant and the propellant requirements, and thus the tug payload capability, could be determined by considering only the equivalent MPS delta-V budget.

The gravity losses which are shown in the tables are based on analyses performed during the Tug Operations and Payload Support Study (Reference 3-5) conducted by Rockwell for MSFC (Contract NAS8-28876). The losses are, in general, applicable to other payload delivery systems with equivalent propulsion system specific impulse values and initial thrust-to-weight ratios.

The second set of delta-V budgets, presented in Tables 3.3-3 and 3.3-4, are for a dual reusable tug. The delta-V requirements are identified by individual tug (Tug A and Tug B). Table 3.3-3 is for a final geosynchronous orbit with an inclination of 28.5 degrees, while Table 3.3-4 is for a geosynchronous equatorial orbit.

The descent delta-V budgets for a reusable payload delivery system are shown in Tables 3.3-5 and 3.3-6. As can be seen from the tables, the impulsive incremental velocity requirements for the major maneuvers are the same as those previously shown in the ascent delta-V budgets. The only differences in the delta-V budgets are the gravity losses and the APS maneuver requirements.

Table 3.3-1. Single Tug Ascent Delta-V Budget  
(Inclination = 28.5 degrees)

Mission Event	Delta-V (ft/sec)		
	MPS	APS	MPS Equiv.
Separate from Orbiter		10	12
Transfer Orbit Insertion (Plane Change = 0 degrees)	7962		8272
Gravity Losses	310		
Midcourse Correction		50	
Geosynchronous Orbit Insertion (Plane Change = 0 degrees)	4814		4923
Gravity Losses	10	30	
Orbit Trim			

Table 3.3-2. Single Tug Ascent Delta-V Budget  
(Geosynchronous Equatorial Orbit)

Mission Event	Delta-V (ft/sec)		
	MPS	APS	MPS Equiv.
Separate from Orbiter		10	12
Transfer Orbit Insertion (Plane Change = 2.2 degrees)	8040		8350
Gravity Losses	310		
Midcourse Correction		50	
Geosynchronous Orbit Insertion (Plane Change = 26.3 degrees)	5847		5956
Gravity Losses	10	30	
Orbit Trim			

Table 3.3-3. Dual Tug Ascent/Return Delta-V Budget for Performance Calculations  
( $i = 28.5$  degrees)

Mission Phase	Tug	Mission Event	Delta-V (ft/sec)		
			MPS	APS	MPS Equivalent
On-Orbit Assembly	B	Separate from orbiter Dock with Tug		10 10	24
	A	Separate from orbiter		10	12
Geosynchronous Transfer Orbit Insertion	A and B	Transfer orbit insertion (plane change = 0 degree) Gravity losses	7962 310		8272
Tug A Return to Shuttle A	A	Separate from Tug B Apogee burn to correct perigee Circularize at perigee Gravity losses Plane change Terminal rendezvous (backup) Dock (backup)	110 $\Delta V_{PA}$ 25 598 100	10 15 10	$\Delta V_{PA}$ plus 876
Ascent to Geosynchronous Orbit	B	Midcourse correction Geosynchronous orbit insertion (plane change = 0 degree) Gravity losses Orbit trim	4814 10	50 30	4923

NOTES:

1. Tug A = First Stage of Dual Tug  
Tug B = Second Stage of Dual Tug (See Figure 3.3-9)
2.  $\Delta V_{MPS} = \Delta V_{MPS} + \left( \frac{I_{SP-MPS}}{I_{SP-APS}} \right) (\Delta V_{APS})$   
 $I_{SP-MPS}$  = MPS Specific Impulse = 470 seconds  
 $I_{SP-APS}$  = APS Specific Impulse = 380 seconds
3.  $\Delta V_{PA}$  = The initial transfer orbit insertion delta-V provided by Tug A.

Table 3.3-4. Dual Tug Ascent/Return Delta-V Budget (Geosynchronous Equatorial Orbit) for Performance Calculations

Mission Phase	Tug	Mission Event	Delta-V (ft/sec)		
			MPS	APS	MPS Equivalent
On-Orbit Assembly	B	Separate from orbiter Dock with Tug A		10 10	24
	A	Separate from orbiter		10	12
Geosynchronous Transfer Orbit Insertion	A and B	Transfer orbit insertion (plane change = 2.2 degrees) Gravity losses	8040 310		8350
Tug A Return to Shuttle A	A	Separate from Tug B Apogee burn to correct perigee Circularize at perigee Gravity losses Plane change Terminal rendezvous (backup) Dock (backup)	110 $\Delta V_{PA}$ 25 598 100	10 15 10	$\Delta V_{PA}$ Plus 876
Ascent to Geosynchronous Orbit	B	Midcourse correction Geosynchronous equatorial orbit insertion (plane change = 26.3 degrees) Gravity losses Orbit trim	5847 10	50 30	5956

NOTES:

1. Tug A = First Stage of Dual Tug  
Tug B = Second Stage of Dual Tug (See Figure 3.3-9)
2.  $\Delta V_{MPS} = \Delta V_{MPS} + \left( \frac{I_{SP-MPS}}{I_{SP-APS}} \right) (\Delta V_{APS})$   
 $I_{SP-MPS}$  = MPS Specific Impulse = 470 seconds  
 $I_{SP-APS}$  = APS Specific Impulse = 380 seconds
3.  $\Delta V_{PA}$  = The initial transfer orbit insertion delta-V provided by Tug A.



Table 3.3-5. Reusable Tug Descent Delta-V Budget  
( $i = 28.5$  deg)

Mission Event	Delta-V (ft/sec)		
	MPS	APS	MPS Equivalent
Transfer orbit insertion Gravity losses	4,814 7		4,821
Midcourse correction		10	12
Phasing orbit insertion and circularization Gravity losses	7,962 24		7,986
Midcourse correction		50	
Backup rendezvous	100	25	193

Table 3.3-6. Reusable Tug Descent Delta-V Budget  
(Geosynchronous Equatorial Orbit)

Mission Event	Delta-V (ft/sec)		
	MPS	APS	MPS Equivalent
Transfer orbit insertion Gravity losses	5,847 7		5,854
Midcourse correction		10	12
Phasing orbit insertion and circularization Gravity losses	8,040 24		8,064
Midcourse correction		50	
Backup rendezvous	100	25	193

Prior to initiating the descent maneuver, the weight of the delivery system is considerably reduced over that prior to the final geosynchronous orbit insertion maneuver. Therefore, the propellant requirements to perform a given delta-V, the resultant burn time, and the gravity losses associated with these maneuvers are reduced. Also included in the descent delta-V budget is an allocation for backup rendezvous of the tug with a shuttle in a low-altitude recovery orbit in the event that the shuttle cannot perform the necessary maneuvers. This backup rendezvous delta-V includes a 100 ft/sec MPS delta-V plus an additional 25 ft/sec APS delta-V resulting in an equivalent MPS delta-V of 131 ft/sec.

A representative set of delta-V requirements for on-orbit maneuvering by a reusable payload delivery system is shown in Table 3.3-7. Included in the table are delta-V's for separation of the tug from the payload, phasing orbit insertion and return to a geosynchronous orbit, midcourse corrections, and rendezvous and docking. In general, with the exception of the phasing orbit maneuvers, the delta-V's must be satisfied by the auxiliary propulsion system. As was the case in the previous tables, an equivalent MPS delta-V is identified again based on a specific impulse of 470 seconds for the MPS and 380 seconds for the APS.

Table 3.3-7. On-Orbit Maneuver Delta-V Budget

Mission Event	Delta-V (ft/sec)		
	MPS	APS	MPS Equiv.
Tug/Payload Separation		10	12
Phasing Orbit Insertion	(1)		
Midcourse Correction		10	12
Geosynchronous Orbit Insertion	(1)		
Rendezvous with Payload	100	10	102
Dock with Payload		15	18
(1) $\Delta V_{TOT} \approx 18.7$ ft/sec per degree of phasing per revolution. (See Figure 3.3-11)			

#### 4.0 RELATED ORBIT CHARACTERISTICS

An examination was made of related orbits for the purpose of supporting the assessment of the desirability and/or feasibility of using orbits other than circular "24-hour" orbits. This section summarizes the significant characteristics of these orbits. For the purposes of this documentation, "related orbits" are defined as orbits other than circular "24-hour" orbits. In this context, related orbits include "24-hour" eccentric orbits as well as orbits which have periods which are an integer multiple of 24 hours.

The method of presentation in this section is to show only the changes in the fundamental relationships developed in Section 3.0, Geosynchronous Orbit Characteristics, which are necessary to define the characteristics of related orbits. Therefore, reference is made to equations and figures previously shown in Section 3.0. In this manner, the derivations of the fundamental relationships are not repeated and only the additional relationships required to define related orbits are developed.

**Page intentionally left blank**

**Page intentionally left blank**

## 4.1 RELATED ORBIT GEOMETRIC CHARACTERISTICS

The fundamental characteristics of related orbits are, as previously discussed in Section 3.1, Geosynchronous Orbit Time Histories, defined by and/or derived from the orbit ground trace time histories. The fundamental relationships defining the ground trace characteristics of related orbits are the same as those previously presented under Ground Trace Characteristics of geosynchronous orbits. The fundamental difference being that the position of the satellite as a function of time with respect to the orbit ascending node is no longer a linear function of the mean orbital motion ( $\eta$ ). In order to determine the position of the spacecraft ( $\theta$ ) with respect to the ascending node, it is necessary to define the spacecraft true anomaly in terms of time since perigee. The time since perigee is defined by

$$\epsilon = \frac{M}{\eta} \quad (4.1-1)$$

where

$M$  = the mean anomaly; measured from perigee

$\eta$  = the mean orbital motion

From Equation (4.1-1)

$$M = \eta t \quad (4.1-2)$$

However,

$$M = E - e \sin E \quad (4.1-3)$$

where

$E$  = the eccentric anomaly

$e$  = the orbit eccentricity

Several methods exist for solving Equation (4.1-3) for  $E$  and one of the simplest is the method of differential corrections given in Reference 4-1.



An initial approximately value of E is found from

$$E_0 = M + e \sin M + \frac{e^2}{2} \sin 2M \quad (4.1-4)$$

and the corresponding value of M found from

$$M_0 = E_0 - e \sin E_0 \quad (4.1-5)$$

The required differential correction is given by

$$\Delta E_0 = \frac{M - M_0}{1 - e \cos E_0} \quad (4.1-6)$$

and the next estimate of E is established from

$$E_1 = E_0 + \Delta E_0 \quad (4.1-7)$$

Successive iterations are performed until  $\Delta E_i$  is sufficiently small.

The spacecraft true anomaly ( $v$ ) is then uniquely determined from

$$v = \cos^{-1} \left( \frac{\cos E - e}{1 - e \cos E} \right) \quad (4.1-8)$$

and

$$v = \sin^{-1} \left[ \frac{(1 + e \cos v) \sin E}{\sqrt{1 - e^2}} \right] \quad (4.1-9)$$

The spacecraft position with respect to the ascending node ( $\theta$ ) is then

$$\theta = \omega_p + v \text{ [MOD } 360] \quad (4.1-10)$$

where

$\omega_p$  = the argument of perigee; measured from the ascending node

The remaining relationships required to define the spacecraft ground trace time history are presented in Section 3.1, Orbit Time Histories.



As can be seen from the above relationships, the in-plane position of a non-circular orbit is non-linear with respect to time. Therefore, the ground trace characteristics of non-circular orbits will not have the symmetrical characteristics previously shown for geosynchronous circular orbits.

The characteristics of the ground traces of representative eccentric "24-hour" orbits are dependent upon the magnitude of the eccentricity, the orientation of the line of apsides, and the orbit inclination. The effects of eccentricity and the orientation of the line of apsides are illustrated in Figures 4.1-1 and 4.1-2 for an orbit inclination of 28.5 degrees. In Figure 4.1-1, the line of apsides is coincident with the line of nodes with perigee in the direction of the ascending node. The ascending and descending nodes occur at the same geographic longitude and a distorted figure-eight ground trace occurs since the time between apsidal passages, and thus nodal crossings, is equal to one-half the orbital period. The effect of orbit eccentricity is to increase the figure-eight distortion with increasing eccentricity.

The effect of orienting the line of apsides 90 degrees from the line of nodes is illustrated in Figure 4.1-2 for an argument of perigee of 270 degrees. For this orbit orientation, the times between successive nodal crossing are not equal resulting in different geographic longitudes of the ascending and descending nodes. As the orbit eccentricity increases, the geographic longitudinal displacement of the nodes increases and, for sufficiently high eccentricities, the "figure-eight" ground trace no longer occurs. The unequal times between successive nodal crossings also result in unequal durations over the northern and southern hemispheres. The effects of eccentricity on the times over each hemisphere are also shown in Figure 4.1-2 by the times since perigee of the nodal crossings.

The effect of orbit eccentricity on the earth surface coverage is primarily one of increasing the area of periodic coverage while decreasing the area of continuous coverage. For orbits with the line of apsides oriented 90 degrees from the line of nodes, the change in coverage of the equator is approximately equal to the geographic displacement of the nodes. Some change in the coverage of the polar regions also occurs due to the change in orbit altitude although the change is relatively small.

The data presented in Figures 4.1-1 and 4.1-2 are equally applicable to eccentric orbits with an argument of perigee of 180 degrees and 90 degrees, respectively. The ground traces of such orbits are obtained by reflecting the curves shown in these figures about the equatorial plane; that is, by replacing the plus latitude by minus latitude and minus latitude by plus latitude.

As discussed previously, the earth coverage characteristics of eccentric orbits will vary from that previously presented for circular orbits. A representative earth coverage capability is presented in Figure 4.1-3 for an orbit with eccentricity of 0.2, an inclination of 60 degrees, and an argument of perigee of 270 degrees. To prevent presenting an unnecessarily cluttered figure, the coverage for only one-half revolution has been presented; that is, the coverage from a true anomaly of zero degrees, through the ascending node, to a true anomaly of 180 degrees. The coverage during the second half of the revolution is, by symmetry, the same as shown for the first half revolution

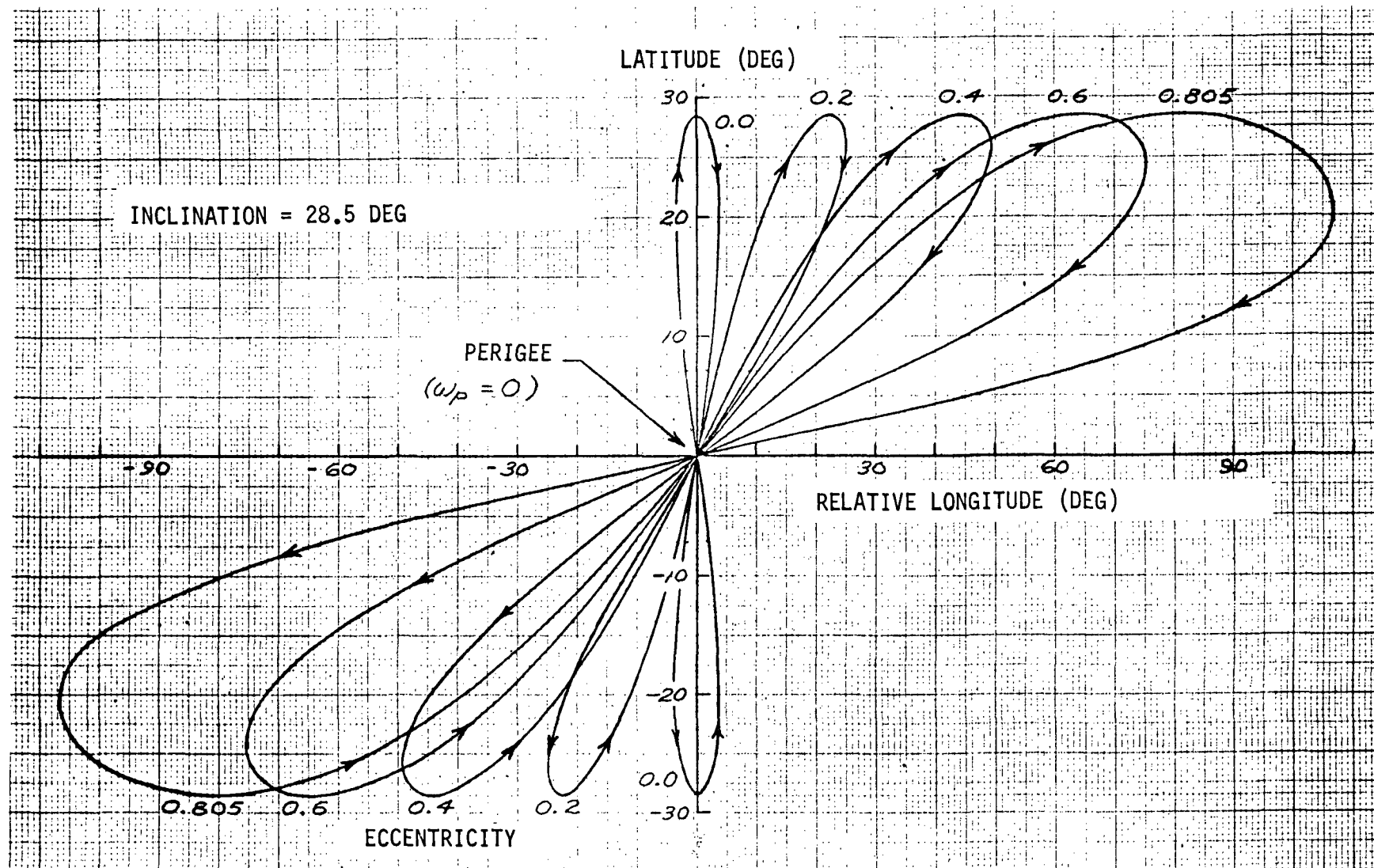


Figure 4.1-1. Eccentric "24-Hour" Orbit Ground Trace ( $\omega_p = 0$ )

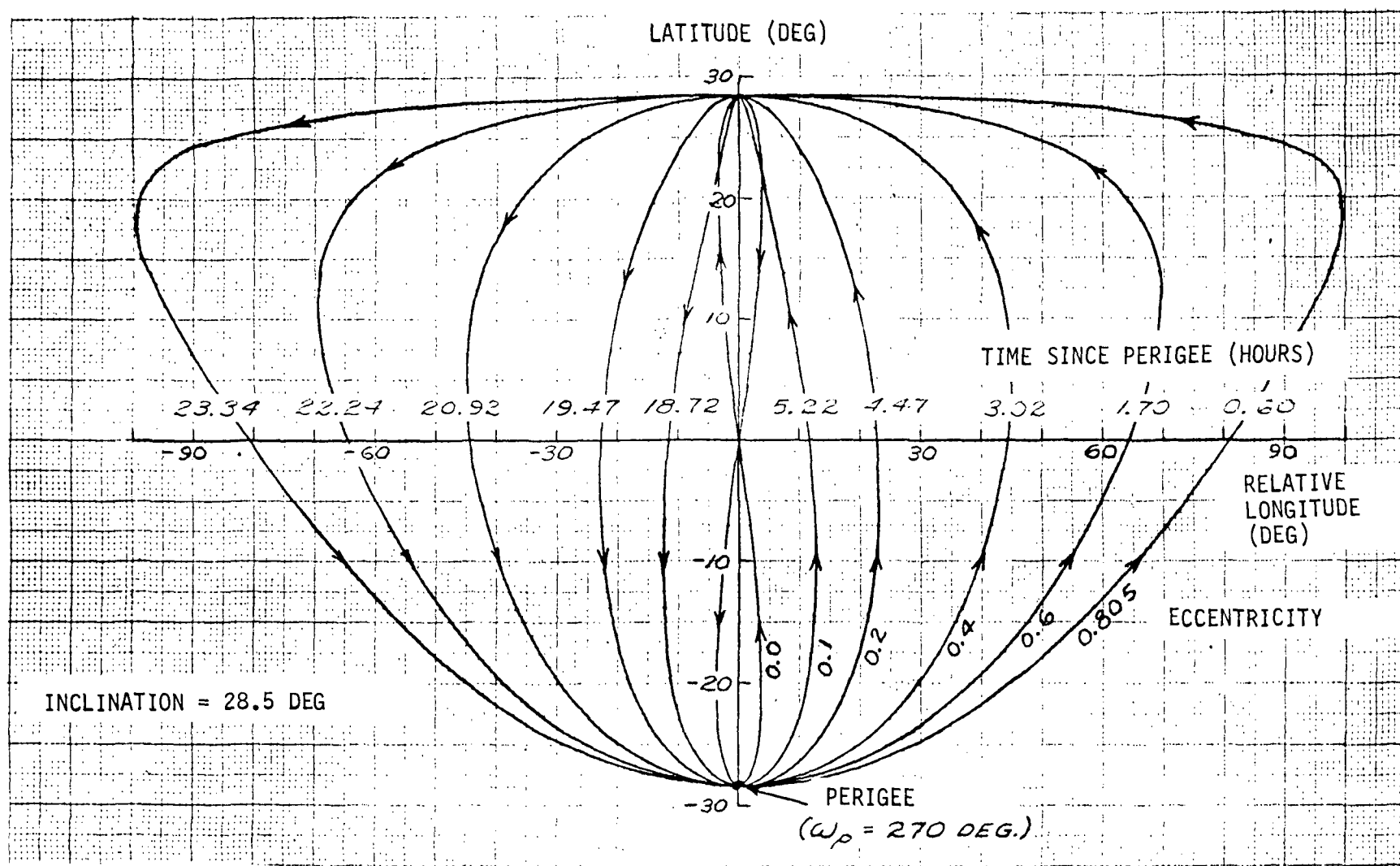


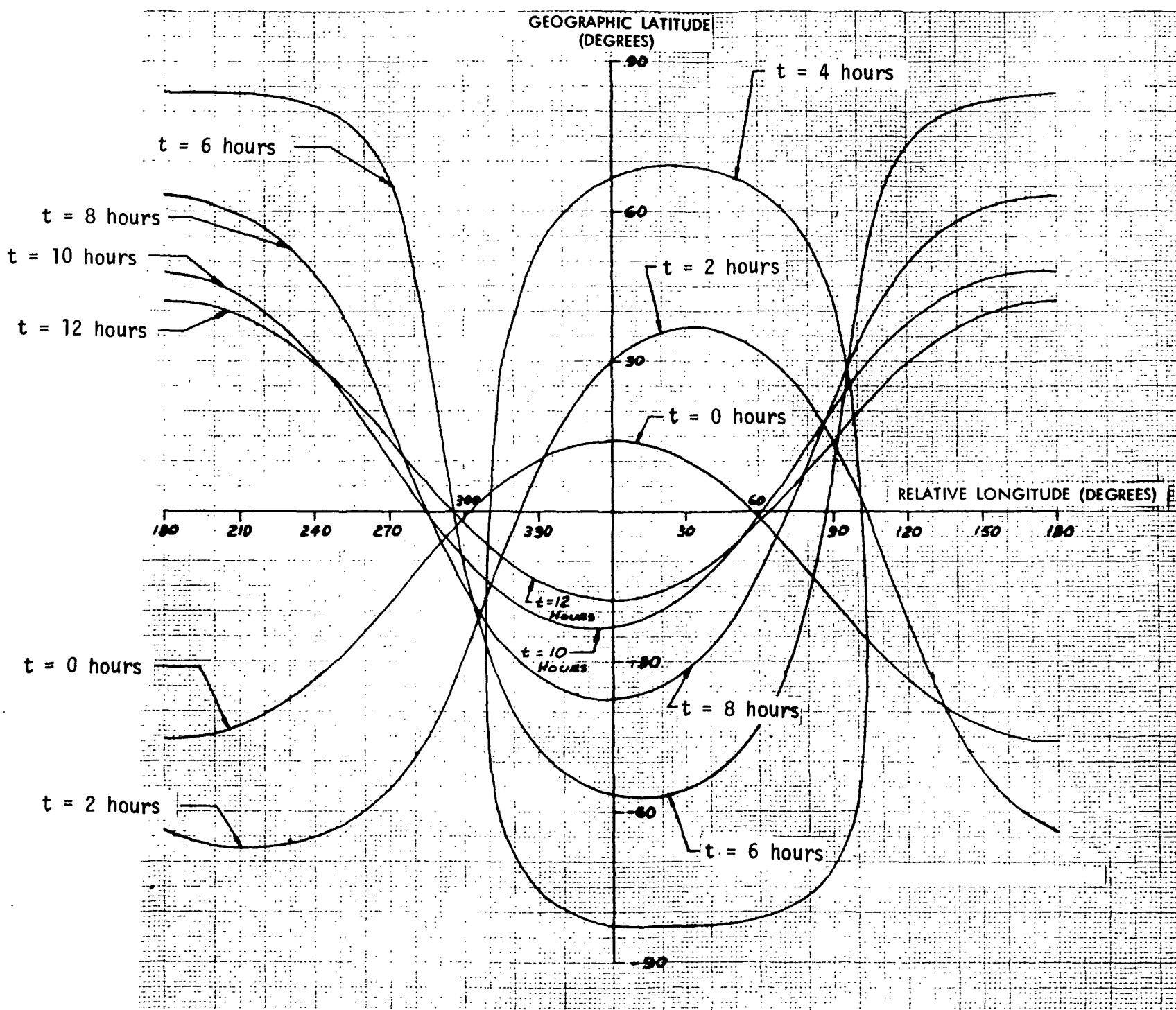
Figure 4.1-2. Eccentric "24-Hour" Orbit Ground Trace ( $\omega_p = 270^\circ$ )

4-7

SD 73-SA-0036-3

**Page intentionally left blank**

**Page intentionally left blank**



- MASK ANGLE = 5 DEGREES
- $t$  = TIME SINCE PERIGEE
- RELATIVE LONGITUDE:  
LONGITUDE MEASURED  
FROM THE GEOGRAPHIC  
LONGITUDE OF PERIGEE
- ARGUMENT OF PERIGEE  
= 270 DEGREES

Figure 4.1-3. Earth Coverage Characteristics ( $i = 60$  degrees;  $e = 0.2$ )

by reflecting the curve about the ordinate. The figure is also applicable to an inclined eccentric orbit which has an argument of perigee of 90 degrees by rotating the traces about the abscissa. Thus, Figure 4.1-3 can be used to define the earth coverage characteristics as a function of time for inclined eccentric orbits which have an argument of perigee of 90 degrees.

When considering the desired orientations of eccentric "24-hour" orbits for the purposes of earth coverage, an additional consideration must be taken into account. That is, the unique characteristics of the ground trace must be considered. As previously shown in Figure 4.1-1, the ground trace of eccentric "24-hour" orbits which have perigee along the lines of nodes results in distorted figure-eight ground traces. For the cases shown in the figure, it can be seen that the ground trace is restricted to two quadrants in terms of geographic longitude and latitude. With the argument of perigee located in the direction of the ascending node, the ground trace is restricted to the "north-east" and "south-west" quadrants. Therefore, the symmetry which characterized circular orbits is no longer evident. When the argument of perigee is either 90 degrees or 270 degrees however, the symmetry with respect to the mean meridian of the ground trace is retained. Therefore, in general, eccentric orbits which have an argument of perigee of either 90 degrees or 270 degrees are preferred from the standpoint of earth coverage characteristics.

Having established the preferred orientation of the line of apsides, the next consideration is the preferred location of the mean meridian of the ground trace. In general, the preferred locations with respect to a geographic ground site are similar to those previously discussed for the circular geo-synchronous orbits.

One additional characteristic of the ground trace of inclined elliptic "24-hour" orbits is worthy of note. By referring to Figure 4.1-2, it can be seen that the period of time that the spacecraft is over the northern hemisphere is greater than the time over the southern hemisphere. Therefore, greater coverage of the northern hemisphere is provided. This fundamental characteristic may be a desirable feature when considering earth resources type experiments which are concerned with viewing the major world land masses since the majority of the land masses are in the northern hemisphere. Also, the major world population centers are located in the northern hemisphere which, for example, make this type of orbit attractive for monitoring environmental pollution.

**Page intentionally left blank**

**Page intentionally left blank**

## 4.2 MISSION PROFILE CHARACTERISTICS

The fundamental relationships previously derived in Section 3.3, Mission Profile Characteristics (for geosynchronous orbits), are generally applicable to the related orbits. The major exception is that the apogee radius and the elliptic "24-hour" insertion velocities must be modified depending on the final eccentricity of the eccentric "24-hour" orbit. Figure 4.2-1 presents the apogee and perigee radius of eccentric "24-hour" orbits as a function of the eccentricity. For the purposes of this study, a limiting eccentricity of 0.8268, which corresponds to a perigee altitude of 500 nautical miles, has been assumed.

The resultant total impulsive incremental velocity requirements for injecting into eccentric "24-hour" orbits are shown in Figure 4.2-2 as a function of total plane change for a range of final orbit eccentricities. As can be seen from the figure, the effect of orbit eccentricity on the total impulsive incremental velocity requirement is to decrease the requirement with increasing orbit eccentricity. It should be noted, however, that the effect of increased eccentricity is to increase the distortion of the ground traces provided by inclined circular "24-hour" orbits. Therefore, the effects on the ability to accomplish mission objectives must also be considered when assessing the applicability of elliptic orbits.

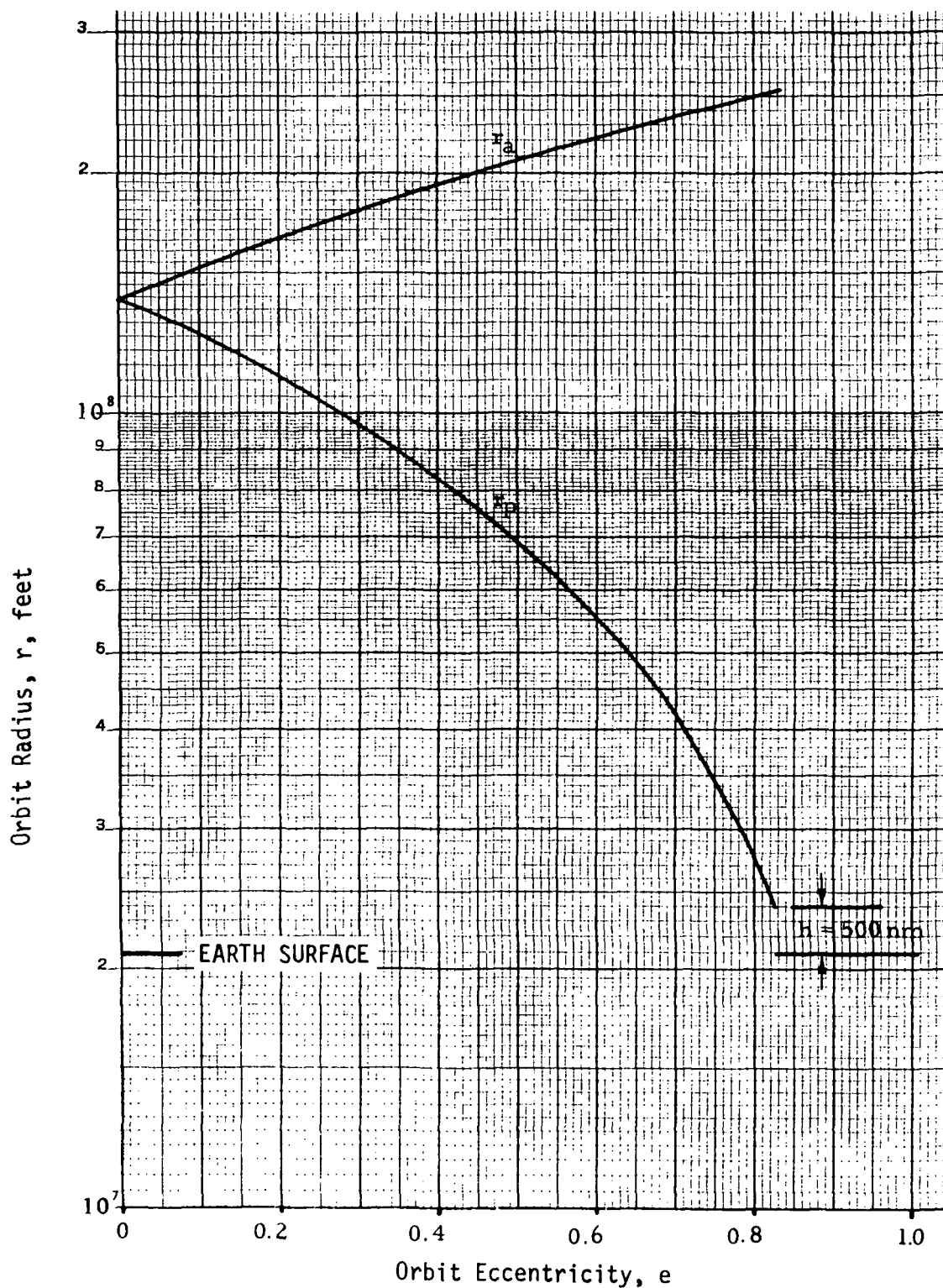


Figure 4.2-1. Elliptic Orbit Radii for "24-hour" Orbits



Space Division  
North American Rockwell

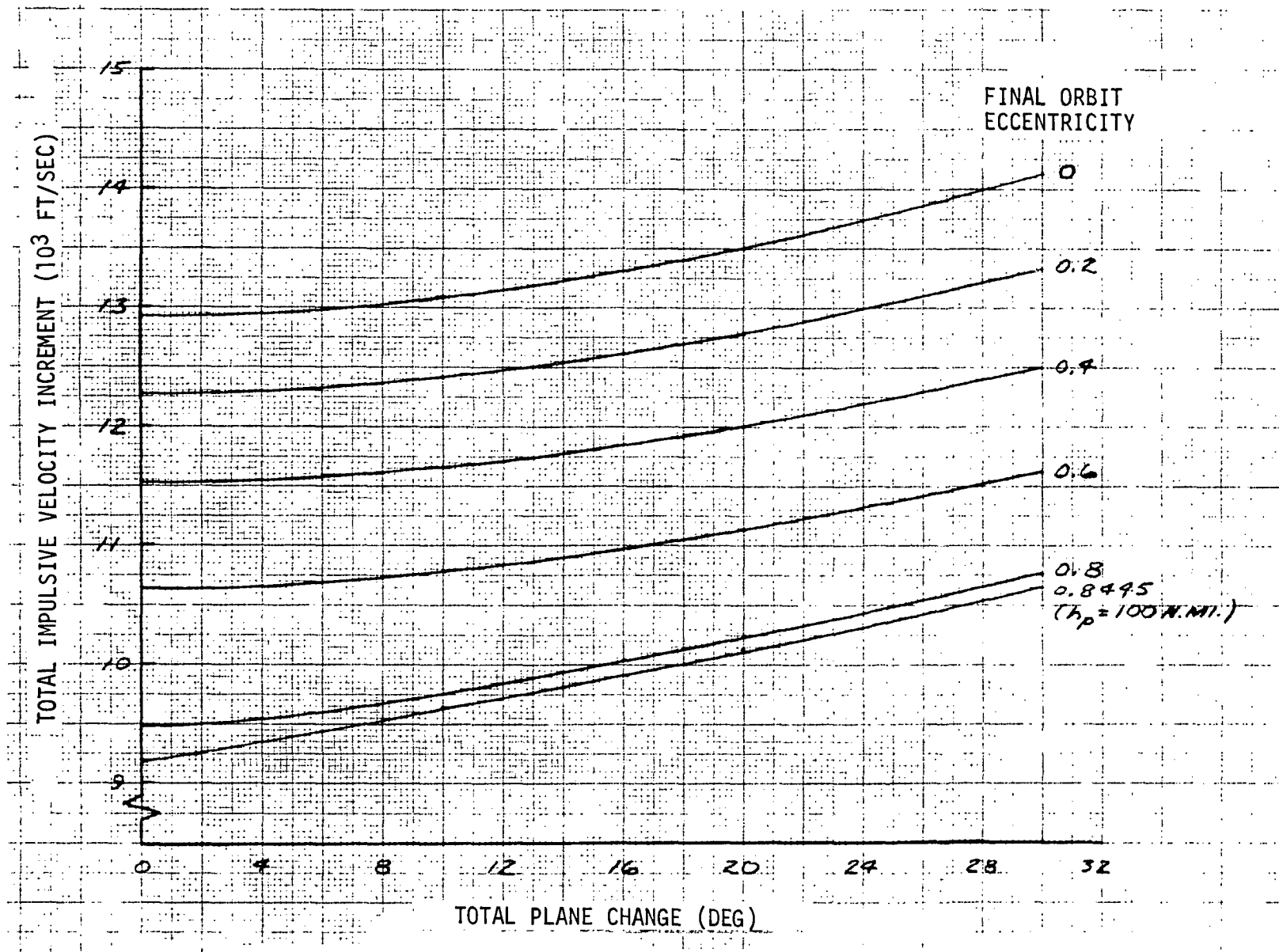


Figure 4.2-2. Impulsive Incremental Velocity Requirements  
(Eccentric "24-Hour" Orbits)

## 5.0 ELECTROMAGNETIC SPECTRUM UTILIZATION

One of the major resources available to the space program is the electromagnetic spectrum. It is used for tracking and ranging, for command and control, for communications, and for sensing and experimentation. Every space vehicle uses some portion of the electromagnetic (EM) spectrum for one or more of the functions mentioned above.

A set of reference data was developed that displays (1) the total EM spectrum, (2) the portions allocated by international and national agreements to space services, (3) atmospheric and weather effects on propagation at different frequencies, (4) weather statistical probability data, (5) techniques and constraints of techniques for multiple frequency usage, and (6) projections of technological status for the time period of this study. Such data is useful in the development of plans and concepts for geosynchronous mission communications links and other EM spectrum associated activities. Operational frequencies and link parameters of transmitter power and antenna size and gain can be derived while accounting for the effects of atmosphere and weather. Utilization of the allocated frequency bands and the limits of frequency use can be established. Part of the data includes the method for calculating and determining orbital spacing limits of identical frequency data relay satellites to perform within international accepted levels of interference. Thus, this set of data can be effectively used in the contention analysis and in development of geosynchronous platform concepts.

This section presents data associated with the EM spectrum and its characteristics. This presentation begins with a general view of the spectrum from low frequencies (LF) to frequencies in the gamma ray region. A set of charts is used to define the usage of broad areas of the spectrum including allocations and natural phenomena. Then, usable portions of the spectrum are identified by examining the propagation characteristics through the atmosphere under normally clear atmospheric conditions.

The World Administrative Radio Conference for Space Telecommunications (WARC-ST), completed July 16, 1971, revised the International Radio Regulations (effective January 1, 1973). As a result, world-wide frequency allocations have been made up to 275 GHz. Based on these new allocations, a tabulation was made of frequencies allocated for space services and those terrestrial services which share these frequencies. Table 5.3-1 covers frequencies from 7 MHz to 275 GHz.

A literature search was performed for data describing the transmission effects and characteristics of communications paths from geosynchronous orbit. Graphs and nomographs were extracted from the literature and are presented; these describe such environmental effects as atmospheric attenuation, attenuation due to rainfall, and noise temperature due to oxygen and water vapor absorption.

**Page intentionally left blank**

**Page intentionally left blank**

## 5.1 USABLE FREQUENCY SPECTRUM

A series of charts has been developed to display the electromagnetic spectrum from low frequencies to frequencies in the gamma ray region. Figures 5.1-1 through 5.1-8 cover the spectrum from  $10^5$  Hz (100 kHz) to  $10^{20}$  Hz. Each chart displays propagation effects and generalized frequency allocations for all types of services. The propagation data shows the effect of the atmosphere and atmospheric disturbances on EM signal transmission, shows solar system influence such as sunspot disturbance, and shows some sources of broadband man-made interference.

The generalized frequency allocations reflect the majority of those allocations made for space telecommunications and those terrestrial allocations which relate to the space allocations (i.e., share the space allocations or provide similar terrestrial services). For those frequencies higher than 300 GHz, no world-wide allocations have been made; however, commonly used frequencies are shown with their applications throughout the infrared, visible, ultraviolet, x-ray, and gamma-ray frequencies.



Space Division  
Rockwell International

CHART ONE: 100 KHz to 1 GHz

PREDOMINANT INTERFERENCE

5-4

SD 73-SA-0036-3

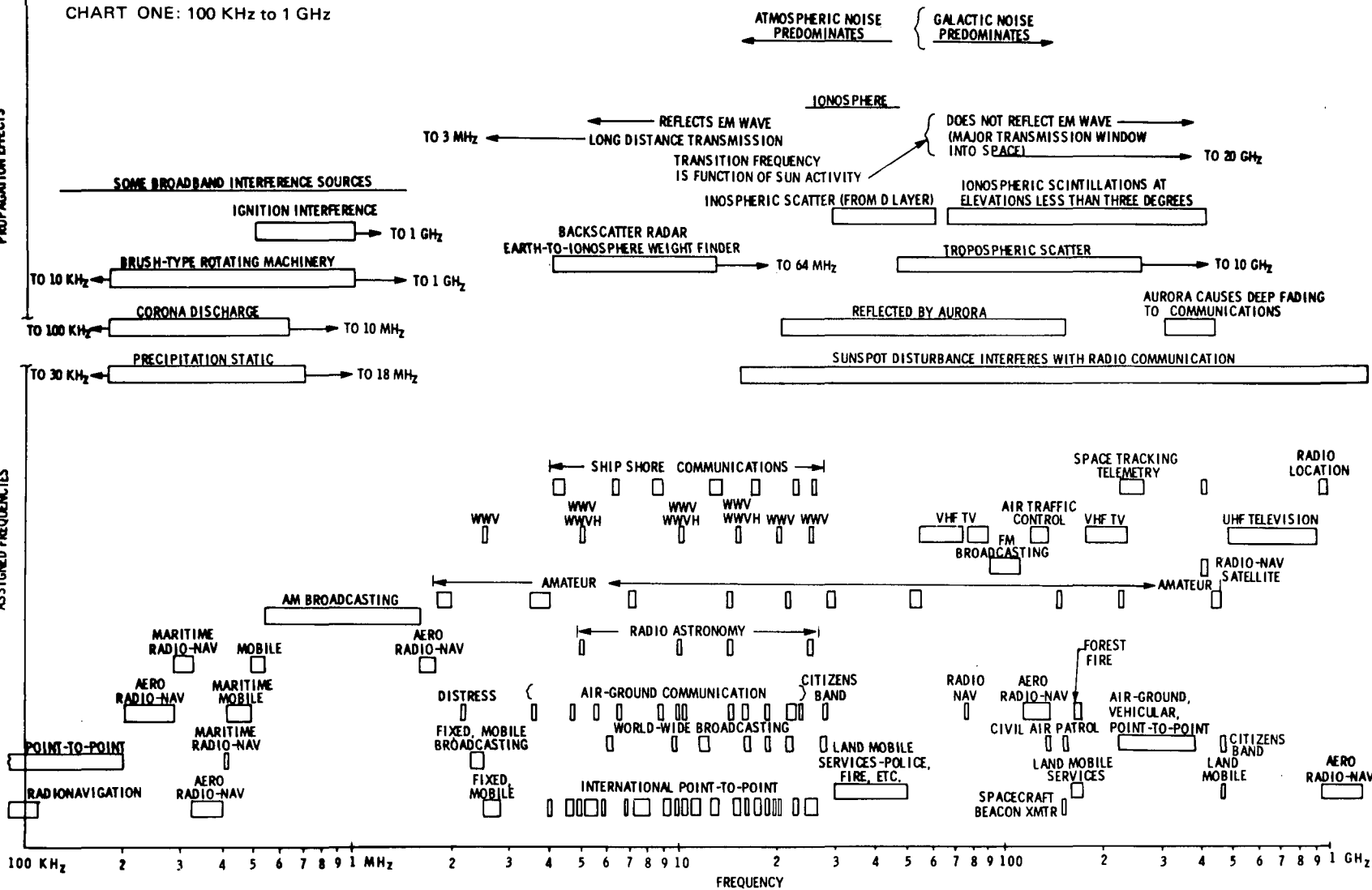


Figure 5.1-1. Frequency Spectrum

CHART TWO: 1 GHz TO 3 GHz

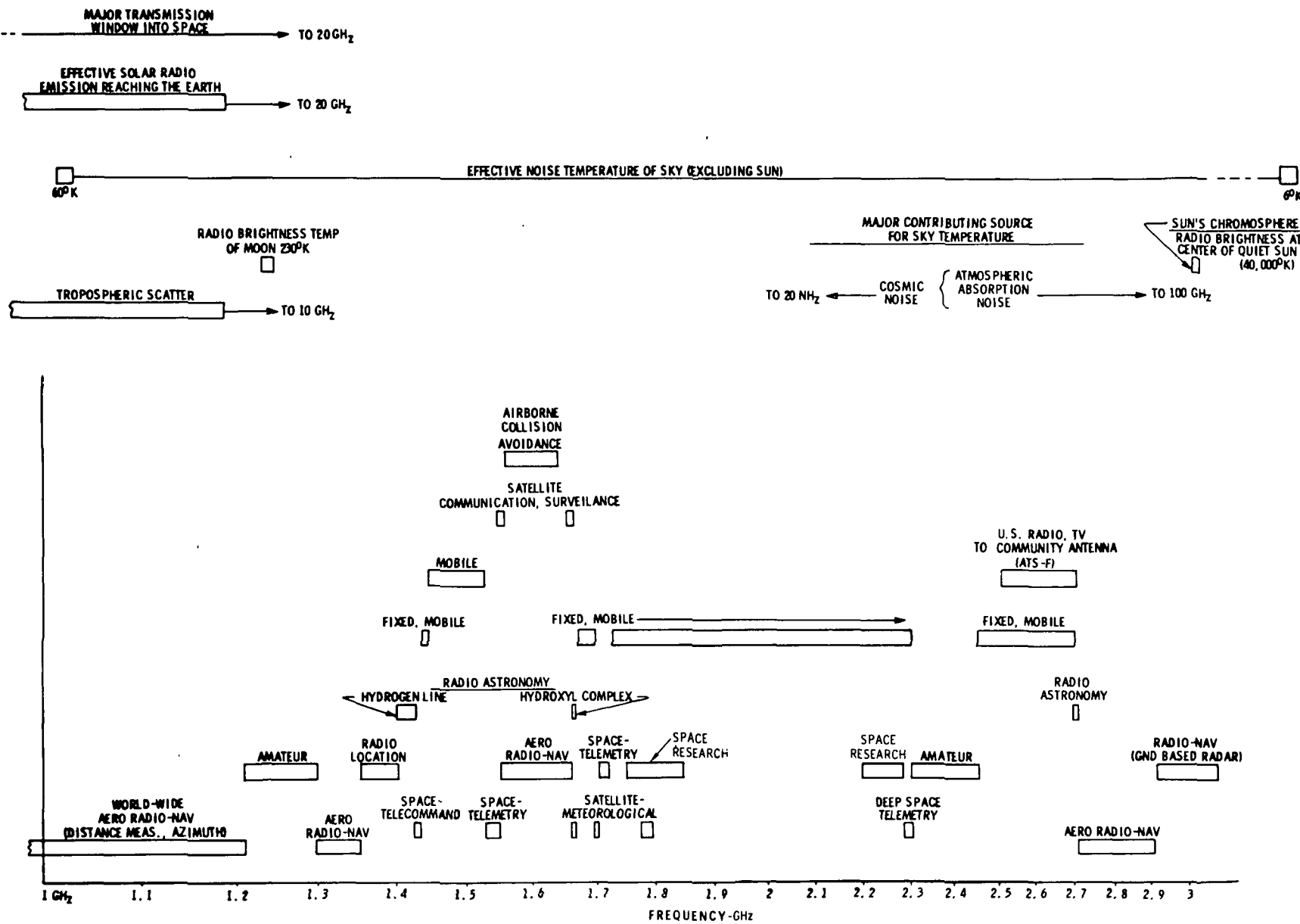


Figure 5.1-2. Frequency Spectrum

CHART THREE: 3 GHz TO 10 GHz

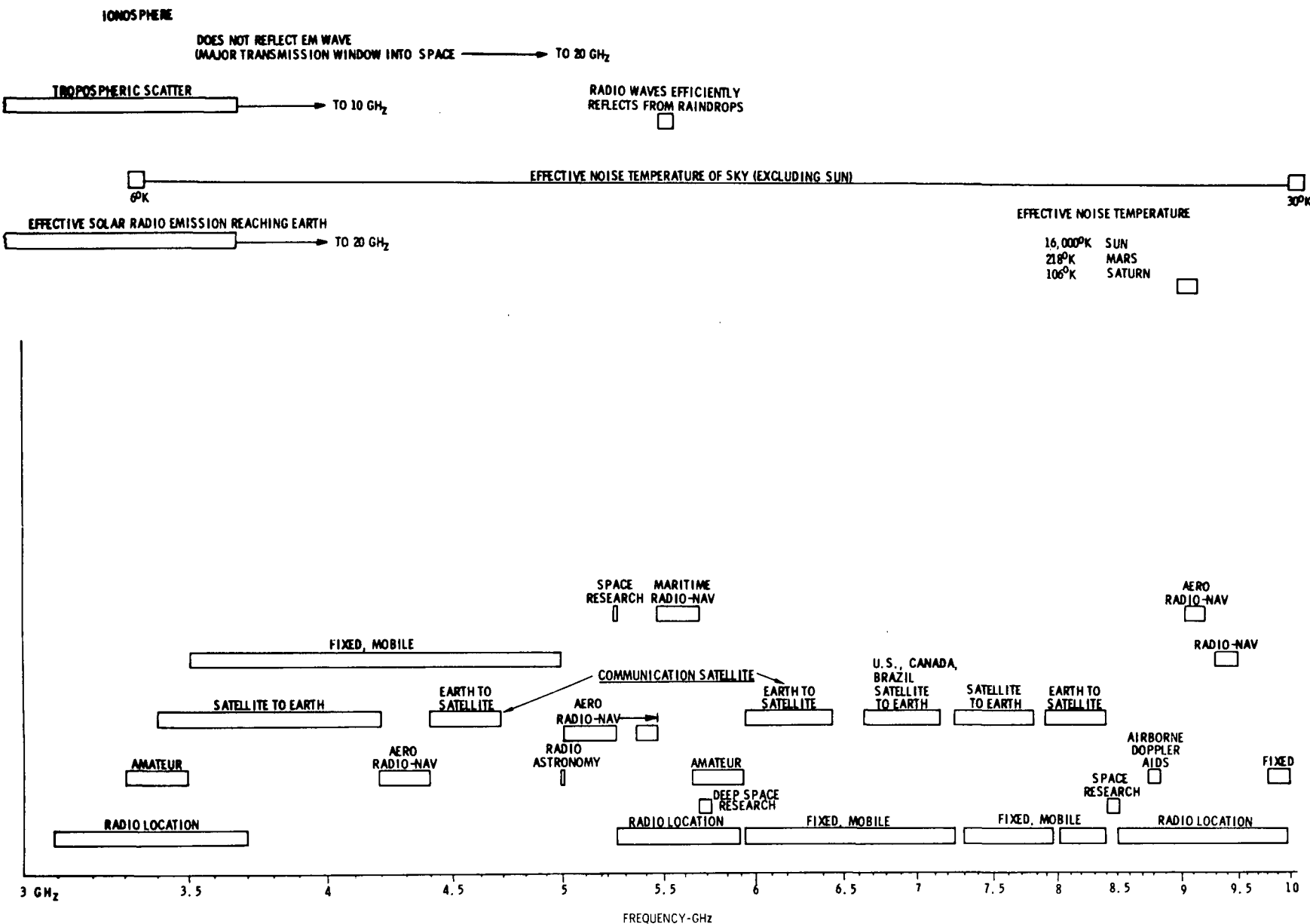


Figure 5.1-3. Frequency Spectrum

CHART FOUR : 10 GH<sub>Z</sub> TO 30 GH<sub>Z</sub>

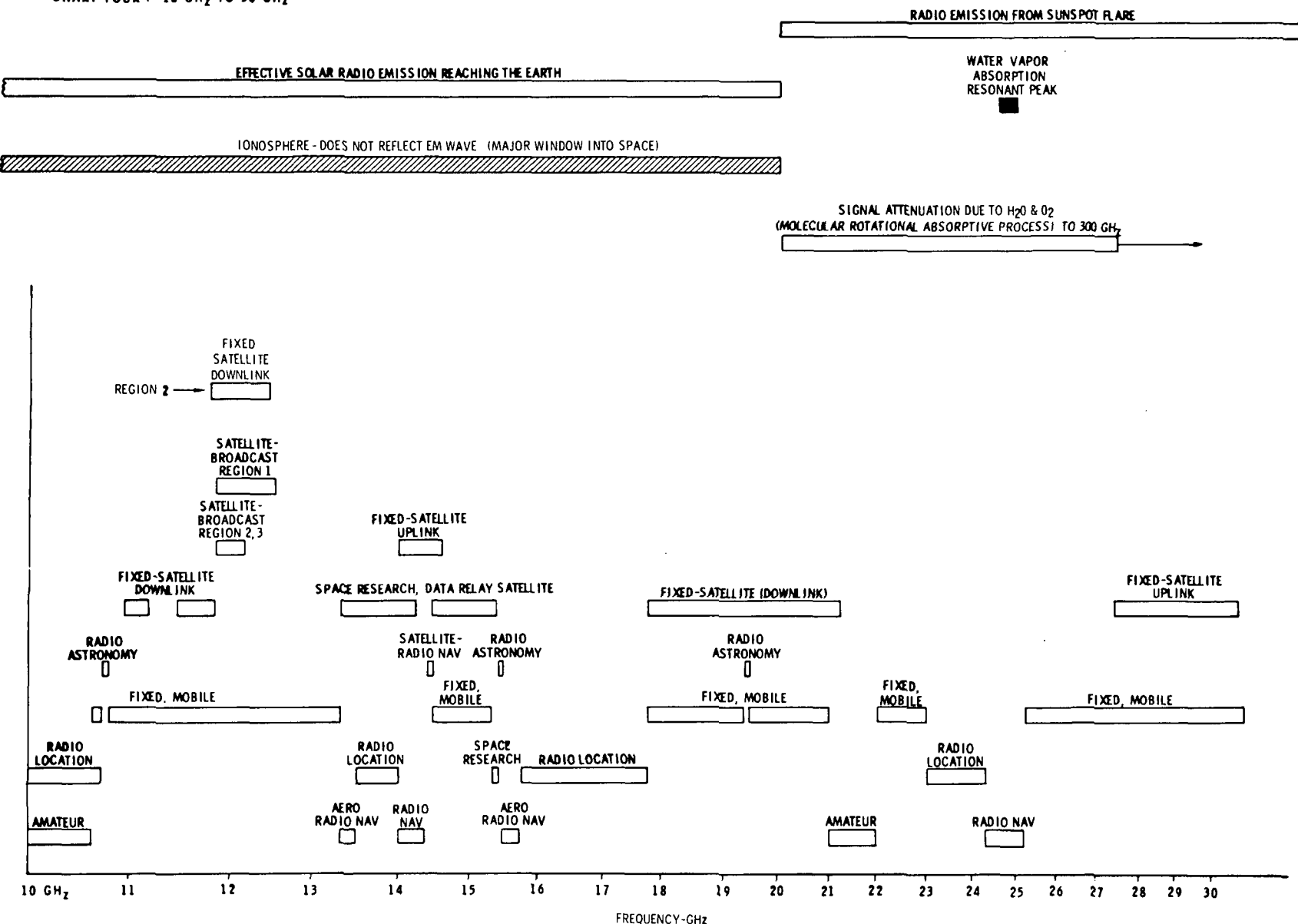


Figure 5.1-4. Frequency Spectrum

CHART FIVE: 30 GH<sub>Z</sub> TO 100 GH<sub>Z</sub>

EM SIGNALS CAN PENETRATE  
PLASMA SURROUNDING  
RE-ENTRY SPACE VEHICLE

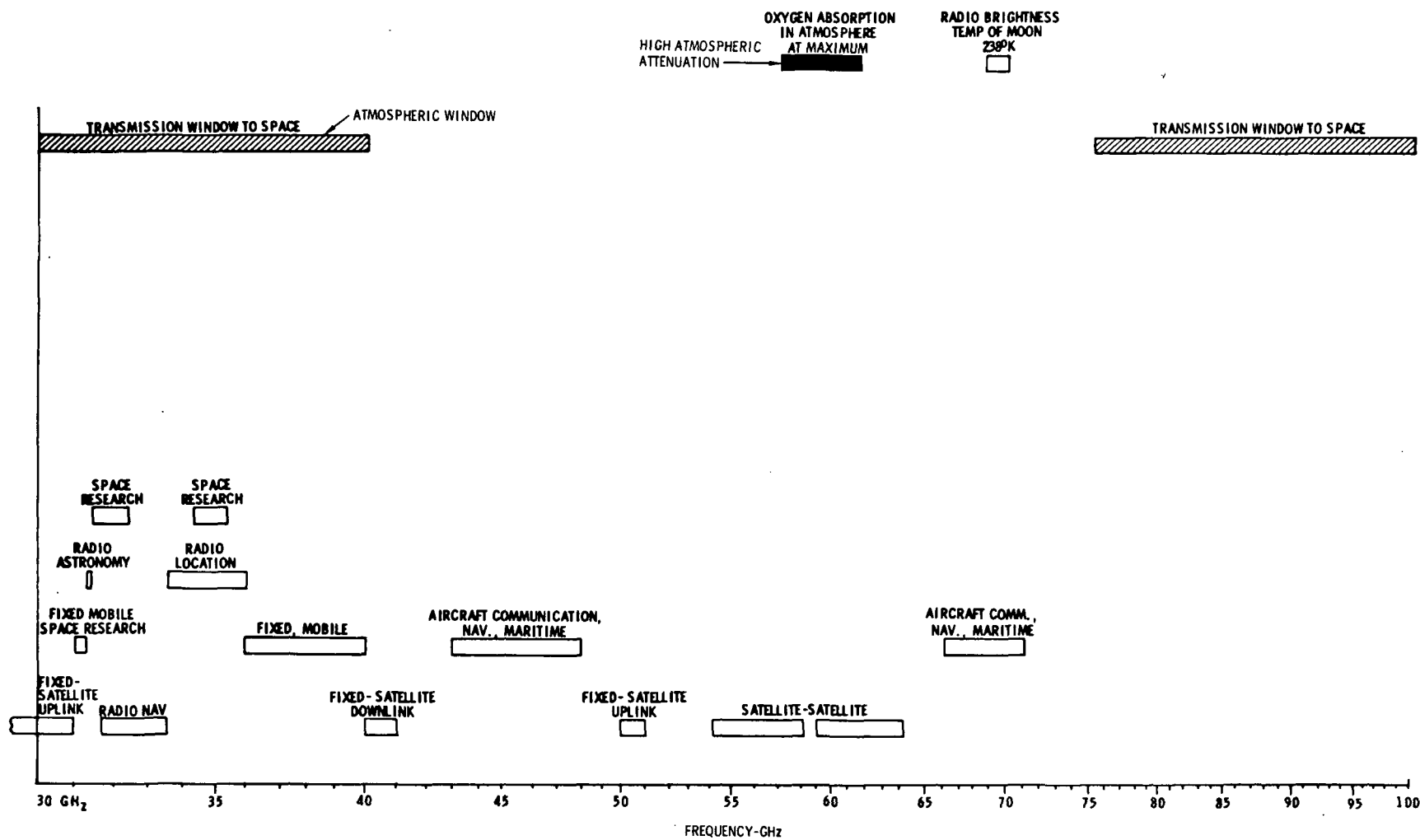


Figure 5.1-5. Frequency Spectrum

CHART SIX : 100 GH<sub>Z</sub> TO 1000 GH<sub>Z</sub>

5-9

SD 73-SA-0036-3

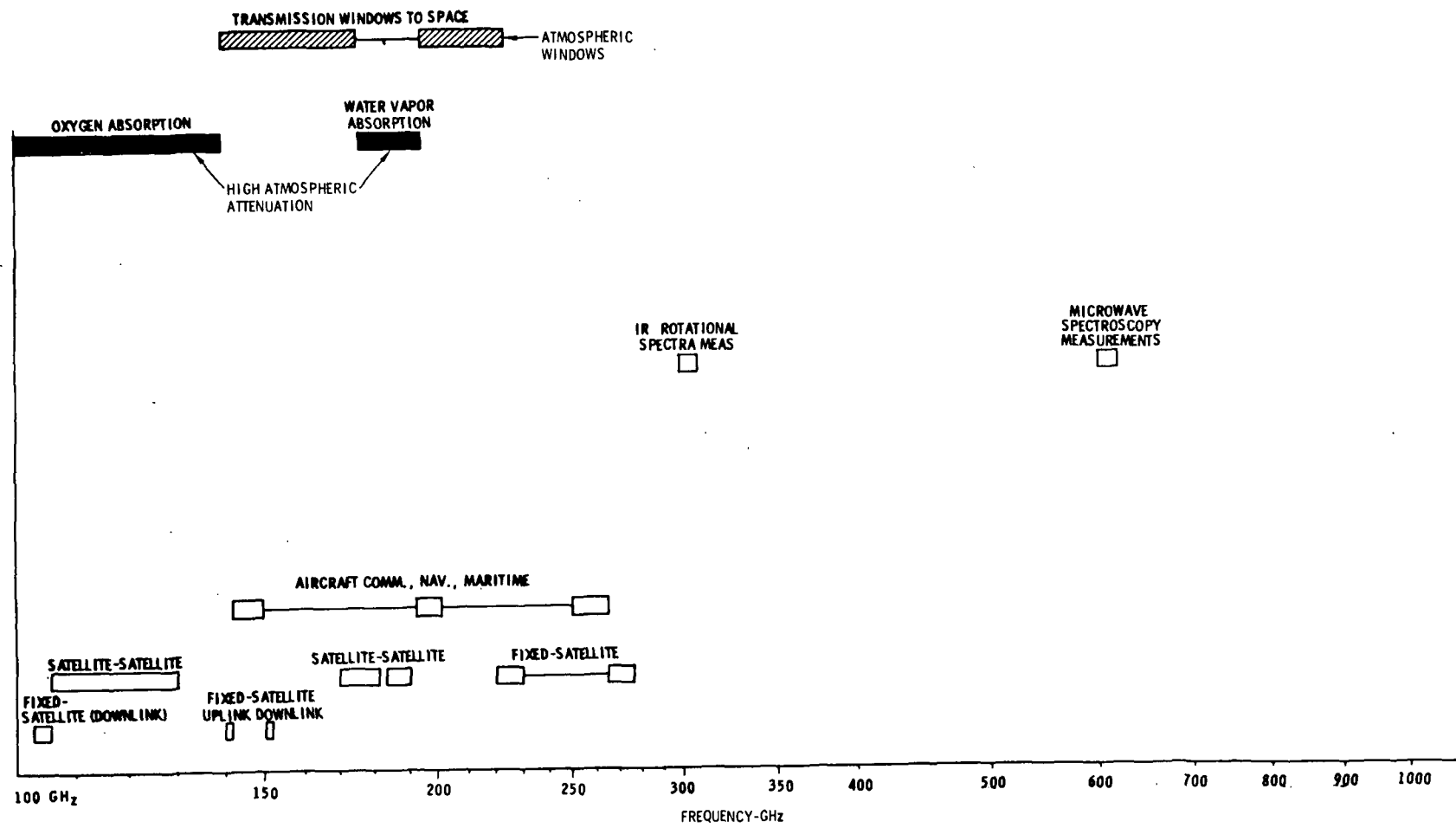


Figure 5.1-6. Frequency Spectrum

CHART SEVEN: 1000 GHz ( $10^{12}$  Hz) TO  $10^{16}$  Hz

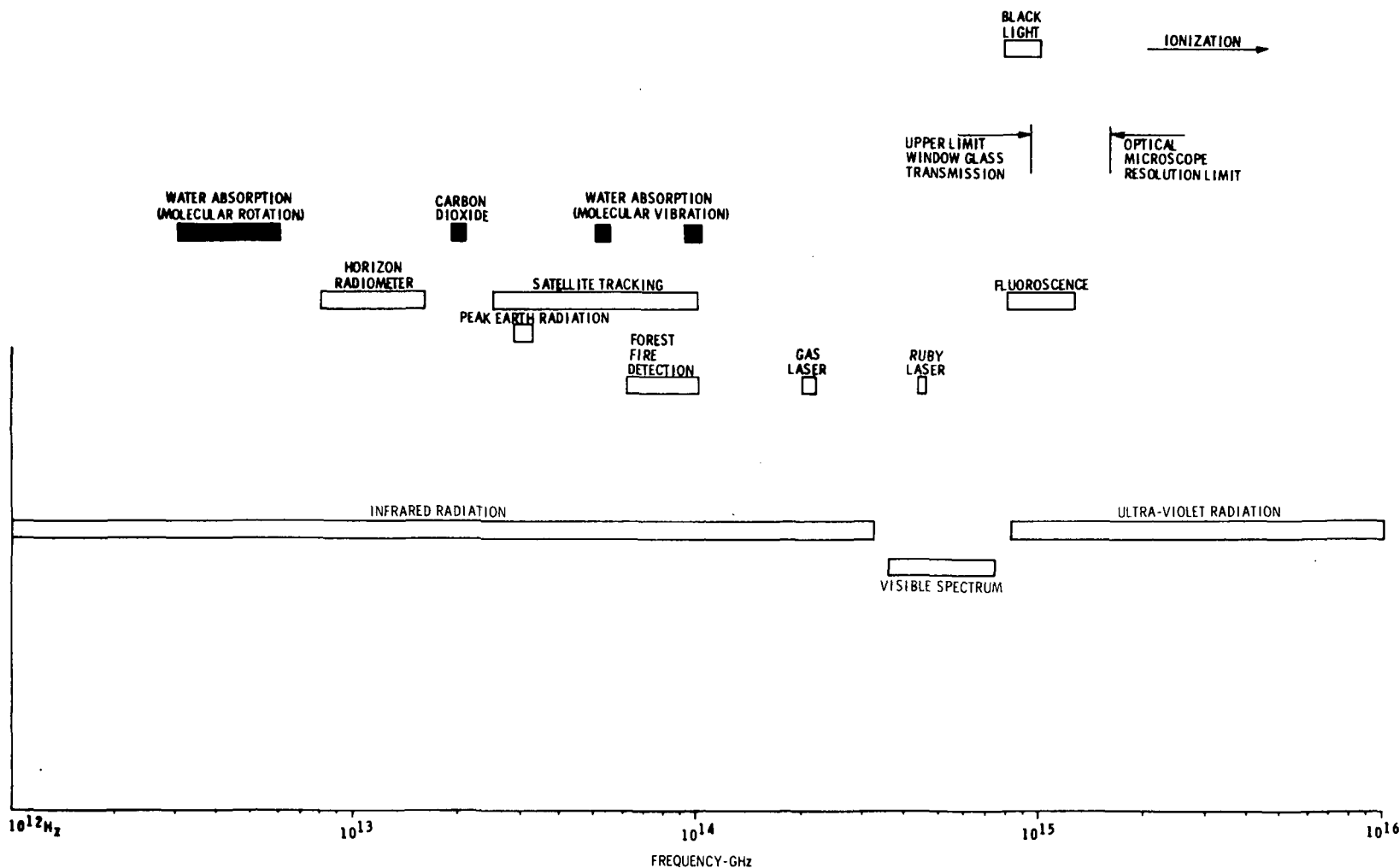


Figure 5.1-7. Frequency Spectrum

CHART EIGHT:  $10^{16}$  Hz TO  $10^{20}$  Hz

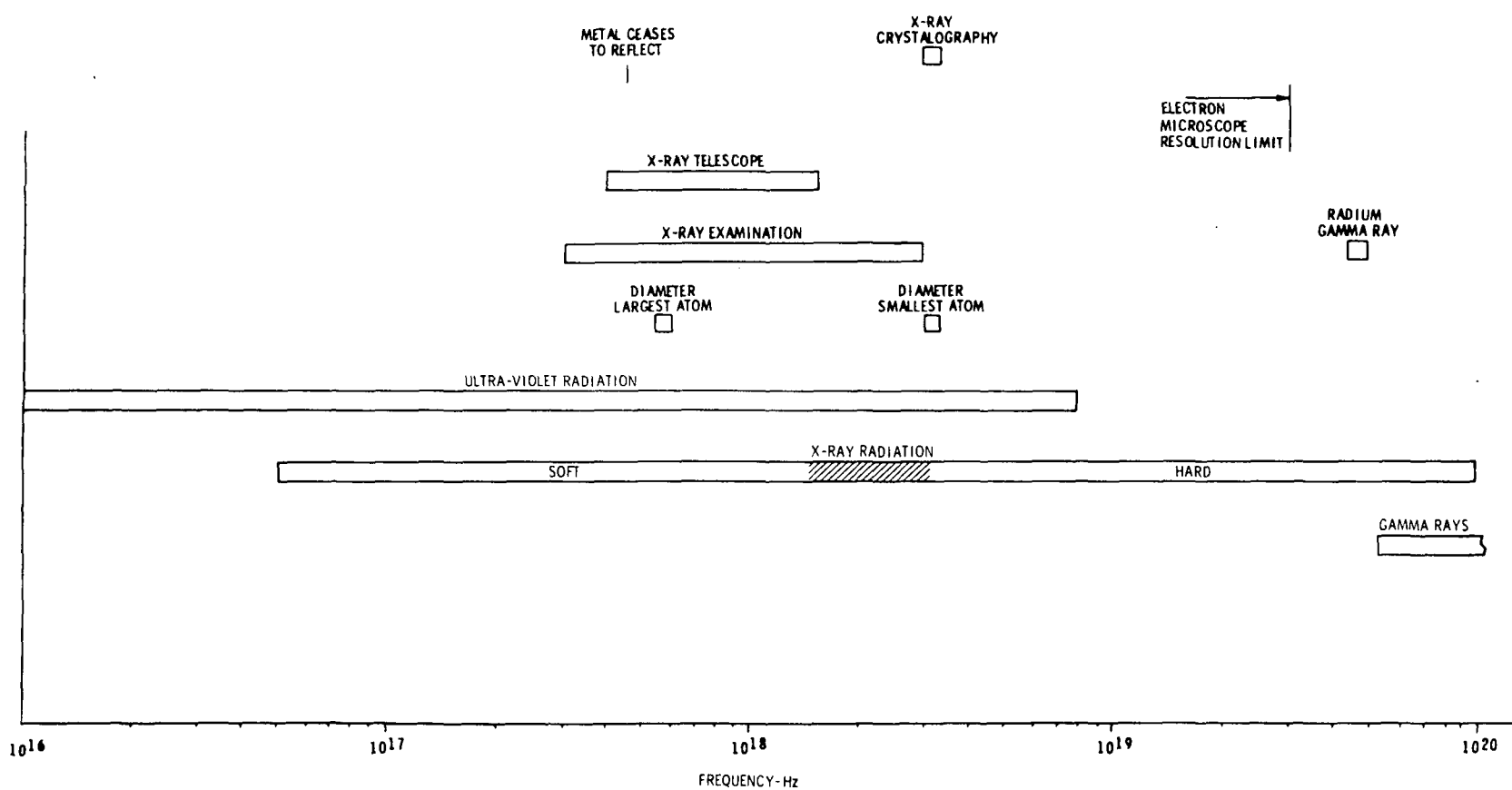


Figure 5.1-8. Frequency Spectrum

**Page intentionally left blank**

**Page intentionally left blank**



## 5.2 ATMOSPHERIC WINDOWS

The earth's atmosphere attenuates electromagnetic radiation in varying degrees according to the frequency (wavelength) of the radiation. Oxygen and water vapor in the atmosphere, clouds and precipitation along the path, layering of the atmosphere, and atmospheric and rain induced noise all contribute to the attenuation. The least attenuation occurs under conditions of clear, dry skies using a radiation path with a small zenith angle to minimize the total amount of atmosphere traversed.

Figure 5.2-1 (Reference 5-1) shows total attenuation as a function of frequency along a path whose zenith angle does not exceed 45 degrees from a high, dry site. Using 3 dB as a threshold for defining windows through the atmosphere (i.e., frequency bands for which the attenuation does not exceed 3 dB are defined as atmospheric windows), we find nine windows: four in the radio frequency region, four infrared windows, and one visible window.

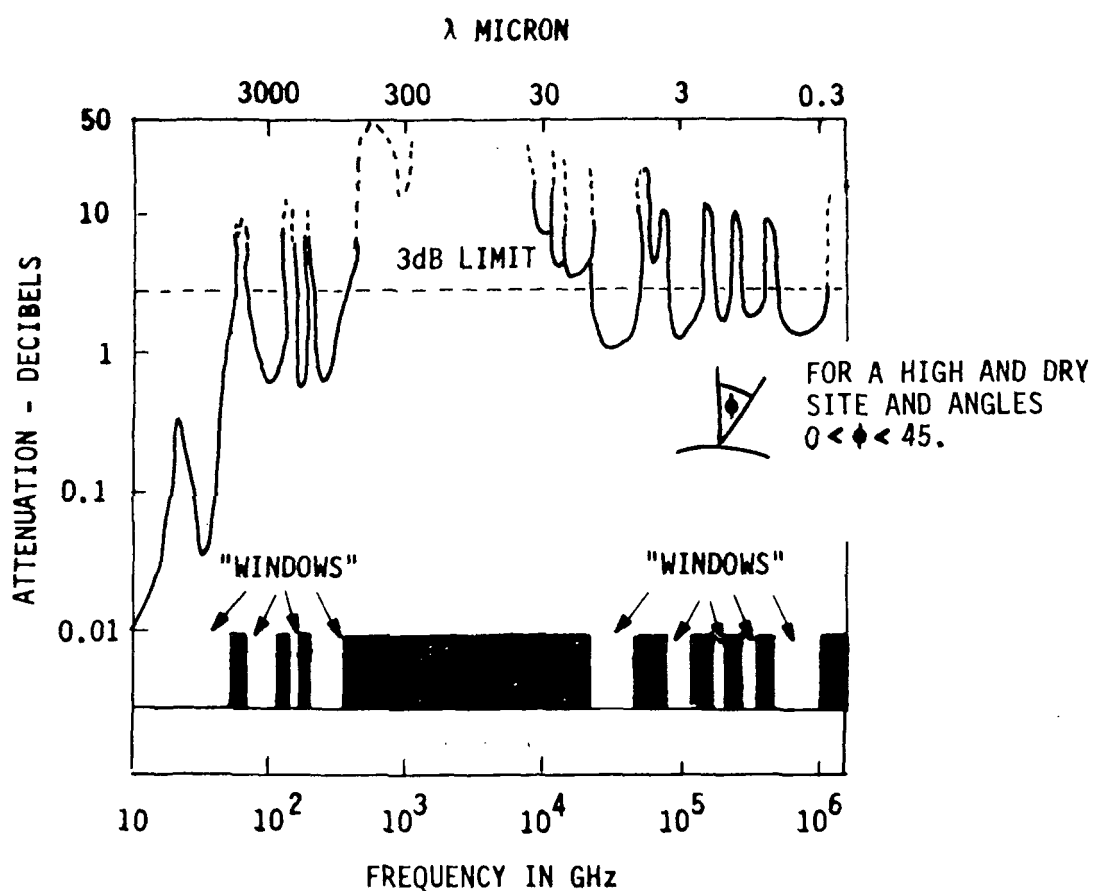


Figure 5.2-1 Atmospheric Windows (Above 10 GHz)

**Page intentionally left blank**

**Page intentionally left blank**



### 5.3 FREQUENCY ALLOCATIONS

The World Administrative Radio Conference for Space Telecommunications (WARC-ST) has allocated bands of frequencies up to 275 GHz for space services. Table 5.3-1 lists all of the allocations from 7 MHz up to 275 GHz. Along with each allocation is listed the bandwidth, the service for which the band is allocated, the service(s) which share the allocated band, and the usage of the band (such as direction of transmission). Most of the bands allocated are for communications between the earth and spacecraft. However, some allocations were made for spacecraft-to-spacecraft communications; these generally coincide with non-windows in the atmosphere.

Inspection of this table shows that for space services 3.2 GHz is allocated below 10 GHz, 41 GHz between 10 GHz and 100 GHz, and 102 GHz above 100 GHz. Furthermore, only frequencies above 275 GHz remain for future allocations. Inspection of Figure 5.2-1 shows that the highest radio frequency window limits future allocations to those frequencies between 275 GHz and 350 GHz.

In several cases the services which share allocation with the indicated space service are different for the three different regions of the world. Such cases are distinguished by the words "Check by Region" in the column of sharing services. Exactly which services share the allocated band in the region of interest can be found by referring to the Radio Regulations as revised by WARC-ST (1971).



Table 5.3-1. World-Wide Spectrum Allocations for Space Services (Based on WARC-ST, 1971, Geneva)

Frequency (MHz)	Bandwidth (MHz)	Service	Shared With	Usage
7.0 to 7.1	0.1	Amateur - satellite	Amateur	
14.0 to 14.25	0.25	Amateur - satellite	Amateur	
21.0 to 21.45	0.45	Amateur - satellite	Amateur	
28.0 to 29.7	1.7	Amateur - satellite	Amateur	
30.005 to 30.010	.005	Space operation	Fixed mobile and space research	Satellite identification
136 to 137	1.0	Space research	Space research, and meteorological satellite	Space-to-earth
137 to 138	1.0	Space operation	Check by region	Telemetry and tracking
143.6 to 143.65	0.05	Space research	Amateur	Space-to-earth
144.0 to 146.0	2.0	Amateur - satellite	Fixed and mobile	Telemetering
149.9 to 150.05	0.15	Radionavigation - satellite	Meteorological - satellite and meteorological aids	400.1 MHz, ±25 kHz
272.0 to 273.0	1.0	Space operation	Meteorological aids	Telemetering
399.9 to 400.05	0.15	Radionavigation - satellite	Earth-to-space	
400.05 to 400.15	0.10	Std. frequency - satellite	Telecommand	
400.15 to 401.0	0.85	Space research	Telemetering	
401.0 to 402.0	1.0	Space operation	Space-to-earth	
406.0 to 406.1	0.1	Mobile - satellite	Space-to-earth	
1427.0 to 1429.0	2.0	Space operation	Fixed and mobile	Space-to-earth
1525.0 to 1535.0	10.0	Space operation	Fixed (by region)	Telemetering
1535.0 to 1542.5	7.5	Maritime mobile - satellite	Maritime mobile - satellite	Space-to-earth
1542.5 to 1543.5	1.0	Aeronautical mobile - satellite	Maritime mobile - satellite	Space-to-earth
1543.5 to 1558.5	15.0	Aeronaut. mobile - satellite	Space-to-earth	
1636.5 to 1644.0	7.5	Maritime mobile - satellite	Earth-to-space	
1644.0 to 1645.0	1.0	Aeronaut. mobile - satellite	Earth-to-space	
1645.0 to 1660.0	15.0	Aeronaut. mobile - satellite	Earth-to-space	
1670.0 to 1690.0	20.0	Meteorological - satellite	Space-to-earth	
1690.0 to 1700.0	10.0	Meteorological - satellite	Meteorological aids, fixed and mobile	Space-to-earth
1700.0 to 1710.0	10.0	Space research	Meteorological aids	Space-to-earth
1750.0 to 1850.0	100.0	Space research	Fixed and mobile	Space-to-earth
2025.0 to 2120.0	95.0	Space research	Fixed and mobile	Earth-to-space (Reg. II)
2200.0 to 2300.0	100.0	Space research	Fixed and mobile	Earth-to-space (Reg. II & III)
2500.0 to 2550.0	50.0	Broadcasting - satellite	Space-to-earth	
2550.0 to 2655.0	105.0	Broadcasting - satellite	Space-to-earth	
2655.0 to 2690.0	35.0	Broadcasting - satellite	Space-to-earth	
3400.0 to 3600.0	200.0	Fixed - satellite	Space-to-earth	
3600.0 to 4200.0	600.0	Fixed - satellite	Space-to-earth	
4400.0 to 4700.0	300.0	Fixed - satellite	Space-to-earth	
5725.0 to 5850.0	125.0	Fixed - satellite	Region I: earth-to-space	
5850.0 to 5925.0	75.0	Fixed - satellite	Regions I and III: earth-to-space	
5925.0 to 6425.0	500.0	Fixed - satellite	Earth-to-space	
7250.0 to 7300.0	50.0	Fixed - satellite	Space-to-earth	
7300.0 to 7450.0	150.0	Fixed - satellite	Space-to-earth	
7450.0 to 7550.0	100.0	Fixed - satellite	Fixed, mobile, and meteorological satellite	
7550.0 to 7750.0	200.0	Fixed - satellite	Space-to-earth	
7900.0 to 7975.0	75.0	Fixed - satellite	Earth-to-space	
7975.0 to 8025.0	50.0	Fixed - satellite	Earth-to-space	
8025.0 to 8175.0	150.0	Fixed - satellite	Earth-to-space	
8175.0 to 8215.0	40.0	Fixed - satellite	Check by region	
8215.0 to 8400.0	185.0	Fixed - satellite	Check by region	
8400.0 to 8500.0	100.0	Space research	Earth-to-space	
(GHz)	(GHz)		Fixed and mobile	Space-to-earth
10.95 to 11.2	0.25	Fixed - satellite	Fixed and mobile	Space-to-earth
11.45 to 11.7	0.25	Fixed - satellite	Check by region	Space-to-earth
11.70 to 12.5	0.8	Broadcasting - satellite	Fixed and mobile	Space-to-earth (Regions I and III)
12.50 to 12.75	0.25	Fixed - satellite	Fixed and mobile	Earth-to-space (Regions I and II)
14.0 to 14.3	0.3	Fixed - satellite	Radionavigation	Earth-to-space
14.3 to 14.4	0.1	Fixed - satellite	Radionav. - satellite	Earth-to-space
14.4 to 14.5	0.1	Fixed - satellite	Fixed and mobile	Earth-to-space

Table 5.3-1. World-Wide Spectrum Allocations for Space Services (Cont)  
(Based on WARC-ST, 1971, Geneva)

Frequency (GHz)	Bandwidth (GHz)	Service	Shared With	Usage
17.7 to 19.7	2.0	Fixed - satellite		Space-to-earth
19.7 to 21.2	1.5	Fixed - satellite		Space-to-earth
21.2 to 22.0	0.8	Earth exploration - satellite	Fixed and mobile	Space-to-earth
22.5 to 23.0	0.5	Broadcasting - satellite	Fixed and mobile	Region III
24.0 to 24.05	0.05	Amateur - satellite	Amateur	
27.5 to 29.5	2.0	Fixed - satellite	Fixed and mobile	Earth-to-space
29.5 to 31.0	1.5	Fixed - satellite		Earth-to-space
40.0 to 41.0	1.0	Fixed - satellite		Space-to-earth
41.0 to 43.0	2.0	Broadcasting - satellite		
43.0 to 48.0	5.0	Aeronautical mobile - satellite		
		Maritime mobile - satellite		
		Aero radionavigation - satellite		
		Maritime radionavigation - satellite		
50.0 to 51.0	1.0	Fixed - satellite		Earth-to-space
51.0 to 52.0	1.0	Space research		
54.25 to 58.2	3.95	Inter - satellite		
59.0 to 64.0	5.0	Inter - satellite		
65.0 to 66.0	1.0	Space research		
66.0 to 71.0	5.0	Aeronautical mobile - satellite		
		Maritime mobile - satellite		
		Aeronautical radionavigation - satellite		
		Maritime radionavigation - satellite		
84.0 to 86.0	2.0	Broadcasting - satellite		Earth-to-space
92.0 to 95.0	3.0	Fixed - satellite		
95.0 to 101.0	6.0	Aeronautical mobile - satellite		
		Maritime mobile - satellite		
		Aeronautical radionavigation - satellite		
		Maritime radionavigation - satellite		
102.0 to 105.0	3.0	Fixed - satellite		Space-to-earth
105.0 to 130.0	25.0	Inter - satellite		Earth-to-space
140.0 to 142.0	2.0	Fixed - satellite		
142.0 to 150.0	8.0	Aeronautical mobile - satellite		
		Maritime mobile - satellite		
		Aero. radionav. - satellite		
		Maritime radionavigation - satellite		
150.0 to 152.0	2.0	Fixed - satellite		Space-to-earth
170.0 to 182.0	12.0	Inter - satellite		
185.0 to 190.0	5.0	Inter - satellite		
190.0 to 200.0	10.0	Aeronaut. mobile - satellite		
		Maritime mobile - satellite		
		Aeronautical radionavigation - satellite		
		Maritime radionavigation - satellite		
220.0 to 230.0	10.0	Fixed - satellite		
250.0 to 265.0	15.0	Aeronaut. mobile - satellite		
		Maritime mobile - satellite		
		Aero radionav. - satellite		
		Maritime radionavigation - satellite		
265.0 to 275.0	10.0	Fixed - satellite		

Note: Frequencies above 275.0 GHz have not been allocated

**Page intentionally left blank**

**Page intentionally left blank**

## 5.4 ENVIRONMENTAL EFFECTS

Three significant detrimental effects of the earth's environment on electromagnetic radiation are discussed in the literature. These three are atmospheric attenuation, attenuation due to rainfall through which the radiation passes, and atmospherically induced noise. The following paragraphs present selected curves and nomographs which illustrate these effects and which may be used in designing communications systems for geosynchronous satellites.

### ATMOSPHERIC ATTENUATION

From Figure 5.2-1 it can be seen that a natural division exists between the radio frequency atmospheric windows and the infrared and visible windows. The following paragraphs treat these regions separately.

#### Radio Frequencies

Figure 5.4-1 is an expansion of the RF portion of Figure 5.2-1. It shows total attenuation along a path for frequencies between 1 GHz and 1 THz (1012 Hz). Figure 5.4-2 (Reference 5-1) is a curve of calculated attenuation per kilometer for a sea-level atmosphere with a water-vapor content of 7.5 grams per cubic meter. These calculated values have been checked experimentally with good correlation (Reference 5-2). The curve shows peaks due to water vapor and oxygen for frequencies up to 150 GHz. Figure 5.4-3 (Reference 5-3) shows four theoretical curves and some experimental measurements of attenuation per kilometer for frequencies between 150 GHz and 350 GHz. These curves and measurements have been normalized to an atmosphere with pressure of 760 mmHg, temperature of 290 K, and 7.5 grams per cubic meter of water vapor.

The two figures just described yield atmospheric attenuation per kilometer for a normalized atmosphere at sea level. Figure 5.4-4 (Reference 5-4) is a nomograph for estimating atmospheric absorption due to an atmosphere typical of Washington, D.C., in August. This chart is limited in its range of frequencies, 10 to 40 GHz; however, these frequencies are receiving a great deal of attention for such applications as TDRS and ATS H&I. As is indicated on the chart, one obtains atmospheric absorption as a function of frequency, elevation of the ground terminal above sea level, and angle of elevation of the path above the horizontal.

ATTENUATION - dB

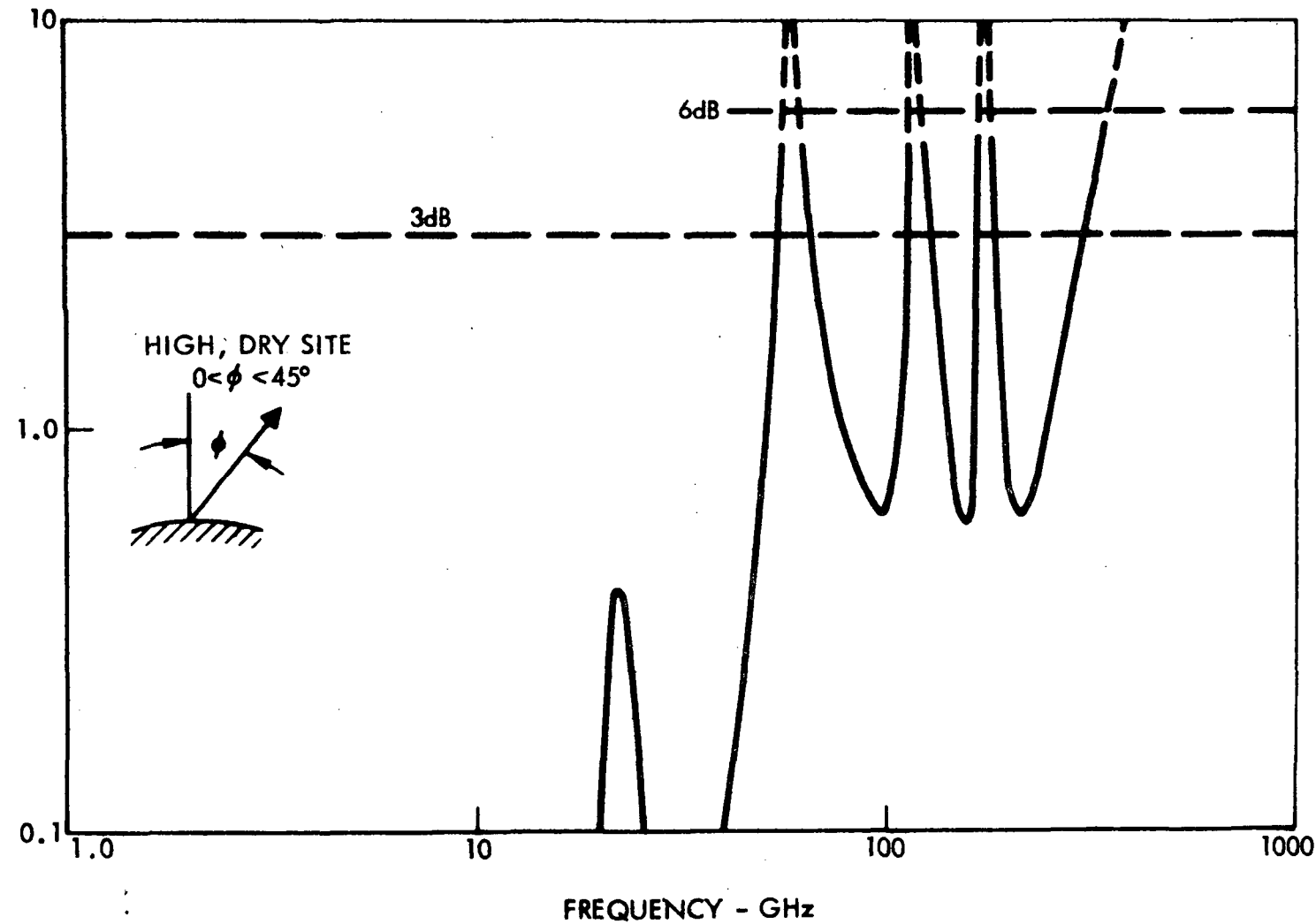


Figure 5.4-1. Transmission Windows

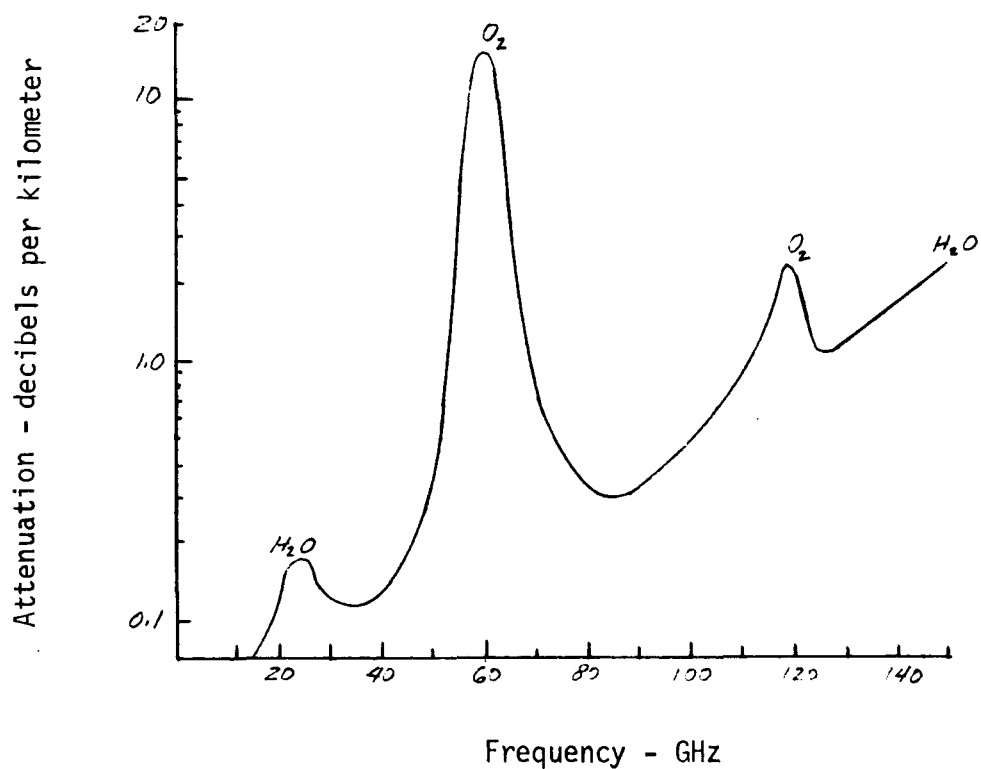


Figure 5.4-2. Effects of Water Vapor and Oxygen

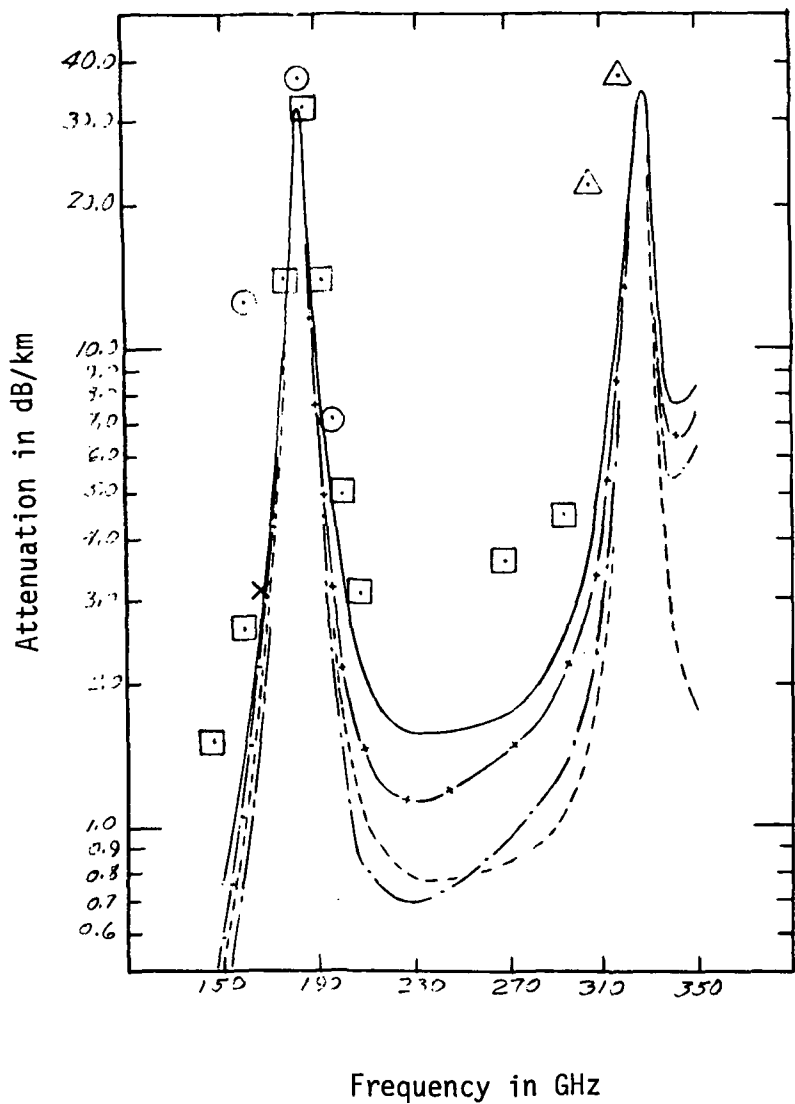
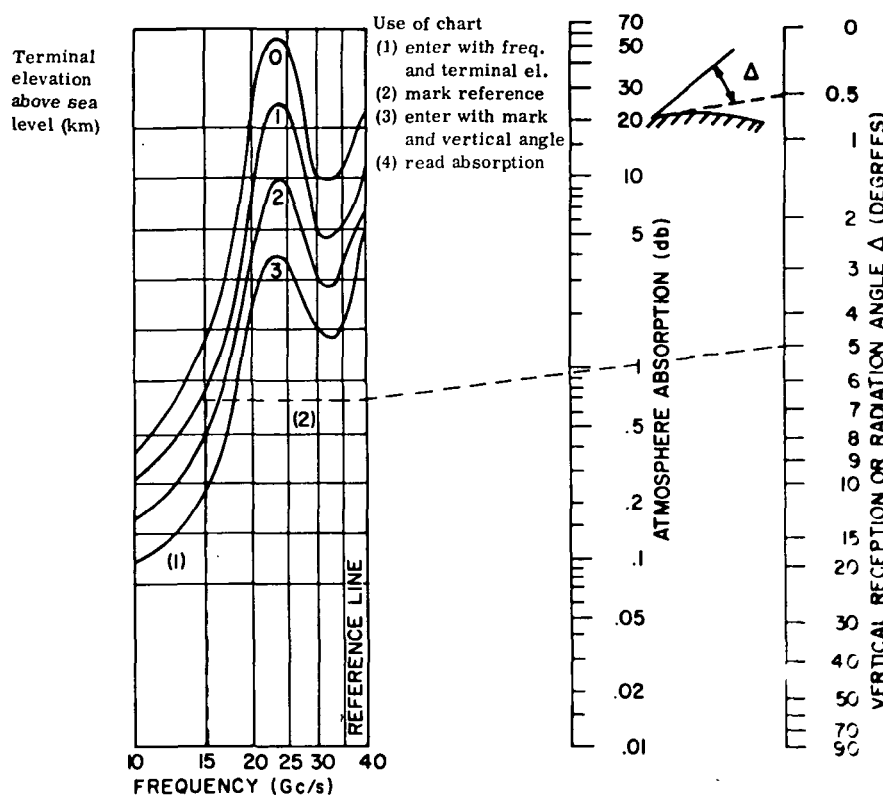


Figure 5.4-3. Atmospheric Attenuation (Between 150 and 350 GHz)  
(Theoretical Curves and Experimental Measurements)



Example:

Frequency 15 GHz  
Elevation 1 km  
Vertical Angle  $5^\circ$   
Absorption 1 dB

Figure 5.4-4. Atmospheric Absorption Nomograph - Frequency vs. Elevation Angle



Note: The reference line in the graph is the 35 GHz line. Horizontally translate values obtained from the graph to the reference line at 35 GHz; plot a straight line from the reference line point to the elevation angle on the right-hand scale and read absorption on the center scale.

Figure 5.4-5, which was plotted from values obtained from the nomograph of Figure 5.4-4 shows attenuation as a function of frequency (10 to 40 GHz) for three elevation angles of interest (assuming a ground terminal at sea level). It is interesting to note, here, that the atmospheric absorption can be kept to a fairly low level by keeping the beam pointed along higher elevation angles, i.e., using greater mask angles.

#### Infrared and Visible Frequencies

Figure 5.4-6 (Reference 5-5) shows the transmission characteristics of the infrared and visible frequency windows. These characteristics are shown as percent transmission normalized to the amount of transmission at the center of the visible window over a 1000-foot path at night. Wavelengths between  $0.55 \mu\text{m}$  and  $14 \mu\text{m}$  (21.4 THz) are covered; three different paths (1000 feet, 3.4 miles, and 10.1 miles) were used with generally the same amount of precipitable water per unit length in each case.

#### RAINFALL ATTENUATION

As mentioned earlier, the lowest value of atmospheric attenuation occurs when the atmosphere is driest. Rainfall along the transmission path contributes additional attenuation to the electromagnetic signal. Figure 5.4-7 (Reference 5-6) shows the amount of attenuation per kilometer for 15 different precipitation rates (1 to 100 mm/hr) for frequencies between 3 GHz and 20 GHz at 18 C. Figure 5.4-8 (Reference 5-7) presents similar data for five precipitation rates (12.5 to 150 mm/hr) for frequencies between 20 GHz and 300 GHz. These curves represent calculated values; however, these calculations have been verified experimentally for frequencies up to 100 GHz. In order to use these curves, one must know the extent of the rainfall and the distribution of rain along the path. Figure 5.4-9 (Reference 5-4) is a nomograph with which attenuation due to rainfall can be found as a function of frequency (5 to 40 GHz), rainfall rate (0.25 to 16 mm/hr), horizontal extent of the rain (1 to 80 km), elevation angle of the beam (0 to 90 degrees), and vertical extent of the rain.

These three figures are useful for specific instances where the rainfall rate and extent are known. In designing a system, however, one cannot know the specific rainfall rate or extent for a given future date. Instead, typical distributions of rainfall are useful. Figure 5.4-10 (Reference 5-7) shows point rainfall rate distributions at six temperate locations. Such data for the specific locations of proposed sites would be needed for system design.

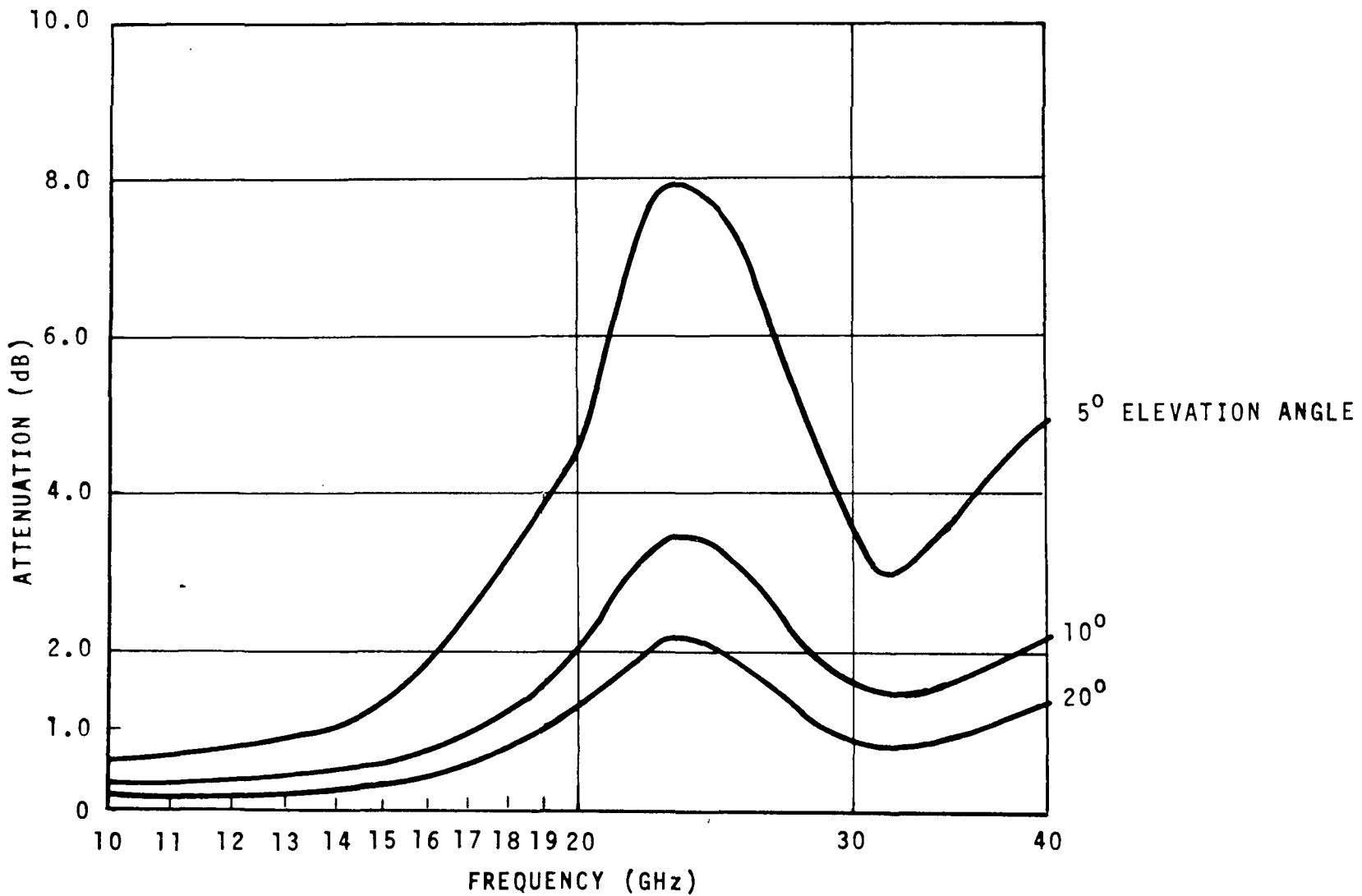
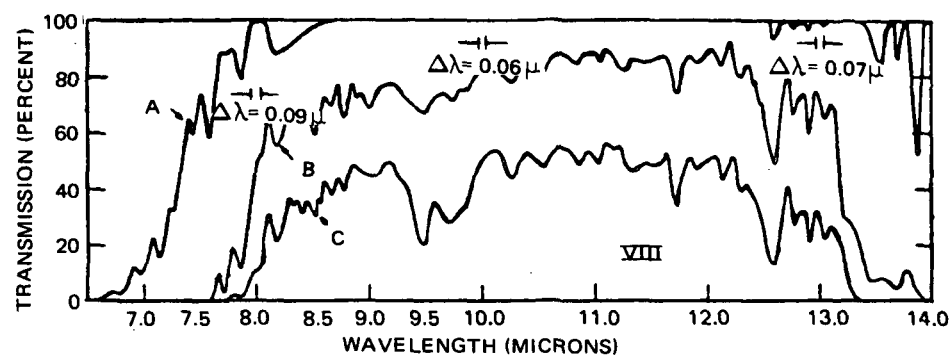
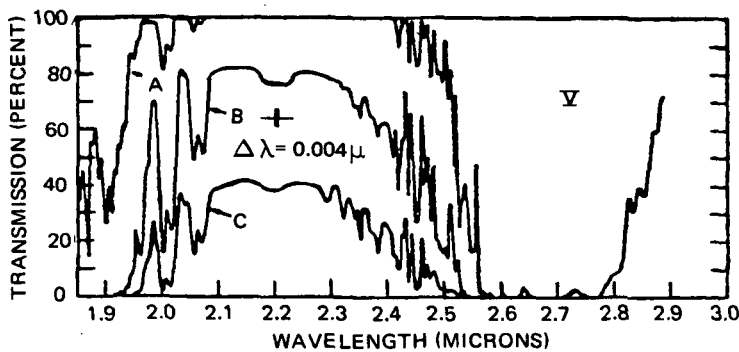
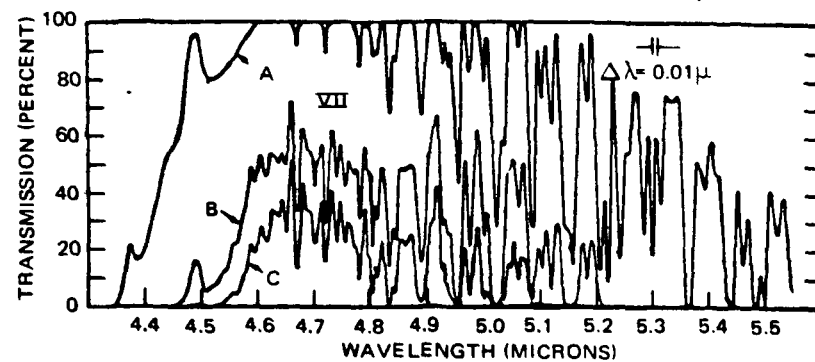
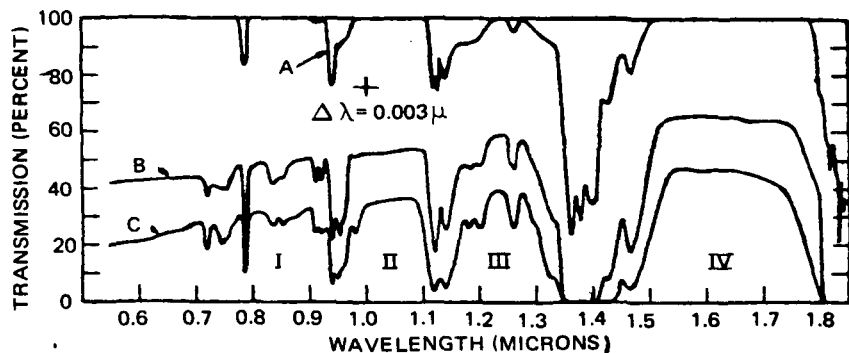
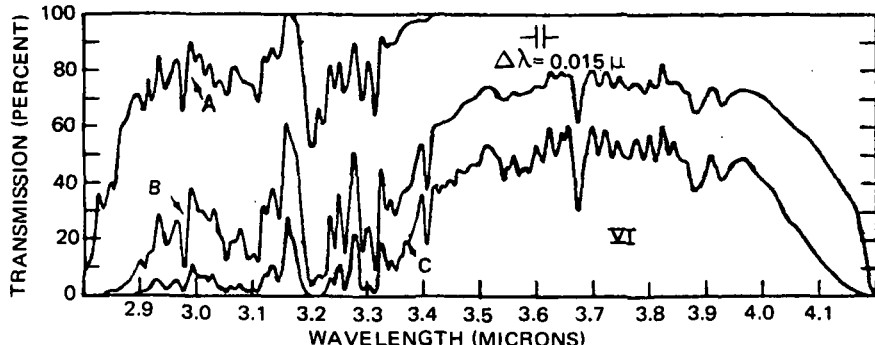


Figure 5.4-5. Atmospheric Absorption as a Function of Frequency and Elevation Angle  
(Sea Level Using an Atmosphere Typical of Washington, D.C. in August)



(MEASUREMENTS MADE OVER HORIZONTAL PATHS)



CURVE	PATH LENGTH	DATE	TIME	TEMP	R H	PRECIPITABLE WATER	VISUAL RANGE
A	1000 FT	3-20-56	3 PM	37°F	62%	1.1 MM	22 MI
B	3.4 MI	3-20-56	10 PM	34.5°F	47%	13.7 MM	16 MI
C	10.1 MI	3-21-56	12 AM	40.5°F	48%	52.0 MM	24 MI

WINDOW DEFINITIONS

I	0.72 TO 0.94 $\mu$	V	1.90 TO 2.70 $\mu$
II	0.94 TO 1.13 $\mu$	VI	2.70 TO 4.30 $\mu$
III	1.13 TO 1.38 $\mu$	VII	4.30 TO 6.0 $\mu$
IV	1.38 TO 1.90 $\mu$	VIII	6.0 TO 15.0 $\mu$

Figure 5.4-6. Atmospheric Transmission in Visible and Infrared Spectrum (Measurements Made Over Horizontal Paths)

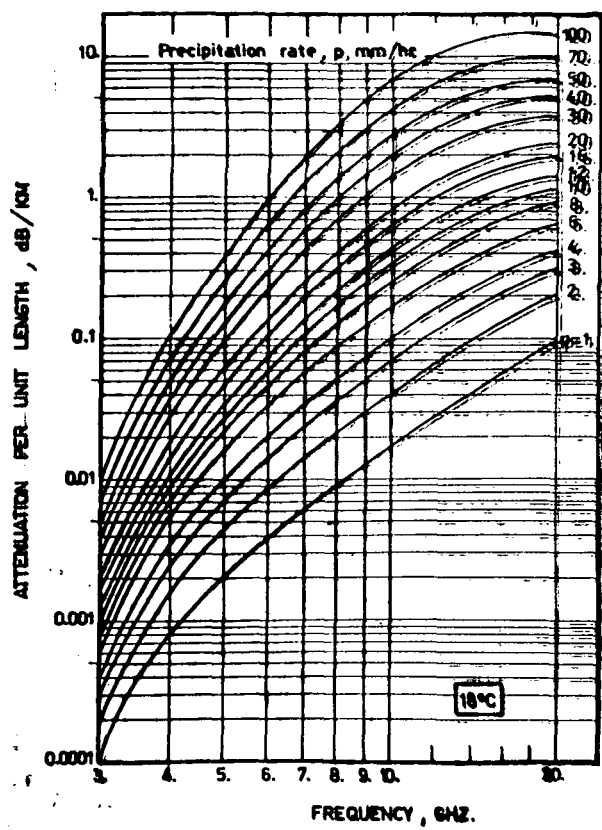


Figure 5.4-7. RF Attenuation Due to Rainfall (3 - 20 GHz)

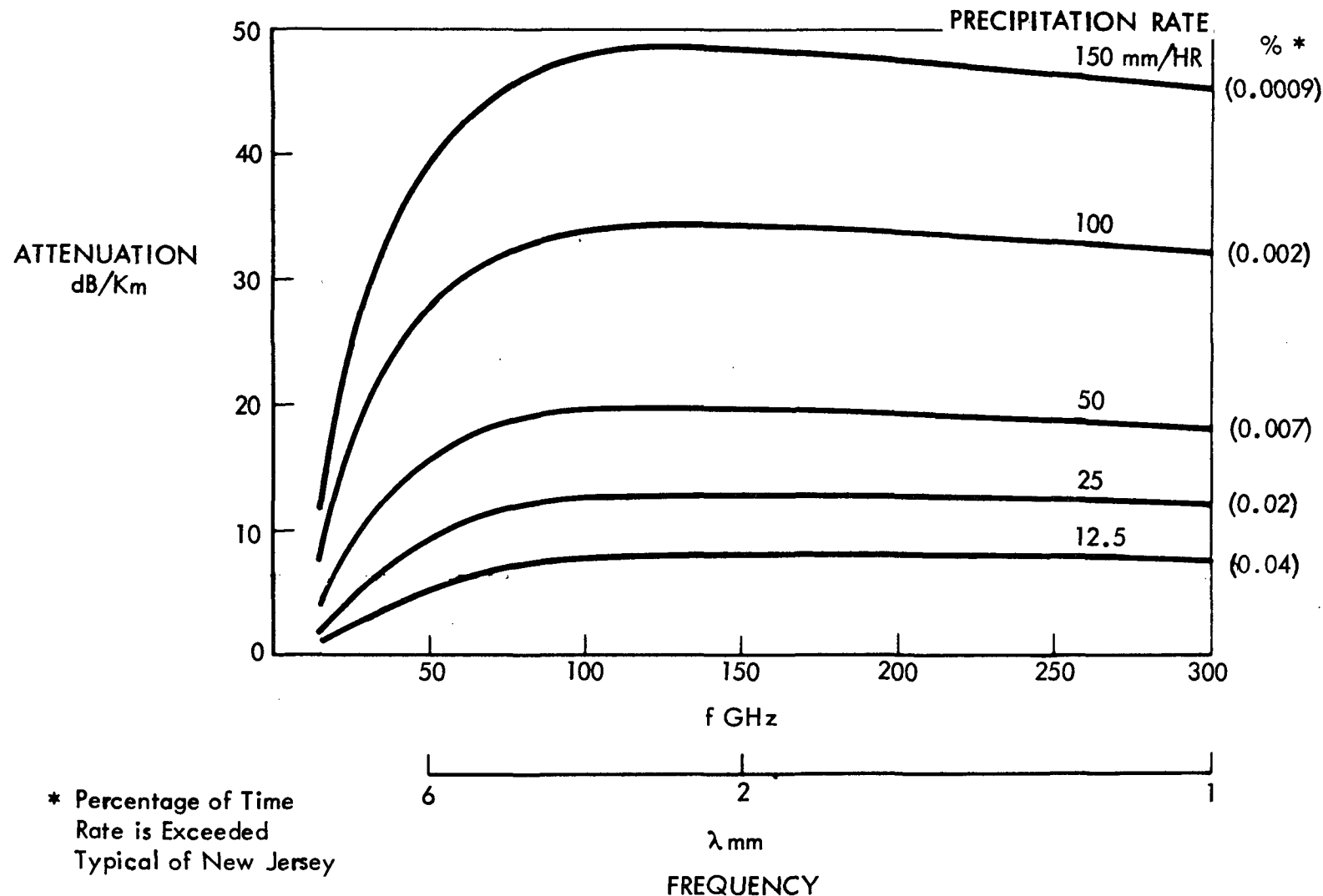
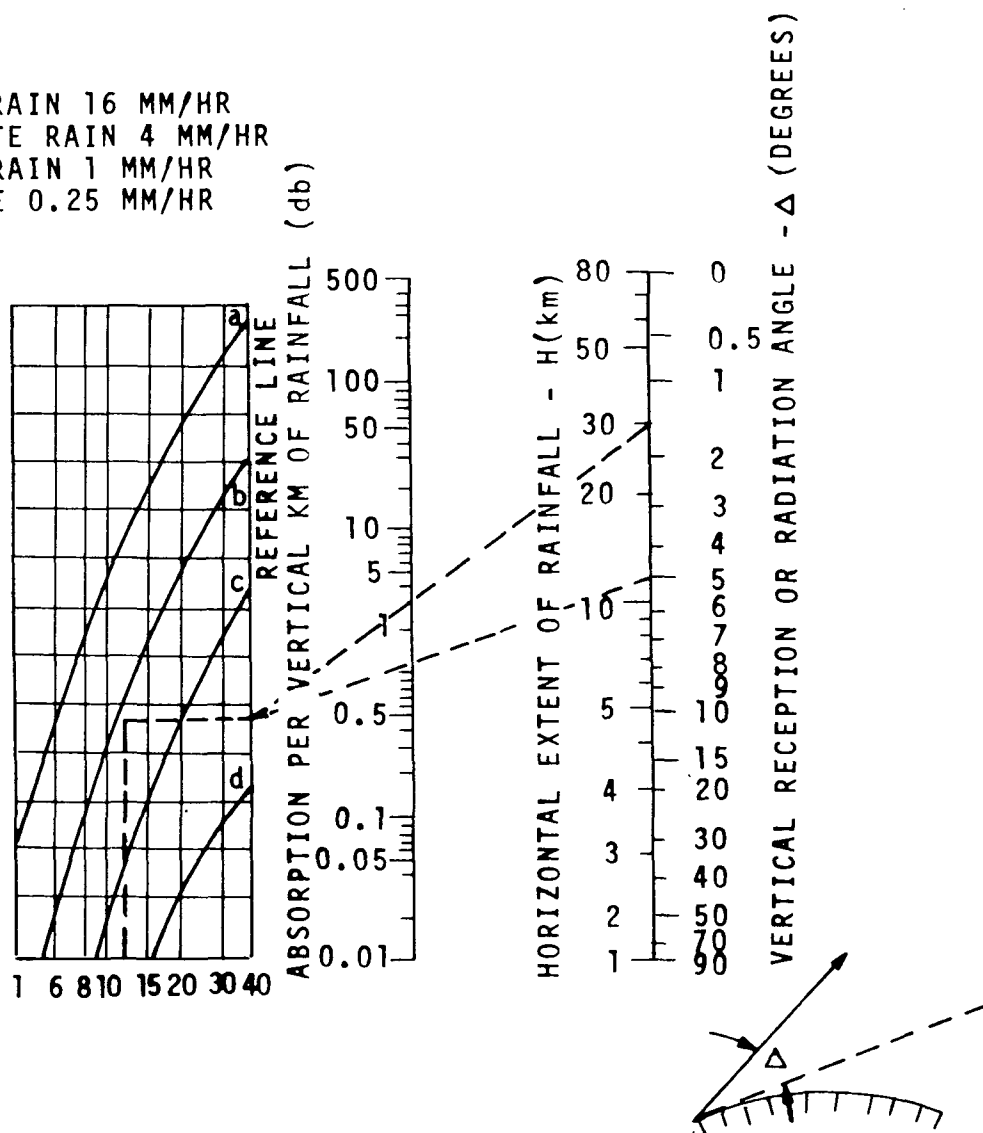


Figure 5.4-8. RF Attenuation Due to Rainfall (Above 10 GHz)

- a = HEAVY RAIN 16 MM/HR
- b = MODERATE RAIN 4 MM/HR
- c = LIGHT RAIN 1 MM/HR
- d = DRIZZLE 0.25 MM/HR



#### CHART TO ESTIMATE ABSORPTION BY RAINFALL

- (1) ENTER WITH FREQ. AND RAINFALL RATE
- (2) MARK REFERENCE LINE
- (3) ENTER WITH MARK AND ( $\Delta$ )
- (4) READ ABSORPTION
- (5) ENTER WITH MARK AND ( $H$ )
- (6) READ ABSORPTION
- (7) MULTIPLY LOWER OF (4) OR (6) BY VERTICAL DEPTH OF RAINFALL

#### EXAMPLE:

AT 12 GHZ IN  
MODERATE RAIN  
2 km IN DEPTH  
EXTENDING 30 km  
ABSORPTION = 2 db  
WHEN  $\Delta = 5^\circ$

Figure 5.4-9. RF Attenuation Due to Rainfall

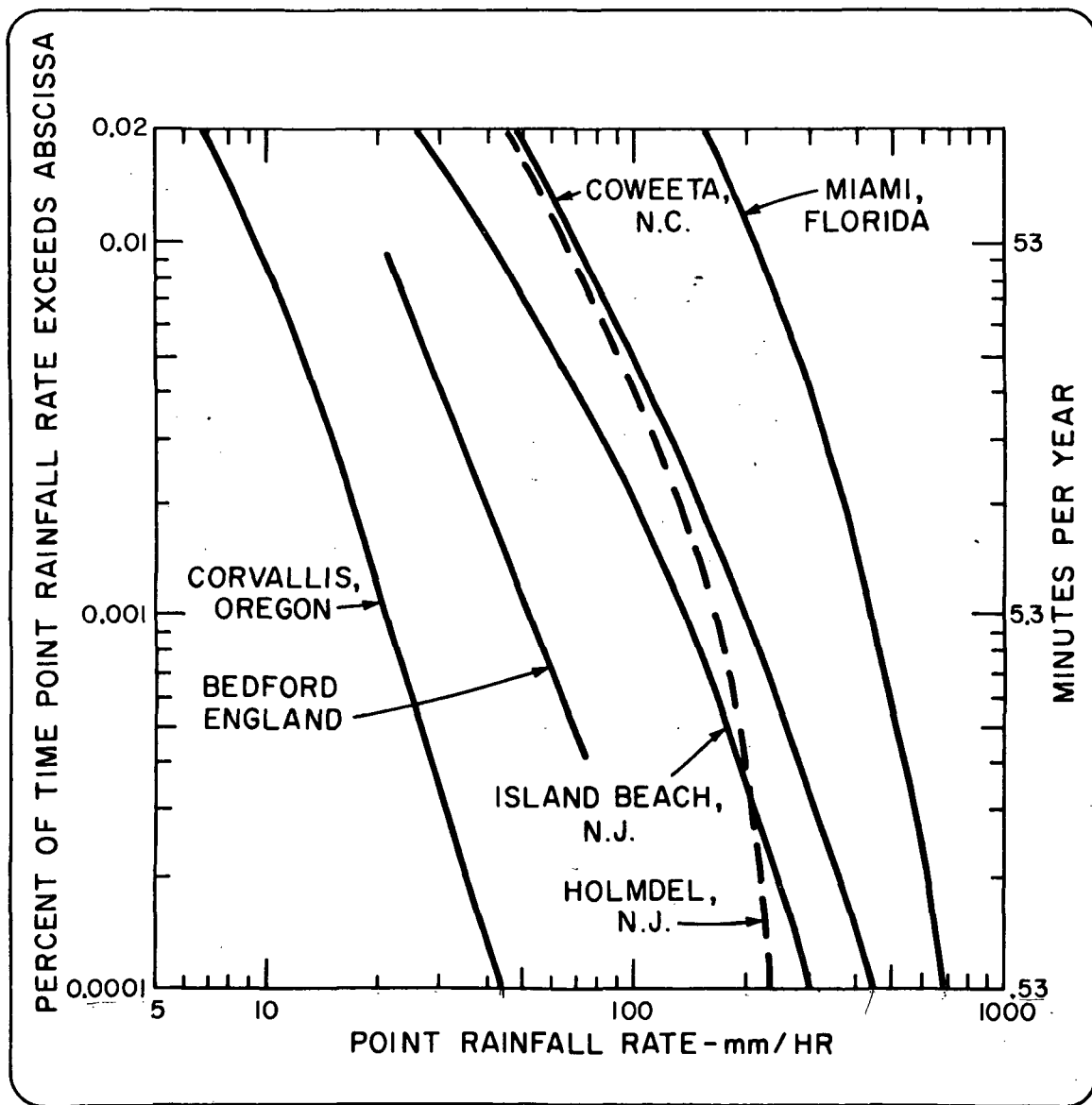


Figure 5.4-10. Point Rainfall Rates Measured in Several Places by Instruments with Rapid Response  
 (Based on a One-Year sample made available through the courtesy of the Illinois State Water Survey)

Figure 5.4-11 (Reference 5-8) shows the time distribution of attenuation due to rain for the 4/6 GHz allocations using a rainfall distribution typical of high rainfall areas. Figure 5.4-12 (Reference 5-8) shows the time distribution of attenuation at 8 GHz for 15 locations. Notice that these curves apply to low elevation angles of the beam. Figure 5.4-13 (Reference 5-7) shows the time distribution of attenuation due to rain at frequencies of 16 GHz and 30 GHz. As noted, these curves are for all elevation angles but daylight hours only at a New Jersey location.

Figure 5.4-14 (Reference 5-2) relates frequency of occurrence of rain cells as a function of cell diameter at altitudes ranging from 5000 feet to 40,000 feet. Note that cells larger than 10 miles in diameter do not occur frequently. Hence, with two ground stations separated by a few miles, one could expect to have one or the other free of rain except in very rare instances. Figure 5.4-15 illustrates this concept of ground station diversity along with a cross-section of a typical thunderstorm. Figure 5.4-16 (Reference 5-7) shows the advantage obtained by using ground station diversity at 16 GHz. Curve 1 shows the percentage of time that a given level of attenuation was experienced at a single ground station; curve 2 shows the percentage of time that a given level of attenuation was experienced while choosing between two ground stations separated by 7 miles (i.e., second station 7 miles from the single station represented on curve 1).

#### SKY NOISE

The oxygen and water vapor absorption phenomena discussed earlier, are manifested in another way. This is illustrated in Figure 5.4-17 (Reference 5-7) which shows the sky noise temperature due to these phenomena. As shown, the sky noise depends on frequency and elevation angle of the beam above the horizon (shown on the right-hand side). Notice that the peaks shown here correspond in frequency to those shown in Figure 5.4-2.



Space Division  
North American Rockwell

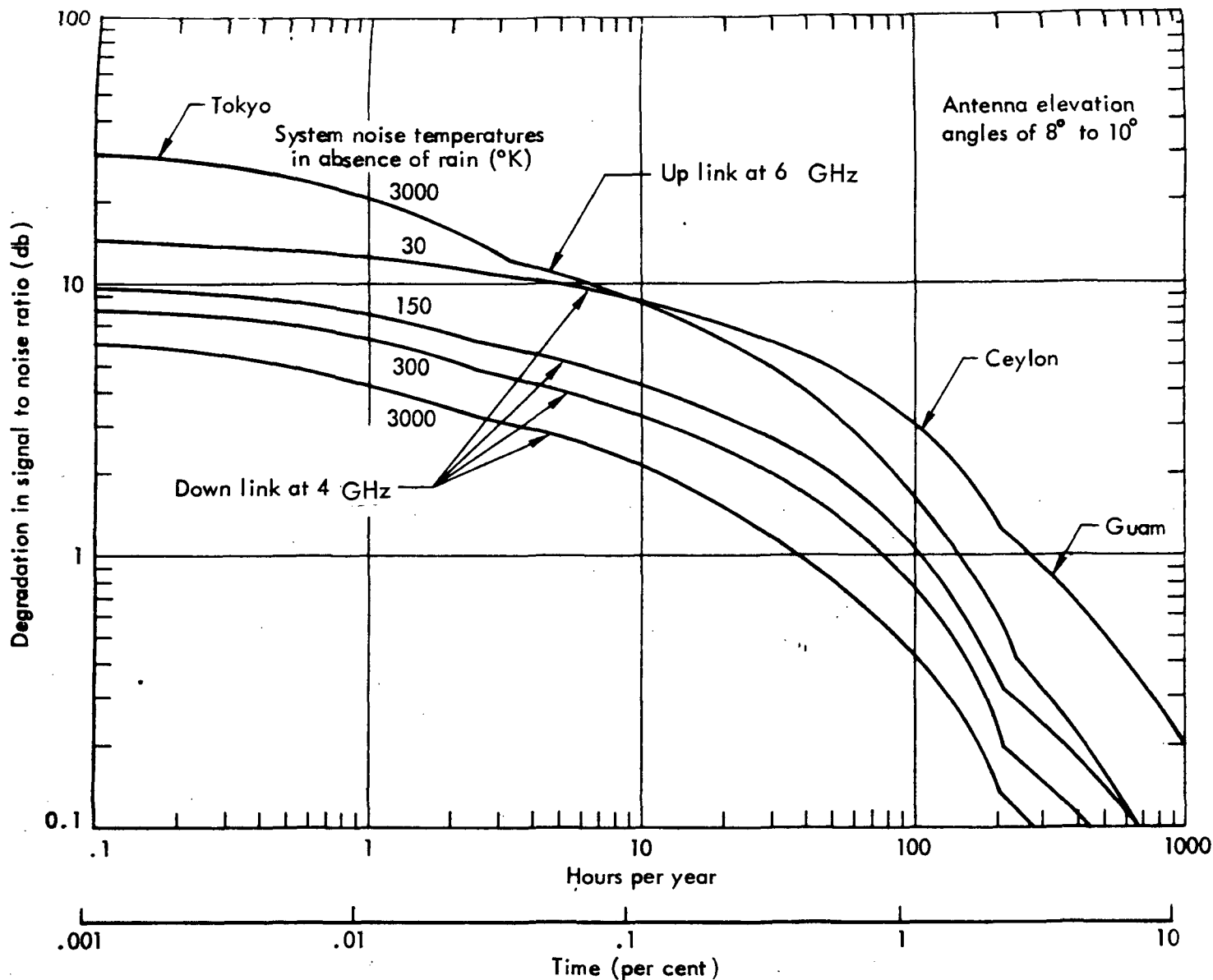


Figure 5.4-11. Typical One-Way System Degradation Due to Rain

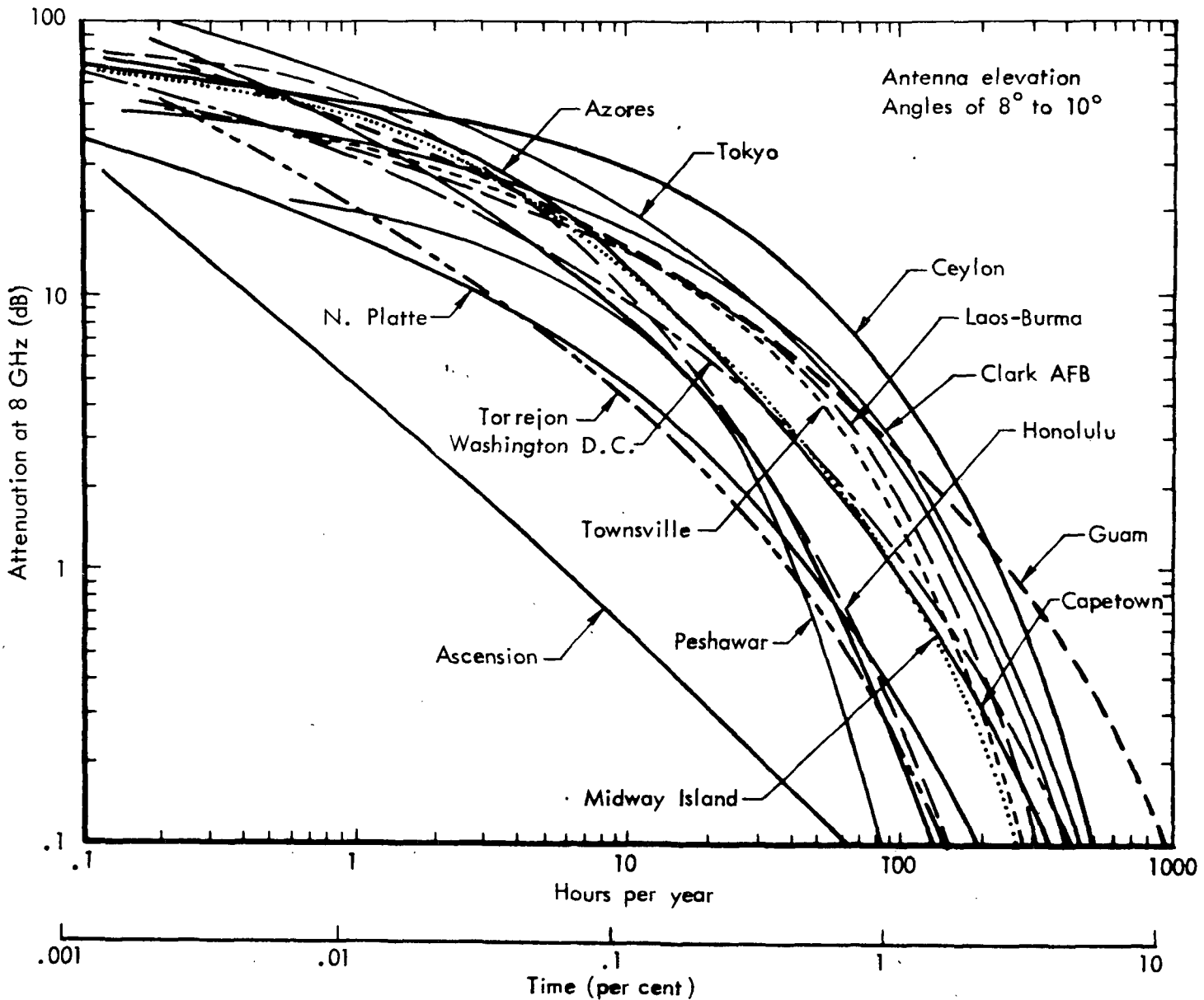


Figure 5.4-12. Precipitation Attenuation (dB) Equalled or Exceeded for Indicated Hours/Year



Space Division  
North American Rockwell

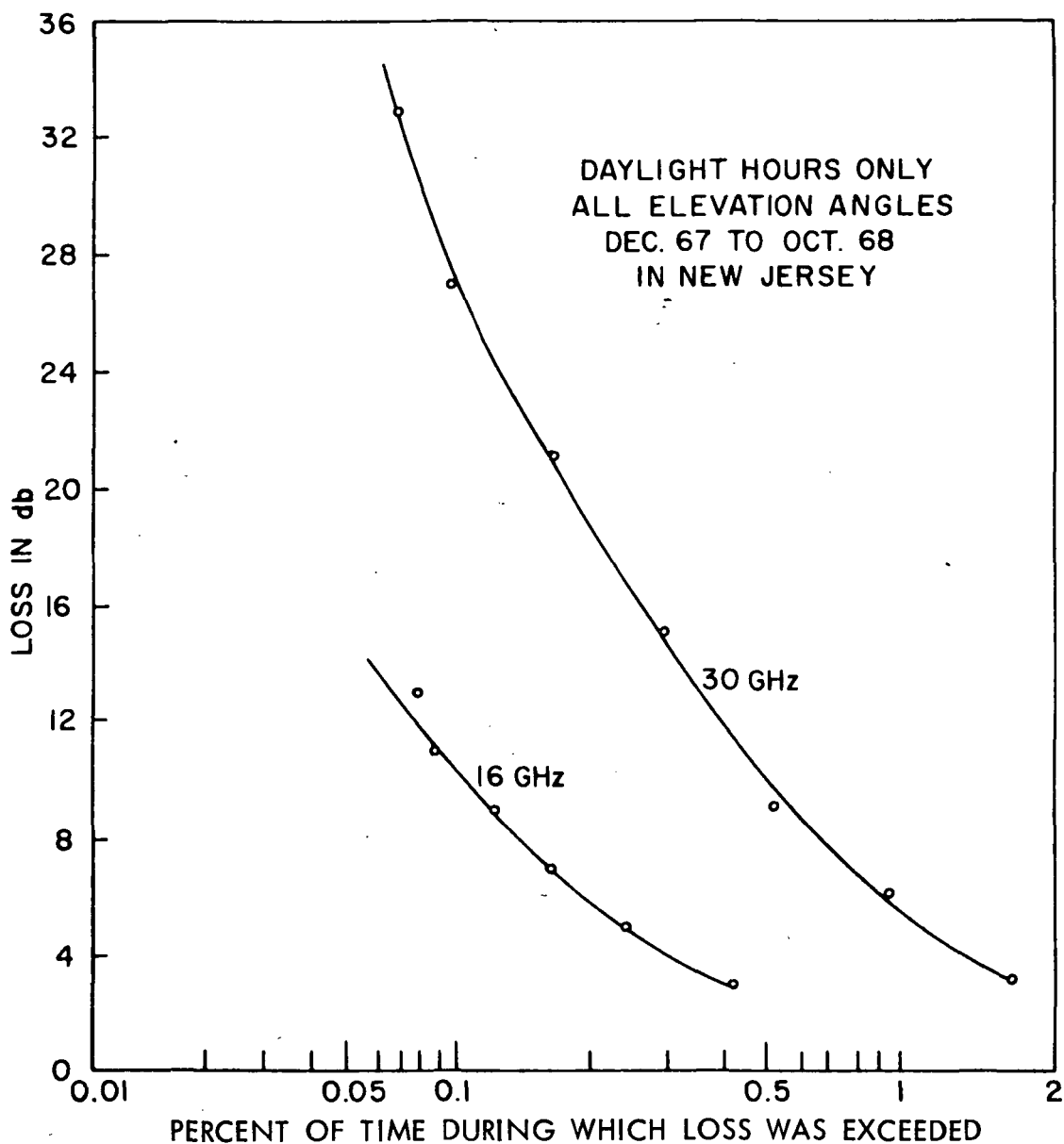


Figure 5.4-13. Atmospheric Attenuation at 16 and 30 GHz as Measured (Using the Sun as a Source)

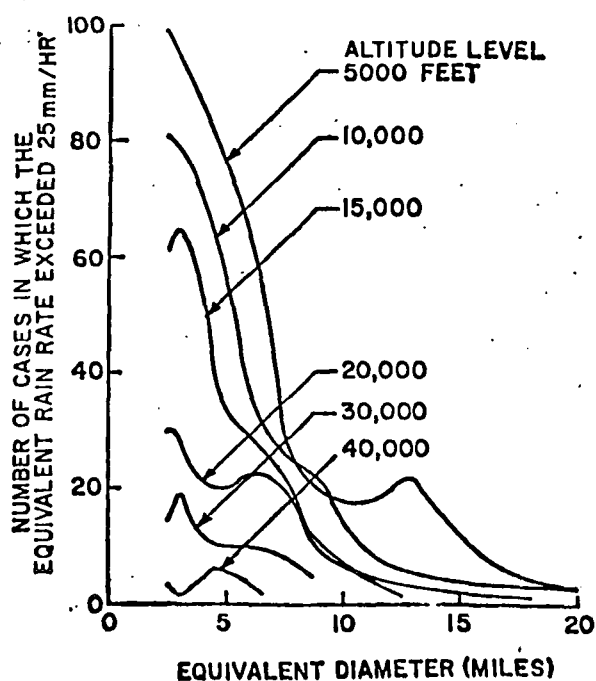


Figure 5.4-14. Frequency of occurrence of rain cells as a function of cell diameter for various altitudes.  
(Based on half-year sample made available through the courtesy of McGill University, Montreal)

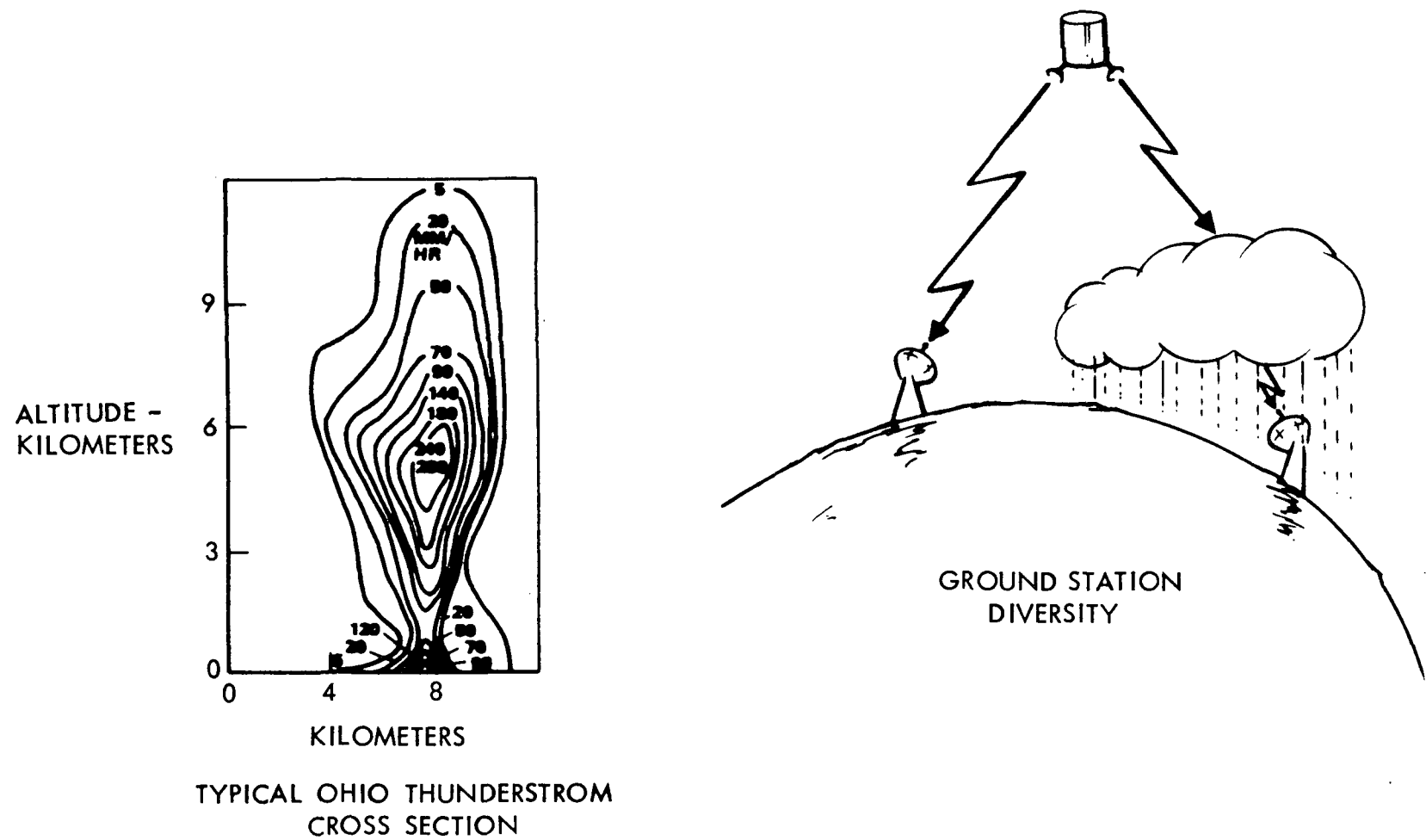


Figure 5.4-15. Ground Diversity Technique to Improve Communication Link Reliability

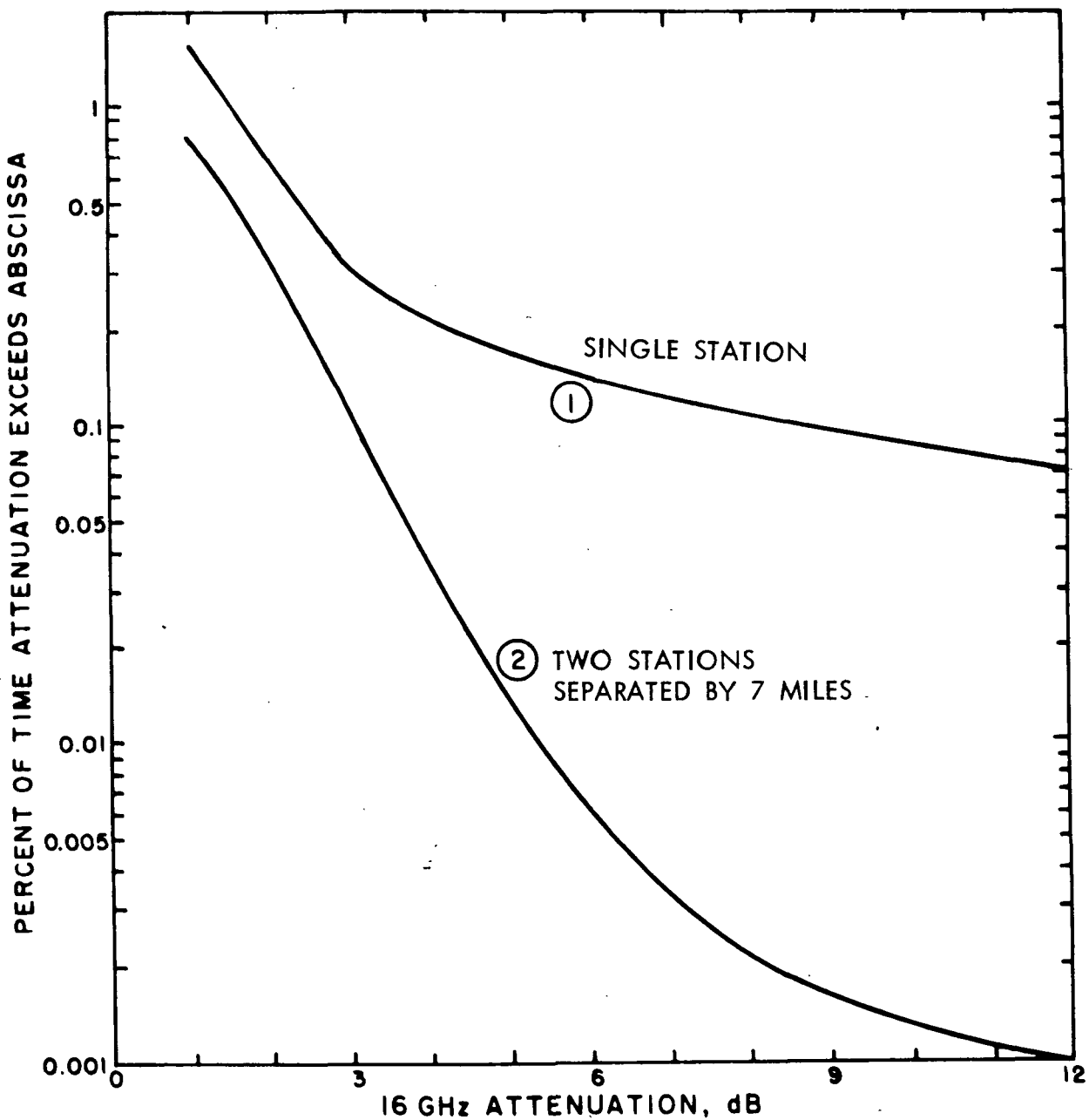


Figure 5.4-16. Diversity Advantage at 16 GHz as Measured for Two Earth Stations Located in New Jersey with Seven-Mile Separation

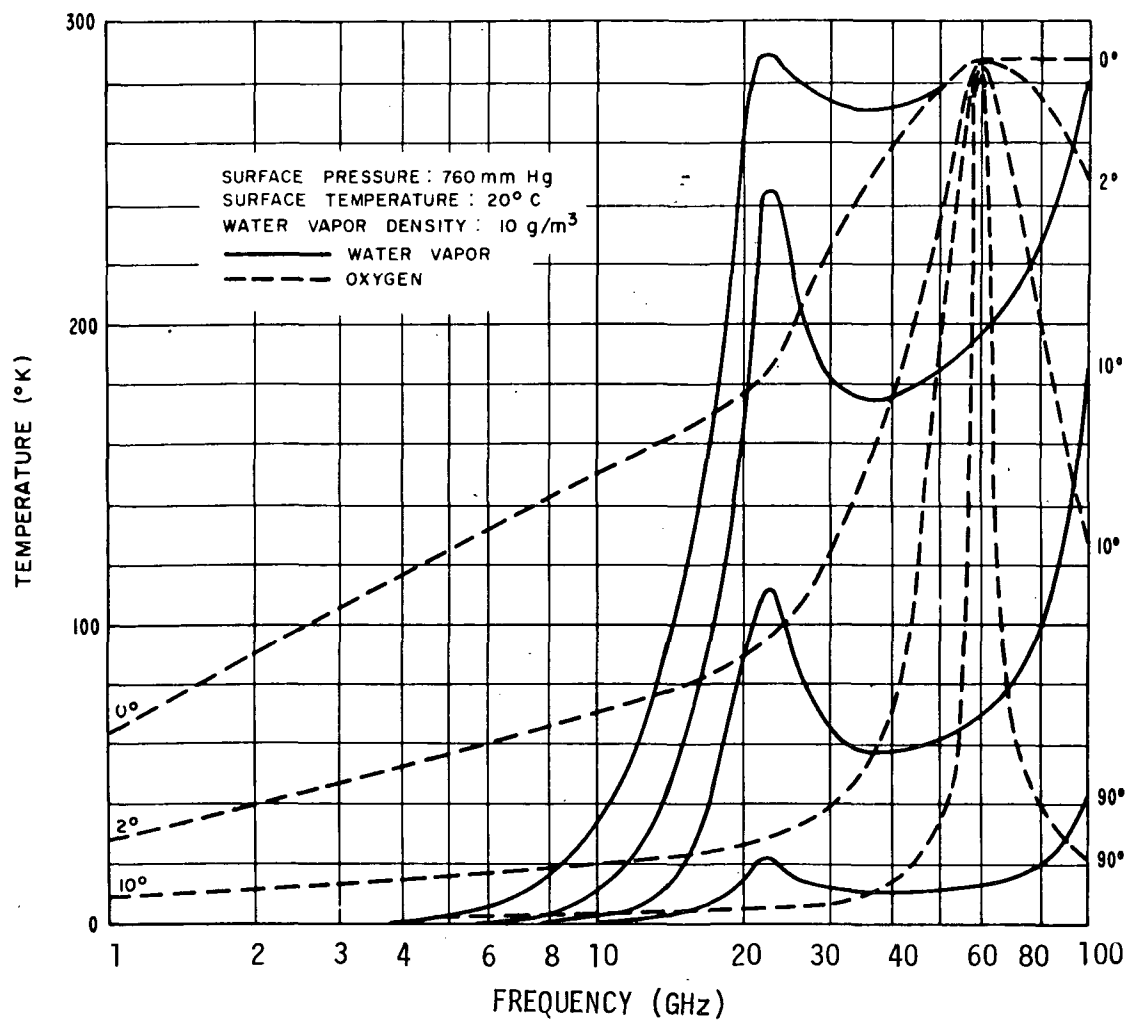


Figure 5.4-17. Sky-Noise Temperature  
Due to Oxygen and Water Vapor Absorption, the Angle of  
Elevation Above the Horizon is Attached to Each Curve



## 5.5 FREQUENCY REUSE TECHNIQUES

Maximum advantage needs to be made of the available portions of the frequency spectrum allocated to space activities. As the previously developed traffic models indicate, the major problem area is in the communications data relay operations. Only a limited amount of the spectrum is available to this function by allocation and by technology limitations in the time period through 1990. Table 5.5-1 illustrates the allocated frequencies and indicates the probable upper frequency limitation from a technology standpoint. For comparative purposes, data rate capability of these bands is shown for single use of these frequency bands. Table 5.5-2 indicates the forecasted data rates for different zones of the world for Domsat and Intelsat functions (derived from the new traffic model forecast). Comparison of these numbers in the year 1990 illustrates the necessity for more than single frequency use in all world zones. Several techniques have been postulated for providing multiple frequency use in particular geographical zones. The following techniques, their implementation, and limitations are discussed in this section:

1. Spatial spacecraft separation utilizing ground station antenna discrimination
2. Orthogonal polarization
3. Spacecraft multiple spot beam earth illumination
4. Time Division Multiple Access (TDMA)
5. Advanced modulation techniques

### GROUND ANTENNA DISCRIMINATION

One of the simplest frequency reuse techniques to apply is that of spatial separation of geosynchronous satellites. Spatial separation is limited by the ground antenna beamwidth. Figure 5.5-1 illustrates the implementation geometry and the numerous desired and undesired link paths. Undesired interfering signals (shown in dotted lines) add to both up and down links at levels defined by the off boresight angle gain of the ground antenna involved.

Development of acceptable satellite spacing versus ground antenna size data was based on the following major assumptions typical of Intelsat or Domsat:

1. Utilization of a system of C-band satellites - downlink  $\approx$  4 GHz, uplink  $\approx$  6 GHz.
2. Each satellite uses 24 transponders, at 40 MHz channel spacing - with two sets of overlapping, orthogonally polarized channels in the 500 MHz bandwidth available
3. Each transponder channel utilizes 34 MHz bandwidth



Table 5.5-1. Allocated Frequency Spectrum and Projected Data Rate Capabilities

Single Frequency Usage					
	Band	Link	Frequency (GHz)	Bandwidth (GHz)	Data Rate Capability (bps)
Probable 1990 Technology Limit	C	Down	3.7 to 4.2	0.5	$4.8 \times 10^8$
		Up	5.925 to 6.425		
	$K_{LO}$	Down	{ 10.95 to 11.2 11.45 to 11.7 }	0.5	$4.8 \times 10^8$
		Up	14.0 to 14.5		
	$K_{HI}$	Down	17.7 to 21.2	3.5	$33.6 \times 10^8$
		Up	27.5 to 31.0		
					Total = $4.3 \times 10^9$
Allocated by WARC	Q	Down	40.0 to 41.0	1.0	$9.6 \times 10^8$
		Up	50.0 to 51.0		
	W	Down	92.0 to 95.0	3.0	$28.8 \times 10^8$
		Up	102.0 to 105.0		
	-	Down	140.0 to 142.0	2.0	$19.2 \times 10^8$
	-	Up	150.0 to 152.0		
	- (not allocated)		220.0 to 230.0 265.0 to 275.0	10.0	$96.0 \times 10^8$
					Total = $15.4 \times 10^9$



Table 5.5-2. Data Rate Forecast - Year 1990  
(Derived from New Traffic Model)  
(Figures 3.4-3, 3.4-5 of Vol. IV, Part 2)

Area	Function	1990 Data Rate Forecast
1. USSR (East) Asia Australia Oceana	Domsat	$27.5 \times 10^{10}$
2. Europe Africa USSR (West)	Domsat	$16.2 \times 10^{10}$
3. North America South America	Domsat	$13.0 \times 10^{10}$
4. Indian Ocean	Intelsat	$6.8 \times 10^9$
5. Pacific Ocean	Intelsat	$6.3 \times 10^9$
6. Atlantic Ocean	Intelsat	$4.7 \times 10^9$

4. Each channel uses FM modulation, utilizing a frequency division multiplexing (FDM) system that puts 1200 voice - circuits with an RMS modulation index of 0.6 and a top baseband frequency of 5.5 MHz on a transponder
5. Satellite spacing is acceptable if the interference noise on the worst case satellite and in the worst case voice circuit is less than 1000 pWOp (pico-watts psophometrically weighted) as recommended by CCIR. This is one-tenth of the total noise budget of 10,000 pWOp allowed. It provides high quality voice reproduction.

Acceptable performance for an FDM/FM voice circuit system outlined above would permit acceptable performance in other services; e.g., television, digital data, etc.

Based on these assumptions a set of data was developed for the C-band case that resulted in the graph of Figure 5.5-2 that depicts acceptable satellite spacing versus antenna size and level of interference noise power for a set of 11 homogeneous satellites. Although this data is for C-band, an extrapolation can be made to the other usable allocated bands, K<sub>L0</sub> and K<sub>H1</sub>. The beamwidth protection ratio is a function of the antenna diameter to wavelength ratio ( $D/\lambda$ ). The  $D/\lambda$  values for antenna diameters are shown next to the antenna size used for C-band. By referring to Table 5.5-3, it is apparent that at

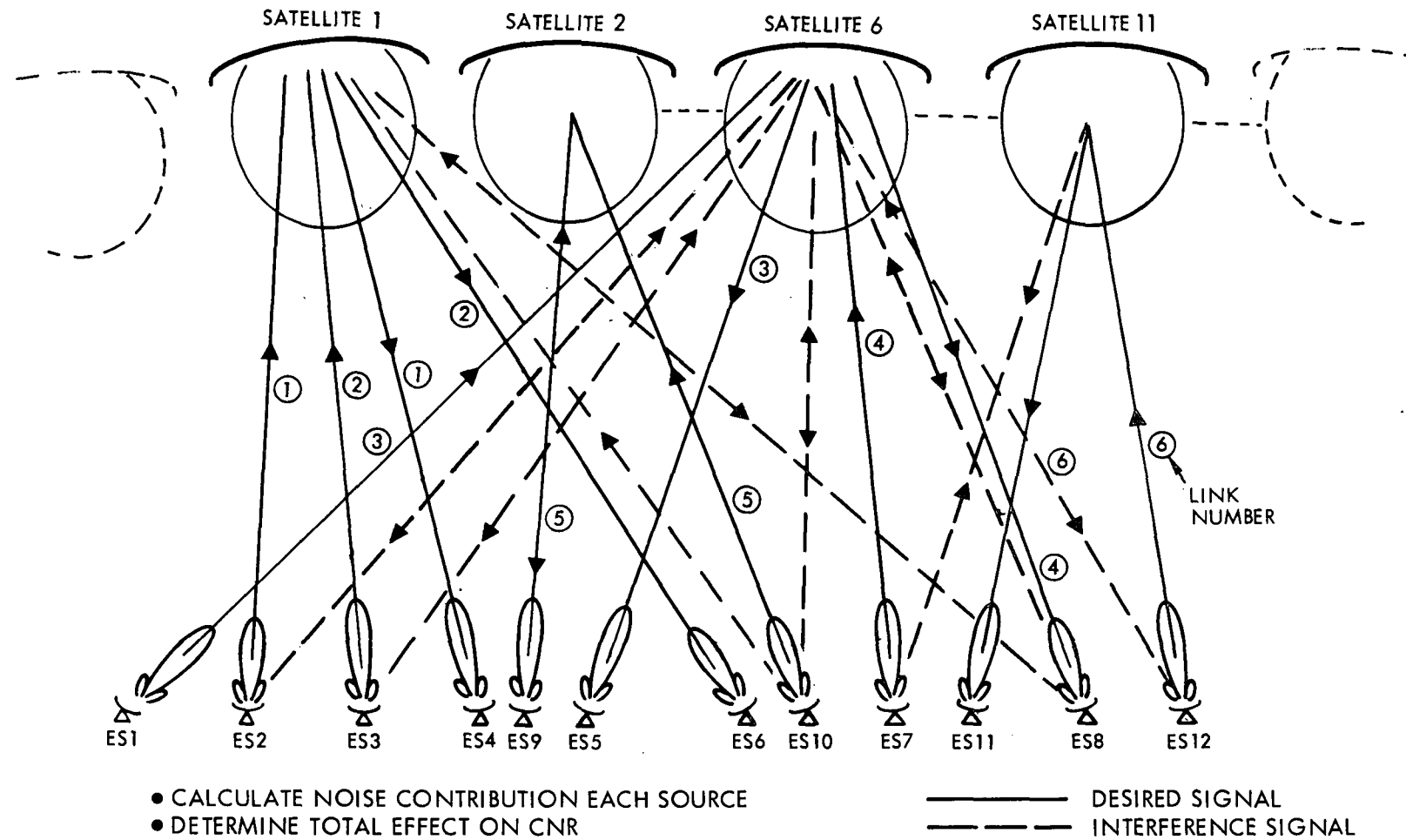


Figure 5.5-1. Interference Modes/Shared Frequency Operation

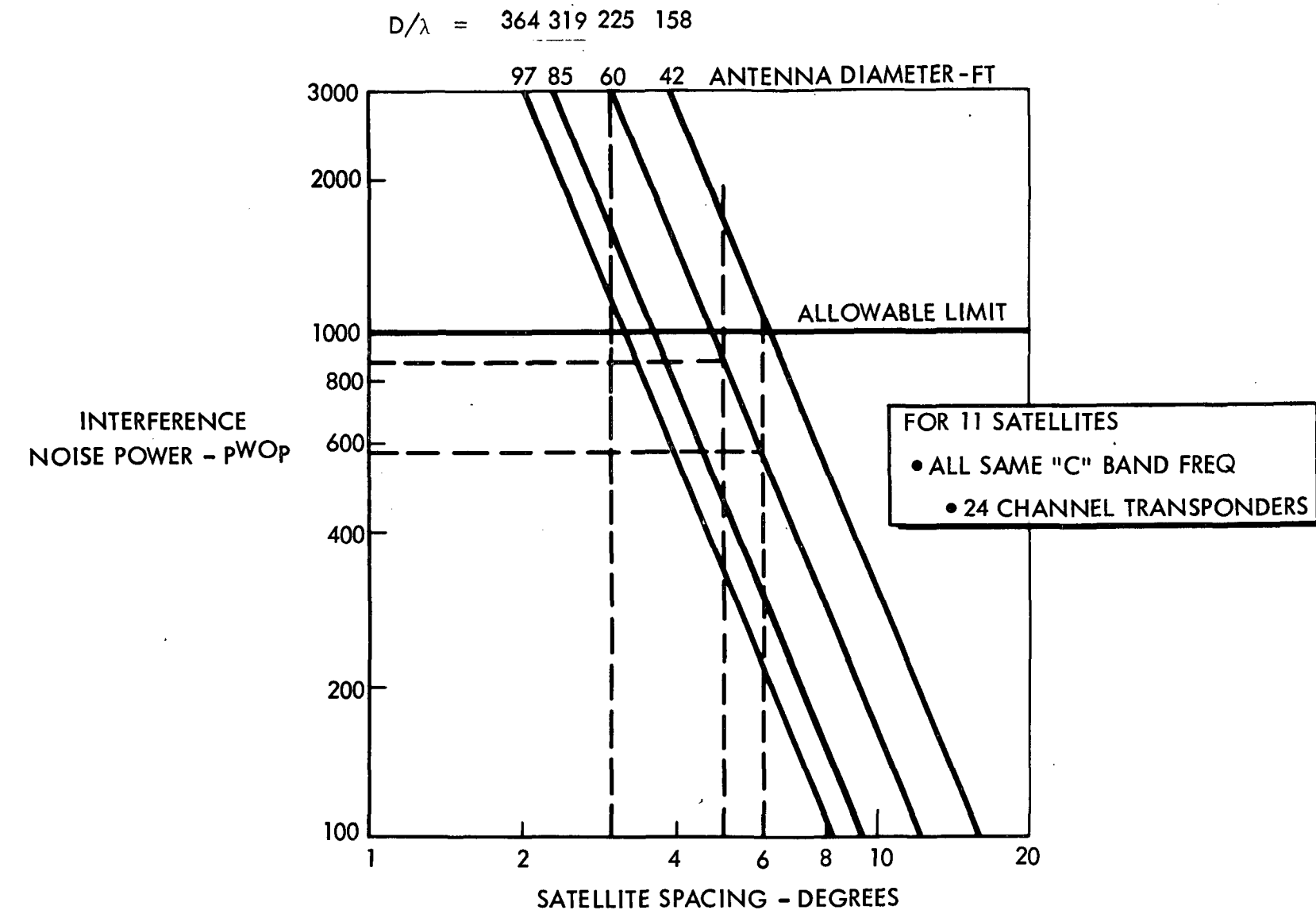


Figure 5.5-2. Interference Noise Versus Satellite Spacing



Table 5.5-3. Antenna Diameter to Wavelength Ratio

Antenna Diameter	C-Band	K <sub>L0</sub> -Band	K <sub>HI</sub> -Band
97	364	1080	1685
85	319	941	1475
60	225	667	1042
42	158	468	733
30	112.5	334	521
15	56.3	167	261

Based on the low end of the down link of each frequency band

C-Band = 3.7 GHz; K<sub>L0</sub>-Band = 11.7 GHz; K<sub>HI</sub>-Band = 17.7 GHz

these higher frequencies, D/λ increases by a magnitude that allows spatial discrimination with relatively small ground antenna. Since the recommended ground antenna size will be at least 30 feet for these higher frequencies, C-band would be the determining frequency for determination of spatial separation.

The Interference Noise versus Satellite Spacing curve (Figure 5.5-2) was derived as follows:

The test tone signal-to-weighted noise power ratio (SNR) in the worst-case (top) telephone channel is related to the carrier-to-interference ratio (CIR) at the receiver input by the expression

$$\text{SNR} = \text{CIR} + \text{IRF} \text{ in dBmOp} \quad (1)$$

IRF = Interference Reduction Factor

The Interference Reduction Factor includes noise weighting and top channel pre-emphasis. It depends on the modulation characteristics of the wanted and unwanted signals. For the case presented here where the interfering carriers are on the same frequency, the IRF is equal to 26.5 dB. It was derived from the following (Reference 5-9):

$$\text{IRF} = 18.8 + 10 \log \left\{ 1 + 9.5 \left[ \frac{1}{\sqrt{10}} \left( \frac{\text{BW}}{0.0084N} - 1 \right) \right]^3 \right\} \text{dB} \quad (2)$$

where

BW = RF bandwidth (MHz)

N = number of voice circuits

Further, the noise in the top channel is related to SNR by,

$$\text{SNR} = 10 \log_{10} \frac{10^9}{N_i} \quad (3)$$

$N_i$  = noise in pWOp

### Interference Relationships

The equations for computing the downlink interference for a single interfering satellite and for uplink interference for a single interfering earth station are developed in Figures 5.5-3 and 5.5-4, respectively. From the carrier-to-interference ratio, the noise in the worst-case telephone channel can be computed as described in the previous section. This is done for each interference source and the total uplink or downlink noise is the sum of each of the contributions. The total noise is the sum of the uplink and downlink noise.

For the case where each of the satellite EIRP's and each of the ground station EIRP's are equal, the equations result in the following since these powers drop out:

$$\text{CIR}_D = G_E - [32 - 25 \log_{10} \theta] + P \quad (4) \text{ downlink}$$

$$\text{CIR}_U = G_U - [32 - 25 \log_{10} \theta] + P \quad (5) \text{ uplink}$$

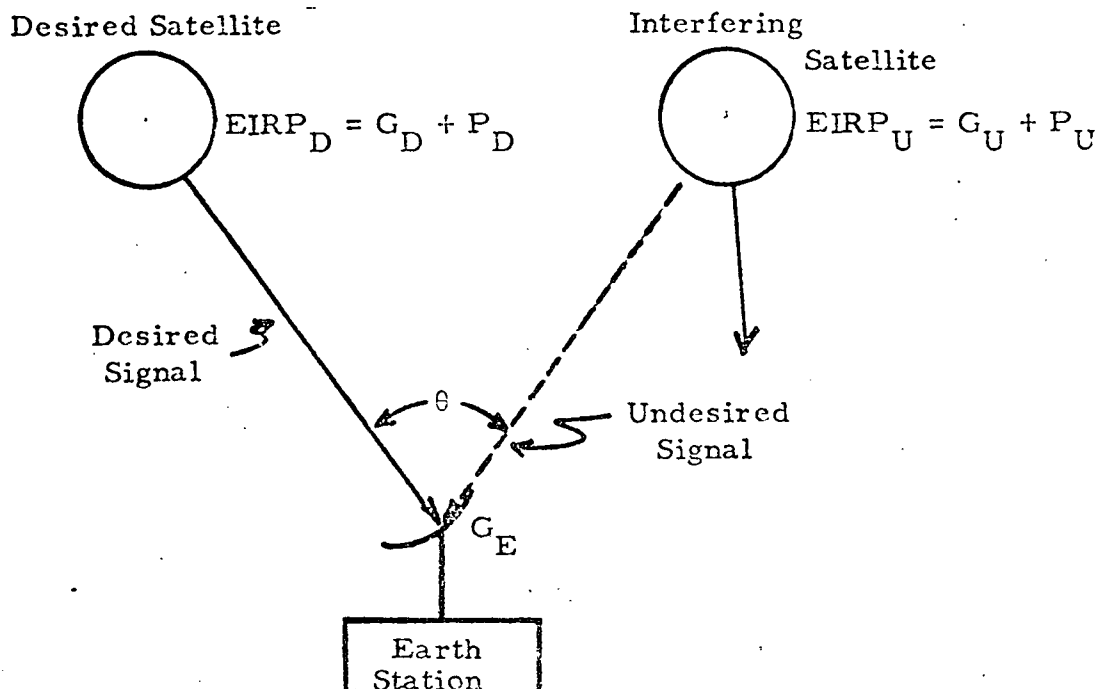
Assuming that the ground antennas are parabolic and have an efficiency of 50 percent, the on-axis gain becomes

$$G = 20 \log_{10} \left( \frac{\pi D}{\lambda} \right) - 3 \text{ in dB} \quad (6)$$

substituting this in Equations (4) and (5),

$$\text{CIR} = 20 \log_{10} \left( \frac{\pi D}{\lambda} \right) - 35 + 25 \log_{10} \theta + P \text{ dB} \quad (7)$$

for either uplink or downlink



$$\begin{aligned} \text{CIR} &= G_E + G_D + P_D - (G_U + P_U) - [32 - 25 \log_{10}(\theta)] + P \quad \text{dB} \\ &= G_E - [32 - 25 \log_{10}(\theta)] + (G_D + P_D) - (G_U + P_U) + P \quad \text{dB} \\ &= G_E - \underbrace{[32 - 25 \log_{10}(\theta)]}_{\text{Antenna Suppression}} + \underbrace{[EIRP_D - EIRP_U]}_{\text{Relative EIRP Adjustment}} + \underbrace{P}_{\text{Polarization Isolation}} \quad \text{dB} \end{aligned}$$

where  $G_E$  (CCIR Standard)

CIR = Carrier to noise (interference) ratio

$G_E$  = Earth station antenna gain (on-axis) - dBi

$G_D$  = Antenna gain of desired satellite - dBi

$P_D$  = Desired satellite transmitter power output - dBW

$G_U$  = Antenna gain of undesired (interfering) satellite - dBi

$P_U$  = Undesired satellite transmitter power output - dBW

$\theta$  = Orbit spacing angle (degrees)

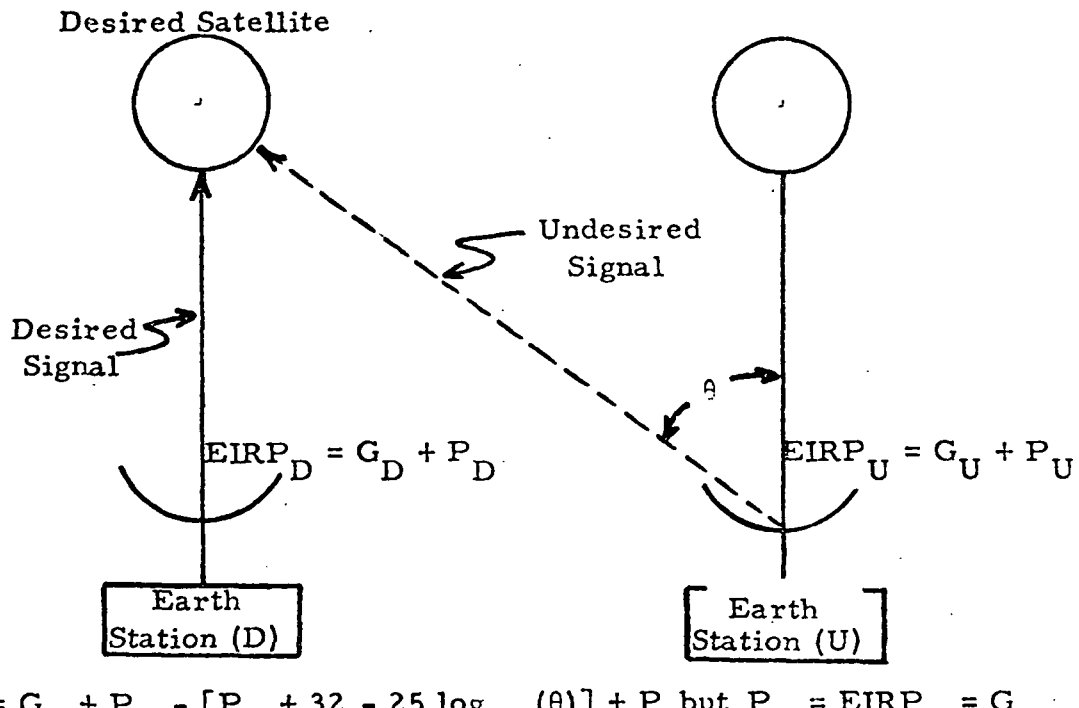
$[32 - 25 \log_{10}(\theta)]$  = Earth station antenna gain at off-axis angle  $\theta$  - dBi

$P$  = Polarization isolation - dB

Assume no satellite antenna directivity, i.e., undesired signal =

$$\text{EIRP}_U = G_U + P_U$$

Figure 5.5-3. Downlink Interference



$$\begin{aligned} CIR &= G_D + P_D - [P_U + 32 - 25 \log_{10}(\theta)] + P \text{ but } P_U = EIRP_U = G_U \\ &= EIRP_D - [EIRP_U - G_U + 32 - 25 \log_{10}(\theta)] + P \quad \text{dB} \\ &= \underbrace{(EIRP_D - EIRP_U)}_{\text{Relative EIRP Adjustment}} + \underbrace{G_U - [32 - 25 \log_{10}(\theta)]}_{\text{Antenna Suppression (Interfering Station)}} + \underbrace{P}_{\text{Polarization Isolation}} + P \end{aligned}$$

where

CIR = Carrier-to-noise ratio - dB

$G_D$  = Desired earth station antenna gain - dBi

$P_D$  = Desired earth station transmitter power output - dBW

$P_U$  = Undesired (interfering) earth station transmitter power output - dBW

$\theta$  = Orbit spacing angle (degrees)

$[32 - 25 \log_{10}(\theta)]$  = Earth station antenna gain at off-axis angle  $\theta$  - dBi

$P$  = Polarization isolation - dB

Assume no satellite antenna directivity to discriminate between  
desired and interfering earth stations

Figure 5.5-4. Uplink Interference



Substituting this in Equation (1),

$$\text{SNR} = 20 \log_{10} \left( \frac{\pi D}{\lambda} \right) - 35 + 25 \log_{10} \theta + P + \text{IRF dBmOp} \quad (8)$$

or assuming no polarization isolation and an IRF of 26.5 dB the equation becomes

$$\text{SNR} = 20 \log_{10} \left( \frac{\pi D}{\lambda} \right) - 35 + 25 \log_{10} \theta + 26.5 \text{ dBmOp} \quad (9)$$

This equation was then used to calculate values for several spacings and ground antenna sizes that were used to produce Figure 5.5-2. Table 5.5-4 shows a typical set of calculations.

#### ORTHOGONAL POLARIZATION

Isolation between two orthogonally polarized beams radiated by a single paraboloid has been determined analytically and experimentally. Isolation levels between orthogonal beams to allow frequency reuse should approach 30 dB. Such isolation is feasible, and can be considered for use in the frequency bands considered in this study for communications relay type satellites.

In practice, two antenna beams are radiated from the same reflector with the beams polarized orthogonally with respect to each other. Linear orthogonal polarization may be implemented by utilizing special feed horns--rectangular corrugated type--that are fed via an ortho-mode transducer (OMT). Overlapping frequencies are fed into the ortho-mode transducer so that the horn illuminates the parabola with these overlapping frequencies whose propagation is orthogonally polarized relative to each other.

Sufficient data has been collected by Comsat, TRW and others to practically demonstrate the feasibility of polarization isolation. Experimental data shows that isolation better than 30 dB can be obtained within the 3 dB contour of the antenna patterns. Figure 5.5-5 illustrates such measurements taken at 7.9 GHz by TRW (Reference 5-10). The numbers at the corners of the grids indicate the level of isolation. Figure 5.5-6 shows isolation of the same order in C-band - Domsat uplink between 5.925 to 6.425 GHz. These figures can be reasonably extrapolated to slightly different beam patterns typical of results on the down link frequency band (3.7 - 4.2 GHz). It is important to realize that such isolation is available within the 3 dB contour of the antenna pattern. As the beam proceeds further off axis this isolation reduces to as low as 10 dB in the sidelobe regions. Thus, when performing spatial interference calculations from ground antenna discrimination, no more than 10 dB advantage should be taken for an assumed alternate orthogonal polarization on adjacent satellites. Within the 3 dB contour, sufficient isolation exists to reuse the frequency band by overlapping frequencies as shown in Figure 5.5-7 for a typical C-band case.

At the higher frequencies, polarization isolation is degraded by rainfall. Figure 5.5-8 shows the effects of rain rate on such isolation at 12 and 18 GHz.

**Table 5.5-4. Typical Interference Calculation**

24-Transponder Spacecraft, 60-Foot Ground Antenna      (homogeneous case, all spacecraft; same EIRP, etc.)

Satellite	Off Boresight Angle from Reference S/C (degrees)	CIR Uplink (6 GHz) dB	CIR Downlink (4 GHz) dB	Interference Reduction Factor	Interference		Interference Power	
					Uplink dBmOp	Downlink dBmOp	Uplink pWOp	Downlink pWOp
5	25	60.7	57.2	26.5	-87.2	-83.7	1.91	4.27
4	20	58.4	54.9	26.5	-84.9	-81.4	3.24	7.25
3	15	55.2	51.7	26.5	-81.7	-78.2	6.78	15.10
2	10	51.0	47.5	26.5	-77.5	-73.0	17.70	50.20
1	5	43.3	39.8	26.5	-69.8	-66.3	105.00	235.00
0	0	-	-	-	-	-	-	-
1	5	43.3	39.8	26.5	-69.8	-66.3	105.00	235.00
2	10	51.0	47.5	26.5	-77.5	-73.0	17.70	50.20
3	15	55.2	51.7	26.5	-81.7	-78.2	6.78	15.10
4	20	58.4	54.9	26.5	-84.9	-81.4	3.24	7.25
5	25	60.7	57.2	26.5	-87.2	-83.7	1.91	4.27

5-49

SD 73-SA-0036-3

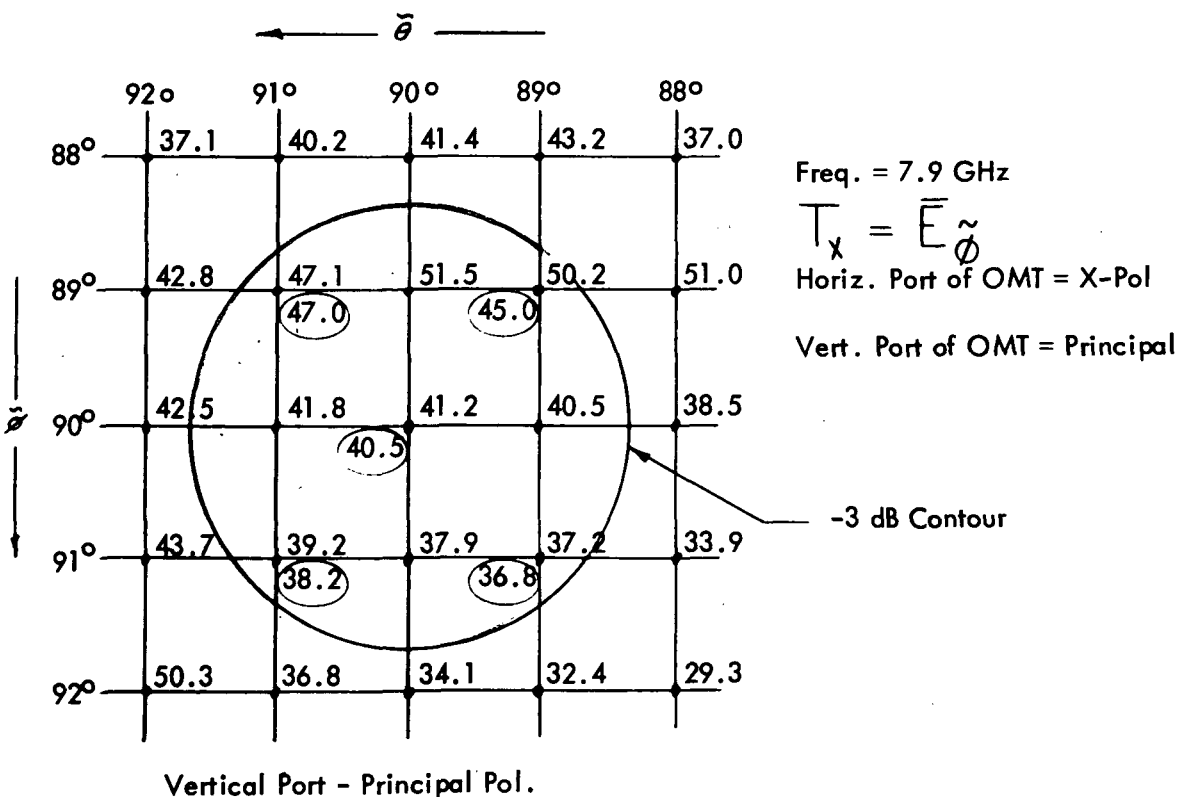
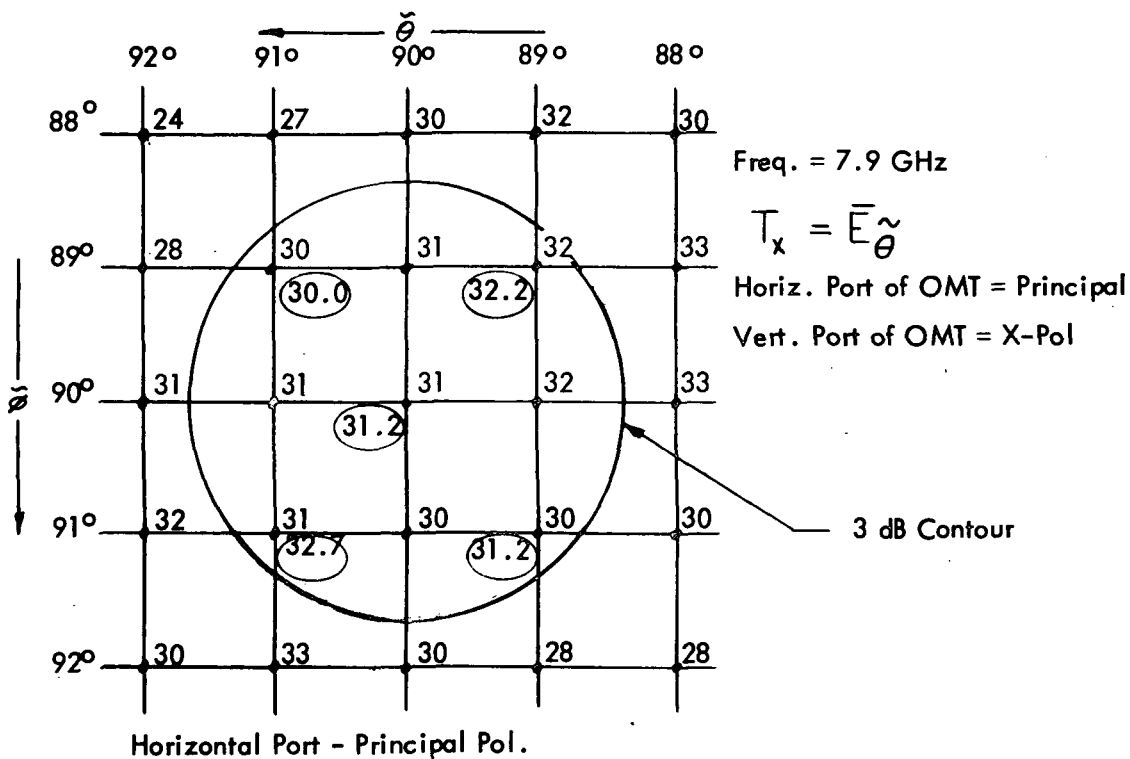
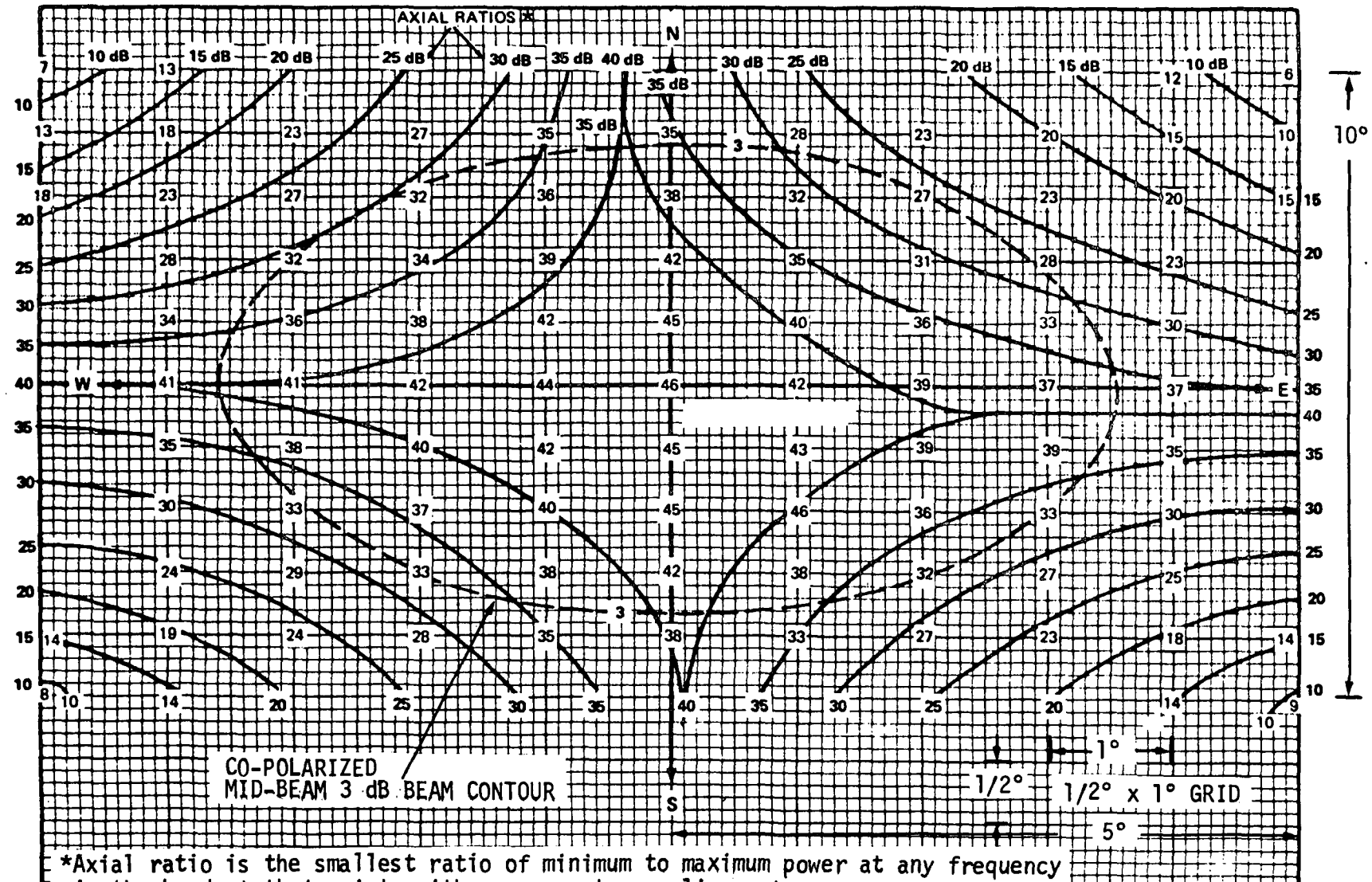


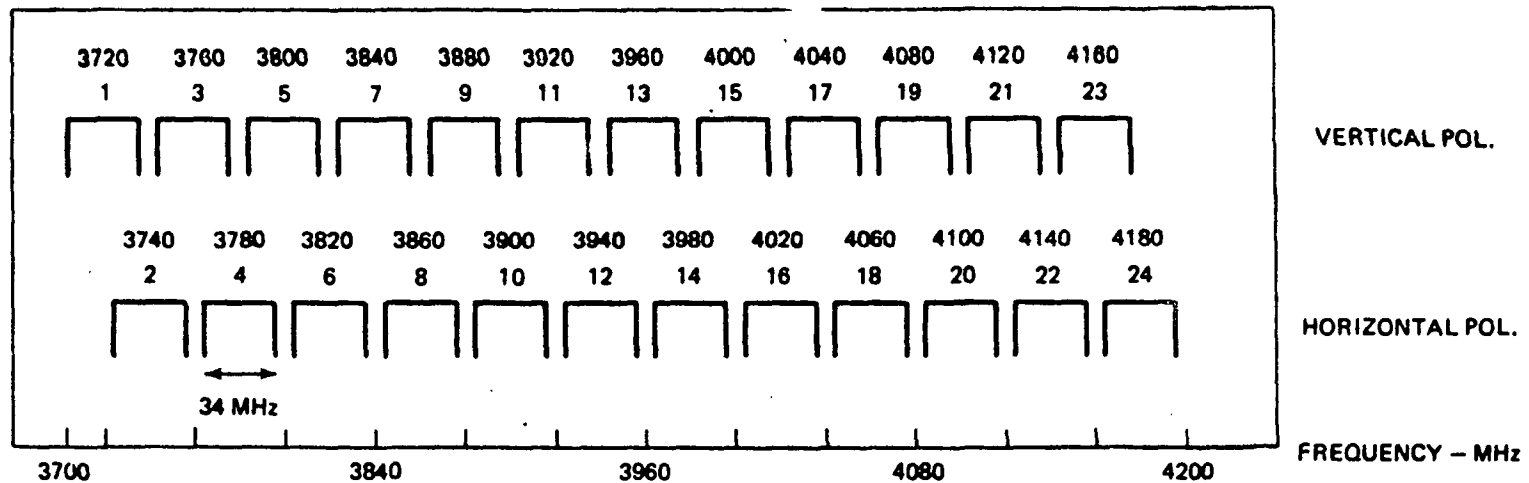
Figure 5.5-5. Polarization Isolation for Coincident Linear Beams



\*Axial ratio is the smallest ratio of minimum to maximum power at any frequency in the band at that point, with source antenna alignment

Figure 5.5-6. Horizontal Polarization (Antenna Without Grating - Angle Aligned)  
5.925 to 6.425 GHz Uplink

DOWN PATH  
(TRANSMIT)

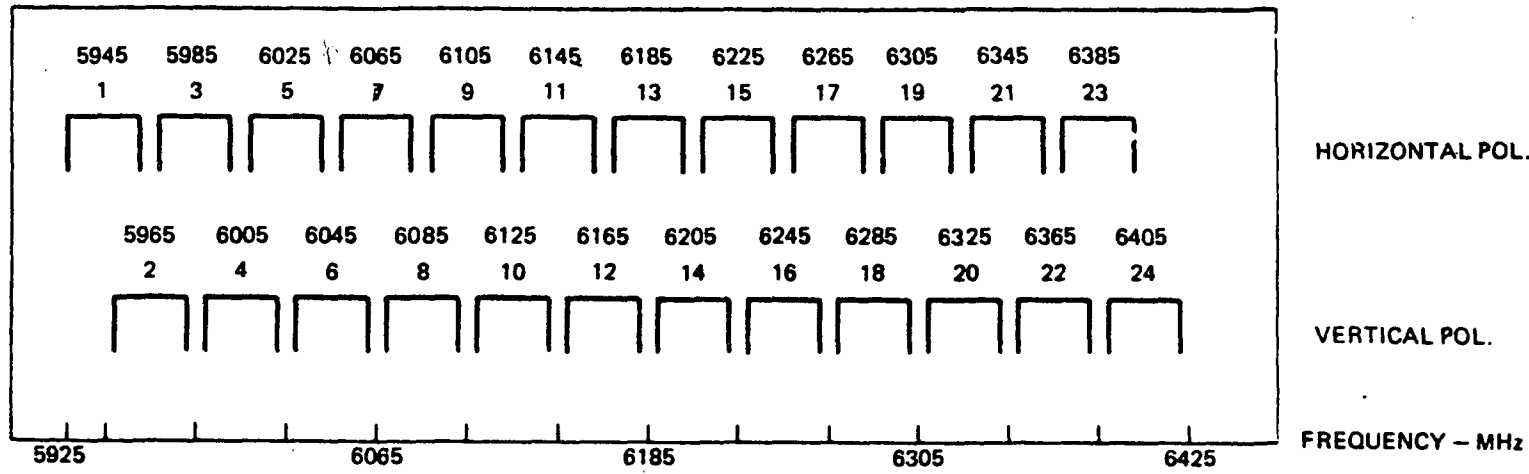


VERTICAL POL.

HORIZONTAL POL.

FREQUENCY - MHz

UP PATH  
(RECEIVE)



HORIZONTAL POL.

VERTICAL POL.

FREQUENCY - MHz

(NOTE: NUMBERS BELOW THE FREQUENCIES REFER TO TRANSPONDER IDENTIFICATION.)

Figure 5.5-7. Typical Frequency Plan Using Orthogonal Polarization

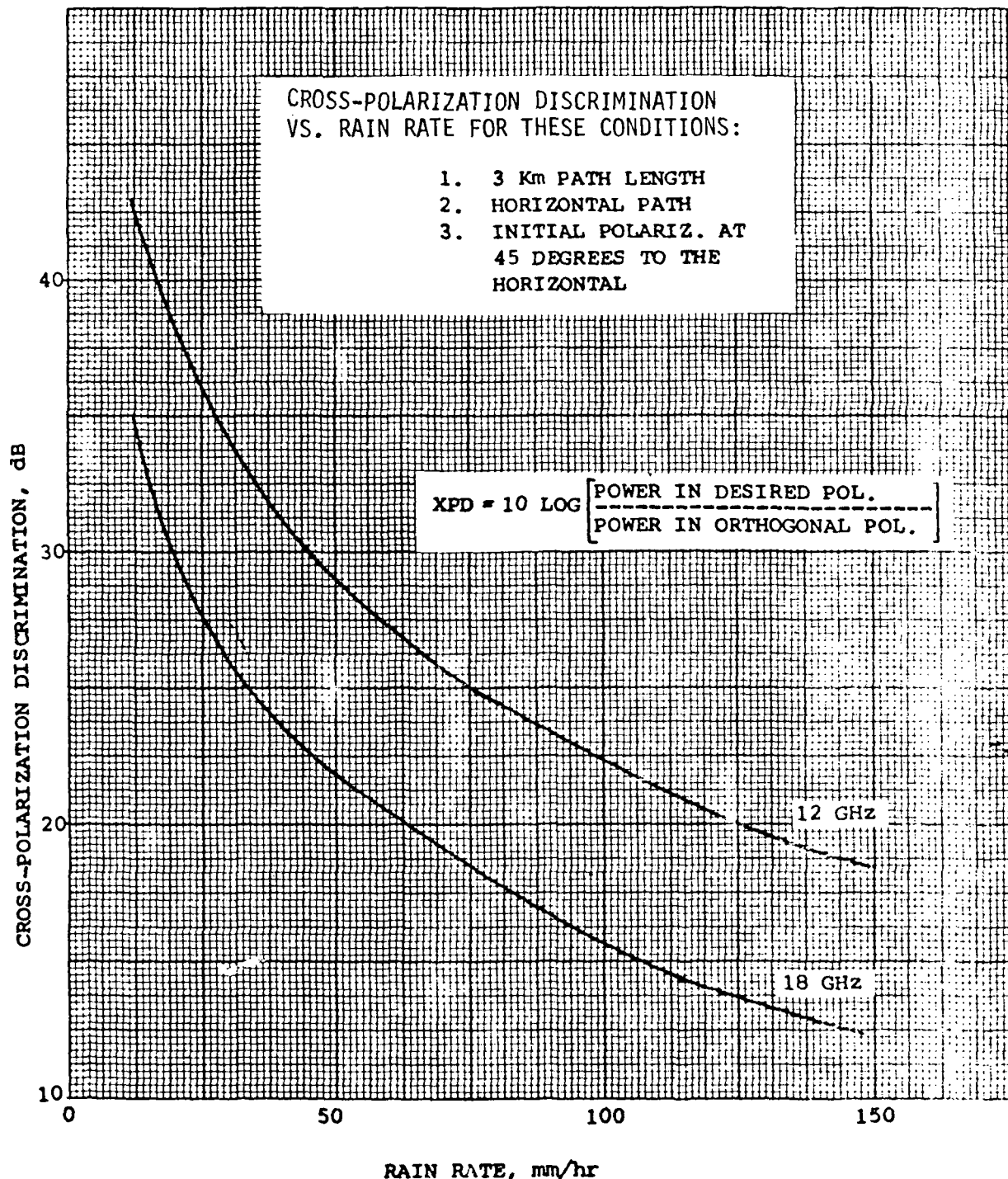


Figure 5.5-8. Cross Polarization Discrimination vs. Rain Rate Effects for a Horizontal Earth Link



## MULTIBEAM SPACECRAFT ANTENNA

By utilizing narrow beam or spot beam antennas on the communications relay satellite, further advantage of antenna discrimination can be used to increase the frequency reuse per degree of orbital arc. Discrimination results from spot beam illumination of the earth and the associated signal drop-off from the peak gain at the center of the beam. The result is quite similar to the discrimination discussed under Ground Antennas. Geographical separation on earth instead of on-orbit accounts for the ability to discriminate. Beam widths of one-half degree at the half-power points are considered to be the minimum feasible size. As a point of reference a one-half degree beamwidth would be approximately 165 miles wide at the 3 dB points. Narrower beams would require large spacecraft antennas, precision attitude control and pointing, and further would illuminate too small an earth area. Figure 5.5-9 displays the pointing angle separation in terms of antenna beamwidths necessary to keep the interference within acceptable levels. This data is based on both beams using the same frequency, thereby accomplishing frequency reuse at a given satellite orbital location. Thus, in a pattern of multiple beams as shown in Figure 5.5-10, frequencies can be reused several times if careful planning of beam targeting and frequency allocation is undertaken.

Spot multiple beam antenna systems should only be considered at frequencies above 10 GHz. Figure 5.5-11 shows antenna sizes versus beamwidth (3 dB) for the K<sub>L0</sub> and K<sub>H1</sub> bands (using the low end frequencies).

Many concepts have been proposed for multiple beam configurations. Because of the problems associated with many feeds with a single reflector due to aperture blockage, consideration is given only to dual beam, single parabolic reflector systems. Multiple beams are therefore provided by using a number of antennas. Attempts to put more than two feeds in a single reflector system result in not only reduced antenna efficiency but also in limiting the minimum spacing between beam pointing angles due to the necessary off-axis feed position. This is particularly severe when feed horns are designed for dual polarization. These feed horns are larger and thus require greater off-axis offset. Table 5.5-5 defines the minimum possible spacing between beams in terms of half-power beamwidths.

Spot-Beam Coverage. When laying out multiple beam coverage plots for specific geographic areas, it is convenient to utilize templates set up to define one degree and two-degree spot beam intersections with earth. The derivation and use of these templates follows.

The radiation pattern of a directive antenna may be idealized as a circular cone with apex at the antenna and centerline along the antenna pointing vector. The apex angle of the cone is called the "antenna beamwidth". Actually, the idealized solid cone (assumed for practical purposes) represents those limits within which the radiated power exceeds one-half the power radiated along the antenna pointing vector.

The intersection of conic radiation patterns with the earth (assumed to be spherical) can be plotted on a map of the earth. The area enclosed within these patterns receives power at levels within 3 dB of maximum radiated power.

BASED ON

$$\Delta\theta = [0.0489S\theta_d^2]^{0.4}$$

Reference 5-17

S = SIDELOBE SUPPRESSION IN dB

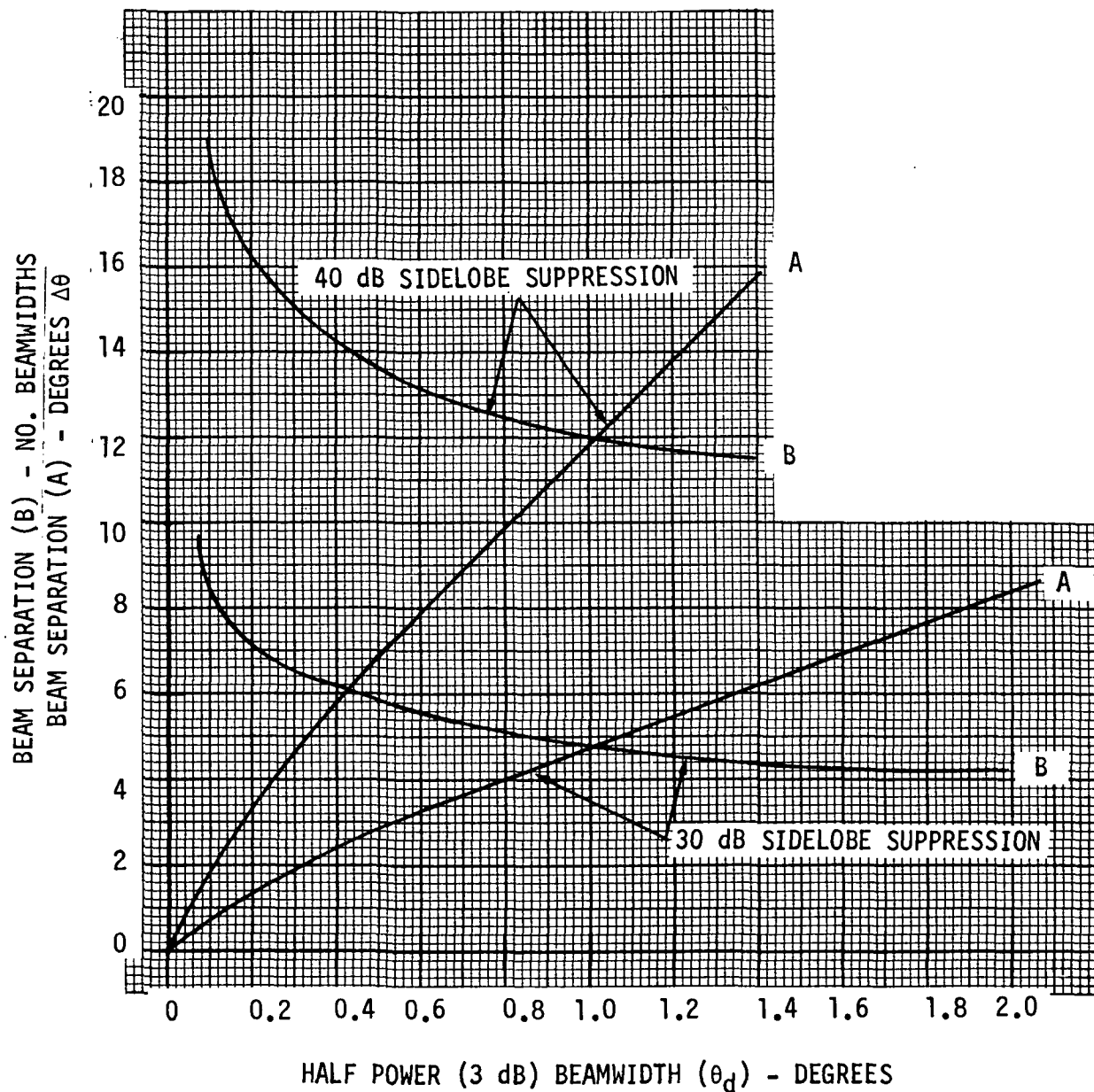
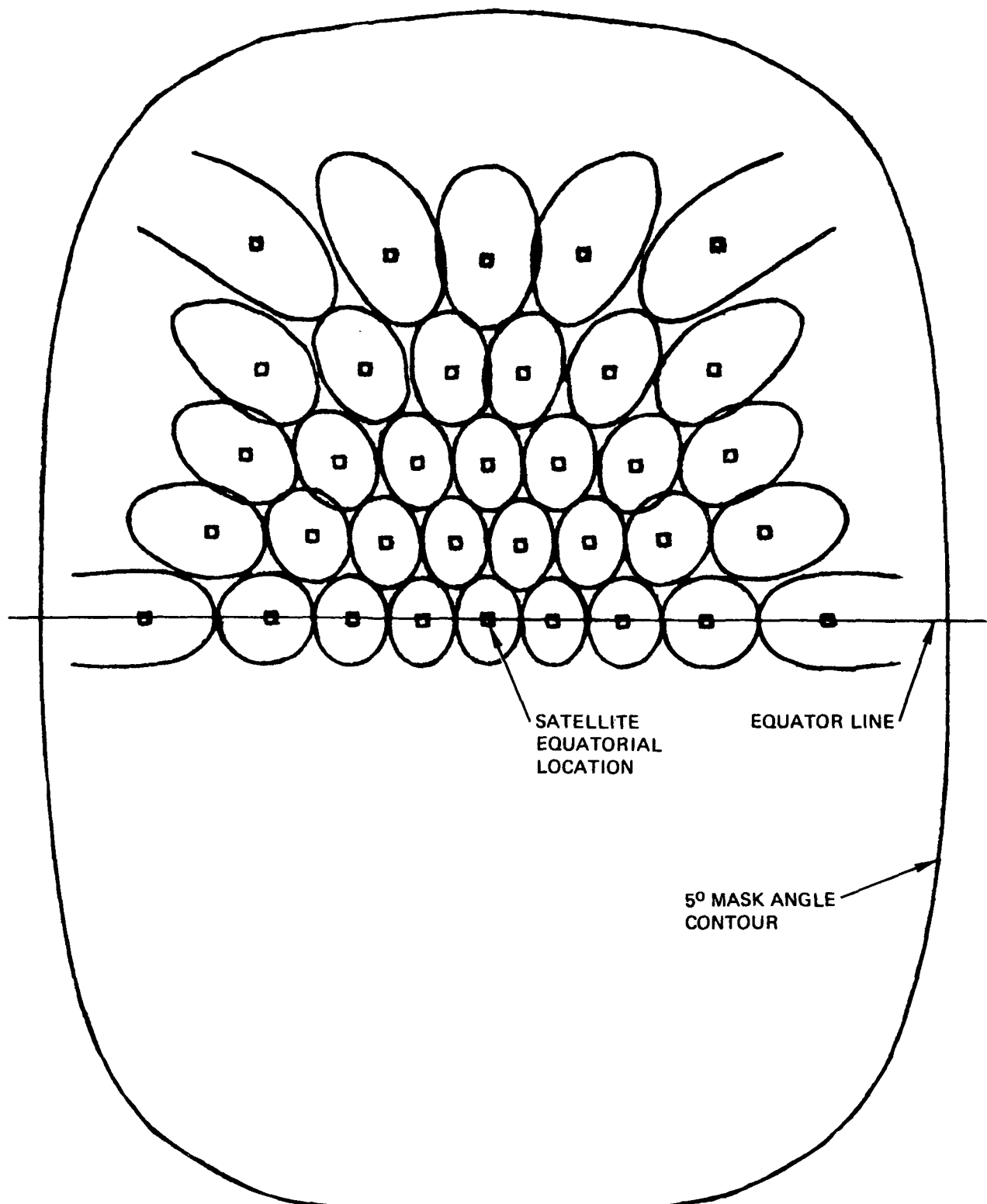
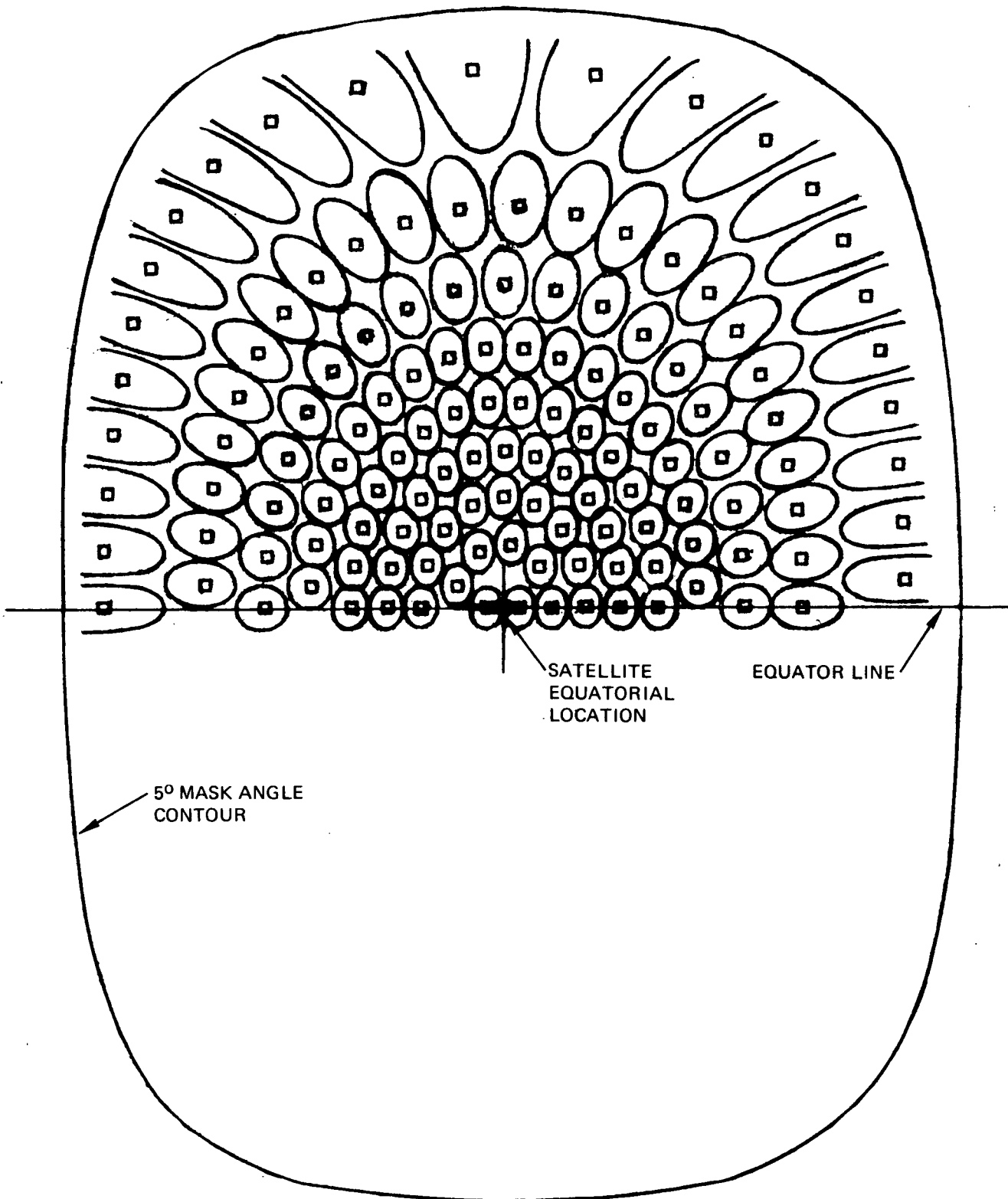


Figure 5.5-9. Multi-Beam Satellite Antenna Use  
(Beam Separation vs. Beamwidth)



(Note: A vellum copy of this template is included for use as an overlay on Figure 5.5-13.)

Figure 5.5-10. Two-Degree Spot Beam Template



(Note: A vellum copy of this template  
is included for use as an  
overlay on Figure 5.5-13.)

Figure 5.5-11. One Degree Spot Beam Template

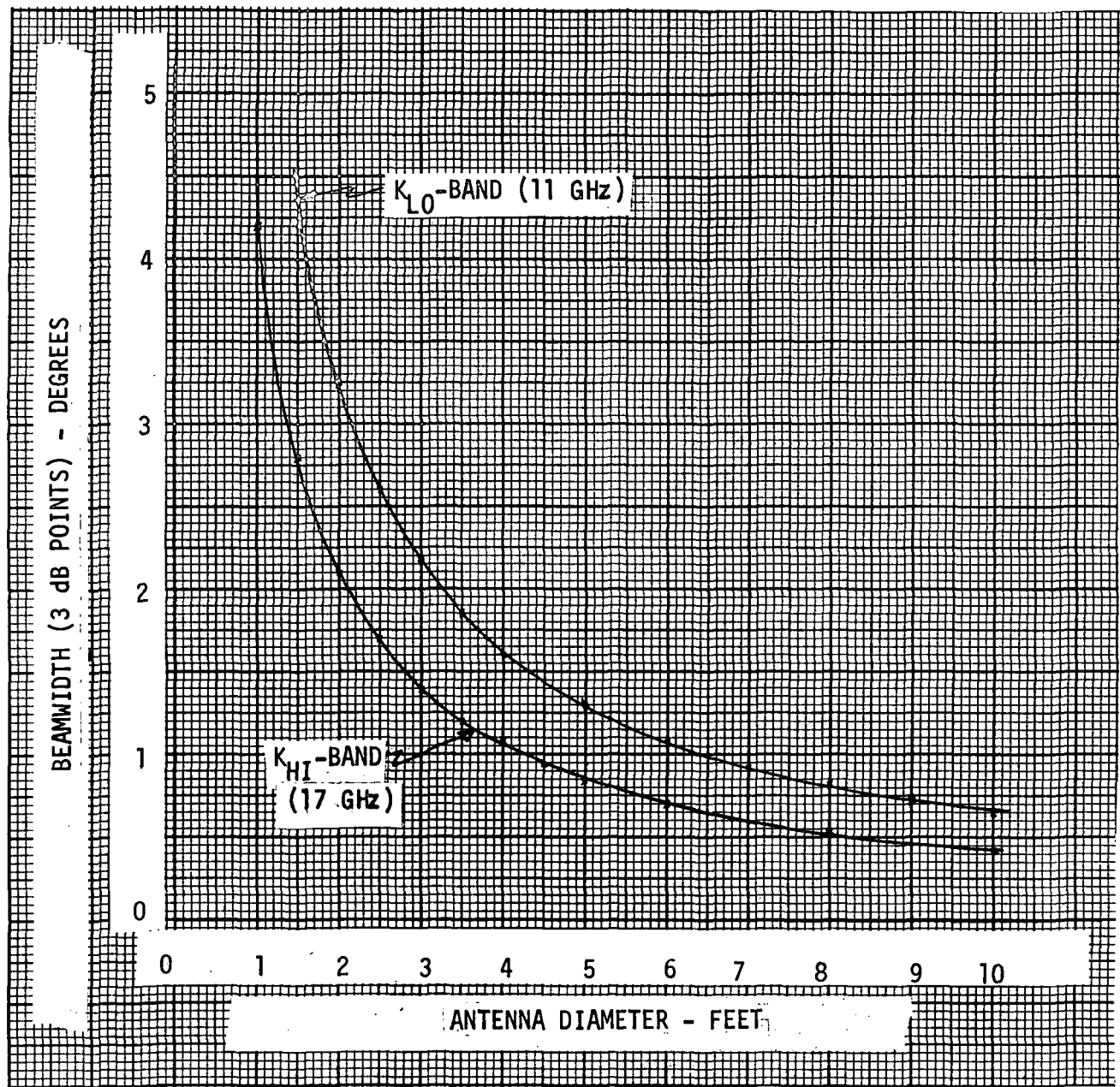


Figure 5.5-12. Antenna Beamwidth vs. Size

Table 5.5-5. Minimum Beamwidth Separation  
for Dual Beam Antennas

	Single Polarization (Standard Feed)	Dual Polarization (Corrugated Horn Feed)
1) H-Plane dimension	$0.7 \lambda$	$1.8 \lambda$
2) Minimum distance between phase centers of two contiguous horns	$0.7 \lambda$	$1.8 \lambda$
3) Beam separation* (for $\frac{F}{D} \approx 0.4$ )	$1.45 \frac{\lambda}{D}$	$3.73 \frac{\lambda}{D}$
4) Half-power beamwidth	$1.2 \frac{\lambda}{D}$	$1.2 \frac{\lambda}{D}$
5) Minimum beam separation (number of half-power beamwidths)  3) ÷ 4)	1.22	3.12
$* \frac{F}{D} = 0.4, \text{ separation} = 0.83 \frac{2}{F} \text{ or } 0.83 \frac{2}{0.4D} = 2.075 \frac{2}{D}$		

In analyzing the geosynchronous platform it was convenient to use the world map (cylindrical projection) shown in Figure 5.5-13. On this map the contour of the intersection of conic radiation with the earth can be computed from the formula shown in Figure 5.5-14. This formula was programmed on a digital computer which could draw the resulting contour when given the location of the subsatellite point, the altitude of the satellite, the aiming point of the antenna beam, and the beamwidth of the radiation pattern.

This program was then used to draw templates of the illumination contours resulting from one degree and two-degree antenna beamwidths, Figures 5.5-10 and 5.5-11, from a geosynchronous satellite. These templates can be positioned on the map so that the center of the template coincides with the subsatellite point on the equator. The template then shows the resulting coverage of the corresponding beamwidth from a geosynchronous satellite at that position. A layout of multiple beam patterns can be generated by proper use of these templates. As is evident from the plots, the beam changes from a circle at the equatorial subsatellite point to a flared-out pattern as the aiming point approaches the tangent. The limit of usable communication link to ground station is defined by the encircling elliptical pattern that shows the location of the position that is limited by a 5-degree ground antenna elevation angle. Such a limitation is imposed to maintain atmospheric attenuation levels low enough for the necessary link margins. Estimates of narrow beam spot coverage can be made using these masks and the map. Actual coverage areas should then be generated by using the computer program to provide more accurate results.

**Page intentionally left blank**

**Page intentionally left blank**

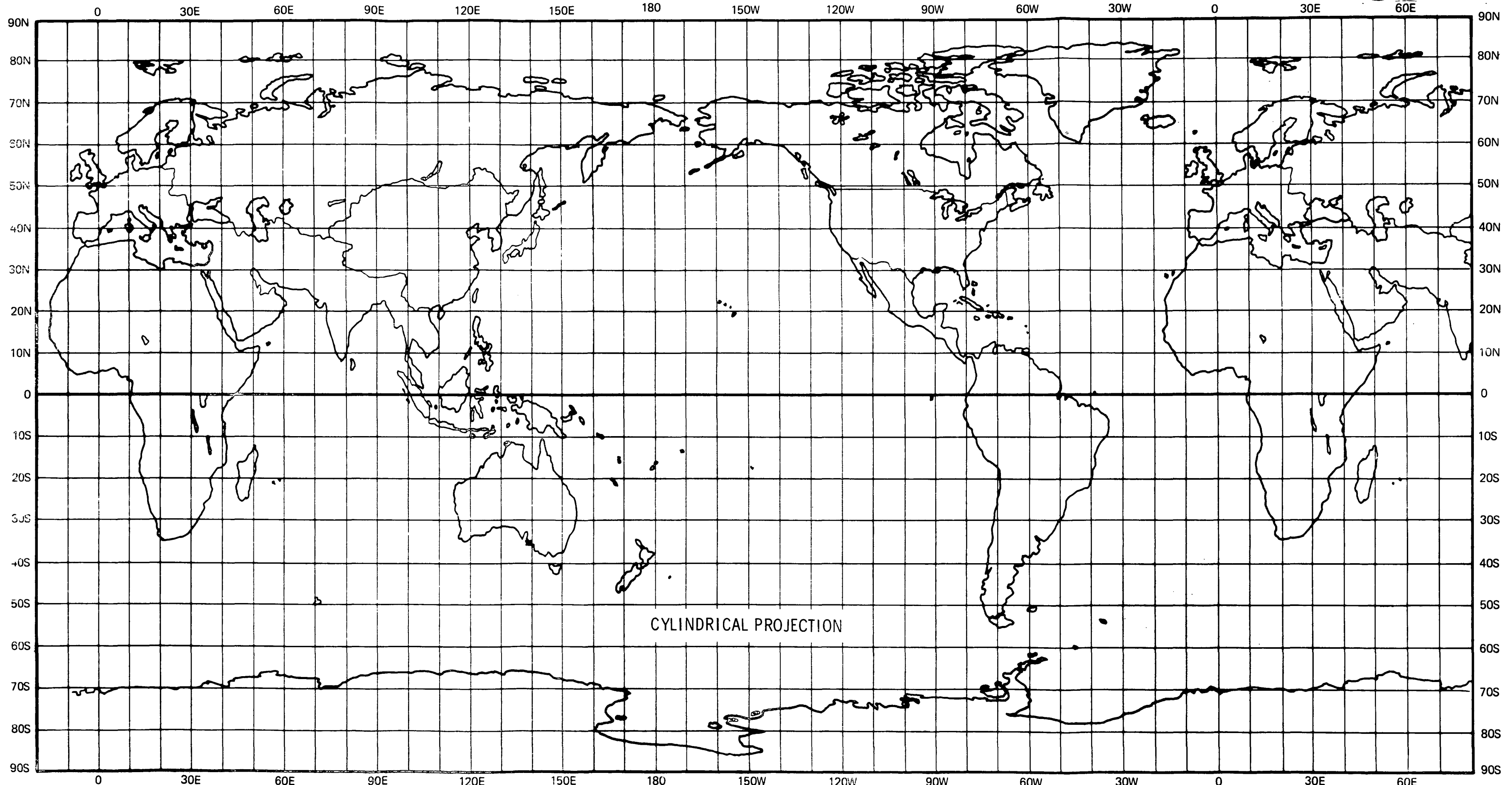
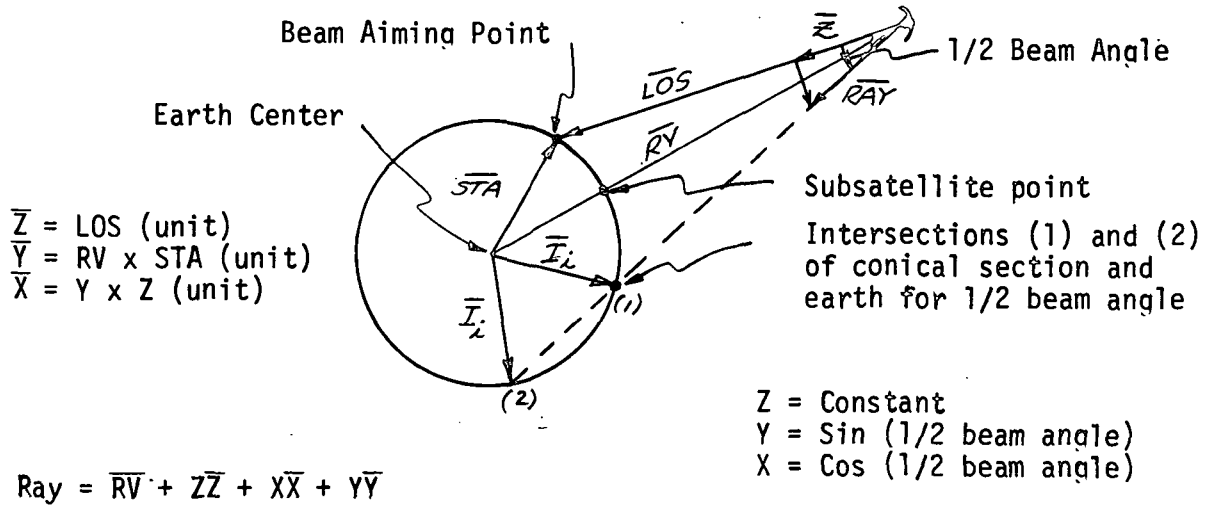


Figure 5.5-13. World Map for Use With Spot Beam Templates



$$M_1 = \frac{\text{Ray}_y - \text{RV}_y}{\text{Ray}_x - \text{RV}_x}$$

$$M_2 = \frac{\text{Ray}_z - \text{RV}_z}{\text{Ray}_x - \text{RV}_x}$$

$$b_1 = \text{Ray}_y - M_1 \cdot \text{Ray}_x$$

$$b_2 = \text{Ray}_z - M_2 \cdot \text{Ray}_x$$

$$A = 1 + M_1^2 + M_2^2$$

$$C = b_1^2 + b_2^2 - R_{\text{earth}}$$

$$B = 2(M_1 b_1 + M_2 b_2)$$

$$I_i = \left[ \begin{array}{l} -B \pm \sqrt{B^2 - 4AC} \\ \hline 2A \\ M_1 \cdot I_{ix} + b_1 \\ M_2 \cdot I_{ix} + b_2 \end{array} \right] \quad i = 1, 2$$

Select smallest  $|RV - I_i|$

Then the latitude of the penetration point =  $\arcsin \frac{I_z}{R_{\text{earth}}}$

And, the longitude of the penetration point =  $\arctan \frac{I_y}{I_x}$

The intersection pattern is the result of iteration of the above relationships for 10 rays around the conical surface.

Figure 5.5-14. Formula for Definition of Penetration Point of Ray Element of Conical Beam with Earth Surface



## TIME DIVISION MULTIPLE ACCESS

Time division multiple access (TDMA) schemes (Reference 5-11) were first tested in a system developed by Comsat (Reference 5-12) via the Intelsat-I (Early Bird) in 1966. The system was channelized for time sharing by earth stations that transmitted their information in bursts rather than continuously. The burst transmissions were synchronized so that all participating transmissions were in a sequence with no overlaps between signals. The test showed that burst synchronism to accuracies in the low nanosecond region can be achieved (Reference 5-13). In 1967, an analysis was given at EASTCON '67 which compared TDMA with Frequency Division Multiple Access (FDMA) and hybrid schemes that also used coding to obtain orthogonality between signals for separation of user transmissions (Reference 5-14). The analysis concluded that of 11 different multiple access system configurations, the use of an ideal orthogonal multiple access modulation technique with a complex demodulation/remodulation satellite offers the best performance. The following advantages were quoted for the latter system:

1. No mutual interference between users.
2. Uplink noise is not repeated as such.
3. Performance is independent of the user station transmitter size relative to average size. This affords a mix of high power and low power users with equal performance for each user.

Comparison between FDMA and TDMA to obtain orthogonality between signals, respectively in the frequency domain or in the time domain, showed obscure differences. A significant improvement occurs using demodulation/remodulation with either scheme. This added function in the system enhances TDMA performance so that it appears more promising. A recent paper (Reference 5-15) points out an area of performance improvement that is attributable to use of digital (PCM) in lieu of analog (FM) techniques. A loss of satellite capacity is experienced when FDM-FM (Frequency Division Multiplex transmitted by Frequency Modulation) multiple access techniques are used. This is due to the nonlinearities of the satellite Traveling Wave Tube Amplifier (TWT) at full power point. The power is sacrificed by backing off the TWT operation into a quasilinear region to reduce intermodulation noise interference in the FM signals. By using digital modulation the relative insensitivity to this interference in voice-activated transmissions affords use of available power more effectively. The relative importance of this feature remains to be evaluated in terms of solid-state power amplifiers but is valid at present in view of the wide use of TWT amplifiers in satellites. A further comparison between PCM-PSK (Pulse Code Modulation transmitted by Phase Shift Keying) and FDM-FM has been reported in the literature (Reference 5-16). From the stand-point of maximum number of one-way voice channels in a 500 MHz band, the report shows that an FDM-FM system with a peak frequency deviation ratio of  $D = 4$  provides 9500 one-way channels, while the PCM-PSK system yields 9120 one-way channels. When orbital separation of satellites is considered, based on interference levels, the PCM-PSK system yields 4200 channels per degree of

orbit compared to 2930 channels for FDM-FM. Further, considering the power required for the latter performance figures shows that for the 2930 channels, FDM-FM required a carrier power (watts) to receiver noise temperature (degrees Kelvin) ratio or  $C/T = 3 \times 10^{-13}$  and for four-level PCM-PSK and an error rate of  $10^{-6}$  plus allowances of 1.0 dB for uplink degradation and 2.0 dB for transmission degradation, the requirement is  $C/T = 2.2 \times 10^{-13}$ . This shows that there is relatively small difference in power requirements. A further advantage for PCM-PSK is in the fact that the problem of carrier dispersal during periods of light load is avoided because there are no idle carriers. On this basis, the foregoing discussion suggests that an optimal system would include use of PCM/PSK/TDMA in a satellite demodulation/remodulation system.

#### TDMA System Functional Description

The TDMA system can be implemented by placing an on-board time division switching system on the satellite. To realize full advantage of TDMA, the satellite system must include means for demodulation and remodulation repeating. A functional block diagram of an on-board switched multiple-access system is shown in Figure 5.5-15.

Each user station transmits a continuous multichannel bit stream consisting of voice-band inputs that are pulse-code modulated (PCM) on a coherent phase-shift-keyed (PSK) carrier. These PSK modulations are time-grouped by destination and have a definite frame period; this supermodulation is also TDM. All user transmissions are frame synchronized as they enter their respective satellite receivers. The signals are demodulated and fed to the satellite distribution system as a PCM bit train. The satellite distribution system acts as a time division switch that connects all traffic consisting of voice-channel timed frames intended for a particular destination in sequence to the appropriate output.

Each output consists of a remodulator and carrier generator. These produce the destination downlink signal containing the PCM-TDM-PSK-TDM modulated single carrier, but this double time division multiplex output is now source-oriented instead of destination-oriented as it was on uplink. Some periodic phase and frequency discontinuities may be present due to the on-board switching. Synchronization sub-units must exist in this system: (1) the user transmissions must be frame-synchronized when they enter the satellite receiver, (2) each coherent PSK demodulator in the satellite must recover the carrier and clock signal of each TDM segment separately because these signals vary from segment to segment, (3) the on-board switching unit must be frame-synchronized to perform the time division switching function, (4) the remodulators on the satellite must provide some indication within each segment to be retransmitted showing where the first bit of the first time slot is located, and (5) the ground receiving station coherent PSK demodulator must recover the downlink carrier and clock signal of each TDM segment.

To accomplish this synchronization, the uplink format shown in Figure 5.5-16(a) and the downlink format, Figure 5.5-16(b), can be used. Assume that Station A is acting as the reference station (an alternative would



Space Division  
North American Rockwell

R - Receiver  
T - Transmitter  
D - Diplexer

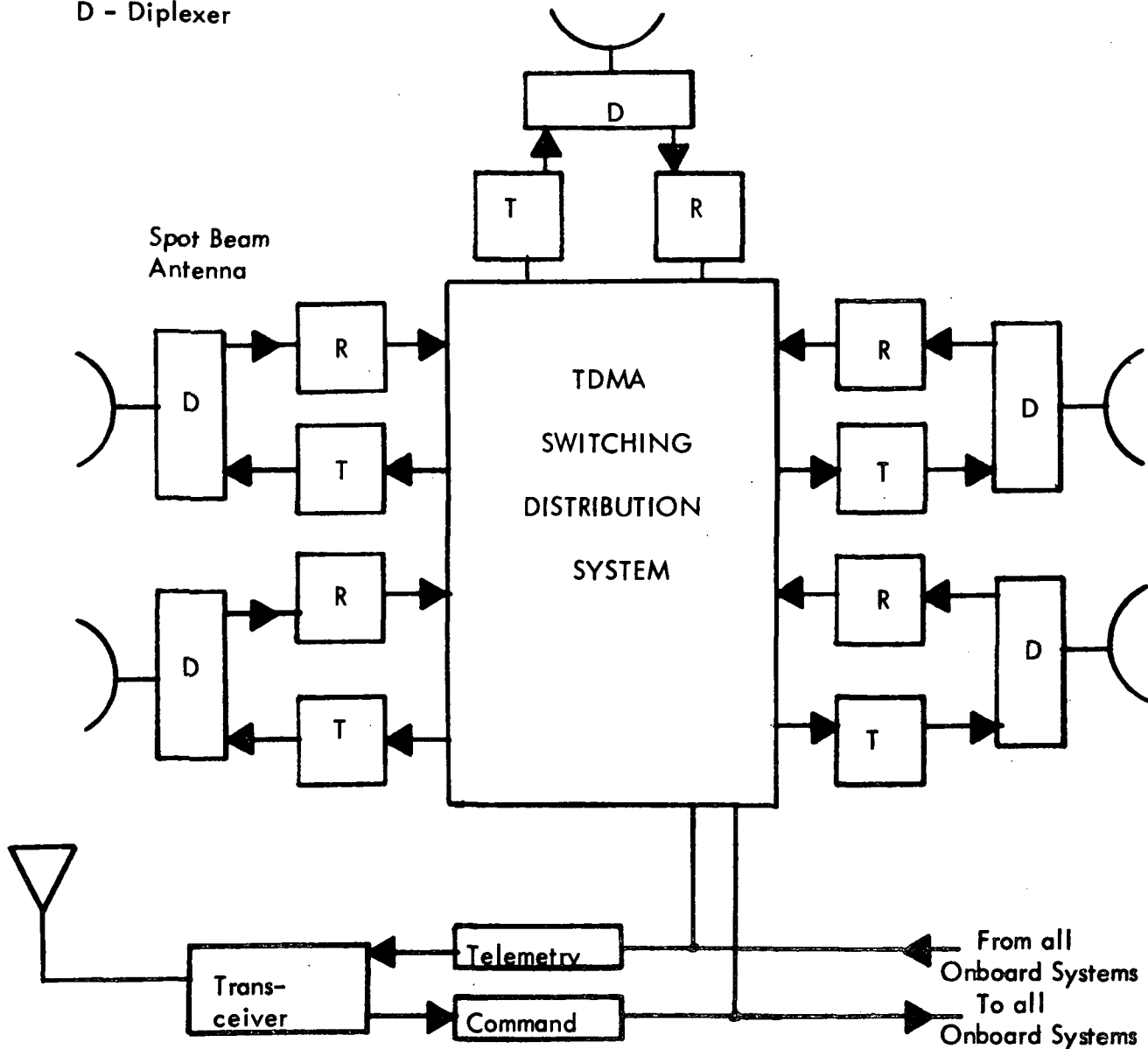


Figure 5.5-15. Satellite TDMA System

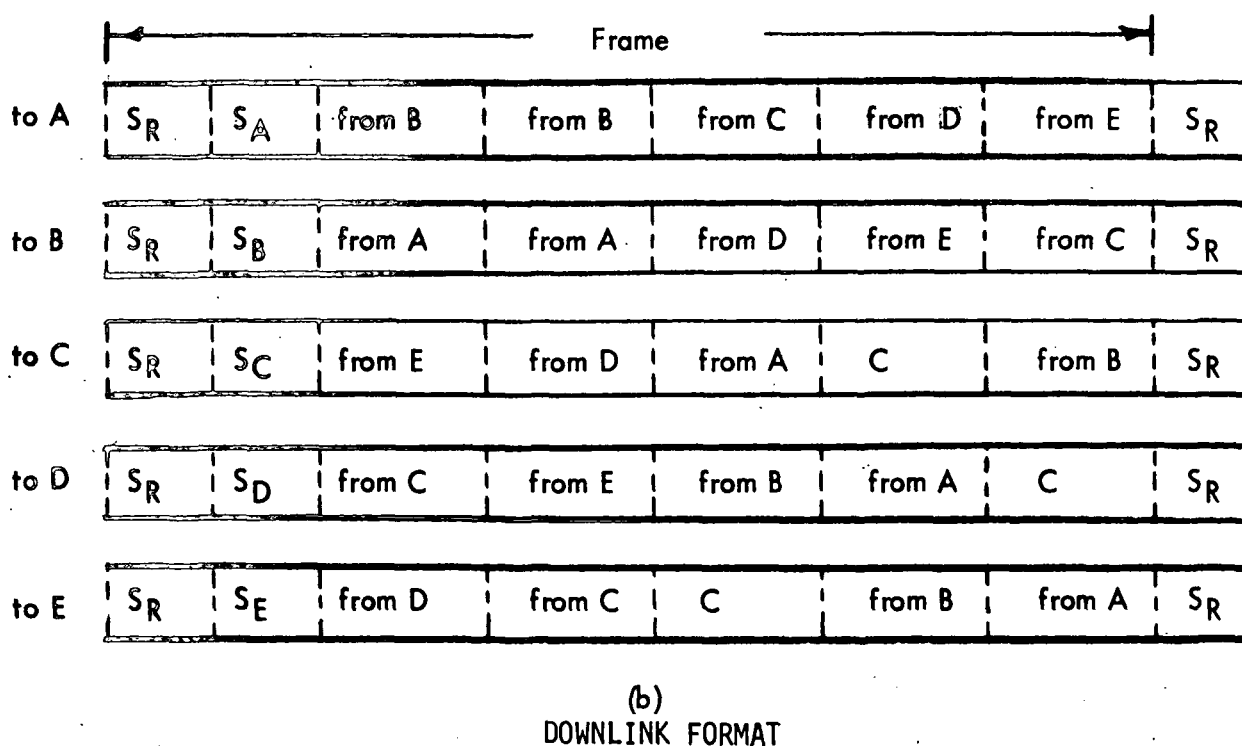
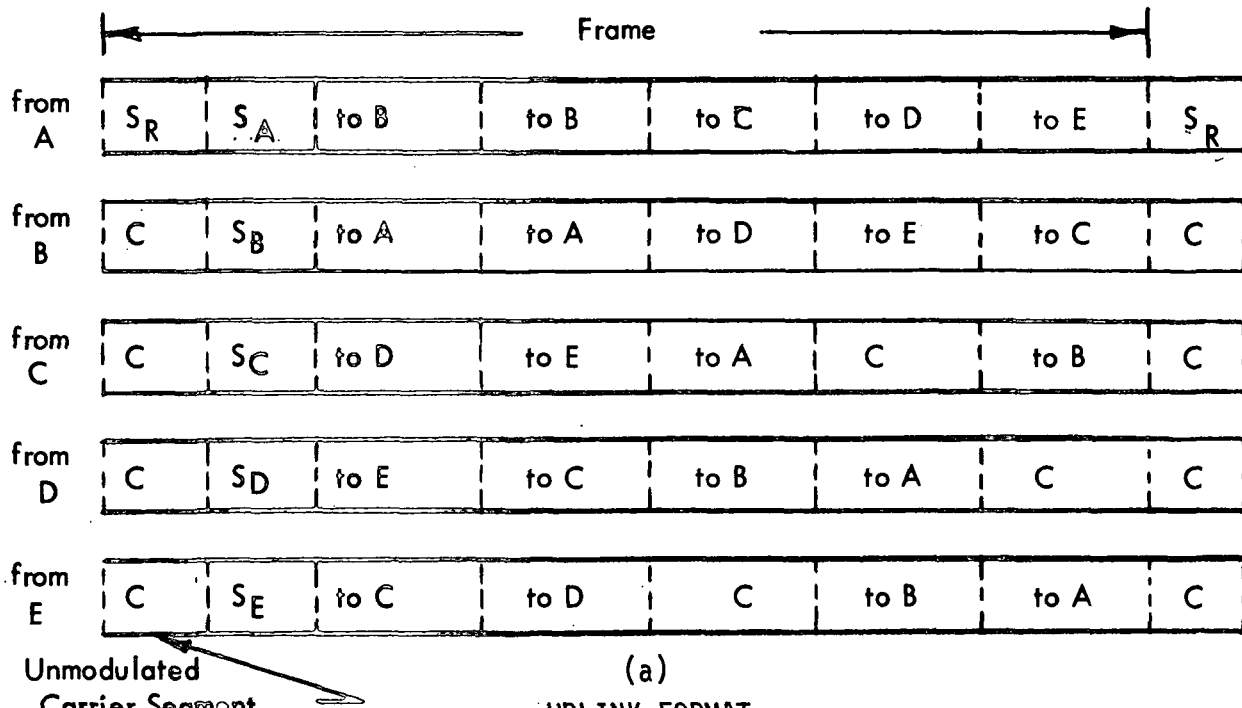


Figure 5.5-16. Formats of a TDMA System

require the satellite to provide frame synchronization with all stations performing synchronization acquisition). With Station A the reference station, the first segment of A's transmission format is a short period containing a codeword for correlation detection by all stations. During this part of the frame, nonreference stations transmit unmodulated carriers. The next segment of the format is also used for synchronization; in this case, all stations transmit their own unique station identification code words.

Up to this point in the format, no voice channel information has been transmitted. Following the two short synchronization segments, the destination-oriented time division grouping of voice channel data starts. These segments as shown are of equal length and capacity. If a station has more traffic for another station than the capacity allowed by one segment, additional segments may be allotted, e.g., the traffic shown between A and B in the format. In order to provide adequate sample time, the frame period should be equal to 125 microseconds or a multiple thereof.

On board the satellite, the switching system is synchronized to the received frame by ground reference Station A. The solid-state switches are then programmed by logic (controlled through the satellite command system) to connect the reference station synchronization segment to all output switch ports. The switch subsequently connects the input directly to the output port for the station identification segment so that, as an example, Station B receives the identification code word of Station B. This time divided return of the uplink signal solves the spot-beam synchronization problem: each user can range its transmissions to maintain frame synchronization by receiving both the reference code word and its own code word. Next, the switching subsystem directs the non-overlapping segments from each station to the satellite output port for that particular station.

With this approach to a multiple access system, though there are five transponders each of bandwidth  $n$ , the actual spectrum used is  $2n$  which is a five-fold decrease over the  $2kn$  normally required, where  $k$  is the number of transponders. There are single up-converter and down-converter chains at the user stations; the satellite EIRP requires no TWT backoff, and multiple users within a spot-beam region can use the conventional TDMA format to share uplink and downlink format.

## 5.6 TECHNOLOGY STATUS

Several areas of communications link performance are examined for projection into future state of art to the year 1985. The year 1985 is chosen as the furthest year of prediction because (1) any later predictions are even more difficult to foresee, and (2) close to 5 years is needed as lead time for state of art that is laboratory stage to proven flight-proven long-life hardware status. The major areas of interest involve microwave and millimeter wave radio frequency components, antenna systems and logic circuitry components that may be used in switching networks for TDMA-like systems.

### FREQUENCY BAND AVAILABILITY

As indicated in Section 5.3, WARC (1971) has allocated frequency bands up to 275 GHz. Several factors are involved in the technological limitations that make use of frequencies above 30 GHz unlikely by 1985. One is the limited capability of components to produce and receive RF signals. Because of atmospheric and weather losses, antenna gains will need to be increased sufficiently to enable use of those components that are available. Increased antenna gains result in narrow beams that impact the stabilization and control of pointing requirements of the spacecraft antenna system. Figure 5.6-1 shows beamwidth versus gain, and indicates that at the 50 GHz band it would be necessary to use an antenna of approximately 0.2 degree beamwidth to obtain sufficient gain to provide acceptable EIRP with a one-watt transmitter. Such limitations are used to provide reasonable input power supply levels. Thus, it seems reasonable to expect that the data relay satellite of the 1980-1990 era will be limited to the use of the K<sub>L0</sub> (12/14 GHz) and K<sub>H1</sub> (20/30 GHz) bands. The K<sub>H1</sub> frequency band supplies seven times the bandwidth of either the 4/6 GHz or 11/14 GHz band. Proper use of all these bands will support a large increase in the communications capacity of geosynchronous orbit by application of frequency reuse techniques. Impact on ground stations and the economics of change will effect the continued push for increasing operational frequency bands from the presently used C-band.

### COMPONENT AVAILABILITY

#### RF Power Amplifier Components

Several candidate types of components will be in use for RF power amplifiers in the 1980-1990 era. These include advancements in traveling wave tubes for use at higher power and higher frequencies, transistor amplifiers in moderate powers up to 10 GHz, varactor multipliers, gunn diode transferred-electron amplifiers and avalanche diodes. The latter group is most applicable to frequency ranges above 10 GHz.

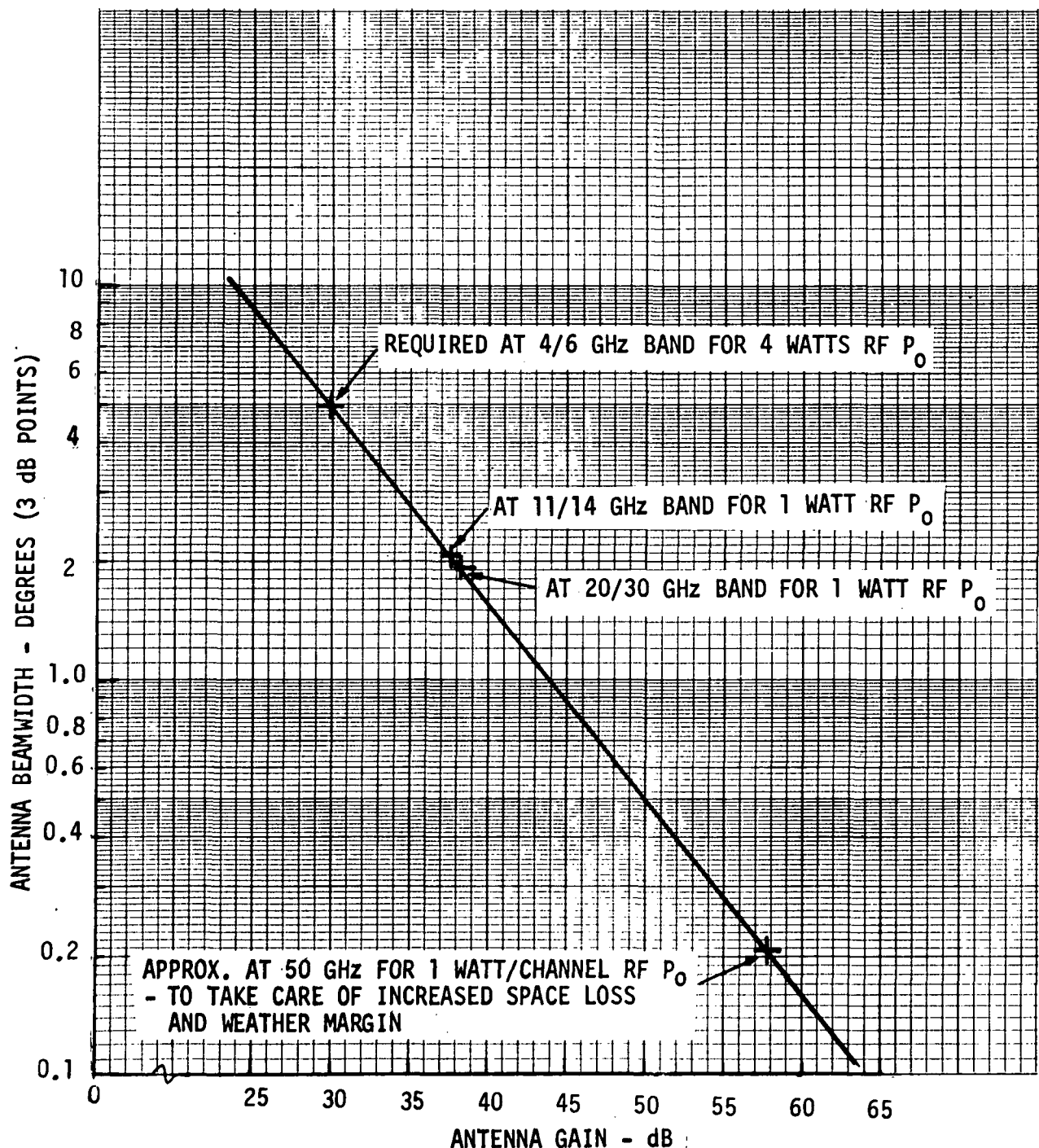


Figure 5.6-1. Antenna Beamwidth vs. Antenna Gain



Transistor amplifiers (using single transistors) are presently being manufactured that can provide 4 watts, Class C, power output at 4.2 GHz and narrow bandwidths to 50 MHz. It is expected that the technology could improve to 10 watts and perhaps to 10 GHz by 1985. Parallel operation can be utilized to provide even higher powers. Such devices presently show gains of only 5.0 dB and efficiencies in the order of 25 percent. A transponder amplifier chain, therefore, uses considerable power to produce a channel (40 MHz) output of 4 watts. By 1990, these devices should improve to efficiencies of 35 percent and gains of 10 to 15 dB, making their use far more attractive.

Traveling wave tubes--as linear broadband amplifiers--presently exist to supply up to 10 watts each at frequencies to 20 GHz for application to space-craft. It is expected that such powers will be available up to 100 GHz by 1985. The lifetime of these units will need to be increased an estimated 4 to 5 years to up to 7 to 10 years to make these tubes attractive for use on communications satellites. Weight and life are the main disadvantages of TWT's. Their efficiency and gain are and will be satisfactory.

Gunn diode-transferred electron amplifiers presently provide from 20 mw to 120 mw at frequencies of 70 GHz and 30 GHz respectively. It is expected that these power outputs could improve to 1 watt at the lower end and 250 mw at 70 to 100 GHz by 1985. Efficiencies run under 5 percent, making heat dissipation the major problem. Efficiencies and heat sinking will need to be improved to make these devices practical. They are highly reliable and have long life, and do not require complex power supplies--like a TWT.

Stable circulator-coupled reflection amplifiers using Impatt diodes have been successfully demonstrated at millimeter wave frequencies. In the 40 to 50 GHz frequency gain, bandwidth products of 15 GHz with power outputs of 100 mw and 8 dB gain have been measured. Increases in frequency and power outputs to levels of 1 watt may be expected by 1985.

It seems that one can predict useful powers of up to 2 watts with 10 percent efficiency by the year 1985 from solid-state devices with reasonable bandwidths at frequencies up to 30 GHz. Such operation would make transmitter equipment for these frequencies feasible with lightweight, solid-state components.

#### Receiver Front Ends

Schottky-barrier mixer diodes and gallium arsenide field effect transistors are destined to be of use as low-noise receiver preamplifiers in the next decade or two. Mixers with Schottky-barrier diode and an integrated L-band IF amplifier have been demonstrated at 40 to 50 GHz with noise figures of 8.5 dB with bandwidths of 500 MHz. Such performance approaches the performance of tunnel diode amplifiers at frequencies up to 15 GHz. It is expected that TDA's will still be useful up to 30 GHz at noise figures of 6 to 7 dB by 1985. Such performance is presently being demonstrated at 15 GHz. It can be expected that noise figures in the order of 6 to 7 dB will be available at frequencies up to 100 GHz by 1985. Bandwidth should not be a problem with either type, within their frequency limitation, being capable of bandwidths up to 5 percent or 10 percent. Receiver preamplifiers should not be limiting devices even up to 100 GHz by 1985. Gallium-arsenide FET's presently being produced in the



laboratory exhibit noise figures of approximately 3 dB at 5 GHz and 6 dB at 20 GHz. In the frequency range from 10 to 30 GHz, these devices should approach noise figures of 4 to 5 dB at 30 GHz by 1985.

### Antennas

The major advances to look for by 1985 are in spacecraft multibeam antenna array systems. Lightweight, deployable antennas capable of 4 to 8 beams are possibilities by 1985. These would be either phased-array or large multifeed parabolic section antennas that would provide the necessary gains and numbers of beams at frequencies up through 30 GHz. Phased arrays can be used in multiple, switchable beam systems. Such advances will allow frequency reuse to the extent necessary for the 1985 era.

### Summary

Table 5.6-1 indicates the projections of usable data rates per orbital degree by 1985, assuming the advances discussed above and the use of advanced modulation techniques, as previously discussed.

Table 5.6-1. Projection of Geosynchronous Orbit Data Rate Capability

Time	Frequency Band	Per Satellite Data Rate Capability (bps)	Frequency Reuse	Spacing (deg.)	Data Rate per Degree (bps)
1975-1980	C	$960 \times 10^6$	2 x	4.6	$205 \times 10^6$
	plus K <sub>LO</sub>	$2.88 \times 10^9$	2 x C 4 x K <sub>LO</sub>	4.6	$626 \times 10^6$
1980-1990	plus K <sub>HI</sub>	$43.2 \times 10^9$	2 x C 4 x K <sub>LO</sub> 6 x K <sub>HI</sub>	4.5	$9.82 \times 10^9$
$\boxed{\text{WORLD RATE*} = 9.82 \times 10^9 \times 360 = 3.5 \times 10^{12} \text{ bps}}$					
<p>*capability of three-band usage as defined</p>					

## 6.0 REFERENCES

- 3-1 Explanatory Supplement to the Astronomical Ephemeris and the American Ephemeris and Nautical Almanac: Prepared Jointly by the Nautical Almanac Offices of the United Kingdom and the United States of America: Issued by H. M. Nautical Almanac Office by Order of the Lords Commissioners of the Admiralty. London: Her Majesty's Stationery Office, 1961.
- 3-2 Perkins, F. M., "Flight Mechanics of the 24-Hour Satellite", AIAA Journal, April 1963, pp. 848-85.
- 3-3 Frick, R. H., "Orbital Regression of Synchronous Satellites Due to the Combined Gravitational Effects of the Sun, the Moon and the Oblate Earth". R-454-NASA, National Aeronautics and Space Administration, Washington, D. C., August 1967.
- 3-4 Michielsen, H. F., and Webb, E.D., "Station Keeping of Stationary Satellites Made Simple", Lockheed Missiles and Space Company, Sunnyvale, California.
- 3-5 Tug Operations and Payload Support Study, Volume 3, Part 1, Mission and Operations Analysis. Rockwell International, Space Division, SD 73-SA-0006-3, DR No. MA-04 (5 March 1973).
- 4-1 Moulton, Forest Ray, PhD., An Introduction to Celestial Mechanics. New York: The Macmillan Co., 1914.
- 5-1 Useful Applications of Earth-Oriented Satellites, N69-27876, National Academy of Sciences, 1969
- 5-2 Hogg, D. C., "Millimeter-Wave Communication through the Atmosphere", Science, Vol. 159, No. 3810, January 1968
- 5-3 Ulaby and Straiton, "Atmospheric Absorption Between 150 and 350 GHz", IEEE Transactions on Antennas and Propagation, Vol. AP-18, No. 4, July 1970.
- 5-4 Haviland, R. P. and House, C. M., Handbook of Satellites and Space Vehicles, D. Van Nostrand Co., Inc., Princeton, New Jersey, 1965
- 5-5 Taylor, J. H. and Yates, H. W., "Atmospheric Transmission in the Infrared", Journal of the Optical Society of America, Vol. 47, No. 3, March 1957
- 5-6 Benoit, A., "Signal Attenuation Due to Neutral Oxygen and Water Vapor, Rain and Clouds", The Microwave Journal, November 1968
- 5-7 Radio Spectrum Utilization in Space, a report of the Joint Technical Advisory Council of the IEEE and the EIA, Vol. 33, Sept. 1970



- 5-8 Feldman, N. E., "Estimates of Communication Satellite System Degradation Due to Rain", P-3027, The Rand Corporation, Santa Monica, Ca. Oct. 1964
- 5-9 "Orbit Spectrum Utilization Study", Vol. IV, prepared by Dr. M. C. Jeruchim and D. A. Kane, Document #TOSD4293, 31 December 1970, General Electric report for Contract OEP-SE-69-102, Office of Telecommunications Policy
- 5-10 "Polarization Isolation Characteristics of a Dual-Beam Reflector Antenna" by J. W. Duncan, J. J. Hamada and W. C. Wong, TWR Systems Group, AIAA Paper 72-531 dated April 24-26, 1972.
- 5-11 D. J. Magill, "Multiple-Access Modulation Techniques", Communications Satellite System Technology. Academic Press, New York, 1966, pp. 661 - 680.
- 5-12 T. Sekimoto and J. G. Puente, "A Satellite Time-division Multiple Access Experiment", IEEE Transactions on Communications Technology, Vol. CDM-16, Aug. 1968, pp. 581-588.
- 5-13 O. G. Gabbard, "Design of a Satellite Time-Division Multiple-Access Burst Synchronizer", IEEE Trans. Comm. Tech., Vol. COM-16, August 1968, pp. 589-596.
- 5-14 J. H. Wittman, "A Comparison of Satellite Multiple Access Techniques", Aerospace and Electronic Systems Technical Convention Record, IEEE, 1967, pp. 165-172.
- 5-15 J. G. Puente, W. G. Schmidt, "Multiple-Access Techniques for Commercial Satellites", IEEE Proceedings, Vol. 59, No. 2, February 1971, pp. 218-229.
- 5-16 "Useful Applications of Earth-Oriented Satellites", National Academy of Sciences, Washington D. C. 1969, pp. 107-118.
- 5-17 Useful Applications of Earth-Oriented Satellites, Panel 9, National Research Council, 1969 (Point-to-Point Communications).
- 5-18 A General Analysis of Domestic Satellite Orbit/Spectrum Utilization, Dale Hatfield, Office of Telecommunications, Dec. 13, 1971, Document PB207-397
- 5-19 Spectrum and Orbit Compatibility Analysis of the Proposed Domestic Satellite Systems, Goddard Space Flight Center, NASA, December 1971
- 5-20 C.C.I.R., XII Plenary Assembly Report (New Delhi, 1970), Volume IV, Part 2, titled "Fixed Service Using Communication Satellites (Study Group 4) and Space Research and Radioastronomy (Study Group 2)", published by the International Telecommunication Union, Geneva, 1970